

Kinetic study of bulk propylene homo-polymerization and
propylene/ethylene gas-phase copolymerization under
industrially relevant conditions

Dissertation

zur Erlangung des
Doktorgrades der Ingenieurwissenschaften
(Dr.-Ing.)

der

Naturwissenschaftlichen Fakultät II
Chemie, Physik und Mathematik

der Martin-Luther-Universität
Halle-Wittenberg

vorgelegt von

Herrn Sina Valaei
geb. am 01.09.1990 in Hamedan, Iran

Gutachter

1. Prof. Dr. M. Bartke
2. Prof. Dr. T. McKenna

Datum der Verteidigung: 22.02.2023 Halle (Saale)

Abstrakt

Polypropylen ist eines der meistgenutzten Polymere und wird über koordinative Polymerisation mit metall-organischen Katalysatoren in verschiedenen Verfahren hergestellt. Bei der koordinativen Polymerisation hängt die Kinetik der Reaktion stark von den verwendeten Katalysatoren ab, die stetig weiterentwickelt werden und sowohl die Effizienz der Verfahren als auch die Eigenschaften der Polymerprodukte stark beeinflussen können.

Ziel dieser Arbeit ist eine kinetische Studie von zwei unterschiedlichen Ziegler-Natta Katalysatoren in mehrstufigen Polymerisations Verfahren, das aus einer Homopolymerisation von Propylen in Masse und einer nachgeschalteten Copolymerisation von Propylen und Ethylen aus der Gasphase besteht.

Zunächst wurde ein existierender Versuchsaufbau mit 5 l Reaktor um eine Kompensationsheizung erweitert, um die Kinetik der Massepolymerisation mit Kompensationskalorimetrie untersuchen zu können. Zur Analyse der kalorimetrischen Daten wurde ein Software-Sensor entwickelt. Die Reaktionskinetik der Gasphasenpolymerisation ist im semi-batch Betrieb durch eine nachdosierend arbeitende Druckregelung untersucht worden, bei der die Gasphasenzusammensetzung mit einem μ -GC eingestellt und überwacht wurde. Diese kombinierte Meßmethode ermöglicht es, heterophasische Copolymerproben mit definiertem Elastomergehalt und kontrollierter Elastomierzusammensetzung zu erzeugen.

In dem beschriebenen Versuchsaufbau ist die Polymerisationskinetik von zwei Ziegler-Natta Katalysatoren untersucht worden. Für die Homopolymerisation lag der Schwerpunkt auf dem Einfluss von Wasserstoff und pre-contacting auf die Polymerisationsaktivität, die nachfolgende Gasphasenpolymerisation fokussierte auf den Einfluss von Gasphasenzusammensetzung auf Comonomereinbau, Aktivitätsprofil und erzeugten Molmassen.

Zur Bestimmung der Monomerkonzentrationen in beiden Verfahrensschritten wurden Sorptionsmessungen und thermodynamische Gleichgewichtsberechnungen durchgeführt.

Abschließend ist basierend auf den experimentellen Ergebnissen ein vereinfachtes, phänomenologisches Modell entwickelt worden, mit dem die Kinetik sowohl der Homopolymerisation in Masse als auch der nachfolgenden Gasphasen-Copolymerisation und die resultierenden Polymere in Abhängigkeit der Reaktionsbedingungen beschrieben werden kann. Über einen schrittweisen Ansatz zur Parameterbestimmung wurden die katalysator-spezifischen Geschwindigkeitskonstanten bestimmt.

Das entwickelte Modell und die ermittelten kinetischen Daten können z.B. für modellbasierte Produktentwicklung und Prozessoptimierung eingesetzt werden.

Abstract

Polypropylene is one of the most widely manufactured polymers and is produced via coordinative polymerization with metal-organic catalysts in different polymerization processes. In coordinative polymerization mechanism, polymerization kinetics depend on the catalyst used, hence both process efficiency and product properties are strongly influenced by the catalyst. Catalysts are constantly developed and optimized, hence there is a constant need for kinetic studies of polymerization catalysts.

Scope of this work is a kinetic study of two different Ziegler-Natta catalysts in a multi-step polymerization of propylene, consisting of a bulk-phase homo-polymerization of propylene and a subsequent gas-phase copolymerization of propylene and ethylene.

For studying kinetics, initially an existing polymerization setup with a 5-liter reactor has been equipped with a compensation heater in order to realize a calorimetric measurement approach for measurement of reaction kinetics in bulk polymerization conditions. For analysis of the calorimetric data, a software sensor has been developed, which allows to estimate the chemical heat flow of the reaction. Reaction kinetics in gas-phase polymerization have been studied by semi-batch operation of the reactor in a pressure control loop, while monitoring and controlling of the gas phase composition with a μ -GC setup. The combined calorimetric and gas-phase kinetic measurement principle enables synthesis of hetero-phasic copolymer samples with defined rubber content and controlled rubber composition.

In the outlined setup, polymerization kinetics of two different Ziegler-Natta catalysts have been studied. For bulk homo-polymerizations, the focus was on studying the hydrogen response and the effect of pre-contacting on polymerization activity. For the subsequent gas-phase polymerization, comonomer incorporation and the effect of gas-composition on polymerization activity profiles and the resulting molecular weight have been studied, for both catalysts.

For determination of monomer concentrations during both steps of the reaction, sorption measurements and thermodynamic phase equilibrium calculations have been performed.

Finally, the experimental results have been compiled in a simplified phenomenological kinetic model. Purpose of the model is to describe both homo-polymerization and copolymerization kinetics and the resulting polymers with respect to the corresponding reaction conditions. Via a stepwise procedure for parameter estimation, the catalyst-specific reaction rate parameters have been determined.

The developed model and the kinetic data determined can be applied for e.g. model-based product development and process optimization.

Acknowledgement

This thesis which is accomplished in the polymer reaction engineering research group of the natural sciences department II at the Martin-Luther-University of Halle-Wittenberg, would not have been possible without the help of many individuals. Here I would like to acknowledge all of them who have helped and supported me during my PhD studies.

First and foremost, I want to express my gratitude to Prof. Dr. Michael Bartke for offering me the opportunity to work in his research group, and for his constructive advice, fruitful discussions and his dedicated guidance and supervision. This work would not have been a possibility without his constant immediate help throughout the years.

I would like to thank Braskem industries for supporting this project financially and to realize the possibility of this research. I am grateful to our project partners at Braskem, including Dr. Craig Meverden, Dr. Gerd Lohse, and Dr. Fernando Da Silva Gomes, for their cooperation and their input from the industry point of view, and for organizing and leading the project. I would like to thank Mr. Robby Elsner and coworkers at Braskem laboratories for testing and analysis of the samples within the framework of this project, including DSC, bulk density, polymer fractionation, intrinsic viscosity and FTIR measurements.

I would like to thank all my colleagues at the polymer reaction engineering research group for their cooperation and support. I learned much from working together with Arkom Drawateep, Dr. Jorik Hill, and Dr. Joana Kettner at the polymerization lab. I would like to further thank our former colleague Dr. Thomas Kröner for his advice and contribution to our research.

I would like to thank Prof. Dr. Hahn and Dr. Jenny Bienias at the industrial chemistry department of Martin-Luther-University, for their help to conduct particle size distribution and porosity measurements.

I would like to thank Dr. Stephanie Krüger and Dr. habil. Gunther Tschuch at the evolution biology research group of Martin-Luther-University for their constant cooperation and for their great help to conduct electron microscopy measurements.

Specially I would like to dedicate this work to my beautiful wife M.Sc. Xinye Li for her endless love and support throughout the years of my master and PhD studies. Without her constant heartfelt dedication and wisdom no accomplishment would have been possible.

Table of Contents

| | | |
|---------|----------------------------------------------------------------|----|
| 1 | Introduction | 1 |
| 1.1 | Polypropylene markets and application | 1 |
| 1.2 | Polypropylene micro-structure and resin types | 1 |
| 1.3 | Processes for production of polypropylene | 4 |
| 1.3.1 | Bulk polymerization | 4 |
| 1.3.2 | Gas-phase polymerization..... | 6 |
| 2 | Theory and literature review | 8 |
| 2.1 | Catalysts for polymerization of olefins | 8 |
| 2.2 | Role of hydrogen..... | 10 |
| 2.3 | Role of pre-polymerization..... | 11 |
| 2.4 | Catalyst activation and pre-contacting..... | 12 |
| 2.5 | Lab scale study of olefin polymerization kinetics | 13 |
| 2.5.1 | Gas and slurry phase | 13 |
| 2.5.2 | Bulk phase | 14 |
| 2.6 | Calorimetric methods for studying polymerization kinetics..... | 14 |
| 2.6.1 | Isothermal calorimetry | 15 |
| 2.6.1.1 | Isothermal heat flow calorimetry | 16 |
| 2.6.1.2 | Isothermal heat balance calorimetry | 17 |
| 2.6.2 | Adiabatic calorimetry | 17 |
| 2.6.3 | Isoperibolic calorimetry..... | 18 |
| 2.6.4 | Power compensation calorimetry..... | 18 |
| 2.7 | Modeling coordinative polymerizations of olefins..... | 19 |
| 2.7.1 | Kinetic scheme..... | 20 |
| 2.7.2 | Meso-scale modeling | 22 |
| 2.8 | Phase equilibria in propylene polymerization..... | 24 |
| 2.8.1 | Vapor-liquid phase equilibria | 24 |
| 2.8.2 | Equilibrium between polymer and penetrant..... | 26 |

| | | |
|-------|--------------------------------------------------------------------|----|
| 2.8.3 | Sorption measurements | 28 |
| 3 | Objectives | 29 |
| 4 | Experimental setup and characterization methods | 30 |
| 4.1 | Polymerization setup | 30 |
| 4.1.1 | Raw materials supply | 31 |
| 4.1.2 | Polymerization reactor..... | 32 |
| 4.1.3 | Control unit..... | 33 |
| 4.1.4 | Gas chromatography setup | 34 |
| 4.1.5 | Software and data collection | 35 |
| 4.2 | Chemicals and catalysts – preparation and handling..... | 36 |
| 4.3 | Polymerization procedures | 38 |
| 4.3.1 | Reactor inertization | 38 |
| 4.3.2 | Homo-polymerization with in-situ pre-polymerization..... | 38 |
| 4.3.3 | Multi-stage impact copolymerization..... | 39 |
| 4.4 | Analysis of the power compensation calorimetry data | 40 |
| 4.4.1 | Raw data power compensation calorimetry | 41 |
| 4.4.2 | Estimation of the reactor heat losses..... | 42 |
| 4.4.3 | Change of filling level | 43 |
| 4.4.4 | Software sensor for online baseline-correction..... | 45 |
| 4.5 | Reaction conditions and experimental plan | 47 |
| 4.6 | Sample characterization | 48 |
| 4.6.1 | Melt mass flow rate indexer..... | 48 |
| 4.6.2 | Porosity measurement | 48 |
| 4.6.3 | Particle size distribution..... | 49 |
| 4.6.4 | Bulk density..... | 49 |
| 4.6.5 | Test of crystallinity..... | 49 |
| 4.6.6 | Microscopy..... | 50 |
| 4.6.7 | Polymer fractionation and measurement of intrinsic viscosity | 50 |

| | | |
|---------|----------------------------------------------------------------------------------------------------------------|-----|
| 4.6.8 | FTIR measurements..... | 50 |
| 5 | Experimental study of propylene polymerization kinetics, with two different Ziegler-Natta type catalysts | 50 |
| 5.1 | Performance of the calorimeter setup..... | 51 |
| 5.2 | Test of reproducibility | 53 |
| 5.3 | Hydrogen response | 56 |
| 5.4 | Influence of pre-contacting | 62 |
| 5.5 | Copolymerization experiments | 67 |
| 5.5.1 | Kinetic measurement principle | 67 |
| 5.5.2 | Establishment of reproducibility | 69 |
| 5.5.3 | Influence of comonomer composition | 71 |
| 5.5.4 | Product molecular weight | 73 |
| 5.6 | Characterization results..... | 78 |
| 5.6.1 | Determination of ethylene content with FTIR method | 79 |
| 5.6.2 | Porosimetry measurements..... | 80 |
| 5.6.3 | Particle size distribution..... | 81 |
| 5.6.4 | Bulk density..... | 83 |
| 5.6.5 | Microscopy..... | 85 |
| 5.6.6 | Determination of crystallinity..... | 88 |
| 6 | Phase equilibria and mass transfer | 89 |
| 6.1 | Vapor-liquid phase equilibria in bulk-phase propylene polymerization | 90 |
| 6.1.1 | Flash calculation procedure..... | 93 |
| 6.1.2 | Determination of liquid level in the reactor..... | 98 |
| 6.2 | Sorption equilibrium..... | 99 |
| 6.2.1 | Sorption balance setup..... | 100 |
| 6.2.2 | Sorption measurement procedure | 101 |
| 6.2.3 | Data interpretation..... | 101 |
| 6.2.3.1 | Effect of swelling..... | 103 |

| | | |
|-------|----------------------------------------------------------------|-----|
| 6.2.4 | Experimental plan | 104 |
| 6.2.5 | Solubility of gases in homo-polymer samples | 104 |
| 6.2.6 | Solubility of gases in copolymer samples | 111 |
| 6.2.7 | Concentration of reaction partners during polymerization | 113 |
| 7 | Kinetic modeling | 114 |
| 7.1 | Model assumptions | 115 |
| 7.2 | Kinetic scheme | 115 |
| 7.3 | Derivation of mass balances | 119 |
| 7.4 | Method of moments | 124 |
| 7.5 | Model implementation and parameter estimation | 128 |
| 7.6 | Model simulation results; hydrogen response | 132 |
| 7.7 | Model simulation results; pre-contact influence | 134 |
| 7.8 | Model simulation results; copolymerization kinetics | 136 |
| 8 | Summary | 142 |
| 9 | List of symbols | 145 |
| 10 | Appendix | 148 |
| | Appendix I | 148 |
| | Appendix II | 150 |
| | Appendix III | 151 |
| | References | 153 |
| | Curriculum vitae | 163 |
| | List of publications | 164 |
| | Eidesstattliche Erklärung | 165 |

1 Introduction

1.1 Polypropylene markets and application

In 2018, global plastics production reached almost 360 million tons. Polypropylene (PP) is one of the most important plastics in the market. Polypropylene belongs to polyolefins family, and with a production of approximately 70 million tons per year, shares around 19 percent of the market. The demand for this material has been growing with a growth rate of about 5%. Packaging, construction, automotive industry, and electronics represent the largest end-use markets. Polypropylene provides a wide range of products with various properties, such as PP films, containers, rigid caps, packaging parts, and fibers. Distribution of European plastics demand by resin type is displayed in figure 1 [1]:

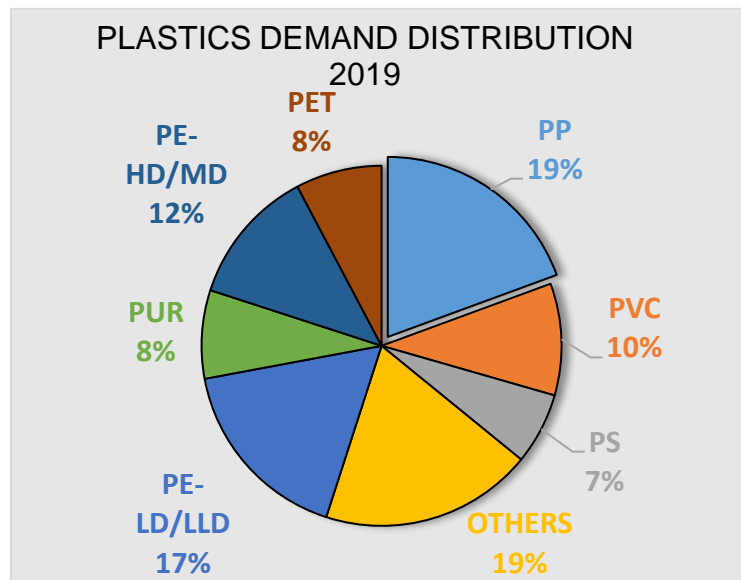


Figure 1. Plastics demand distribution in 2019

Some major polypropylene manufacturers can be named as [2]: China Petroleum & Chemical Corp. (Sinopec Corp.), LyondellBasell Industries N.V., Borealis AG, China National Petroleum Corporation (CNPC), Saudi Basic Industries Corp. (SABIC), Total S.A., Reliance Industries Ltd., China Energy Investment Corporation (China Energy), ExxonMobil Corporation, and Braskem S.A.

1.2 Polypropylene micro-structure and resin types

Polypropylene is a stereoregular polymer. A repeating unit of the polypropylene chain is shown in figure 2.

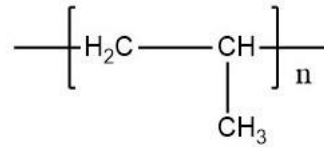


Figure 2. The repeating unit of polypropylene backbone

The repeating unit of polypropylene chain is asymmetrical and contains a chiral center. Since propylene is an asymmetrical molecule, polypropylene can be synthesized with different stereochemical configurations. Depending on the stereo-regularity of the chiral atom [3] in a chain, the chain's stereo-specificity can be categorized into three different types, as displayed in figure 3.

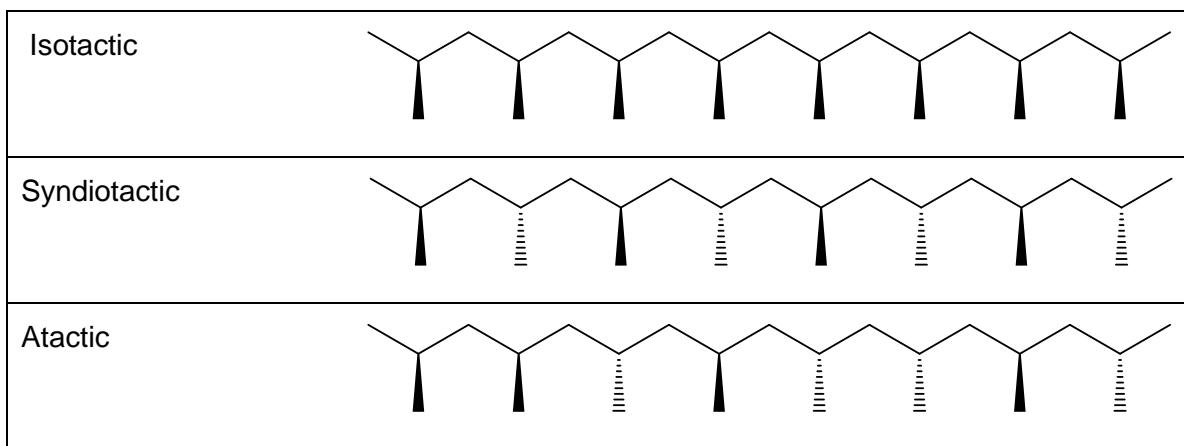


Figure 3. Three polypropylene configurations

- 1) **Isotactic:** where all the methyl groups are placed on one side of the chain. This allows the chains to line up next to one another to form a crystalline structure. The isotactic polypropylene has the highest share of the market among polypropylene stereoisomers, and is produced by modern transition metal catalysts (e.g. heterogeneous Ziegler-Natta, or metallocene catalysts) alongside a metal alkyl cocatalyst [4]. Isotactic polypropylene is characterized by the high crystallinity and a melting temperature of between 160-165 [°C] [5].
- 2) **Syndiotactic:** where the methyl groups are alternatively placed on the opposite sides of the chain. Syndiotactic polypropylene has the ability of crystallization as well, with a melting temperature of around 130 [°C]. Syndiotactic polypropylene can be produced with certain kinds of metallocene catalysts and has much less widespread commercial use [6].
- 3) **Atactic:** where the methyl groups are randomly placed on different sides of the chain following no specific order. The random positioning of the methyl groups prevents crystallization. Atactic polypropylene is an amorphous material (soft and sticky) and has little commercial value.

Tacticity significantly influences crystallinity of polypropylene [7], since Stereo defects disrupt the length of the crystallizable isotactic sequences. State of the art catalysts for PP manufacturing, result in a high fraction of iso-tactic material, with minor presence of atactic polymer.

In addition to tacticity, further important parameters of the PP chain, which influence the properties, include the molecular weight, polydispersity, and comonomer composition in case of copolymers. Factors such as production process (unimodal, or bimodal production), catalyst used, and polymerization reaction components such as hydrogen, that acts as the chain transfer agent can influence the molecular weight and the molecular weight distribution of the products. Polypropylene products, synthesized with multi-site heterogeneous Ziegler-Natta catalysts typically consist of a broad molecular weight distribution with polydispersity index of above 4 [8]. Whereas single-site catalysts such as metallocene catalysts result in a narrow molecular weight distribution and polydispersity of around 2 [9].

Commercial PP products have a weight average molecular weight of between 200 to 600 [kg/mol]. PP is a light weight material with densities between 900 to 920 [kg/m³] [4], Young modulus of between 1300 to 1800 [MPa], melting temperature of 162 to 168 °C, and glass transition temperature of 0°C [5].

Polypropylene materials can be categorized in three main types of resins:

Homo-polymer is the most widely used polypropylene material, herein the polymer backbone only consists of propylene monomers. Homo-polymers have properties such as good tensile strength and stiffness, high thermal stability, and good solvent resistance. However, the poor impact property of the isotactic polypropylene limits some of its applications [4,5].

Random copolymer are resins, in which a small ethylene content of typically below 7 [Mass%] is copolymerized with propylene. Random copolymers have better impact properties, higher clarity and lower melting temperature compared to homo-polypropylene. The random presence of ethylene species in polymer back bone acts as chain defects, resulting in lower criticizability [10].

Hetero-phasic impact copolymers (ICP) consist of a matrix-material (either homo-polypropylene or random copolymer) and an elastomeric ethylene-rich copolymer, which is not miscible with the matrix material and acts as impact modifier. In industrial practice, these resins are produced in at least two reactors in series. In the first reactor, the matrix is generated, and in a subsequent gas-phase reactor the rubber phase copolymer is produced and dispersed in the matrix material. An advantage of this type of resin is the high low-temperature impact strength. One important parameter of these kind of products is the rubber content, which means the amount of elastomeric ethylene/propylene copolymer related to the amount of the

product. High impact copolymers typically have a rubber content of up to 40 [Mass%], and the rubber phase copolymer has typically ethylene compositions between 20 to 60 [Mass%]. An increase in rubber content of the ICP product results in higher impact resistance, however this is at the expense of the stiffness (flexural modulus) of the product. Furthermore, high-impact polypropylene copolymers display high thermal stability and improved blush resistance [5,11,12]. Applications of this type of resin can be found in the fields of packaging and automotive industry as bumper material.

1.3 Processes for production of polypropylene

In early examples of PP production processes (introduced by Montecatini), polymerization was carried out in a diluent. Slurry processes use a diluent ($C_3H_8-C_6H_{14}$) that is a nonsolvent for crystalline polyolefins to suspend the crystalline polymer particles and to dissolve the amorphous fraction. The process would operate in semi-batch mode, where the monomer would be added to a mixture of the diluent and catalyst and the rest of the chemicals required. Subsequently the catalyst would be deactivated with alcohol, and removed from the diluent, by means of treatment with water. Continuous modes of operation in slurry process were introduced as the demand for PP increased, however, the slurry processes posed several disadvantages, namely, requirement for the purification, removal, and recycling of the solvent, likelihood of significant reactor fouling due to dissolving of amorphous polymer in the diluent, and limitation in the range of available products. Eventually this process was replaced by more advanced technologies [13].

There are several industrial processes for production of polypropylene. The more recent and prominent processes are, gas-phase and bulk-phase polymerization, herein polymerization is carried out either in gaseous or liquid monomer. These processes are more cost effective, higher polymerization rates are achieved, and a broader range of products is available. Bulk-phase polymerizations are typically carried out in loop reactors or autoclaves and gas-phase polymerizations are conducted in fluidized bed or stirred bed reactors. For production of different PP resins such as hetero-phasic impact copolymers, various configurations of these reactors in hybrid processes are developed by PP manufacturers [14].

1.3.1 Bulk polymerization

In bulk process, propylene is polymerized in an environment of liquid pool of propylene acting both as slurry media and monomer. This is an improvement compared to the traditional slurry

polymerizations, since propylene can be separated from the polymer by flashing, and hence an extensive diluent recovery is no longer required. A further advantage of the bulk process is the high monomer concentration compared to the slurry and gas-phase processes, which leads to a higher reaction rate and polymerization yield. Furthermore, liquid propylene provides a more efficient heat removal capability compared to the gas-phase polymerization [14]. The pressure in bulk polymerization processes is always above propylene saturation pressure, varying from about 26 [bar] at 60 [°C], and up to 38 [bar] at 80 [°C]. Typical hybrid industrial processes consist of a bulk-phase stage for production of homo-polymer or random copolymer matrix, and based on the product required, a subsequent gas phase stage for copolymerization with ethylene.

A major industrial bulk-phase polymerization process is the Spheripol™ process by LyondellBasell. In the Spheripol™ technology, a small loop reactor is used to carry out pre-polymerization at mild conditions, subsequently the main polymerization (either homo-polymer or random copolymer) is carried out in one or two loop reactors. In case, hetero-phasic impact copolymers are targeted, an additional fluidized bed reactor (FBR) for subsequent gas-phase copolymerization might be added to the process setup. For impact modification a gas-phase reactor is used, due to lower solubility of ethylene in liquid propylene as well as possibility of dissolution of rubber phase copolymer in liquid propylene. A high-temperature flash separation is included between the liquid and gas phase sections of the hybrid process to transition to gas-phase operation condition and remove the excess hydrogen in the reactor. A simple schematic view of the Spheripol™ process is presented in figure 4 [15].

A competing technology is the Hypol™ process by Mitsui. First-generation Hypol™ technology is a hybrid process, which uses a bulk stirred tank reactor for the first stage and a gas phase stirred bed reactor for the second stage. In the second-generation Hypol™ II units, a bulk loop reactor is used for the first stage. In either case, homo-polymer or random copolymer matrix is made in bulk-phase polymerization, and impact copolymers are subsequently manufactured in the second stage, gas-phase stirred bed reactor [16].

A further example of a bulk-phase polymerization process is the Borstar™ technology by Borealis. This process consists of a loop reactor, followed by one or two fluidized bed reactors for production of homo-polymer or random copolymer matrix and depending on the type of product required, one or two additional fluidized bed reactors connected in series for impact copolymerization. Even though the process setup looks similar to Spheripol™ process, one distinct difference of the Borstar process to Spheripol™ process is that, in the first gas-phase reactor, matrix material is produced as well, which offers good opportunities for a bimodal molecular weight distribution of the matrix material.

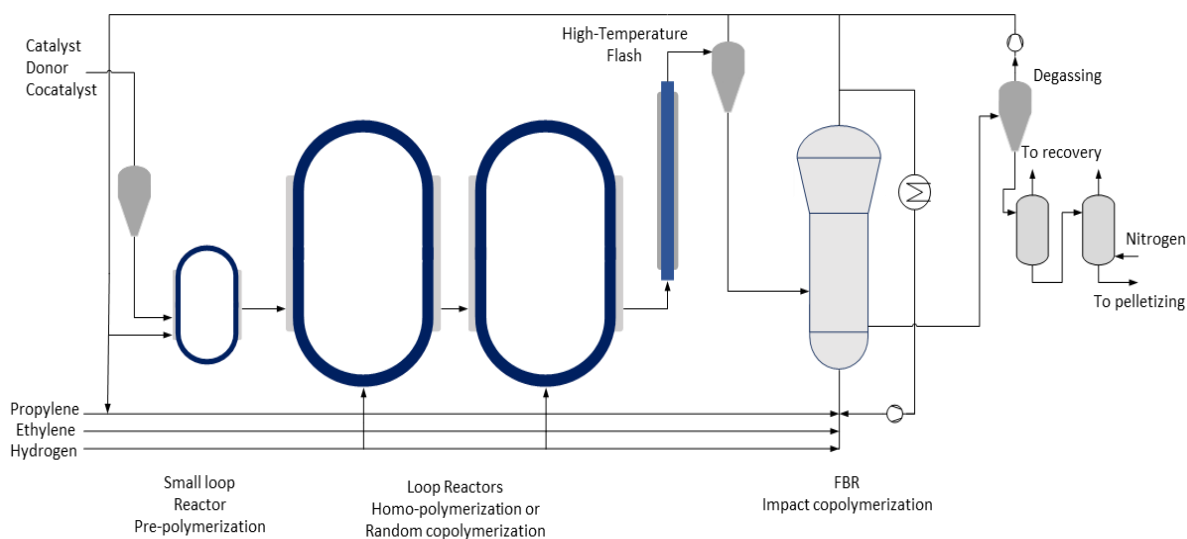


Figure 4. The Spheripol™ process

1.3.2 Gas-phase polymerization

The gas phase polypropylene production technologies have simpler configuration and are more cost and energy efficient, compared to slurry and bulk processes. In gas phase operation, separation of polymer and the unreacted propylene is easier, and diluent recovery step or flashing of liquid propylene in case of bulk phase operation is eliminated. A drawback of operation in the gas phase, is the limited heat transfer ability compared to liquid phase. A common solution in fluidized bed reactors is the condensed cooling method, in which recycled monomer in liquid form is fed to the reactor, and polymerization heat is removed by evaporation of the liquid feed upon entering the reactor [17].

An example of a gas-phase polypropylene production process is the Novolen™ technology (originally developed by BASF), which includes one or two vertical stirred bed reactors, operating in gas phase at pressures above 20 [bar] and temperatures between 70 [°C] and 90 [°C]. In this process uniformity of the reaction conditions is achieved by agitation rather than bed fluidization. This technology deploys condensed mode cooling with flash evaporation of liquified reactor gas, mixed with fresh feed. The two reactors can be operated in parallel or cascade for production of homo-polymer or random copolymers, and if impact copolymers is targeted, the reactors are operated in cascade mode, wherein the first reactor is used to produce the matrix polymer and the rubber phase copolymer is manufactured subsequently in the second reactor [18].

Unipol™ process, originally developed by Union Carbide for gas-phase polymerization of ethylene, was deployed for polypropylene production since 1980's. This process includes a large, fluidized bed reactor that operates at pressures between 25 to 30 [bar] and temperatures between 60 [°C] to 70 [°C], for production of homo-polymer and random copolymer. A smaller fluidized bed reactor is deployed in series for impact copolymerization [19].

LyondellBasell has introduced the Spherizone™ process. In the Spherizone™ process, the matrix material is produced in a special type of circulating bed reactor with two reaction zones. The growing polymer particles are circulated between the two different zones of the reactor with separate polymerization conditions. This development broadens the range of available products [20].

Further examples of gas-phase processes are Inovene process by Ineos and the Horizone™ process by Japan propylene corporation, which deploy two stirred powder bed reactors, that can be operated in parallel or cascade mode, where in parallel mode both reactors produce homo-polymer or random copolymer, and in cascade mode the second reactor is used for impact copolymerization.

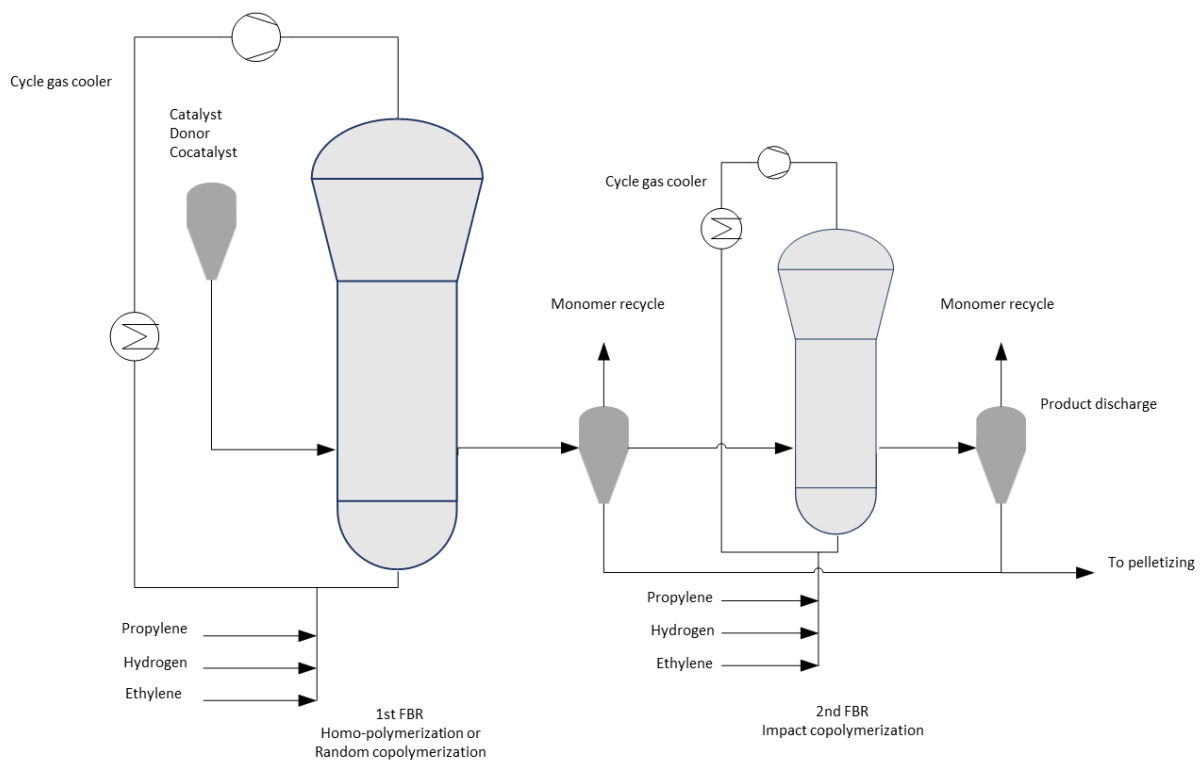


Figure 5. The Unipol process

2 Theory and literature review

2.1 Catalysts for polymerization of olefins

Commercial production of polyolefins is mainly carried out by catalytic coordinative polymerization, with the exception of low-density polyethylene which is produced by high pressure radical polymerization. Catalytic polymerization enables the reaction to be operated at relatively mild conditions ($T=70-100$ [°C], $P=20-40$ [bar]). There are four major families of catalysts for olefin polymerization, namely Ziegler–Natta, Phillips, metallocene and late-transition metal catalysts.

Phillips catalysts, which were developed in the 1950s, are based on chromium oxide, and are still widely used in the industry for production of high density polyethylene [14].

The Ziegler-Natta (ZN) catalyst was developed following the discovery made by Karl Ziegler in 1953, that a transition metal compound based on titanium was capable of polymerizing ethylene molecules [21]. Natta successfully produced polypropylene using a similar catalyst with a tacticity of up to 90%, with the catalyst system including $TiCl_3$ and Aluminum alkyl compound as a cocatalyst. Ziegler-Natta catalyst is defined as a transition metal compound (typically halide) of metal groups IV to VIII, paired with a metal alkyl of the groups I to III, typically aluminum alkyl compounds such as trimethyl aluminum (TMA), triethyl aluminum (TEA), or diethyl aluminum chloride (DEAC) as cocatalyst. The cocatalyst activates the catalyst by reduction and alkylation of the transition metal, forming an active metal-carbon bond, that enables the system, to carry out repeating insertions of olefin molecules.

Ziegler-Natta catalysts can be either heterogeneous or homogeneous [22]. Heterogeneous ZN catalysts are typically supported by magnesium chloride ($MgCl_2$) or silica (SiO_2). Homogeneous ZN catalysts are generally vanadium based and are mostly used for production of ethylene-propylene-diene elastomers (EPDM).

Heterogeneous (supported) ZN catalysts are multi-site catalysts, which contain several types of active centers, and since various centers differ in their kinetic response, the polymer product consists of a mixture of fractions each produced by a different type of active center. presence of multiple types of active sites, leads to a broad molecular weight distribution with poly dispersity indexes of typically between 3 to 10 [23–25].

Since the discovery, multiple generations of Ziegler-Natta type catalysts have been developed, and various aspects of the catalyst performance such as achieving higher activities, higher stereo-selectivity, as well as better control of polymer morphology have been improved.

What is generally known as the first generation of commercial ZN catalyst, included aluminum reduced and activated TiCl_3 compound alongside DEAC as the cocatalyst. The first generation of ZN catalyst had a typical productivity of about 1 $[\text{kg}_{\text{Polymer}}/\text{g}_{\text{cat}}]$, with an iso-tactic index of 90%, and required removal of atactic polymer fraction and catalyst residue from the product [26].

The second generation of ZN catalysts was introduced by Solvay with addition of a Lewis base (di-isoamyl ether) into the catalyst system. This catalyst had a higher surface area and yielded five times the productivity compared to the first generation. The Solvay catalyst resulted in tacticity index of about 95% [27].

In the third generation of ZN catalyst, the TiCl_4 compound was immobilized on activated MgCl_2 support material. For stereoregularity, a Lewis base was added to the catalyst system (internal donor), typically ethyl benzoate. The internal donor plays its role during the preparation of the catalyst, it competes with TiCl_4 for coordination to the MgCl_2 support [28]. Incorporation of the support material has the effect of increasing the number of active species throughout polymerization, which can be explained in terms of a high dispersion of the active titanium species on the large surface of MgCl_2 support [23]. In this system alongside catalyst and cocatalyst, an additional external donor (typically Methyl p-toluate) is introduced to the reaction environment. Electron donors tend to coordinate to non-stereospecific catalyst sites, and thus increase overall tacticity of the product, resulting in productivities between 15 to 30 $[\text{kg}_{\text{Polymer}}/\text{g}_{\text{cat}}]$ and iso-tacticity index of 90-95%.

Further research led to development of the fourth generation of ZN catalyst in the 1980's, which included alkyl phthalates as internal donor and alkoxy silane as external donors. Phthalate catalysts offered a better productivity/stereo-regularity balance compared to benzoic acid esters, and to this day are widely used for production of polypropylene, with higher productivity of 30-60 $[\text{kg}_{\text{Polymer}}/\text{g}_{\text{cat}}]$ and iso-tacticity index of 95-99% [29].

The fifth generation of ZN catalysts were developed by introduction of diethers or aliphatic ester (succinate) [30] as internal donors, resulting in extremely high catalyst activity and stereo-regularity without the need for addition of external electron donors to the system [31].

A further development in catalyst research in polyolefin industry is the use of the metallocene catalysts for olefin polymerization. Metallocene catalysts are generally transition metals of group IV (elements such as Ti, Zr and Hf) coordinated with two organic ligands (typically cyclopentadienyl or cyclopentadienyl-derivative) in a sandwich-like molecular structure [32].

Kaminsky and Sinn discovered methylaluminoxane (MAO) to be a suitable co-catalyst to activate and stabilize the metallocene precursors [33]. As opposed to ZN catalysts,

metallocene catalysts are single site catalysts, which under stable polymerization conditions result in polymers with uniform properties, chemical composition, and narrow molecular weight distribution (PDI~2). While metallocene-catalysts are commercially used for production of polyethylene to some extent, for commercial production of polypropylene, metallocens are practically not used. One reason for this are the high costs for syntheses of bridged metallocene complexes needed for polymerization of isotactic polypropylene. [9,34]

2.2 Role of hydrogen

Hydrogen is commonly used as the chain transfer agent in industrial practice to control the product molecular weight in olefin polymerizations [35–37]. Moreover, hydrogen enhances catalyst activity in propylene polymerizations. Hydrogen response in catalytic polymerizations of propylene has been investigated in several studies, as an example, Guastlla investigated the influence of hydrogen on polymerization kinetics of propylene using supported Ziegler-Natta catalysts, and reported an increase of activity by 150% caused by the presence of hydrogen [38]. A similar type of response has been reported in other references as well [39–44], however in case of ethylene polymerizations, hydrogen presence leads to a decline in activity [45].

A reported hypothesis for explaining the activation influence of hydrogen on propylene polymerizations is the dormant site reactivation theory. A propylene molecule can be inserted to a growing polymer chain either via regio-regular 1,2 insertion, or regio-irregular 2,1 mis-insertion displayed in the following figure 6 [36]. The 2,1 mis-insertion of propylene to the active titanium-carbon bond, forms a dormant chain. Due to the steric hindrance caused by the methyl group adjacent to the titanium center, dormant chains are non-reactive to further propagation. This dormant chain, however, can be reactivated by reacting with a small molecule such as hydrogen, ending the polymer chain, and hence releasing a vacant active site that can in turn react with other monomer molecules. Reactivation of dormant sites by hydrogen leads to a higher concentration of active sites throughout polymerization, which explains the activation effect of hydrogen. Soares reported that the hydrogen influence is reversible [40], meaning that removing hydrogen from the polymerization environment leads to a drop, in catalyst activity, and with reintroduction of hydrogen, the catalyst activity increases once again. This reversibility is in-line with the dormant site activation theory.

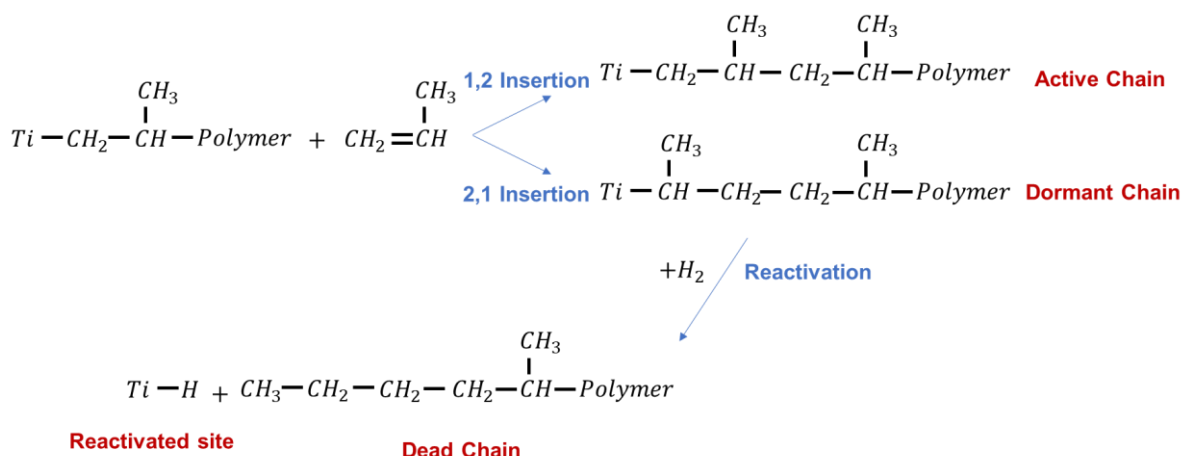


Figure 6. Hydrogen effect; The dormant site theory

2.3 Role of pre-polymerization

A challenge associated with highly active coordination catalysts is heat removal from the catalyst particles. When catalysts are injected into a polymerization reactor at temperatures between 60 to 80 [°C], the catalyst is activated very fast and reaches a high initial polymerization rate, which due to the exothermic nature of the polymerization reaction, generates a significant chemical heat flux (the formation enthalpy of polypropylene in liquid propene is $\Delta H_f = -84$ [kJ/mol]). This chemical heat flux at the initial stages of polymerization can cause thermal deactivation of the catalyst active sites and lead to an overall decline of the catalyst activity. Furthermore, the high initial polymerization rate can adversely influence the polymer particle morphology, and lead to production of fine powder, which can cause fouling or plugging in process setup.

A common solution to this challenge is deployment of a pre-polymerization stage in the production process. Pre-polymerization refers to starting the polymerization in mild conditions, wherein the catalyst is injected at lower temperature (close to room temperature). In industrial practice, pre-polymerization is carried out in a separate smaller reactor, prior to the main polymerization reactor. In lab-scale studies, the pre-polymerization can be carried out in the same reactor (in-situ pre-polymerization) by injecting the catalyst at lower temperature (10-25 [°C]), and after a certain duration of pre-polymerization the reactor is heated up to the main polymerization reaction temperature (60 to 80 [°C]).

At pre-polymerization stage, the catalyst/polymer particles grow in size to a certain extent in mild conditions, providing a larger heat transfer area for the particles at the main polymerization stage. This improves the heat removal ability from the polymerization active centers and helps avoiding the thermal deactivation. As a result, higher overall catalyst activity is achieved in the

main polymerization stage. In addition to the influence on catalyst activity, since the fragmentation of catalyst particles occur in a more controlled manner, the pre-polymerization can improve the particle morphology and reduce the final fraction of fine powder in the product [46–48].

Influence of pre-polymerization on catalyst activity has been studied by several researchers [47,49,50]. Samson reported an increase in polymerization activity of liquid propylene by 30% with carrying out the pre-polymerization prior to the main polymerization. Pater investigated the influence of pre-polymerization on the resulting particle morphology in bulk phase propylene polymerization [47].

It must be added that factors like pre-polymerization temperature and duration can play a crucial role on the degree of pre-polymerization (pre-polymer mass produced per mass of catalyst), and thus influence the main polymerization reaction kinetics. Kettner studied the polymerization kinetics of a metallocene catalyst in liquid propylene and reported an optimum pre-polymerization degree for the catalyst used [51].

2.4 Catalyst activation and pre-contacting

Valance state of titanium plays a significant role in polymerization kinetics of Ziegler-Nata catalysts. Before any reaction titanium is originally at state Ti^{4+} . It was reported by Ray that the titanium valance state is reduced to Ti^{3+} in an instantaneous reaction with cocatalyst (in this case TEA):



The active species for propylene polymerization is Ti^{3+} , therefore reduction of titanium from the original state by cocatalyst is necessary for catalyst activation [52,53]. Shimizu reported [54] that in order to activate the Ziegler-Natta catalyst for propylene polymerization, the catalyst needed to be treated with TEA prior to polymerization and introduction to monomer. Shimizu observed that pre-treatment with TEA is necessary for catalyst activation, and without treatment, polymerization rate significantly diminishes. Valance state of titanium can be further reduced to Ti^{2+} by TEA.



It was reported by Ray that further reduction of titanium to Ti^{2+} is not instantaneous. it is known that the Ti^{2+} species is not active for polymerization of propylene [55], and thus over reduction of Titanium to Ti^{2+} can adversely influence polymerization rate. Ray reported that catalyst aging

(contact between TEA and catalyst before polymerization at room temperature and without agitation) for durations up to 90 minutes will lead to a decline in polymerization rate of bulk propylene, that can be explained by over reduction titanium centers to Ti^{2+} . Contradicting results about pre-contacting have been reported in literature. Jose reported that pre-contacting adversely influenced activity of Ziegler-Natta catalyst in gas phase propylene polymerizations [56]. Jose indicated that despite having lower overall productivity, polymerizations with pre-contacting display higher initial activity. This might be due to the activation of a larger number of catalyst sites in pre-contacting step. Jose suggested that the more gradual nature of catalyst activation in polymerizations without any pre-contacting might help avoid the thermal deactivation of catalyst active centers in initial stages of polymerization. As opposed to aforementioned publications, Raissi's research [57] indicated that pre-contacting did not have a notable influence on polymerization kinetics of propylene using Ziegler-Natta catalyst. Aigner on the other hand reported an optimal pre-contact time for polymerization of ethylene using Ziegler Natta catalyst [58], where it was observed that polymerization activity of the Ziegler-Natta catalyst increases with an optimal pre-contact duration and by longer pre-contacting durations the polymerization rate is adversely influenced. These results were explained by modeling the mass transfer of TEA in catalyst particles and reaching the optimum TEA concentrations. Tan reported that pre-contacting enhances the polymerization rate of Ziegler-Natta catalysts in bulk polymerization of propylene [59], however in the study, experiments with or without pre-contacting were investigated and duration of pre-contacting was not varied. Polymerization process can be of importance in this regard as well, for example in industrial practice in gas-phase propylene polymerization processes such as Innovene™ and Unipol™ the catalyst is introduced to the reaction environment without any pre-contacting, whereas in bulk-phase polymerization such as Spheripol™ and Borstar™ process, catalyst and cocatalyst are contacted before polymerization. It appears that each catalyst system might react differently towards pre-contacting. This can be due to the mass transfer differences among different catalysts, or the activation behavior of the catalyst according to its chemical nature, therefore for new catalyst systems studying the activation behavior of the catalyst is relevant.

2.5 Lab scale study of olefin polymerization kinetics

2.5.1 Gas and slurry phase

For lab scale studies of gas-phase olefin polymerizations, reaction kinetics can be obtained by semi-batch operation of the reactor and feeding monomer in a pressure control-loop at isothermal and iso-baric conditions. Many researchers have studied kinetics of propylene polymerization in gas-phase [50,60–64]. Choi and Ray investigated the kinetics of gas-phase

propylene polymerizations using Ziegler-Natta catalysts and studied the influence of reaction temperature on reaction kinetics and product properties. Meier used the polymerization rate curves obtained by semi-batch operation of reactor in gas phase to develop a reaction kinetics model. Kettner studied the influencing factors such as hydrogen concentration and reaction temperature on the behavior of various Ziegler-Natta catalysts in gas-phase polymerizations of propylene [63]. A similar experimental approach has been used by authors in order to investigate the kinetics of propylene/ethylene copolymerization in gas-phase; Kröner studied the copolymerization kinetics using Ziegler-Natta catalysts and developed a combined mass-transport and reaction kinetics model [65]. Debling and Ray [66] investigated the hetero-phasic copolymerization kinetics of propylene and ethylene system, and focused on the morphological development of the resulting product. Kinetics of olefin polymerizations in slurry phase can be studied with the outlined methodology as well. References [67–70] are notable examples of kinetic study of olefin polymerization in slurry phase.

2.5.2 Bulk phase

In case of bulk-phase polymerization, the approach described for gas-phase polymerizations is not feasible, and the reactor is often operated in batch mode, hence extraction of reaction rate information from mass flow of reactants into the reactor is not possible. Often the only kinetic information obtained from an experiment in batch mode bulk propene polymerizations is the polymerization yield obtained by weighing of the polymer product [71–73]. Reaction dilatometry has been used for kinetic studies of olefin polymerization. As an example, Al-haj deployed reaction dilatometry in a fully filled (with liquid propylene) reactor, to study polymerization kinetics of bulk phase propylene [39]. Another example of a similar method is the work of Patzlaff, that investigated the polymerization kinetics of liquid propylene mixed with pentane in a partially filled reactor by tracking the pressure drop in the reactor due to consumption of propylene throughout the polymerization [74]. Various calorimetric methods have been developed to study kinetics of olefin polymerization reactions. In the following sections different types of reaction calorimetry setups and various modes of operation are reviewed.

2.6 Calorimetric methods for studying polymerization kinetics

Reaction calorimetry is a well-established method for studying kinetics of chemical reactions by means of thermal analysis. Numerous reaction calorimetry modes and methods are

available in published literature. Calorimetry methods can be categorized based on the heat flow measurement principle, and temperature control mode.

In general terms, the heat released by an exothermal polymerization reaction, is proportional to the polymerization rate and is described as:

$$\dot{Q}_{chem} = R_p V_R (-\Delta H_f) \quad 2.1$$

The reaction heat release is represented as \dot{Q}_{chem} [W], R_p is the polymerization rate, V_R is the reaction volume, and ΔH_f [W] is the reaction enthalpy. The global expanded heat balance for a reaction calorimeter can be written as [75]:

$$\dot{Q}_{acc} = \dot{Q}_{chem} + P + \dot{Q}_{stirr} + \dot{Q}_{mix} + \dot{Q}_{phase} + \dot{Q}_{dos} - \dot{Q}_{jacket} - \dot{Q}_{loss} \quad 2.2$$

Where \dot{Q}_{acc} [W] is accumulated heat in the setup, P [W] is the heat flow by an internal heater (calibration probe or compensation heater), \dot{Q}_{stirr} [W] is the heat generated by stirring, \dot{Q}_{mix} [W] is the heat exchange due to possible mixing of different fluids, \dot{Q}_{phase} [W] is the heat exchange caused by possible materials phase change in the reactor, \dot{Q}_{dos} [W] is the heat released or absorbed by dosing of materials in to the reactor during the course of the reaction, \dot{Q}_{jacket} [W] is the heat flow from the reactor content to the jacket, and \dot{Q}_{loss} [W] is the heat loss to the environment. Based on the reaction conditions, reactant materials and the operating mode of a reaction calorimeter, various terms from equation 2.2 can be eliminated and the heat balance can be simplified.

2.6.1 Isothermal calorimetry

An isothermal reaction calorimeter setup maintains the reactor temperature at a constant value throughout the chemical reaction and measures the chemical heat flow. Isothermal calorimetry has the advantage of defined and controlled reaction conditions. Many physical and kinetical parameters and properties in a polymerization reaction are temperature dependent, therefore an isothermal operation is desirable. For isothermal calorimetry two methods are known, isothermal heat flow calorimetry and isothermal heat balance calorimetry [76]. The main distinction among these two methods is the measurement principle. In the heat flow calorimeter, the energy balance is based on the heat flow through the reactor wall to the jacket measured by the temperature difference in between reactor and jacket. In contrast, in the heat balance method, the energy balance is based on the heat transfer to the reactor jacket measured by the temperature difference of the thermostating liquid throughout the jacket.

2.6.1.1 Isothermal heat flow calorimetry

When implementing the heat flow measurement principle, the heat flow to the jacket at any given moment of the reaction must be estimated. The simplified heat balance (ignoring heat of stirring) at the heat flow calorimeter is as follows:

$$\dot{Q}_{chem} = k_l A (T_r - T_j) + \dot{Q}_{loss} \quad 2.3$$

Where k_l is the heat transfer coefficient and needs to be estimated by performing calibration experiments. k_l strongly depends on properties of the reaction mixture (such as temperature, viscosity, etc.) [77], and stirring conditions (such as stirrer type and rpm) [78–80]. “ A ” denotes the heat transfer area of the reactor, T_r is the reactor temperature, and T_j is the average jacket temperature. It must be noted that in this mode of operation the heat accumulation in the jacket coolant must be negligible and the temperature difference between jacket coolant inlet and outlet streams is maintained typically below 0.1 [°C].

While operating isothermal heat flow calorimetry, to estimate the heat flow to the jacket, and thus determine the chemical heat release (\dot{Q}_{chem}), it is essential to have an estimation of the values of ($k_l A$). A further challenge is that $k_l A$ might change during reaction, e.g. due to worsening of heat transfer condition, e.g. via increase of solids content, increase of viscosity, decrease of filling level and so on. Therefore, calibration experiments are required, in which a known constant energy is given to the system by a calibration heater for a defined period in absence of chemical reactions. Changes in reactor filling level, i.e. effective heat exchange area during batch reactions, due to reactant conversion must be considered.

Samson introduced an isothermal heat flow calorimeter for studying bulk propylene polymerization kinetics, wherein the reactor temperature was controlled by means of using two thermostats; one for cooling and one for heating the jacket fluid, connected with a PID controller [81]. The same reactor setup was deployed by Pater [47] to study the influence of temperature, hydrogen and monomer concentration and pre-polymerization method on polymerization kinetics of propene. Use of an isothermal heat flow calorimeter for investigation of the propylene slurry and bulk-phase polymerization with a silica-supported metallocene/MAO catalyst has been reported by Korber [82]. Tisse presented a heat flow reaction calorimeter to study slurry-phase polymerizations of ethylene using different types of supported catalysts [76].

2.6.1.2 Isothermal heat balance calorimetry

The simplified heat balance of a heat balance calorimeter setup at steady state conditions is given as:

$$\dot{Q}_{chem} = \dot{m}_j C_{p_j} (T_{jin} - T_{jout}) + \dot{Q}_{loss} \quad 2.4$$

Where \dot{m}_j is the mass flow of the coolant in the jacket, C_{p_j} is the heat capacity of the jacket coolant, and T_{jin} , T_{jout} are the inlet and outlet temperatures of the coolant. As seen in equation 2.4, the heat balance is established on the reactor jacket coolant. This is a distinction between the heat balance calorimeter and a heat flow calorimeter outlined in previous section. One advantage of heat balance calorimetry is that the term $k_l A$, which might change during a reaction, is not needed for analysis of the measurements. On the other hand, to have a good sensitivity of heat balance calorimetry, for lab-scale reactors, often the coolant flux must be reduced compared to heat flow calorimetry, which in turn reduces the heat removal capacity via the jacket. Hence heat balance calorimetry is more suitable for larger reactors where the difference between the inlet and outlet jacket temperatures is significant. An example of a heat balance calorimeter was developed by Lahti [77] and used for studying kinetics of ethylene polymerizations in slurry phase. In this operating method, it is essential to determine the heat capacity, and the mass flow of the jacket coolant.

2.6.2 Adiabatic calorimetry

An adiabatic calorimeter consists of an insulated vessel, where the reaction takes place, and the reaction heat release is measured by means of monitoring the changes in temperature of the vessel. The heat balance can be written as [83]:

$$\dot{Q}_{chem} = m_r C_{p_r} \frac{dT_r}{dt} \quad 2.5$$

Where m_r is the mass of the reactor content, C_{p_r} is the heat capacity of the reactor content, and $\frac{dT_r}{dt}$ indicates the changes in temperature. Herein the system is not in isothermal condition and temperature dependent kinetic parameters are thus influenced. A further challenge while operating an adiabatic calorimeter is that, the changes in temperature can be significant for a highly exothermic reaction such as polymerizations, which might pose a process safety concern [84]. An adiabatic calorimeter was used by Ali El Haj [85] to study bulk propylene polymerization kinetics.

2.6.3 Isoperibolic calorimetry

In isoperibolic calorimeters the jacket temperature is kept at a certain constant value, therefore when an exothermic reaction takes place, the reactor temperature will rise. The heat balance for a reactor operating in isoperibolic mode can be written as:

$$\dot{Q}_{chem} = m_r C p_r \frac{dT_r}{dt} + k_l A (T_r - T_j) + \dot{Q}_{loss} \quad 2.6$$

It is essential for this mode of operation to have an estimation of the values of k_l and $C p_r$, which can change during the course of a non-isothermal polymerization reaction, due to the reaction heat release and temperature change. This method has been used to study kinetics of bulk propylene polymerizations and the hydrogen response by Ali El Haj [39].

2.6.4 Power compensation calorimetry

A power compensation calorimeter setup consists of an internal electrical heater submerged in the contents of a reactor paired with an external cooler. The jacket temperature is always kept at a constant value, a few degrees below the reactor temperature. Hence, there is a heat flow from the reactor to the jacket. If no reaction takes place, this heat flow to the jacket is compensated by the power dissipated from the electrical heating element to maintain isothermal condition. Once an exothermal reaction such as polymerization takes place, less electrical power is needed by the compensation heater, in order to keep the reactor in thermal equilibrium. The heat flow released by the exothermal chemical reaction is basically accessible by the difference of the compensation power needed with and without chemical reaction. The heat balance in isothermal conditions can be written as the following [80,86]:

$$P + \dot{Q}_{chem} = \dot{Q}_{jacket} + \dot{Q}_{loss} = k_l A (T_r - T_j) + \dot{Q}_{loss} \quad 2.7$$

Wherein \dot{Q}_{chem} represents the heat generated by the polymerization reaction, the energy provided by the electrical heater is P , and the heat flow to the jacket (\dot{Q}_{jacket}) is equal to the term " $k_l A (T_r - T_j)$ ". where k_l is the heat transfer coefficient, A represents the heat transfer area, $(T_r - T_j)$ is the temperature difference between the reactor content and the jacket, and \dot{Q}_{loss} is the heat loss. In case of a bulk propylene polymerization process liquid propylene has a low viscosity, and since there is nearly no change in viscosity, \dot{Q}_{stirr} is at a constant negligible value, therefore the chemical heat flow is derived as:

$$\dot{Q}_{chem} = \dot{Q}_{jacket} - P + \dot{Q}_{loss} = k_l A (T_r - T_j) - P + k_{loss} (T_r - T_{amb}) \quad 2.8$$

An early example of this type of calorimetry being put to use was presented by Andersen [68,87] where a reaction calorimeter equipped with an internal compensation heater was used to study the kinetics of emulsion polymerizations of styrene. Dobre used a power compensation calorimeter to study kinetics of emulsion polymerization of a sugar monomer [88]. A power compensation calorimeter equipped with a cooling peltier element has been deployed by Zogg [89] to study kinetics of chemical reactions, and Schlegel reported the use of a power compensation calorimeter for kinetic study of styrene polymerizations, the setup proved instrumental in keeping the operation strictly isothermal [80].

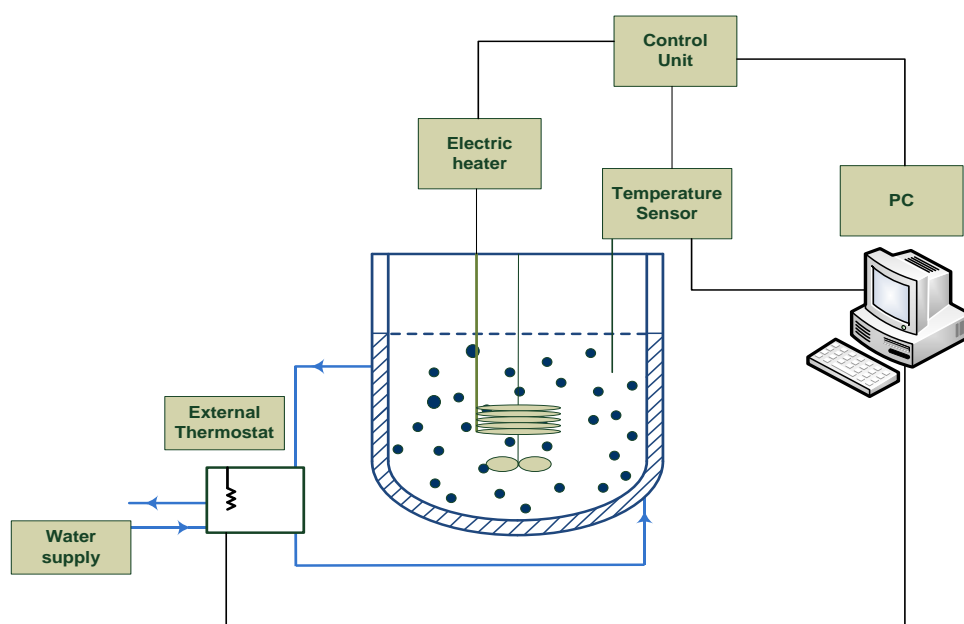


Figure 7. A schematic presentation of a power compensation calorimeter setup

2.7 Modeling coordinative polymerizations of olefins

Coordination polymerization of olefins through Ziegler-Natta catalysts is a complex phenomenon and various approaches have been introduced towards modeling the polymerization kinetics. In published literature this problem has been treated in different length scales:

- I) Macro-scale
- II) Meso-scale
- III) Micro-scale

In macro-scale, (above 1 meter) phenomena such as the reactor hydrodynamics, product particle size distribution, and reactor residence time distribution are studied. As an example Debling modeled product molecular weight grade transition in loop and fluidized bed reactors producing propylene homo-polymer and copolymers [90]. Zacca studied the kinetics of liquid propylene polymerization in loop reactors and in macroscale, focused on the concentrations of monomer in different positions in the loop reactor as well as particle velocity profiles and effect of recycle ratios on the reactor performance [91]. Work of Yiannoulakis [92] is another example of macroscale modeling wherein the authors focused on the dynamic modeling of the molecular weight and long chain branching distributions in a continuous solution metallocene-catalyzed ethylene polymerization reactor. Matos [93] proposed a simple kinetics scheme for polymerization of bulk propylene, and the model was used to predict the effect of hydrogen concentration in reaction medium on reaction rate constants. Luo modeled the bulk propylene production in Hypol technology by using a multisite approach, and appeared to successfully model the molecular weight distribution of plant product data [94]. Khare presented a dynamic model for continuous gas phase production of propylene homo-polymer as well as impact copolymers in stirred bed reactors [95].

In meso-scale (1mm to 1cm) modeling, focus is on interparticle and intraparticle interactions, such as mass and heat transfer [96]. Modeling the growth and morphology of polymer particles can be categorized in meso scale [97].

In micro-scale, one focuses on the catalyst active centers, their activation and deactivation and the elementary reactions of the polymerization which determine the product micro-structure. Crystallization of the polymer is another important topic at the micro-scale.

Phenomenon occurring at different scales are naturally inter-related and can cause a kinetic model to become very complex, therefore based on the desired objectives of a study, the kinetic model can focus more on phenomenon taking place on a certain scale while simplifying or neglecting the other length-scales. In the following sections the kinetic scheme of coordination polymerization, taking place at the micro-scale and examples of models published at meso-scale are reviewed.

2.7.1 Kinetic scheme

Catalytic olefin polymerizations occur via coordinative polymerization mechanism. In a Ziegler-Natta catalyst, the polymerization active species are formed by reaction between the transition metal compound of the catalyst and the organo-metallic cocatalyst. A widely accepted mechanism for coordinative olefin polymerizations with Ziegler-Natta catalyst has been

proposed by Cossee and Arlman [98–100], herein it is indicated that polymer chain growth further takes place by a two-step process of first coordination of the monomer molecules with the transition metal atom at the catalyst active center and secondly insertion of the coordinated monomer in between the chain and the active center. Coordination polymerizations are very complex, with several elementary reactions take place simultaneously. Kinetics of polymerization reactions can be described via reaction rate expressions for the corresponding elementary reactions. Different catalysts have their own unique kinetic response, and hence reaction rate parameters are catalyst specific for coordinative polymerization. Many researchers have presented reaction kinetic models for describing propylene polymerizations. The kinetic scheme of the elementary reactions adopted in a reaction kinetic model, can be established based on experimental investigations of reaction kinetics. In general the following basic steps in propylene polymerizations are known to occur [61,72,101–104]:

- I. Activation
- II. Chain initiation
- III. Chain propagation
- IV. Chain transfer
- V. deactivation

In the first step catalyst's metal centers are typically activated by reacting with cocatalyst, however (re-)activation via other species such as hydrogen or monomer is possible as well. These activated catalyst sites in turn react with monomers in reaction environment and initiate a polymer chain. The polymer chains grow further in propagation step, wherein repeated insertion of monomers (or monomer and comonomer in case of copolymerizations) into the growing chain via catalyst active site takes place. In chain transfer reaction, the active site of a growing polymer chain is transferred to another reaction partner, which results in a vacant active site and a dead polymer chain. In practice, hydrogen is used as chain transfer agent for controlling the product molecular weight of polyolefins, however chain transfer to other species such as monomer, polymer or cocatalyst or spontaneous chain transfer are possible as well. Finally, the decay in activity of the catalyst throughout the polymerization is explained by the deactivation step, herein an active chain is terminated either by reacting with other species or spontaneously, resulting in a dead chain and a dead catalyst site. Ziegler-Natta catalysts have multiple types of active sites with different kinetic responses. In many reaction kinetics models several types of active sites are adopted in the model to describe the distribution of product properties more accurately [40,105–108]. In this case, the kinetic parameters might vary for each individual type of active site resulting in very complex reaction schemes and parameter sets. An overview of possible reaction steps and corresponding rate parameters are listed in the following table:

| Reaction step | Chemical equation | Rate constant |
|--------------------------|----------------------------------------|-----------------|
| Activation | $Ti^P + CoCat \rightarrow Ti^*$ | $k_{act,CoCat}$ |
| Chain initiation | $Ti^* + M \rightarrow P_1^*$ | k_0 |
| Chain propagation | $P_n^* + M \rightarrow P_{n+1}^*$ | k_p |
| Chain transfer | | |
| To hydrogen | $P_n^* + H_2 \rightarrow D_n + Ti^*$ | $k_{tr,H}$ |
| To Monomer | $P_n^* + M \rightarrow D_n + P_1^*$ | $k_{tr,M}$ |
| To Cocatalyst | $P_n^* + CoCat \rightarrow D_n + Ti^*$ | $k_{tr,CoCat}$ |
| Spontaneous | $P_n^* \rightarrow D_n + Ti^*$ | $k_{tr,\beta}$ |
| Deactivation | $P_n^* \rightarrow D_n$ | k_d |

Table 1. Typical elementary reactions for the kinetic modeling of coordinative polymerization

The activation effect of hydrogen on propylene polymerization is explained by the dormant site theory. 2,1 mis-insertion of a propylene molecule to a growing polymer chain creates a dormant chain. The dormant chains are not active, yet they can be reactivated by a small molecule such as hydrogen. The kinetic scheme for these steps is presented in table 2.

| Reaction step | Chemical equation | Rate constant |
|----------------------------------|---------------------------------|---------------|
| Dormant site formation | $P_n^* + M \rightarrow R_{n+1}$ | $k_{dorm,f}$ |
| Dormant site reactivation | | |
| By hydrogen | $R_n + H_2 \rightarrow P_n^*$ | $k_{dorm,aH}$ |
| Spontaneously | $R_n \rightarrow P_n^*$ | $k_{dorm,aS}$ |

Table 2. Dormant site formation and reactivation, reaction steps

2.7.2 Meso-scale modeling

Physical approaches towards the polymer particle in meso scale, can be categorized in three commonly used type of models.

Firstly, the core-shell model assumes that polymer forms around a solid catalyst particle, and the active site is at the surface of the particle and catalyst breakage is ignored. This approach was incorporated by Schmeal [109]. By considering only one type of active site, this model failed to predict the broad molecular weight distributions that are expected for polymers produced by Ziegler-Natta type catalysts and predicts unrealistically high mass-transfer resistances. Subsequently, the polymer flow model (PFM) was proposed by Schmeal and

Street. The PFM assumes that growing polymer chains and catalyst fragments form a pseudo-homogeneous phase. Heat and mass transfer occur through the pseudo-homogeneous polymer matrix, in which the catalyst particles are distributed. Bartke and Reichert presented a model for molecular weight distribution as a function of the radial position within a growing polymer particle by applying the PFM approach [110] for gas-phase polymerization of butadiene.

A more sophisticated model is the multi-grain model (MGM). This model structure, and mass balances considering the mass transport phenomena was originally proposed by Yermakov [111]. The MGM assumes, that the polymer phase consists of a porous agglomerate of micro-grains. The micro-grains themselves are considered to include a catalyst fragment surrounded by polymer layer. Mass and heat transfer are formulated at the two levels of macro (porous agglomerate), and micro particle (micro grain). Nagel [112] used this approach and modeled the molecular weight distribution in polymerization of olefins by Ziegler-Natta catalysts. Unlike the PFM model, the MGM model takes the heterogeneous nature of polymer particles into account. In MGM model the polymer particles consist of an agglomerate of micro particles. Floyd [113] formulated the polymerization rate in regard to mass balances proposed for MGM model, and presented regimes for macro-grain micro-grain diffusion resistance in regards to polymerization rate. In subsequent publications, Floyd studied mass transfer limitations at the growing particle boundary layer in slurry and gas phase polymerizations. Hutchinson [114] presented a model using the MGM approach and by considering the mass transfer phenomena, predicted the polymerization rates as well as particle growth and morphology. Kröner applied a modified MGM approach, considering clusters of fused micro grains as relevant length scale for mass-transfer. The cluster sizes were determined via sorption experiments. Combining this mass transfer model with a polymerization kinetics scheme, Kröner was able to describe the polymerization rates as well as transport phenomena in gas phase polymerization and Impact copolymerization of propylene [65].

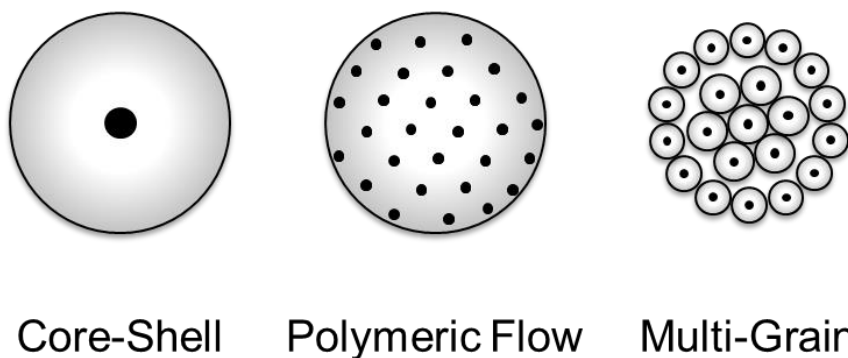


Figure 8. Schematic description of core-shell, polymeric flow, and multi-grain models

2.8 Phase equilibria in propylene polymerization

2.8.1 Vapor-liquid phase equilibria

A substance at pressure equal or greater than its bubble-point will exist in a state of equilibrium between vapor-liquid phases. Figure 9 displays an isotherm curve of propylene density at 75 °C indicating the existence of two phases in pressures above saturation (33.92 [bar]). [115].

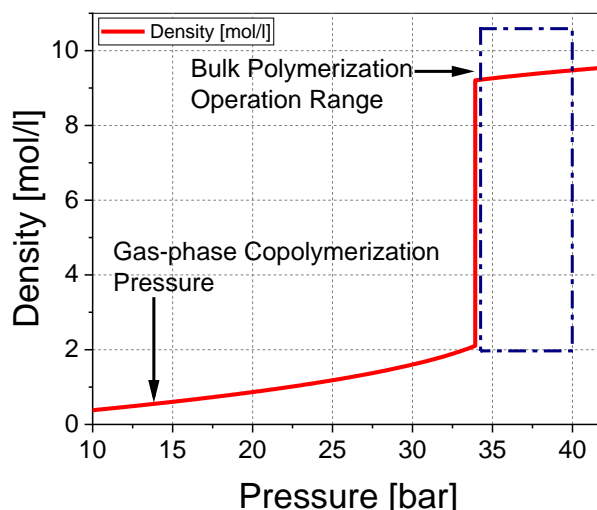


Figure 9. Propylene density isotherm at 75°C and pressure range of 0 to 40 [bar]

Bulk polymerizations are performed in pressures between 34 to 40 [bar], therefore propylene coexists in a vapor-liquid equilibrium in this range. The existence of propylene in two phases of vapor and liquid is called the flash phenomena. Gas-phase propylene polymerization or ethylene/propylene copolymerization are typically carried out at lower pressures (14 [bar] in this work), therefore propylene solely exists in gas phase. As opposed to propylene, ethylene has a much lower critical temperature ($T_c=282.35$ [K]), and thus it only exists in gas form over the pressure range of common polymerization processes.

During the bulk polymerization, in addition to propylene, typically hydrogen is present in both phases in a binary mixture with propylene and acts as chain transfer agent. In such a system, multiple phases are in equilibrium, when the chemical potential of each species is equal in all phases [116]. Chemical potential of a component in an ideal mixture is defined as:

$$d\mu^{id} = \frac{RT}{P}dP = RTd\ln(P) \quad 2.9$$

When considering real fluids, such as propylene used in this study, ideal gas law is no longer applicable specially at higher pressures, therefore the chemical potential of a real fluid is redefined by introduction of the concept of fugacity (f):

$$d\mu^{real} = \frac{RT}{P} dP = RT d\ln(f) \quad 2.10$$

The change in fugacity of a real fluid regarding pressure is therefore derived as:

$$\left(\frac{\partial f}{\partial P}\right)_T = \frac{v}{RT} \quad 2.11$$

And thus:

$$\ln(f) = \int_0^P \frac{v}{RT} dP \quad 2.12$$

Here v indicates the molar volume of the real fluid. The volume of a real fluid can be estimated by an equation of state (such as virial, or cubic equations of state). Fugacity coefficient of a substance is defined as the following:

$$\varphi = \frac{f}{P} \quad 2.13$$

Naturally for an ideal gas the fugacity coefficient is equal to one. According to the definition of fugacity and equation 2.10, the equilibrium criterion for a substance between two phases of vapor and liquid is defined as:

$$\hat{f}_i^v = \hat{f}_i^l \quad 2.14$$

The terms \hat{f}_i^v, \hat{f}_i^l refer to the fugacities of component "i" in liquid and vapor mixture. This condition can be extended to the propylene and hydrogen mixture existing in polymerization reactor used in this study. Fugacity of a component in vapor phase relative to pressure and the mole fraction of the component in vapor is defined as:

$$\hat{f}_i^v = \hat{\varphi}_i^v P_i = \hat{\varphi}_i^v y_i P \quad 2.15$$

A common method for expression of phase equilibrium is called the gamma-phi formulation of the phase equilibria [116]. In this formulation, fugacity of a component in liquid phase can be expressed in terms of activity and standard fugacity:

$$\hat{f}_i^l = x_i \gamma_i f_i^0 = \hat{f}_i^v = \hat{\phi}_i^v y_i P \quad 2.16$$

with:

$$f_i^0 = \phi_i^l P_i^l \exp\left(\frac{P - P_i^l}{\rho_i^l RT}\right) \quad 2.17$$

herein the activity (γ_i) can be formulated by Henry's law or Flory-Huggins theory and standard fugacity (f_i^0) is described by the fugacity at vapor pressure of the pure component multiplied by a correction term for pressure called the Poynting factor ($\exp\left(\frac{P - P_i^l}{\rho_i^l RT}\right)$). A further approach towards describing a multi component phase equilibrium is the so-called phi-phi formulation which is more commonly used in case of systems at high pressure:

$$y_i \hat{\phi}_i^v = x_i \hat{\phi}_i^l \quad 2.18$$

With,

$$K_i = \frac{y_i}{x_i} = \frac{\hat{\phi}_i^l}{\hat{\phi}_i^v} \quad 2.19$$

Herein K_i is the equilibrium constant of component "i". In this approach typically an equation of state is used to calculate the fugacity coefficient of components in each phase (equations 2.12 and 2.13), and thus calculate the mole fraction of each component and the corresponding equilibrium constant [117].

The mathematical procedure for calculating the material balance in each phase in a vapor-liquid multi component equilibrium, as well as fraction of each component in both phases is called flash calculations. In case of bulk phase polymerization of propylene in a partially filled reactor, by flash-calculations, the partitioning of propylene between liquid and gas-phase can be determined. In this work to estimate liquid and vapor fugacity of components in mixture, and equilibrium constants, and to perform the flash calculation procedure, Peng-Robinson equation of state is used (see chapter 6.1).

2.8.2 Equilibrium between polymer and penetrant

In addition to the material balance between the liquid and vapor phases in polymerization reactor, the phase equilibria between forming polymer particles and the reaction medium (liquid propylene or gaseous propylene/ethylene mixture) is an area of focus in this work.

Polypropylene does not dissolve in liquid propylene, and polymer particles are suspended in a liquid pool of monomer during bulk polymerization. In coordinative olefin polymerization, reaction occurs at the catalyst active centers. As the polymerization continues the catalyst is surrounded by the forming polymer particle, hence reactant molecules must transport through the polymer phase to the catalyst active site. The phase equilibrium between the penetrating reactants and the amorphous fraction of polypropylene is what determines the concentrations of reaction partners at the active center.

It has been established in literature that penetrants are solely soluble in amorphous fraction of the polymer [118,119]. This justifies application of a simple two-phase fugacity rule for describing the equilibrium between propylene or ethylene and polypropylene. Amorphous polymer is considered to act as a liquid, which is at equilibrium with liquid propylene during bulk polymerization or with gases during a gas-phase polymerization.

In case of small penetrating molecules and lower concentrations in polymer, the interaction between polymer and penetrant can be neglected, and the equilibrium between polymer and penetrant can be described by Henry's law. In equation 2.17 the standard fugacity can be replaced with Henry's constant:

$$P_i \hat{\phi}_i^v = x_i \gamma_i H_i \quad 2.20$$

In case of ideal vapor and liquid phase ($\hat{\phi}_i^v, \gamma_i = 1$) the Henry's law is simplified as:

$$P_i = x_i H_i \quad 2.21$$

Henry's law can be used to describe the equilibrium between ethylene gas and polypropylene [120]. The validity of Henry's law is limited for higher concentrations since the monomer-polymer interactions starts to influence gas solubility. For instance, in case of propylene gas and polypropylene at higher pressures, the Henry's law is not capable of describing the solubility of propylene in polymer.

In this case one common approach is to use the Flory-Huggins theory, wherein the penetrant activity over an amorphous polymer is calculated, and the equilibrium can be described by the gamma-phi formulation (equation 2.17). The Flory-Huggins theory formulates the activity as [121]:

$$\ln(a_i) = \ln(v_i) + (1 - v_i) + \chi(1 - v_i)^2 \quad 2.22$$

The interaction parameter (χ) can be adjusted to fit the experimentally obtained data or can be calculated by theoretical means.

A further approach is to consider the phi-phi formulation of equilibrium, this time between a penetrant and amorphous polymer:

$$y_i \hat{\phi}_i^v = x_i \hat{\phi}_i^l \quad 2.23$$

By assuming the fraction of polymer in the penetrant vapor phase is negligible ($y_i = 1$) the above formulation is simplified as:

$$\hat{\phi}_i^v = x_i \hat{\phi}_i^l \quad 2.24$$

Here an equation of state can be used to formulate the fugacity of penetrant and polymer phase and to estimate the solubility of the penetrant in polymer. In this work the Sanchez-Lacombe equation of state is used to describe the equilibrium between propylene penetrating gas and the amorphous fraction of polypropylene (see chapter 6.2). Sanchez-Lacombe equation of state belongs to the family of the cubic equations of state and is often used to describe the solubility of olefins in polyolefins [122–124]. A semi-empirical approach was proposed by Hutchinson, to describe gas solubility of penetrant in polymer at higher pressure range, where Henry's law is no longer applicable [125]:

$$C_i = A_H P_i e^{B_H C_i} \quad 2.25$$

Here C_i indicates the penetrant concentration in amorphous polymer, and A_H and B_H are adjustable parameters that are fitted to match the experimentally obtained values for penetrant concentration.

2.8.3 Sorption measurements

The equilibrium solubility in polymer is defined as the mass ratio of absorbed penetrant and polymer:

$$S_{eq} = \frac{m_i}{m_p} \quad 2.26$$

The effective (amorphous) monomer concentration that directly influences polymerization rate can be calculated by number of moles of penetrant relative to (swollen) amorphous polymer volume:

$$C_{am} = \frac{n_i}{V_{am}} \quad 2.27$$

In order to determine the volume of amorphous polymer it is essential to have an estimation of the degree of crystallinity of the polymer under investigation. The polymer crystallinity can be determined by methods such as differential scanning calorimetry (DSC), or X-ray diffraction (XRD). Furthermore, the swelling effect due to solution of penetrants in amorphous polymer must be considered.

Equilibrium solubility of a penetrant gas in polymer can be experimentally investigated via various methods. Sorption experiments are a well-known method for measuring the solubility of penetrants in semi-crystalline polymer. In open literature different methods have been introduced for performing sorption measurements:

Sato used a gravimetric method to investigate the influence of Crystallinity and temperature on solubility of propylene in different polypropylene samples [126,127]. Patzlaff used a sorption balance to investigate the mass transfer rate in iso-tactic PP powder and film samples. Bartke et al [128] performed similar investigations on high-Impact polypropylene samples, wherein sorption measurements were performed with pressed polymer films and corresponding homo- and copolymer powders. Kröner and Bartke studied the solubilities of ethylene and propylene in high impact copolymer films and powder samples, and presented a model for mass transport in polypropylene [129]. Ben Mrad deployed a sorption balance to investigate the diffusivity of multicomponent gas Mixtures in polyethylene [130,131]. A gravimetric apparatus based on a magnetic suspension balance was used by Novak to measure the sorption of ethylene and 1-hexene in polyethylene samples at various temperatures, and the experimental measurements were compared with the predictions of PC-SAFT equation of state [132]. Furthermore, inverse gas chromatography method was used by Sliepcevich [133] to measure solubility and diffusivity of olefins in polypropylene.

3 Objectives

The target of this work is to study and compare polymerization kinetics of two different Ziegler-Natta catalysts in multi-step polymerization conditions. The process is a combination of a bulk-phase homopolymerization and a subsequent gas-phase copolymerization. While for gas-phase polymerization, established procedures for measurement of polymerization kinetics are existing, for bulk-phase polymerization, often the only kinetic information observed, is the yield after polymerization.

Hence, one first objective for this work is to upgrade an existing reactor with power compensation calorimetry and develop the necessary procedures in order to obtain more

kinetic information from bulk-phase polymerization stage. One important target is to precisely predict and control the amount of homopolymer made in bulk-phase stage.

The second objective is to carry out a detailed experimental study on polymerization kinetics in the upgraded reactor, for both catalysts.

In homo-polymerization, the effect of hydrogen content on course of activity and molecular weight produced shall be studied for both catalysts. In addition, the effect of pre-contacting of the catalyst and cocatalyst on homo-polymerization kinetics shall be studied and compared for both catalysts.

In the subsequent gas-phase copolymerization, the comonomer response, the comonomer incorporation as function of the gas-phase composition shall be studied as well as the resulting activity profiles and product properties such as molecular weight and particle morphology.

The third objective is to compile the generated experimental data in a phenomenological model for description of the multi-stage polymerization process. The model shall be based on equilibrium solubilities, either determined experimentally or calculated based on adequate thermodynamic models. For both catalysts, the relevant kinetic parameters, such as reactivity ratios and kinetic rate constants shall be determined.

The developed model shall be a basis for further model-based product development and process optimization.

4 Experimental setup and characterization methods

4.1 Polymerization setup

In this work, polymerization experiments have been carried out in a polymerization reactor setup, suited for performing bulk phase and gas phase polymerizations. A scheme of the setup is presented in figure 10. The setup includes raw materials supply and purification unit, the polymerization reactor, the control unit, and the data acquisition and interpretation unit. In the following sections different parts of the setup are illustrated further.

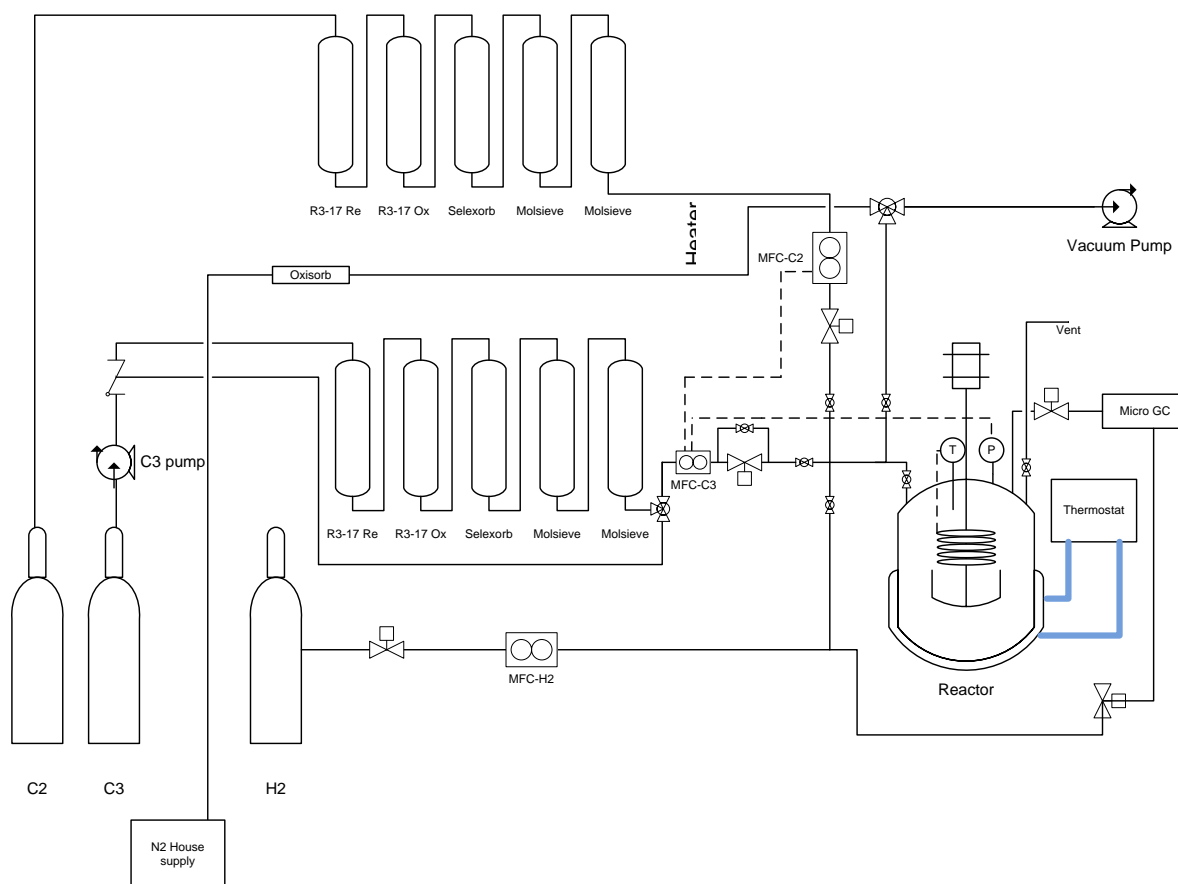


Figure 10. Polymerization reactor setup

4.1.1 Raw materials supply

For the homo-polymerization experiments, bottled liquid propylene supplied by Air Liquide (3.5 purity level) as monomer, and hydrogen supplied by Linde AG (5.0 purity level) as the chain transfer agent were used. In-house nitrogen (purity level 5.0) was used for purging and inertization of the reactor prior to the polymerization experiments. For the copolymerization experiments additionally gaseous ethylene, supplied by Air Liquide (3.5 purity level) was used as comonomer.

| Gas | Supplier | Purity |
|------------------|-------------|--------|
| Propylene | Air Liquide | 3.5 |
| Ethylene | Air Liquide | 3.5 |
| Hydrogen | Linde | 5.0 |
| Nitrogen | Air Liquide | 6.0 |

Table 3. Raw material supply and quality

A challenge in using Ziegler-Natta catalysts for polymerizations, is the sensitivity of the catalysts to poisoning. In general terms moisture, oxygen, carbon dioxide, carbon monoxide as well as polar compounds will poison the Ziegler-Natta catalyst and hinder the ability to

observe the polymerization kinetics in industrially relevant activity levels. A multi-stage purification system has been applied to purify the monomer and comonomer supply, as depicted in figure 10. In the first purification column, an oxidized copper catalyst (PuriStar® R3-12, by BASF) was used for removal of sulfur, arsine, H₂S and COS compounds. Second column contained, PuriStar® R3-17 (BASF) to remove carbon monoxide. A 50:50 in mass mixture of Selexsorb® CDL/COS (BASF) has been installed to adsorb a range of polar compounds. The fourth and fifth columns contained molecular sieve with a pore size of 4 [Å], to remove traces of moisture.

A diaphragm pump (LEVA E12-314 765) was used, to pressurize the liquid propylene up to 40 [bar]. To further ensure the purity of monomer supply, the liquid propylene stream, was recycled multiple times through the purification columns, prior to feeding to the reactor.

Since ethylene exists above the critical point in storage and polymerization conditions, it is supplied in high pressure filled bottles. Gaseous ethylene was directed through a separate purification unit, similar in configuration as for propylene.

To further purify the inhouse nitrogen supply, an Oxisorb cartridge (by Linde), was installed to remove traces of oxygen from the nitrogen stream. The hydrogen supply is not further purified.

4.1.2 Polymerization reactor

In this work a 5-liter stainless steel Büchi reactor suited for carrying out bulk and slurry as well as gas-phase polymerizations of propylene was used. The reactor jacket was water cooled, by an external thermostat (Single Type STW 1-6-50-K5D) operating with running water with maximum heating power of 3.5 [kW] and cooling power of 11.5 [kW]. The inlet and outlet water temperatures through the jacket were monitored with PT100 temperature sensors. The reactor temperature was measured by a separate PT100 temperature sensor placed inside the reactor. The reactor could operate in pressures between vacuum to 60 [bar] and temperatures 10 [°C] to 90 [°C]. A pressure gauge (Rosemount GmbH, model 2088) enabled monitoring the reactor pressure. A power compensation calorimeter setup, (purchased from Polymer Reactor Technology GmbH, Ahaus, Germany) has been added to the reactor, the calorimeter included an internal heater and thermocouple placed inside the reactor, and an additional control unit coupled with the reactor temperature sensor. The power compensation calorimeter setup enabled online monitoring of bulk phase propylene polymerization kinetics. A double ribbon helical stirrer driven by a Büchi three phase variable gear motor has been built and added in a fashion to accommodate the internal heater (figure 11).



Figure 11. 5-liter Büchi reactor, power compensation heating element, double ribbon helical stirrer

Raw materials including propylene, hydrogen and ethylene were each dosed into the reactor using separate mass flow controllers (Flomega 5882, Brooks Instruments). This enabled to accurately monitor and control the amount of materials in the reactor both in batch and semi-batch modes of operation.

4.1.3 Control unit

The reactor setup was operated in two different modes of operation. Batch mode operation for bulk-phase homo-polymerization experiments, and semi-batch mode, wherein the gas-phase impact copolymerization experiments were conducted.

In batch mode, the power compensation calorimeter setup coupled with the external thermostat maintain isothermal condition. The power compensation calorimeter setup consists of an electrical heating element submerged in the contents of the reactor (in this case liquid propylene), PT100 temperature sensor, a 3126 Eurotherm PID controller, a further 3216I Eurotherm PID controller as temperature safety limiter, and a thermocouple. The heating element can provide a maximum of 660 [W] of power. The internal heater can only operate while fully submerged in liquid, therefore it is only used during bulk phase polymerization experiments. During bulk-phase experiments the external thermostat maintains the jacket temperature a few degrees below the reactor temperature at a constant value. The internal heater compensates for the heat flow to the jacket and heat losses and keeps the reactor in thermal equilibrium. The heating is controlled using the 3216 Eurotherm PID controller (PID 1 in figure 12). The input for this controller is the PT100 temperature sensor installed in the reactor. To prevent the heater from overheating a 3216I Eurotherm is used as a temperature

safety limiter. (PID 2 in figure 12). The input for this controller comes from the thermocouple installed at the surface of the internal heater.

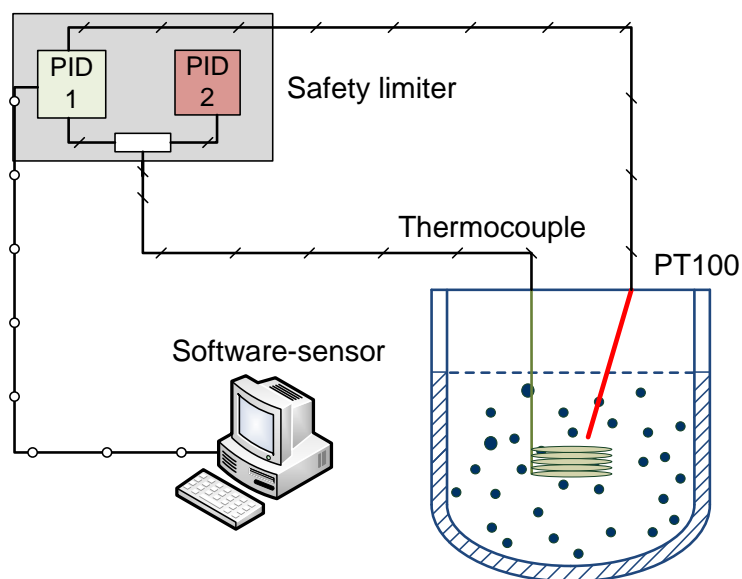


Figure 12. Power compensation calorimeter setup control sketch [134]

The data from the temperature sensor and the heater is transferred to the data acquisition software, where it can be viewed online during the polymerization reaction, and the polymerization rate information is extracted from (chapter 4.4).

During the gas-phase impact copolymerization experiments, the reactor is operated in semi-batch mode, wherein gaseous monomer is converted to solid polymer material. This causes a pressure drop in the reactor, due to the much higher density of the polymer compared to gaseous monomer. This pressure drop is compensated by the monomer feed in a closed pressure-control loop. As long as temperature, pressure and gas composition are constant, the monomer feed into the reactor is equal to monomer consumption. Iso-baric conditions in semi-batch mode of operation is maintained via a pressure control loop, herein the pressure sensor installed on the reactor, relays the data to a PID controller (Eurotherm), which compares the value with the pressure set point and transmits the signal to the mass flow controller, that adjusts the mass flow of the monomer accordingly. Temperature in gas-phase experiments is controlled by means of a PID controller controlling the jacket temperature in order to keep the reactor temperature in isothermal condition.

4.1.4 Gas chromatography setup

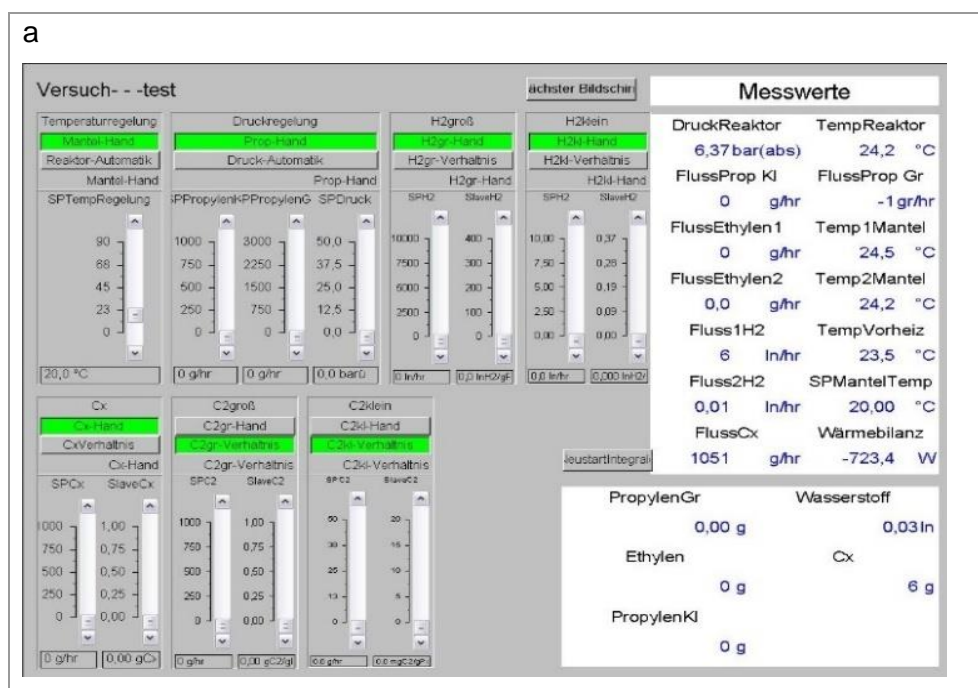
A micro gas chromatography setup (μ -GC, Varian CP 4900) has been used to monitor the concentration of gases in the reactor during gas-phase propylene/ethylene copolymerization experiments. The gas composition measured by the μ -GC setup was used to control the mass

flows of propylene and ethylene into the reactor in order to maintain constant conditions throughout the copolymerization.

In detail, the μ -GC was connected to the polymerization reactor through a sampling line on top of the reactor. A 1-micron filter was installed on the line to avoid any solid polymer particles entering the μ -GC. Next in line, a micro pressure regulator was installed to reduce the sample gas pressure down to 1 [bar]. It is important to minimize the internal volume of all equipment in the sample line to avoid long dead times and hence long response times from the μ -GC. The sampling line was heated with an electrical heating band, to avoid any condensation of gaseous propylene. The used Varian CP 4900 μ -GC included three measurement columns with the ability to detect the following gases: propylene, ethylene, hydrogen, nitrogen, oxygen, and hexane. The raw peak information collected by the μ -GC was processed by a MATLAB program to calculate the species mole fractions in gas-phase. The μ -GC is calibrated for propylene, ethylene, and hydrogen.

4.1.5 Software and data collection

Information from the setup, such as reactor pressure, reactor temperature, jacket temperature, and mass flow of the materials, were transferred and collected in a DasyLab 9.0 software, in which the user could monitor, and set the values for jacket and reactor temperatures, reactor pressure, and flow rates of materials. The calorimeter data such as heater power and reactor temperature were collected in a separate VEE pro software by Agilent, displayed in figure 13.



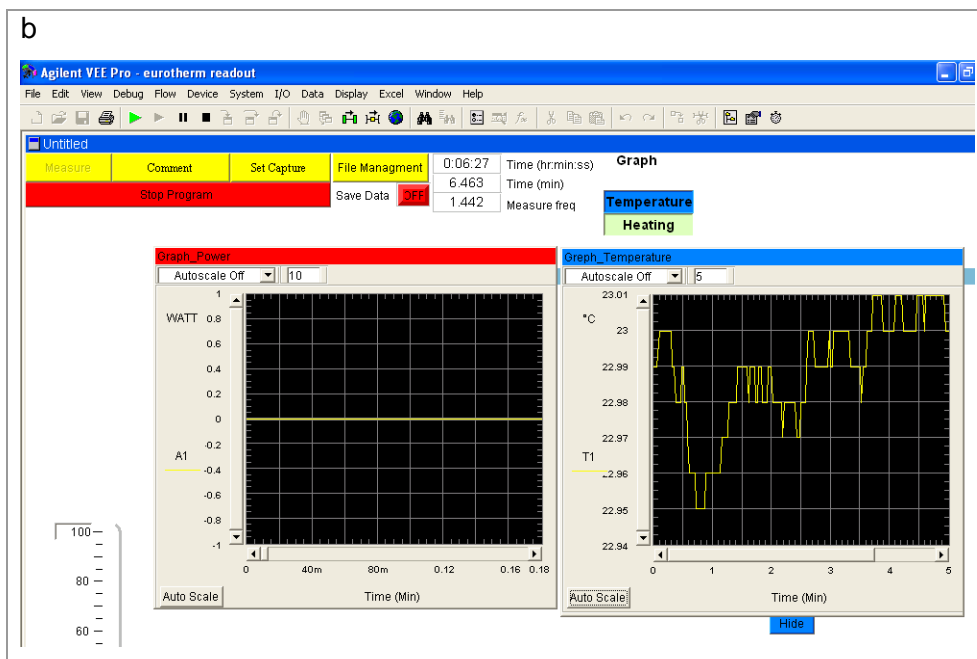


Figure 13. a) DasyLab data acquisition software b) VEE pro data acquisition software by Agilent

4.2 Chemicals and catalysts – preparation and handling

In this work polymerization behavior of two different Ziegler-Natta type catalyst of different generations, provided by industrial partner of this project have been studied. The catalysts are called catalyst A and catalyst C. Active component of both catalysts is titanium. The two catalysts show different polymerization kinetics both in propylene homo-polymerization and multi-stage copolymerization experiments.

| Property | Catalyst A | Catalyst C |
|---------------------|------------|------------|
| Active component | Titanium | Titanium |
| Density [g/l] | 1700 | 1800 |
| Porosity [Volume %] | 72 | 73 |

Table 4. Properties of the used catalysts

As cocatalyst a 1.0 [M] solution of triethylaluminium (TEA) in hexane (Sigma-Aldrich) was used. TEA acts as cocatalyst by activating the titanium active centers as well as scavenging the propylene from any remaining impurities. Cyclohexyltrimethoxysilane (1.0 [M] solution in hexane, Sigma-Aldrich) was used as external electron donor (fixed Si/Ti ratio of 10 [mol/mol]), and hydrogen was used as the chain transfer agent for controlling the product molecular weight. Hexane (99.9%, Carl Roth) has been used for diluting the donor, and for preparing catalyst suspension. Ethanol (96%, Carl Roth) was used to quench the polymerization reaction when a faster quenching was required. Liquid propylene and gaseous ethylene are used as monomer and comonomer.

Ziegler-Natta catalysts are prone to poisoning by any contact to air or moisture, and TEA is a highly reactive substance with air and water and must be handled with high precaution. All handling of catalyst and chemicals is conducted in a neutral environment in a dry glove box (by *Jacomex*®), where the amount of water and oxygen are kept under 0.1-ppm level [135].



Figure 14. Jacomex dry box

For transferring the catalyst and other chemicals from the glove box to the reactor, injection feeders were used. A feeder consists of two stainless steel chambers (1.4 [ml] volume) enclosed with three Swagelok VCR valves on each side:



Figure 15. Injection feeder

For each polymerization experiment two feeders have been used. The first feeder containing only TEA, and the second feeder containing TEA and donor in the chamber on top and the required amount of catalyst suspended in hexane, in the other chamber at the bottom (once installed on the reactor). After preparation, the feeders were installed on the reactor under nitrogen flow. To inject the catalyst and other components into the reactor the feeder's valves are opened, and the components were injected into the reactor under the flow of liquid propylene pressurized to 40 [bar] by the membrane pump.

4.3 Polymerization procedures

4.3.1 Reactor inertization

Thorough reactor inertization has been conducted prior to each polymerization experiment to avoid traces of impurities and to obtain the full potential productivity of the catalyst under the given conditions. In the inertization procedure, the reactor temperature was set at 90 [°C] and the reactor was placed under vacuum for two hours. After hot vacuum, the reactor was left under nitrogen purge over-night for the next polymerization run. After each polymerization run the reactor was opened, whipped clean with heptane, dried and closed again.

4.3.2 Homo-polymerization with in-situ pre-polymerization

After inertization, the reactor was again vacuumed for 30 minutes at room temperature to remove the remaining nitrogen used for purging from the reactor. The required amount of hydrogen was dosed via a mass flow controller into the reactor. 1.4 [kg] of propylene was fed to the reactor, using a mass flow controller to track the amount of flowing propylene. Using the first feeder 1.4 [ml] of 1 [M] TEA solution in hexane was injected into the reactor alongside the flow of liquid propylene. The injection line was kept under inert condition using nitrogen purging and vacuuming the line before filling with liquid propylene. Injection of TEA prior to the beginning of the reaction serves the purpose of scavenging the bulk monomer for 10 minutes. After TEA was injected into the reactor, stirring the reactor content at 100 [rpm] was started. The reactor temperature was set at the desired value for the pre-polymerization stage (25 [°C] for catalyst A and 15 [°C] for catalyst C). For controlling the temperature during the pre-polymerization stage, the jacket temperature was set at 2 degrees below the desired temperature and the compensation heater was turned on to provide enough power to keep the reactor in isothermal condition.

The second feeder contained catalyst suspended in 1 [ml] of hexane in one chamber, and 0.4 [ml] of 1 [M] TEA, and the required amount of donor based on catalyst amount used in each polymerization in the second chamber. In case pre-contacting of catalysts and cocatalyst was required, the valve between the two chambers of the injection feeder was opened and components were contacted. After the required pre-contacting duration, by injection of the catalyst and other components into the reactor, pre-polymerization was started.

For each injection around 50 [g] of liquid propylene was used. After 10 minutes of pre-polymerization at mild conditions, the reactor was heated up to main polymerization reaction temperature (75 [°C]). The jacket temperature was set at a value between 68 and 72 [°C],

based on the expected activity of the catalyst and the resulting heat release. The setup enabled a swift heat up of around 8 minutes. After the heat-up stage, the power compensation calorimeter setup controlled the temperature at the desired value, and iso-thermal condition was maintained throughout the polymerization, wherein the temperature fluctuations were below 0.04 [°C].

To end the polymerization, the compensation heater was shot off, stirring was stopped, and the remaining monomer amount in the reactor was vented off. A visual depiction of the homo-polymerization procedure with in-situ pre-polymerization is displayed in figure 16.

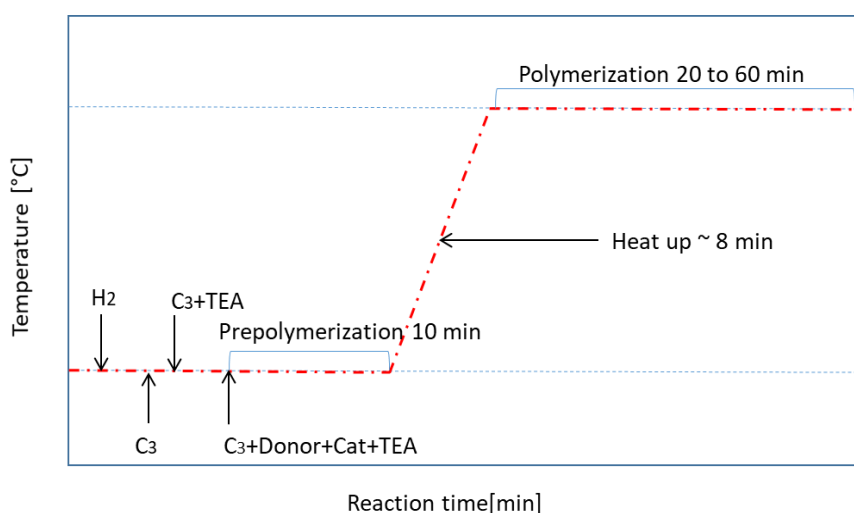


Figure 16. Homo-polymerization procedure, In-Situ pre-polymerization

4.3.3 Multi-stage impact copolymerization

In industrial processes, such as Spheripol™ process, for production of high impact resins, the homo-polymer powder is transferred to a second gas-phase reactor, wherein copolymerization takes place. In this study, since both stages of bulk homo-polymerization and gas-phase impact copolymerization are carried out in the same reactor, there is a transition period for reaction conditions (pressure, gas composition) between the two stages. The transition period between the different stages is an uncontrolled regime, during which reaction kinetics measurement is not possible, and should be as short as possible.

To transition to copolymerization stage:

- The internal heater was shot off and temperature control was achieved only by controlling the jacket temperature with the external thermostat.
- The sampling by μ -GC was started.

- Propylene was partially vented out until the reactor pressure dropped down between 7~11 [bar] (based on the partial propylene pressure required in the gas-phase copolymerization stage). Since the saturation pressure of propylene at the reaction temperature (75 [°C]) is at 33.9 [bar] the remaining propylene in the reactor existed only in the gas phase.
- Since with venting propylene the hydrogen gas in the reactor is mostly vented as well, an additional 2 [mol%] of hydrogen in the gas mixture in the reactor was added to the reactor batch-wise.
- To reach the copolymerization reaction pressure (14 [bar]), the reactor was filled with ethylene with maximum flow rate (300 [g/hr]) to shorten the transition period.

After the reactor pressure reached 14 [bar], iso-baric condition was maintained by the pressure control loop, and simultaneous flow of propylene and ethylene was started. As long as pressure, temperature, and the composition of materials in the reactor are constant, the reaction is in steady state conditions, and the combined mass flow rates of propylene and ethylene into the reactor, are equal to the gross consumption rate of polymerization. The composition of the gases was monitored by the gas chromatograph setup with a response time of below 2 minutes. It is observed by μ -GC measurements, that for constant monomer feed ratios, the monomer composition remains constant as well. The copolymerization was stopped by venting out the remaining of the gases in the reactor.

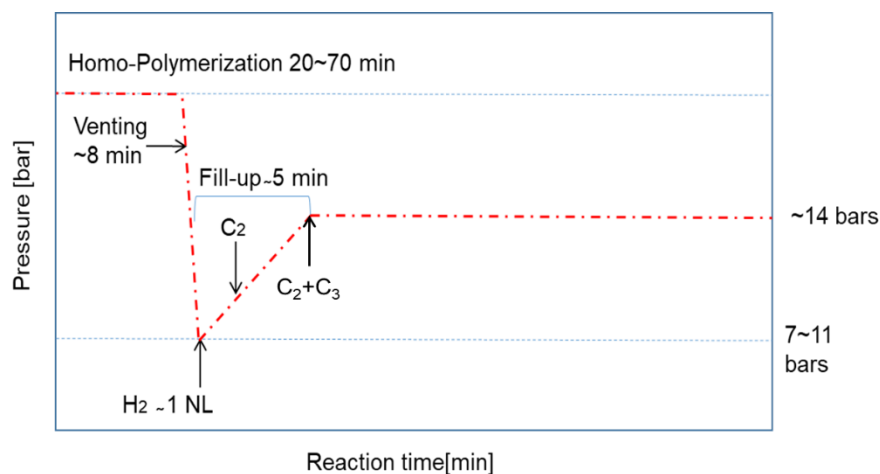


Figure 17. Gas-phase copolymerization procedure

4.4 Analysis of the power compensation calorimetry data

In this section, analysis of the power compensation calorimetry data is outlined. For extraction of the kinetic information from the raw data of the compensation calorimetry, the heat-balance of the reactor setup is applied. The heat losses from the setup are measured, the effective heat transfer coefficient of the reactor setup is determined, and the calorimeter calibration method

is presented. Furthermore, the software sensor developed for online evaluation of the obtained calorimetric measurements is demonstrated.

4.4.1 Raw data power compensation calorimetry

For illustration of the raw data obtained from power compensation calorimetry, an example of a bulk-phase polymerization run with a Ziegler-Natta catalyst at 75 [°C] in the outlined setup is depicted in figure 18. The heater power before injection of the catalyst is shown as P_0 in figure 18 and is equal to about 295 [W]. As polymerization with injection of the catalyst begins, a sharp drop in power provided by the electrical heater is observed. This drop can be attributed to the heat released by the polymerization reaction. The reactor temperature at injection of the catalyst only increases about 0.2 [°C] for about 2 minutes. After an hour of polymerization, the reaction is quenched by injecting ethanol into the reactor. The heat flow to the jacket after the end of the reaction, noted as P_f in the figure, is about 240 [W]. The observed change in the heat flow to the jacket is due to the changes in the heat transfer area during polymerization and must be considered for further analysis of the calorimetry experiments.

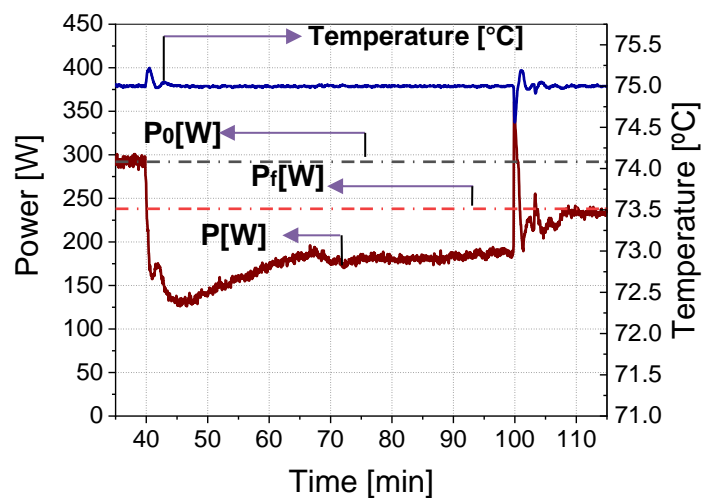


Figure 18. Example of compensation heater power and reactor temperature in bulk-phase polymerization run. As was demonstrated in section 2.6.4, the heat balance in a reaction calorimeter equipped with a compensation heater can be simplified for isothermal conditions and negligible power dissipation via stirring to:

$$P + \dot{Q}_{chem} = \dot{Q}_{jacket} + \dot{Q}_{loss} = k_l A (T_r - T_j) + \dot{Q}_{loss} \quad 4.1$$

For determination of the chemical heat flow and thus the reaction rate, all other terms of the heat balance must be known and quantified.

4.4.2 Estimation of the reactor heat losses

The heat loss term itself can be expanded as

$$\dot{Q}_{loss} = k_{loss}(T_r - T_{amb}) + \dot{Q}_{disp} \quad 4.2$$

k_{loss} [W/K] is the heat loss coefficient, T_r is the reactor temperature, T_{amb} is the ambient temperature, and \dot{Q}_{disp} is the heat dissipation at ambient temperature. In absence of any chemical reaction the term for chemical heat flow (\dot{Q}_{chem}) disappears from equation 4.1 and the heat balance is simplified as:

$$P = k_l A(T_r - T_j) + k_{loss}(T_r - T_{amb}) + \dot{Q}_{disp} \quad 4.3$$

To estimate the heat losses of the reactor, a series of measurements were performed, in which the average jacket temperature (T_j) and the reactor temperature (T_r) were set at the same value, and thus the heat transfer to jacket is minimized. In these conditions, the power provided by the compensation heater to keep the reactor in isothermal condition is equal to the heat losses:

$$P = \dot{Q}_{loss} = k_{loss}(T_r - T_{amb}) + \dot{Q}_{disp} \quad 4.4$$

This measurement has been performed at various reactor temperatures and an ambient temperature of 24 [°C] and stirring speed of 100 [rpm]. The intercept from the linear fit presented in figure 19 indicates the heat dissipation of the operating setup at stirring speed of 100 [rpm] at the ambient temperature (\dot{Q}_{disp}). The polymerization experiments in this work have been performed at 75 [°C], the heat loss at this temperature and a stirring speed of 100 [rpm] is about 100 [W] and is independent of the filling level of the reactor.

| Parameter | Value | Description |
|------------------|------------|----------------------------------|
| k_{loss} | 1.28 [W/K] | Heat loss coefficient |
| \dot{Q}_{disp} | 30.36 [W] | Heat loss at ambient temperature |

Table 5. Heat loss parameters of the reactor setup; Ambient temperature=24 [°C]; N=100 [rpm]

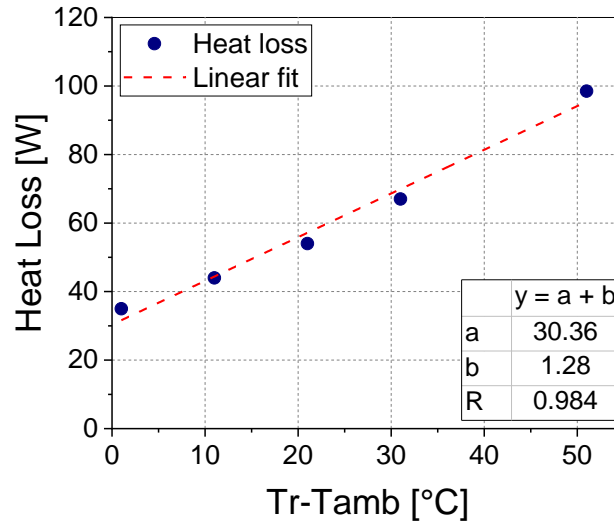


Figure 19. Reactor setup heat loss vs temperature; $T_{amb}=24$ [°C], $T_r= 24-75$ [°C], $N=100$ [rpm]

4.4.3 Change of filling level

A challenge in application of power compensation calorimetry for bulk phase polymerization of propylene is the change of filling level. In a batch wise bulk phase polymerization process, due to the much higher density of polypropylene compared to liquid propylene [136], the liquid volume level in the reactor is decreasing. Thus, the heat transfer area decreases with conversion as well.

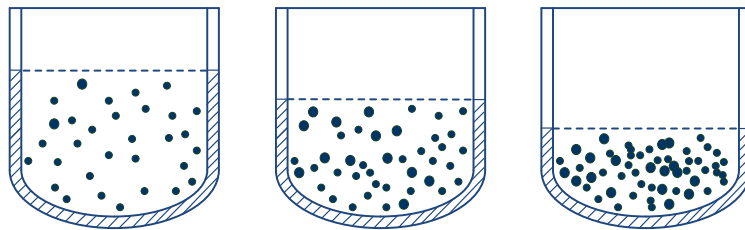


Figure 20. Schematic depiction of the change in heat transfer area during a batch bulk-phase polymerization run. In order to determine and quantify the change of the heat transfer conditions, calibration experiments with different filling levels and temperature differences have been carried out. Therein, the heat flow to the jacket for different filling levels has been measured in absence of any chemical reaction, which means the term for chemical heat flow (\dot{Q}_{chem}) is equal to zero. The resulting heat balance of the reactor during the calibration experiments is as follows:

$$P = \dot{Q}_{jacket} + \dot{Q}_{loss} = k_l A \Delta T + \dot{Q}_{loss} \quad 4.5$$

Figure 21 shows a typical calibration curve in absence of polymerization reaction at 75 [°C] and 100 [rpm] stirring speed. For this example, the reactor has been filled with 1.2 [kg] of propylene, and the power required to keep the reactor in isothermal condition in absence of polymerization reaction for three different temperature differences ($\Delta T=3,5,7$ [°C]) has been measured.

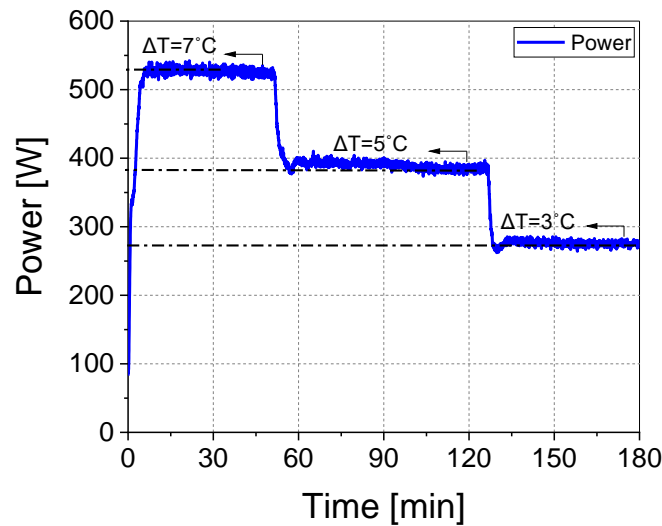


Figure 21. A typical calibration measurement: reactor filled with 1.2 [kg] of propylene; $T=75$ [°C]; $N=100$ [rpm]. Similar calibration experiments have been performed with different filling levels in the reactor. The data for the heat flow to the jacket, depending on filling level and temperature difference is plotted in figure 22. The heat loss of the reactor setup to the environment (\dot{Q}_{loss}) at 75 [°C] are determined to be around 100 [W], independent of filling level. As expected, the heat flow to the jacket is increasing both with filling level and with temperature difference. The volume occupied by liquid propylene has been calculated through the flash calculation procedure (see chapter 6.1), and the heat transfer area at a given filling level is extracted from the design of the used autoclave (possible vortexes due to stirring were neglected). The reproducibility of the calibration experiments has been checked by repeating the measurements throughout this work. The heat flow to the jacket is estimated to have an error range of about 4%.

By inserting the measured heat loss in equation 4.5, the heat flow to the jacket and hence the heat transfer coefficient k_l can be calculated. k_l depends strongly on properties of the reaction mixture (such as temperature, density, viscosity) and stirring conditions. For the given reactor setup at 75 [°C] with a double-ribbon helical stirrer at 100 rpm stirring speed, the heat removal can be characterized by a heat transfer coefficient k_l of about:

$$k_l = 700 \pm 8\% [W/m^2K]$$

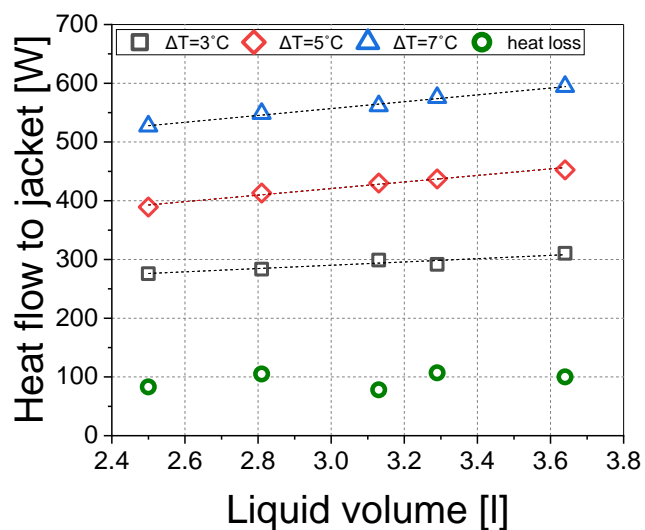


Figure 22. Heat flow to jacket vs filling volume; $T=75$ [°C]; $N=100$ [rpm]

4.4.4 Software sensor for online baseline-correction

Since the heat transfer area is changing during a polymerization reaction, the heat flow to the jacket is changing as well. For a corresponding baseline correction, a software sensor has been developed, which couples the power compensation calorimetry data with a material balance for propylene and flash calculations in order to determine the filling level and heat flow to the jacket, online during a polymerization run. A flowsheet of the software sensor is depicted in figure 23.

At the start of an experiment, first the initial amount of propylene, the amount of catalyst and the temperature difference between reactor and jacket must be provided. In the software sensor, for the current amount of liquid propylene in the reactor, a flash-calculation is performed to determine the vapor and liquid fraction of propylene and thus the liquid filling level in the reactor. With the filling level and the temperature difference between reactor and jacket, the heat flow to the jacket (\dot{Q}_{jacket}) is estimated based on the calibration measurements illustrated in figure 22. By determining \dot{Q}_{jacket} and the measured compensation power (P), the chemical heat flow (\dot{Q}_{chem}) is calculated by equation 4.5. From the chemical heat flow, the rate of propylene consumption can be concluded (based on equation 2.1), and hence the polymer production and the new filling volume can be updated.

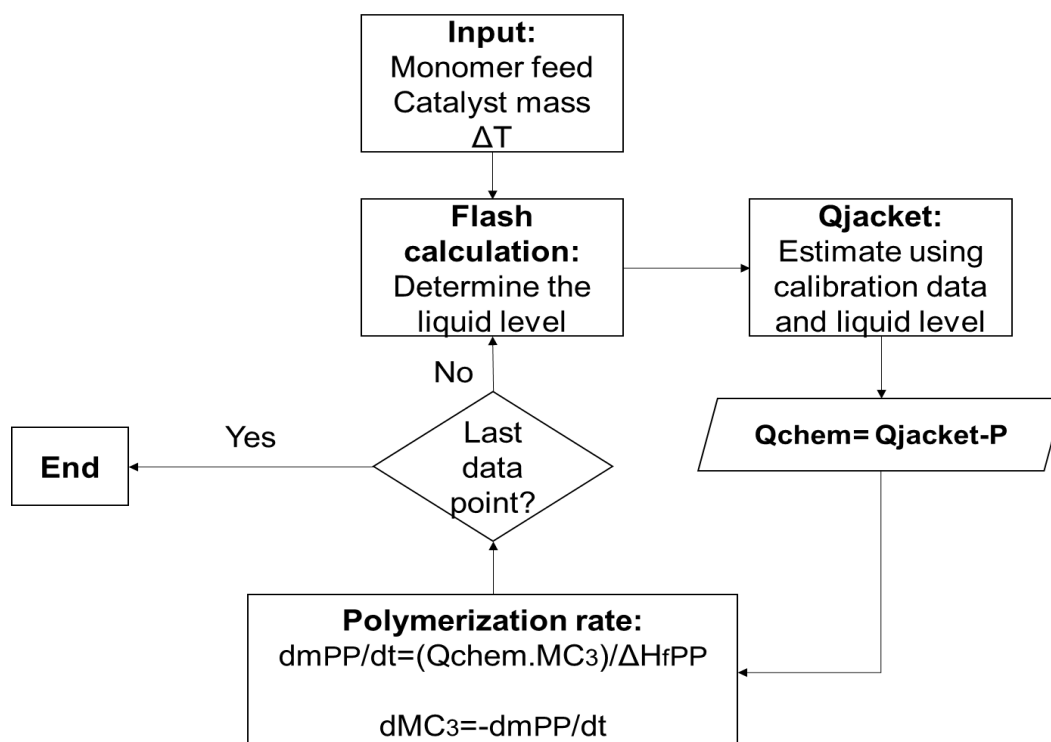


Figure 23. Algorithm for the online processor, estimating the heat flow to the jacket, calculating the chemical heat flow, estimating rate of production, repeating flash calculations, and updating the baseline heat flow

The program continues in this order until the last data point is obtained. The software sensor is programmed in a separate MATLAB procedure, which calls, the data acquired by Agilent software recording the power compensation calorimeter input. The online software-sensor provides a non-linear baseline correction for the heat flow to the jacket, based on the kinetics of the corresponding experiment. An example can be seen in figure 24.

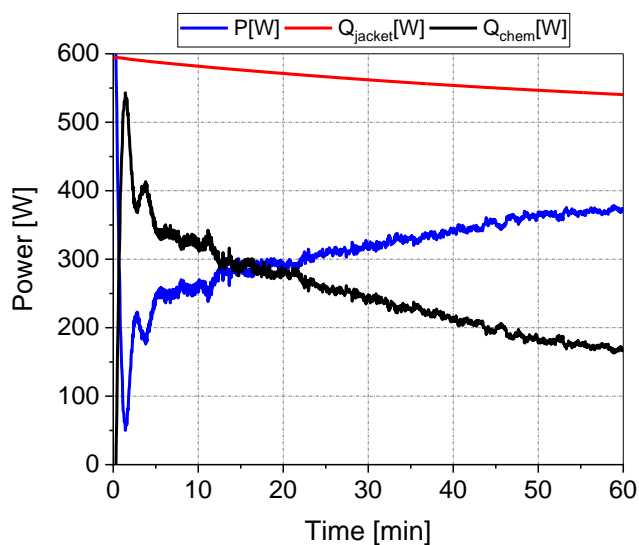


Figure 24. A typical curve showing the power provided by the internal heater, heat flow to the jacket and the chemical heat flow.

4.5 Reaction conditions and experimental plan

In the experimental study, the influence of hydrogen concentration, as well as catalyst injection conditions (pre-contacting) on homo-polymerization kinetics of two different Ziegler-Natta type catalysts has been studied (catalysts A, and catalyst C). In addition to homo-polymerization experiments the influence of comonomer composition on copolymerization kinetics of both catalysts has been investigated.

The amount of TEA for all experiments was kept fixed at 216 [mmol], and thus the Ti/Al ratio varied between 400 to 600 [mol/mol] based on the catalyst amount used. The donor amount has been adjusted for each experiment to keep a constant Si/Ti ratio of 10 [mol/mol].

Hydrogen response was studied by varying the hydrogen amount used in homo-polymerization reactions between 0-15 liters in normal conditions [NI] which corresponds to 0 to 1.8 [mol%] of hydrogen in the feed. Moreover, the influence of pre-contacting on homo-polymerization kinetics has been investigated, herein pre-contacting of catalyst and cocatalyst was carried out at room temperature and without mixing, prior to polymerization, the duration of pre-contacting was varied (0 to 300 [s]).

In the multi-stage copolymerization runs the initial homo-polymerization stage conditions were kept fixed at standard conditions (1.0 [mol%] H₂ and 10 [min] of pre-polymerization and 10 [s] pre-contact). The amount of ethylene in the copolymer was varied from 27 to 60 [mol%] ethylene in rubber (x_{C2}), which corresponds to 11 to 30 [mol%] ethylene in the gas mixture in the reactor (y_{C2}), to observe the resulting effect on copolymerization kinetics.

The experimental conditions of polymerization experiments, in this study are summarized in the following table:

| Factor studied | Variation range | Experiment type | Reaction Temperature [°C] | Si/Ti [mol/mol] | Al/Ti [mol/mol] |
|--------------------|-----------------------------|---------------------|---------------------------|-----------------|-----------------|
| Hydrogen response | 0-1.8 [mol%] H ₂ | Homo-polymerization | 75 | 10 | ~400 |
| Pre-contact time | 0~300 [s] | Homo-polymerization | 75 | 10 | ~400 |
| Ethylene in rubber | 27~60 [mol%] | Copolymerization | 75 | 10 | ~400 |

Table 6. Experimental plan for polymerization experiments; catalyst A and catalyst C

4.6 Sample characterization

4.6.1 Melt mass flow rate indexer

Molecular weight of polypropylene can be measured using high temperature gel permeation chromatography [137]. A less sophisticated and well-known technic used to compare the molecular weights of polyolefins is melt flow rate (MFR). A polymer with higher molecular weight will naturally have a lower melt flow rate, an experimental correlation between MFR and weight average molecular weight (M_w) [kg/mol] of Homo-polypropylene is proposed by Bremner [138]

$$M_{w,hp}[\text{kg/mol}] = 538.445 [MFR_{hp}]^{-0.249} \quad 4.6$$

In this work, the MFR method has been used to compare molecular weights of different reaction products. Measurements have been carried out using the CSI-127 MF micro-melt flow indexer. The measurements were performed under 230 [°C], using the standard weight of 2.16 [kg].

The measuring result of this μ -MFR is given in form of time, which is required for the melted polymer to press through the die for a specific distance. The time measured is converted into MFR value using the following experimental calibration equation:

$$MFR_{[2.16]} = 517[\text{time}]^{-1.115} \quad 4.7$$

The calibration equation has been established by measuring the flow time of polymer samples with known molecular weights and melt flow rate provided by the industrial partner of this project.

4.6.2 Porosity measurement

Porosity of the polymer samples has been measured at the industrial chemistry department of Martin-Luther University, Halle-Wittenberg. The measurements were carried out using a Pascal-140 porosimeter (Thermo Finnigan) the porosity reported in this work is calculated by combining measurements in low pressures (up to 400 [kPa]) with high pressure measurements (up to 400 [Mpa]). The porosity data conveys information about the morphology of the polymer powders produced by different polymerization conditions and materials composition.

4.6.3 Particle size distribution

In this research sieve grading technic has been used to measure particle size distribution of samples produced in different conditions (homo-polymer and copolymer). A Retsch vibratory sieve shaker (AS 200 digit) polymer with a sieve size range of 100 to 5000 microns has been used with an amplitude of 60 [1/s] for 10 minutes to determine the particle size distribution of polymer samples. Around 300 [g] of the product were used for each measurement. The measurements were carried out at the industrial chemistry department of Martin-Luther University, Halle-Wittenberg.

4.6.4 Bulk density

Bulk density of a powder is defined as its mass divided by the volume occupied by the powder. This volume includes the spaces between the particles. The results of bulk density measurements depend strongly on the packing method. In this work, tapped bulk density of the powder products has been measured and reported. The polymer was packed in a volumetric cylinder, the aerated sample was tapped, and the mass packed into the specific volume (20 [ml]) was measured on a laboratory balance. This measurement has been repeated at least five times to ensure reproducibility.

$$\rho_{bulk} = \frac{m_p}{V_{cylinder}} \quad 4.8$$

4.6.5 Test of crystallinity

Scanning differential calorimetry has been used to determine the degree of crystallinity of polymers produced in this work. A "NETZSCH DSC 204F1 Phoenix" device has been used. About 6 [mg] of each sample were used for each measurement. The sample has been heated up to 200 [°C], with a heating ramp of 10 [K/min]. The measurements have been carried out at the polymer chemistry research group of Martin-Luther University of Halle-Wittenberg. The area under the curve of the first heating ramp has been used to calculate the degree of crystallinity. The first heating ramp has been chosen because this resembles more the conditions of the polymer powder in the reactor. In contrast, for characterization of final polymer pellets, often the 2nd melting peak is analyzed. To calculate the crystallinity from the DSC curves the area under the curve for the first heating ramp is considered and divided by the melting Enthalpy of 100% crystalline PP ($\Delta H^0=207$ j/g) [139]:

$$X_{cr} = \frac{\Delta H_m}{\Delta H_{m(100\%)}} * 100 \text{ [Mass\%]}$$

4.9

4.6.6 Microscopy

Morphology of the polymer particles produced in this work has been studied by means of scanning electron microscopy. "XL 30 ESEM-FEG" electron microscope device has been used at the evolution biology department of Martin-Luther university. The polymer powder has been placed on the double-sided tape, and was coated by gold sputtering, to make the sample visible to electron beams in the microscopy setup. The coating was done using PECS system and had a thickness of between 20 to 30 Nanometers. The samples have been analyzed under high vacuum (10^{-6} [mbar]), and measurements were performed at 1.2 [kV].

4.6.7 Polymer fractionation and measurement of intrinsic viscosity

Polymer fractionation (fractionation of matrix and rubber material) using boiling xylene has been carried out at laboratories of the industrial partner of this project. In order to estimate the molecular weight of the rubber phase copolymer, intrinsic viscosity of the copolymer rubber fraction of the samples has been determined using a capillary method.

4.6.8 FTIR measurements

Fourier transform infrared spectroscopy (FTIR) measurements have been carried out at laboratories of the industrial partner of this project. All FTIR spectra were recorded on a Brucker "Tensor 27 ATR FT-IR" device. Using hot pressed films with thickness of about 600 microns, the measurements have been carried out aiming to determine the fraction of ethylene in copolymer samples.

5 Experimental study of propylene polymerization kinetics, with two different Ziegler-Natta type catalysts

In this chapter, the experimental results of the bulk-phase homo-polymerizations and multi-staged copolymerizations are presented. The influence of the different reaction conditions on catalyst activity, the activity profiles and the resulting product's properties are discussed for

both catalysts. The experimental observations are adopted for the derivation of the reaction kinetic model presented in chapter 7.

5.1 Performance of the calorimeter setup

In polymerization reactions of propylene, the relationship between the chemical heat flow and polymerization rate is given as:

$$\dot{Q}_{chem} = R_p V_R (-\Delta H_{fPP}) \quad 5.1$$

Activity of the catalyst at any given moment of the homo-polymerization reaction (t) can be written as:

$$Activity(t) \left[\frac{kg}{g \text{ Cat} \cdot hr} \right] = \frac{m_p}{m_{cat} t} = \frac{V_R R_p M_{wC3}}{m_{cat}} = \frac{\dot{Q}_{chem} M_{wC3}}{m_{cat} (-\Delta H_{fPP})} * 3.6 \left[\frac{s \text{ kg}}{hr \text{ g}} \right] \quad 5.2$$

$Activity(t) \left[\frac{kg}{g \text{ Cat} \cdot hr} \right]$ is the mass of polymer produced per gram of catalyst during each hour of polymerization, M_{wC3} [g/mol] is the molar mass of the monomer (propylene in case of homo-polymerization experiments), m_{cat} [g] represents the amount of catalyst used in the polymerization experiment, and ΔH_{fPP} is the enthalpy of formation of polypropylene, which has a value of $\Delta H_{fPP} = -84000$ [J/mol] [14] [140] in case of polypropylene produced in bulk phase. As was described in section 4.4, the chemical heat flow of propylene polymerization is measured by power compensation calorimetry method, through the procedure depicted in figure 23. The chemical heat flow can be converted to activity by equation 5.2. By plotting the current activity over reaction time, the activity profile of a polymerization reaction is established.

A typical activity profile obtained by calorimetric measurements and calculated by equation 5.2 is depicted in figure 25. The standard polymerization procedure consists of a 10-minute pre-polymerization step followed by ~8 minutes of heat up, wherein the reactor temperature is raised after the pre-polymerization stage to 75 [°C]. The calorimetric measurements from the moment that the system reaches the desired reaction temperature (75 [°C]) are used to establish the activity profiles. The system requires typically less than 5 minutes to stabilize, and achieve constant reaction temperature, therefore the first 2 to 3 minutes (marked in green in the plot) in the activity profiles do not convey significant kinetical information and are affected by the control unit stabilizing the temperature.

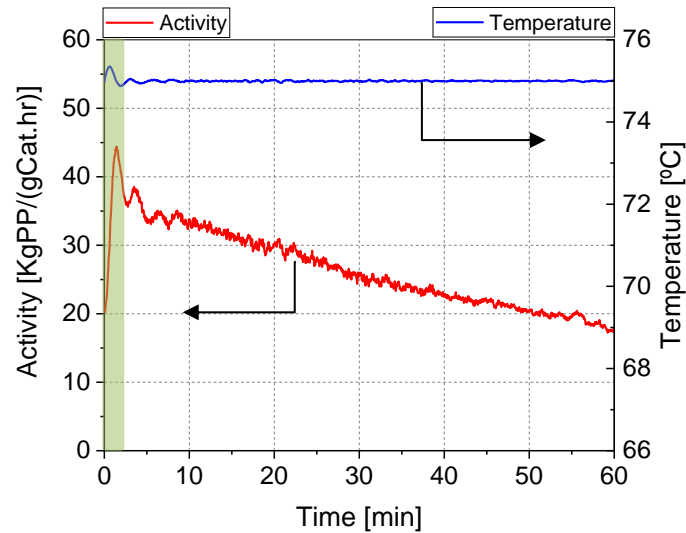


Figure 25. Typical activity profile; Cat A; T=75 [°C], H₂=1 [mol%], 10 [min] pre-polymerization, 10 [s] pre-contact
 The total production of polypropylene during the homo-polymerization can be calculated by integrating the chemical heat flow over reaction time.

$$m_{hp}[kg] = \frac{M_{wC3}(\int_0^t \dot{Q}_{chem})}{\Delta H_{fPP} 1000 [\frac{g}{kg}]} \quad 5.3$$

The accuracy of the data obtained by the calorimeter, can be validated by comparing the predicted yield by equation 5.3, with the actual yield at the end of the polymerization by means of weighing the product. As depicted in the parity diagram in figure 26, by using the data provided by the outlined calorimeter setup and the online software-sensor, one can predict the polymerization yield with an acceptable accuracy (typically well below 10% error). Possible sources of error can be:

1. Production during the pre-polymerization and heat-up stages is the main source of error. This value must be estimated by separate experiments and cannot be directly measured during the polymerization experiments.
2. Possible error in calibration measurements of the calorimeter setup: reproducibility of the calibration measurements is checked and an error range of below 4% (in figure 22) is observed.
3. Any vortex created by stirring is neglected. Formation of a vortex can lead to changes in the heat transfer area and might lead to errors in estimation of the heat flow to the reactor jacket.

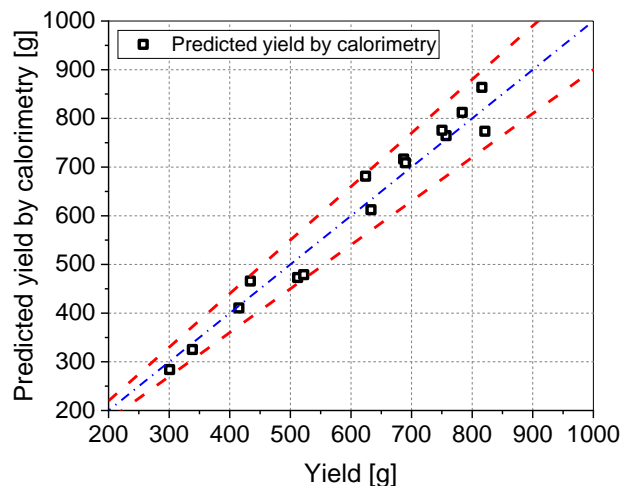


Figure 26. Validation of calorimetric measurements; Comparison experimental and calculated yield bulk phase polymerizations; $T=75$ [°C], $H_2=0-1$ [mol%], dashed lines represent a 10% error range

In addition to the obtained activity profiles, the overall average activity of polymerization experiments is used as a quantity to compare the influence of the different reaction conditions on the polymerization results, defined as:

$$Activity \left[\frac{kgPP}{gCat.hr} \right] = \frac{Yield[kg]}{m_{cat}[g]t_{poly}[hr]} \quad 5.4$$

Experimentally, the average activity of a polymerization run is calculated via equation 5.4 starting from the final yield. In This equation the term $Yield$ [kg] indicates the polymer mass weighted at the end of polymerization run, m_{cat} [g] is the catalyst mass used, and t_{poly} [hr] indicates the polymerization time and does not include the pre-polymerization and heat-up stage times.

5.2 Test of reproducibility

Standard homo-polymerization experiments for catalysts A and C have been performed to establish reproducibility of the polymerization procedure and catalyst activity. Standard reaction conditions are listed in the following table 7:

| Reaction conditions | Pre-polymerization temperature | Polymerization temperature | Polymerization time | Stirrer speed |
|---------------------|------------------------------------|----------------------------|---------------------|---------------|
| Range | 25 [°C] (Cat A) 15 [°C] (Cat C) | 75 [°C] | 60 [min] | 100 [rpm] |

Table 7. Reaction condition for standard homo-polymerization experiments for both catalysts, used for establishing reproducibility

The standard polymerization recipe for both catalysts is listed in the following table 8:

| Catalyst | TEA | Hydrogen feed concentration | propylene | Donor nature | Pre-contact time | Si/Ti |
|-------------------------------------------|------------|----------------------------------|-----------------|--------------|------------------|--------------|
| Cat A ~ 18 [mg] suspended in 1[ml] Hexane | 1.9 [mmol] | 1 [mol%] (≈ 10 [NI]) | ~ 1.5 [kg] | C-Donor | 10 [s] | 10 [mol/mol] |
| Cat C ~ 10 [mg] suspended in 1[ml] Hexane | 1.9 [mmol] | 1 [mol%] (≈ 10 [NI]) | ~ 1.5 [kg] | C-Donor | 10 [s] | 10 [mol/mol] |

Table 8. Reaction Recipe for standard homo-polymerization experiments for both catalysts, used for establishing reproducibility

The reproducibility of the polymerization procedure has been established for both catalysts by repeating the standard polymerization enough times, wherein the overall average activity as well as activity profiles over the course of polymerization are within an acceptable margin of error (below 10%). It is noteworthy that catalyst C shows much higher activity in similar conditions. In figure 27 the average overall activity for five repetitions of standard polymerization for both catalysts are presented. The statistics of these standard polymerizations for both catalysts are displayed in the following table:

| Catalyst | Mean activity [KgPP/(gCat.hr)] | Number of runs | Standard deviation [KgPP/(gCat.hr)] | Coefficient of variation |
|--------------|--------------------------------|----------------|-------------------------------------|--------------------------|
| Cat A | 35.08 | 5 | 1.09 | 3.11 |
| Cat C | 72.58 | 5 | 2.42 | 3.33 |

Table 9. Statistics; reproducibility of standard homo-polymerization conditions

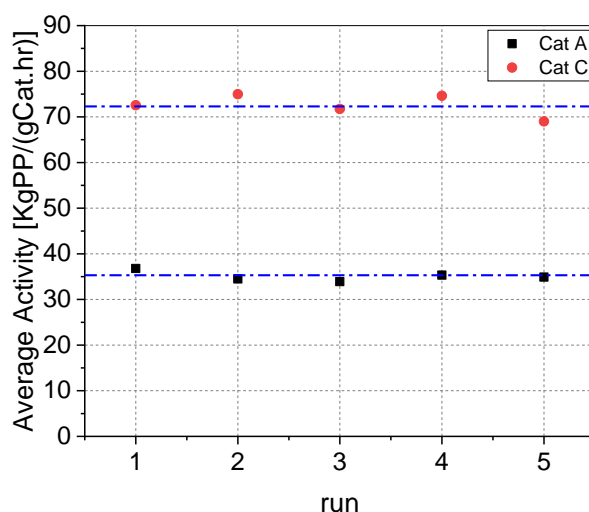


Figure 27. Reproducibility of the homo-polymerization average activity; Cat A vs Cat C; T=75 [°C], H₂=1 [mol%], 10 [min] pre-polymerization, 10 [s] pre-contact

The activity profiles of the standard polymerizations show acceptable reproducibility for both catalysts and are presented in figure 28. A significant difference between the activity levels of catalyst A and catalyst C is observed. Catalyst C shows nearly double initial activity:

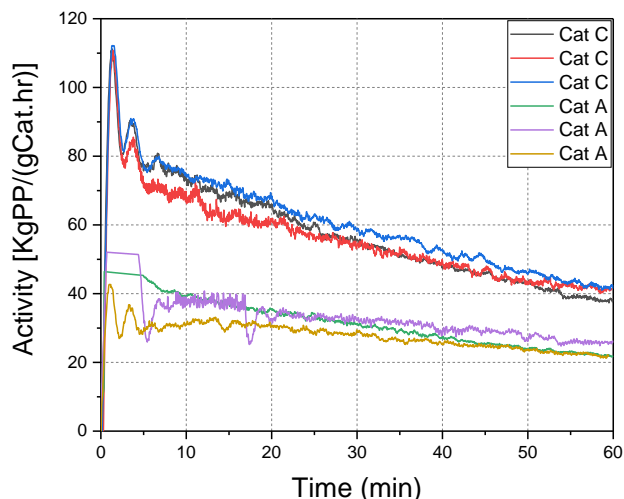


Figure 28. Reproducibility of the homo-polymerization activity profiles; Cat A vs Cat C; T=75 [°C], H₂=1 [mol%], 10 [min] pre-polymerization, 10 [s] pre-contact

In a typical homo-polymerization of propylene with Ziegler-Natta catalysts, a decline in activity is always observed. This decline is due to deactivation of active centers of the catalyst and is inevitable. Normalized activity profiles of standard experiments for both catalysts A and C are compared in figure 29:

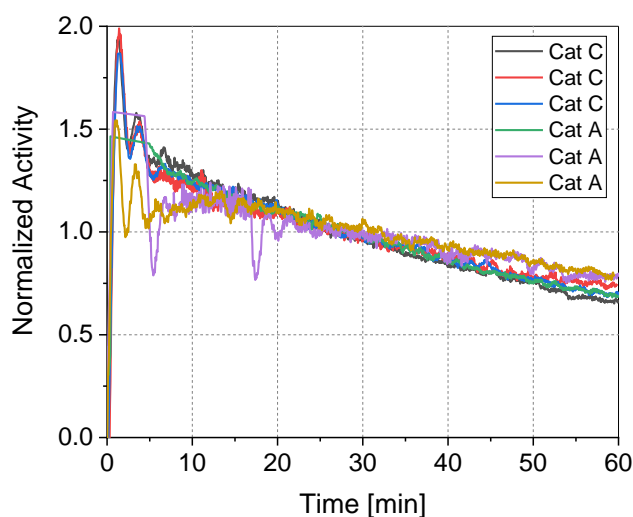


Figure 29. Normalized activity profiles; Cat A vs Cat C; T=75 [°C], H₂=1 [mol%], 10 [min] pre-polymerization, 10 [s] pre-contact

Despite the disparity between the activity levels of the two catalysts, the normalized activity profiles look similar. This indicates a similarity in the deactivation behavior of the two catalysts.

5.3 Hydrogen response

As described in chapter 2.2, hydrogen is used as chain transfer agent in coordination polymerizations of propylene. The transfer reaction to hydrogen controls the kinetic chain length and thus molecular weight of the polymer product. A known effect of hydrogen on propylene polymerizations is increasing polymerization rate and thus the activity of the catalyst. To study the effect of hydrogen on the polymerization kinetics of the catalysts used in this work, polymerization experiments following the polymerization procedure described in chapter 4.3.2 have been performed, wherein the amount of hydrogen in the feed has been varied. The polymerizations were carried out with an in-situ pre-polymerization at 25 [°C] (15 [°C] in case of catalyst C) for 10 minutes followed by a heat-up stage, and main polymerization at 75 [°C] for one hour. Hydrogen has been fed into the empty reactor before filling the reactor with liquid propylene, the amount of hydrogen has been varied between 0 to 1.8 [mol%] in the feed (mol H₂/mol feed). The reaction conditions and the polymerization recipe for studying the hydrogen response are listed in table 10 and 11.

| Reaction conditions | Pre-polymerization temperature | Polymerization temperature | Polymerization time | Stirrer speed |
|---------------------|------------------------------------|----------------------------|---------------------|---------------|
| Range | 25 [°C] (Cat A) 15 [°C] (Cat C) | 75 [°C] | 60 [min] | 100 [rpm] |

Table 10. Reaction condition for studying hydrogen response

| Catalyst | TEA | hydrogen feed concentration | propylene | Donor nature | Pre-contact time | Si/Ti |
|-------------------------------------------------|---------------|-----------------------------|-----------|--------------|------------------|-----------------|
| Cat A ~ 18 [mg] suspended in 1[ml] Hexane | 1.9 [mmol] | 0-1.8 [mol%] | ~1.5 [kg] | C- Donor | 10 [s] | 10 [mol/mol] |
| Cat C ~ 10 [mg] suspended in 1[ml] Hexane | 1.9 [mmol] | 0-1.8 [mol%] | ~1.5 [kg] | C- Donor | 10 [s] | 10 [mol/mol] |

Table 11. Reaction recipe for studying hydrogen response

The influence of hydrogen on the average activity of the homo-polymerizations of catalyst A is depicted in the following figure:

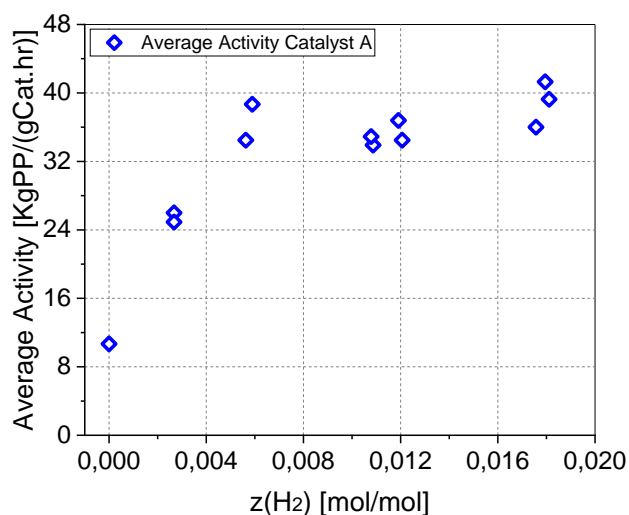


Figure 30. Hydrogen response; Cat A; T=75 [°C], H₂=0-1.8 [mol%], 10 [min] pre-polymerization, 10 [s] pre-contact
 As seen in figure 30, polymerization with no hydrogen shows around only 25% of the maximum activity of catalyst A in these conditions (about 10 [kgPP/(gCat.hr)]). By increasing the hydrogen fraction in the feed to around 0.5 [mol%] the catalyst average activity increases and reaches a plateau (about 40 [kgPP/(gCat.hr)] maximum activity) thereafter. Further increase in hydrogen fraction in the feed does not result in a significant increase in activity.

The activity profiles obtained by polymerization of catalyst A and various hydrogen amounts are plotted in figure 31. As expected, the polymerization without hydrogen shows the lowest activity during the course of reaction, and by an increase in hydrogen amount the overall activity increases and reaches a plateau.

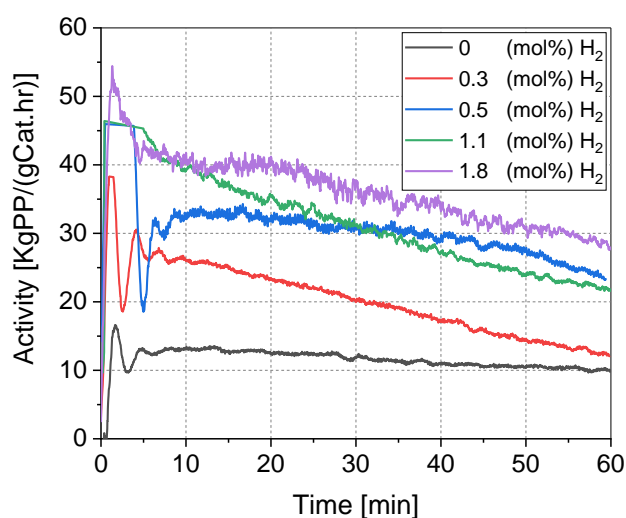


Figure 31. Hydrogen response activity profiles; Cat A; T=75 [°C], H₂=0-1.8 [mol%] (0-15 [NI]), 10 [min] pre-polymerization, 10 [s] pre-contact

To study the influence of hydrogen concentration on the deactivation behavior of catalyst A during the one-hour course of polymerization, the activity profiles have been normalized and plotted in the following figure 32:

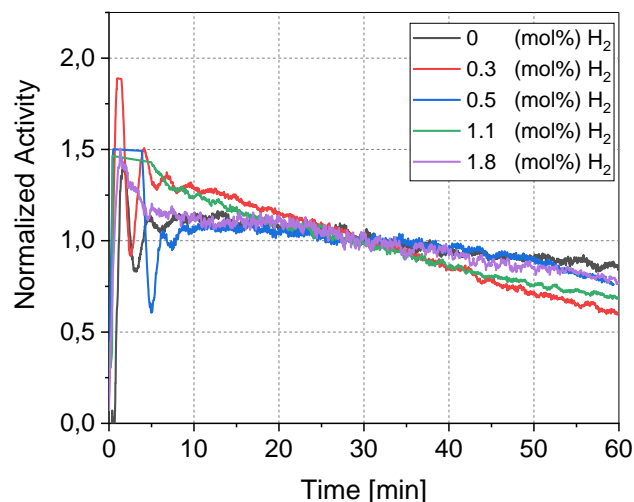


Figure 32. Hydrogen response normalized activity profiles; Cat A; T=75 [°C], H₂=0-1.8 [mol%] (0-15 [NI]), 10 [min] pre-polymerization, 10 [s] pre-contact

The normalized profiles have relatively similar slopes and the slight differences do not convey significant kinetical information. Therefore, it can be concluded that hydrogen does not influence the deactivation behavior of catalyst A in a significant manner.

To investigate the effect of hydrogen on the molecular weight of the homo-polymer products, the melt flow rate of the samples has been measured according to the method described in chapter 4.6.1. The following figure 33 shows the melt flow rate results of the samples produced with a range of hydrogen used in the homo-polymerization process regarding mole fraction of hydrogen in the feed. The samples produced without any hydrogen display extremely low MFR values (about 0.3 [g/10min]).

The MFR values increase with the rise in the hydrogen fraction in the feed, which corresponds to a decrease in the molecular weight of the product. For the samples produced with 1.8 [mol%] in the feed, MFR values of over 100 [g/10min] have been measured. Values of weight average molecular weight have been calculated according to equation 4.6 and are depicted in figure 34. M_w decreases from around 830 [kg/mol] corresponding to experiments performed without presence of hydrogen, down to 175 [kg/mol] for higher hydrogen amounts.

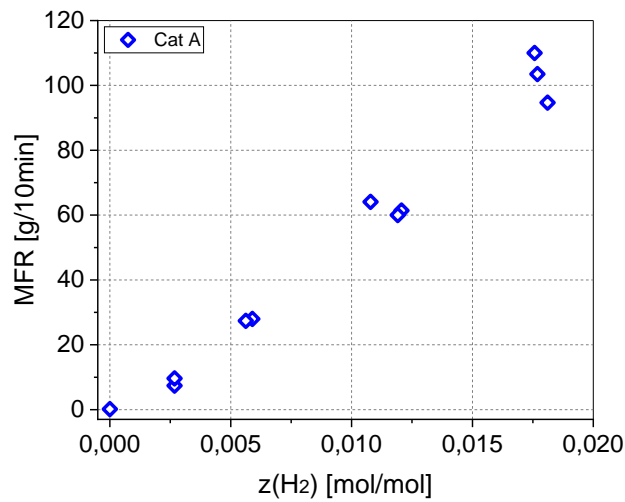


Figure 33. Homo-polymer MFR; Cat A; T=75 [°C], H₂=0-1.8 [mol%], 10 [min] pre-polymerization, 10 [s] pre-contact

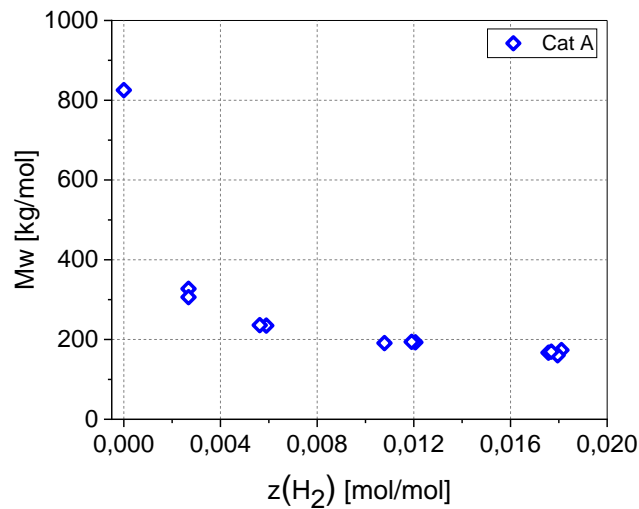


Figure 34. Homo-polymer weight average molecular weight; Cat A; T=75 [°C], H₂=0-1.8 [mol%], 10 [min] pre-polymerization, 10 [s] pre-contact

The hydrogen variation experiments were performed for catalyst C as well. Variation of the total amount of hydrogen from 0 to 1.8 [mol%] in the feed leads to an increase in activity from about 20 [kgPP/(gCat.hr)] corresponding to experiment without hydrogen up to maximum 78 [kgPP/(gCat.hr)] for experiments with 0.5 [mol%] hydrogen in the feed. As expected, after a rise in activity, a plateau is reached. Overall, catalyst C always shows higher activity levels compared to catalyst A. Average activity of the two catalysts are compared in figure 35 for different hydrogen mole fractions in the feed:

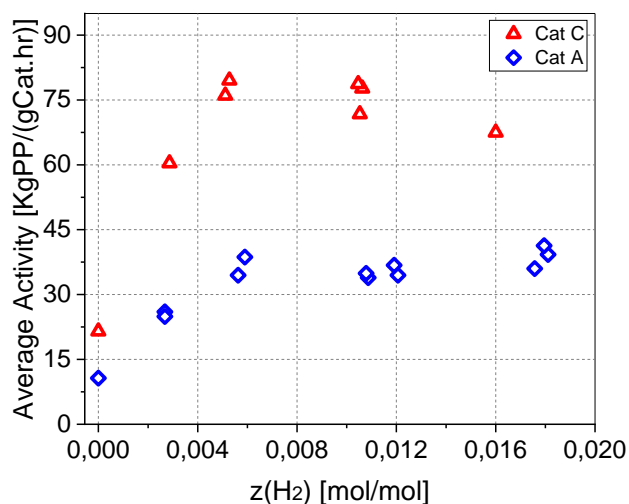


Figure 35. Hydrogen response; Cat A vs Cat C; T=75 [°C], H₂=0-1.8 [mol%], 10 [min] pre-polymerization, 10 [s] pre-contact

Activity profiles of catalyst C are depicted in the following graph. As expected, the experiment with no hydrogen displays the lowest activity level. Activity increases for experiments with higher hydrogen and reaches a plateau with presence of 0.5 [mol%] in the feed:

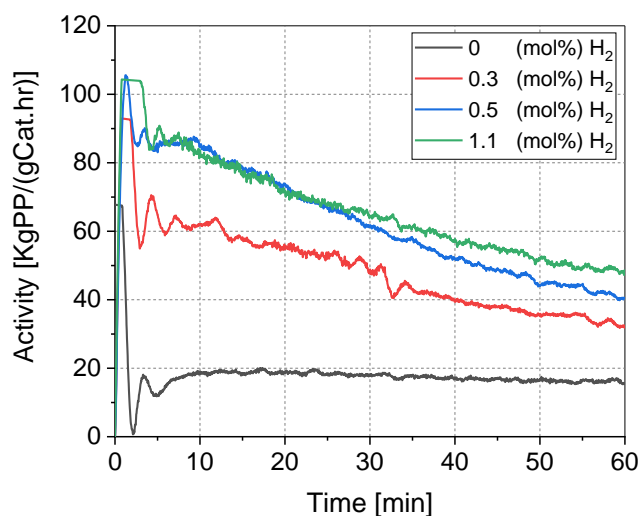


Figure 36. Hydrogen response; activity profiles; Cat C; T=75 [°C], H₂=0-1.1 [mol%] (0-10 [NI]), 10 [min] pre-polymerization, 10 [s] pre-contact

To compare the deactivation behavior of experiments with different hydrogen concentration, the normalized activity profiles of catalyst C, are compared in figure 37:

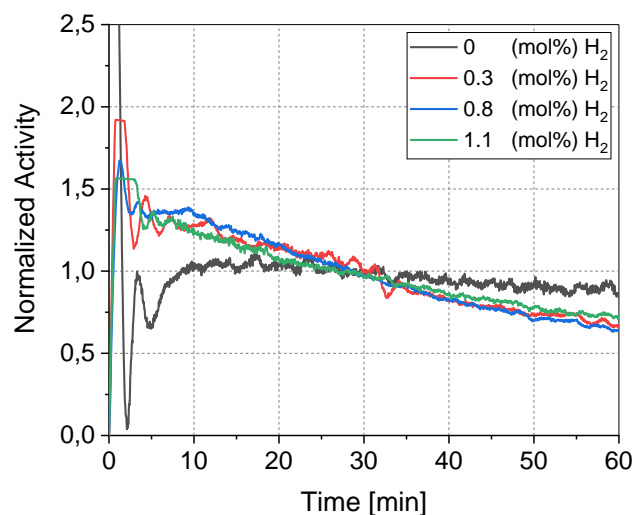


Figure 37. Hydrogen response; Normalized activity profiles; Cat C; T=75 [°C], H₂=0-1.1 [mol%] (0-10 [NI]), 10 [min] pre-polymerization, 10 [s] pre-contact

Experiments show similar deactivation behavior except for the experiment without presence of hydrogen, where the deactivation occurs with a milder slope. Melt flow rate of the samples produced by both catalysts using different hydrogen mole fractions in the feed are plotted in figure 38. Melt flow rates of both catalysts follow a similar trend. The weight average molecular weight of synthesized samples by both catalysts are compared in figure 39, and as is apparent by the MFR values, samples produced by both catalysts display similar molecular weights in standard polymerization conditions range.

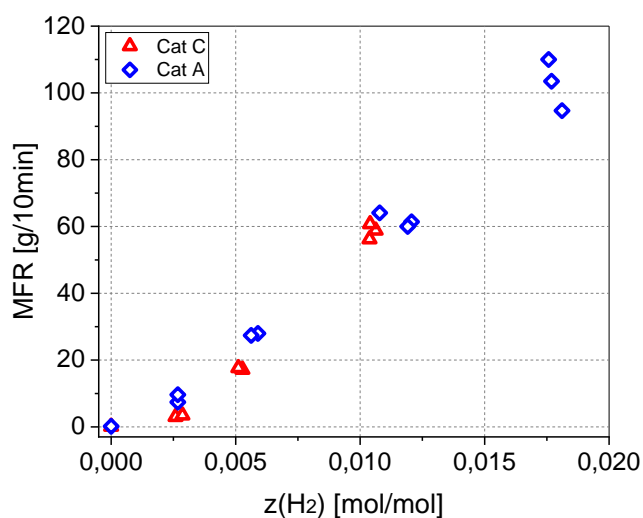


Figure 38. Homo-polymer MFR; Cat A vs Cat C; T=75 [°C], H₂=0-1.8 [mol%], 10 [min] pre-polymerization, 10 [s] pre-contact

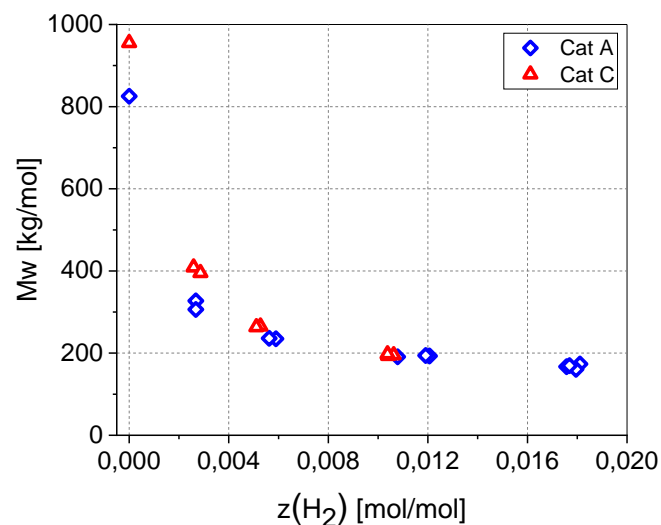


Figure 39. Homo-polymer weight average molecular weight; Cat A vs Cat C; T=75 [°C], H₂=0-1.8 [mol%], 10 [min] pre-polymerization, 10 [s] pre-contact

5.4 Influence of pre-contacting

Influence of pre-contacting on kinetics of homo-polymerization of propylene has been studied for both catalysts. Pre-contacting has been carried out prior to polymerization between catalyst and cocatalyst in the injection feeder at room temperature and without any agitation, as described in chapter 4.3.2. The duration of contact between catalyst and TEA has been varied between 0 to 300 seconds. Homo-polymerization has been carried out in otherwise standards conditions and procedure. Homo-polymerization recipe and conditions for both catalysts used to study the influence of pre-contacting are listed in tables 12 and 13:

| Reaction conditions | Pre-polymerization temperature | Polymerization temperature | Polymerization time | Stirrer speed |
|---------------------|------------------------------------|----------------------------|---------------------|---------------|
| Range | 25 [°C] (Cat A) 15 [°C] (Cat C) | 75 [°C] | 60 [min] | 100 [rpm] |

Table 12. Reaction condition for studying influence of pre-contacting

| Catalyst | TEA | hydrogen feed concentration | propylene | Donor nature | Pre-contact time | Si/Ti |
|-------------------------------------------|------------|-----------------------------|-----------|--------------|------------------|--------------|
| Cat A ~ 18 [mg] suspended in 1[ml] Hexane | 1.9 [mmol] | 1.8 [mol%] | ~1.5 [kg] | C-Donor | 0-300 [s] | 10 [mol/mol] |
| Cat C ~ 10 [mg] suspended in 1[ml] Hexane | 1.9 [mmol] | 1 [mol%] | ~1.5 [kg] | C-Donor | 0-300 [s] | 10 [mol/mol] |

Table 13. Reaction recipe for studying influence of pre-contacting

After one hour of homo-polymerization the resulting overall average activity of catalyst A is depicted in figure 40 with regard to the duration of pre-contact. The polymerization experiments with no pre-contacting show on average, activity levels of around 20 [KgPP/(gCat.hr)], with 10 seconds of pre-contacting activity levels increase to around 40 [KgPP/(gCat.hr)] maximum activity. This indicates that pre-contacting with cocatalyst is of significant importance for activating catalyst A. With increasing the pre-contact time to 60 and further to 300 seconds activity levels decline. With 300 seconds of pre-contacting activity decreases by 25% compared to the optimum pre-contact time, which is assessed to be 10 seconds. This can be attributed to the over reduction of titanium centers of the catalyst by reacting with TEA during the pre-contacting time as described in chapter 2.4.

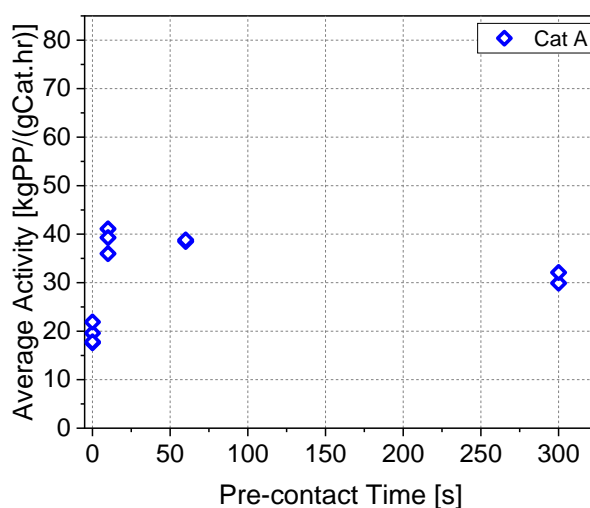


Figure 40. Influence of pre-contacting; homo-polymerization average activity; Cat A; T=75 [°C], H₂=1.8 [mol%], 10 [min] pre-polymerization, pre-contact=0-300 [s]

The activity profiles of catalyst A, resulting from different pre-contact times are depicted in the following figure 41. It is observed that, the experiment with 10 seconds of pre-contact shows the highest activity, and the polymerization run without any pre-contacting (0 seconds) shows the least activity. Pre-contact times of longer than 10 seconds (60, 300 seconds) result in a decline in activity. Based on these results it is concluded that the optimum pre-contact time for catalyst A is 10 seconds.

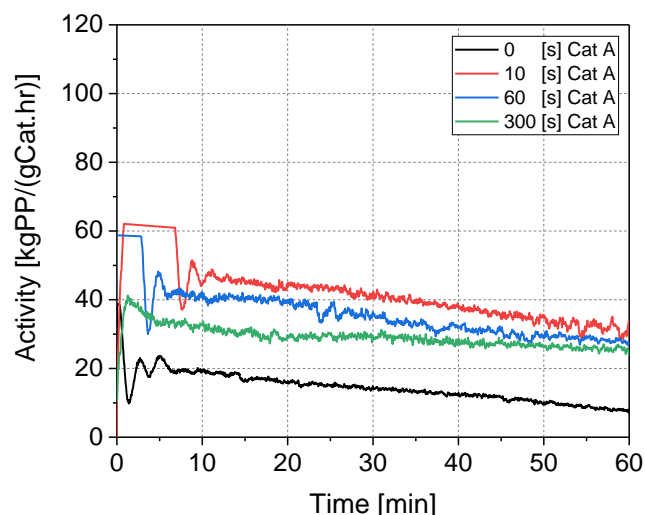


Figure 41. Influence of pre-contacting; homo-polymerization activity profiles; Cat A; T=75 [°C], H₂=1.8 [mol%], 10 [min] pre-polymerization, pre-contact=0-300 [s]

To study the influence of pre-contact time on deactivation behavior of the catalyst, normalized activity profiles of catalyst A are plotted in the following graph:

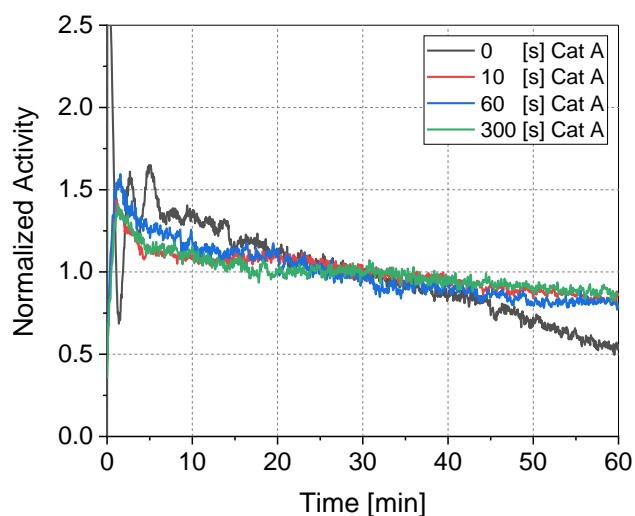


Figure 42. Influence of pre-contacting; Normalized homo-polymerization activity profiles; Cat A; T=75 [°C], H₂=1.8 [mol%], 10 [min] pre-polymerization, pre-contact=0-300 [s]

The normalized activity profiles of the experiments with pre-contacting are similar, except the experiment without pre-contacting, which shows a slightly more rapid deactivation.

For catalyst C, the effect of pre-contacting on average activity has been studied. Results are depicted in the following figure 43. As opposed to catalyst A, it is apparent that pre-contacting does not significantly affect the polymerization kinetics of catalyst C. Catalyst C appears to be activated easily in the reactor, and without any need for activation by pre-contacting prior to injection, since polymerizations without pre-contacting are displaying similar activity levels as

experiments with pre-contact at around 72 [KgPP/(gCat.hr)]. By increasing the pre-contact time, a meaningful decline in activity of catalyst C is not observed and catalyst C displays opposing behavior to catalyst A in this regard as well.

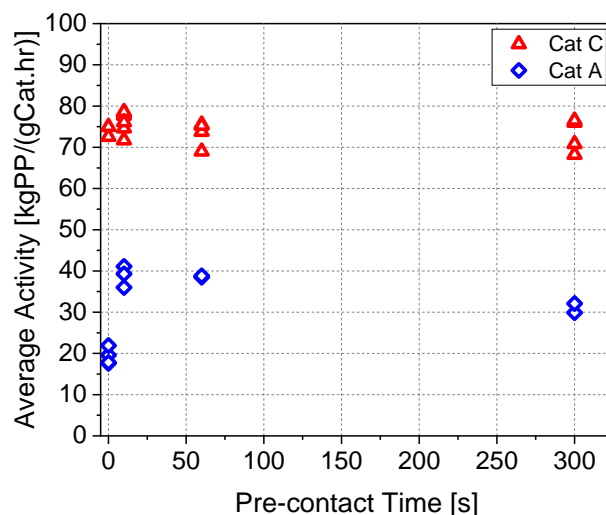


Figure 43. Influence of pre-contacting; homo-polymerization average activity; Cat A vs Cat C; T=75 [°C], H₂=1.8 [mol%] for Cat A, H₂=1.0 [mol%] for Cat C, 10 [min] pre-polymerization, pre-contact=0-300 [s]

Activity profiles of catalyst A and catalyst C with different pre-contact times are compared in figure 44. As opposed to catalyst A, activity profiles of catalyst C are similar for different pre-contacting times, however 10 seconds of pre-contacting still leads to slightly higher activity for catalyst C as well.

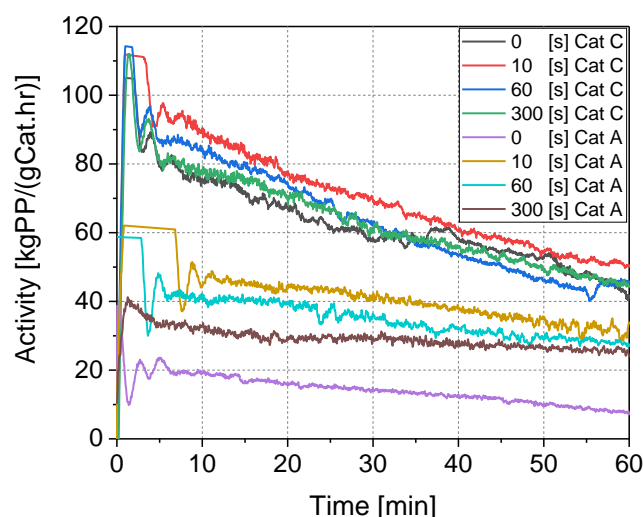


Figure 44. Influence of pre-contacting; homo-polymerization activity profiles; Cat A vs Cat C; T=75 [°C], H₂=1.8 [mol%] for Cat A, H₂=1.0 [mol%] for Cat C, 10 [min] pre-polymerization, pre-contact=0-300 [s]

Normalized activity profiles of catalyst C are similar despite having different pre-contact times. It can be concluded that pre-contacting does not affect the deactivation behavior of catalyst C.

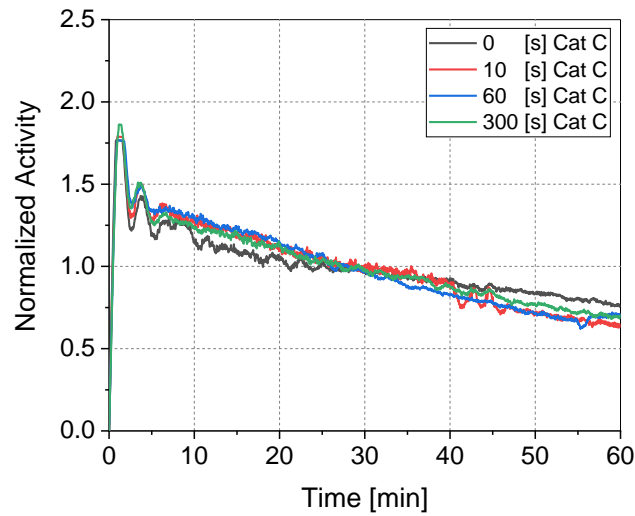


Figure 45. Influence of pre-contacting; normalized homo-polymerization activity profiles; Cat C; T=75 [°C], H₂=1.0 [mol%], 10 [min] pre-polymerization, pre-contact=0-300 [s]

To study the influence of pre-contacting on the molecular weight of final product, melt flow rate of samples produced with different pre-contact times have been measured. In the following graph, MFR is plotted vs pre-contact time. A meaningful trend in MFR of the product with respect to pre-contact time cannot be observed. The observed differences can be attributed to other experimental factors such as slight differences in hydrogen concentration.

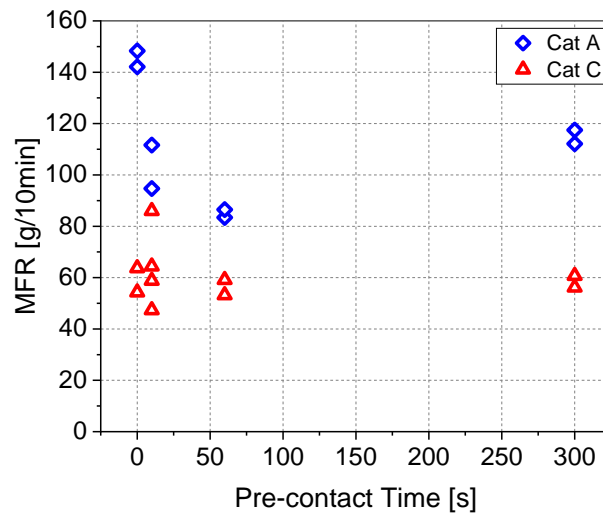


Figure 46. Influence of pre-contacting; product MFR; Cat A vs Cat C; T=75 [°C], H₂=1.8 [mol%] for Cat A, H₂=1.0 [mol%] for Cat C, 10 [min] pre-polymerization, pre-contact=0-300 [s]

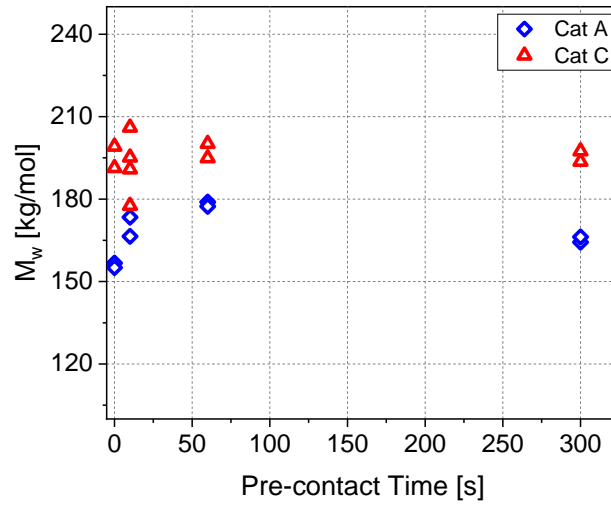


Figure 47. Influence of pre-contacting; product molecular weight; Cat A vs Cat C; T=75 [°C], H₂=1.8 [mol%] for Cat A, H₂=1.0 [mol%] for Cat C, 10 [min] pre-polymerization, pre-contact=0-300 [s]

5.5 Copolymerization experiments

In this section the measurement principle of reaction kinetics during gas phase copolymerization is demonstrated. The outlined combined method of calorimetry during homo-polymerization, and semi-batch operation of reactor during gas-phase copolymerization, is used to compare the kinetics of multi-stage impact-copolymerization for both catalysts.

5.5.1 Kinetic measurement principle

In the gas-phase copolymerization stage, the reaction rate is measured by semi-batch operation of the reactor in a pressure control loop. As long as reaction conditions such as pressure, temperature, and gas composition in the reactor are constant, the mass flow of the components into the reactor is equal to the gross consumption rate of polymerization reaction. During the copolymerization stage, propylene (monomer) and ethylene (comonomer) flow simultaneously into the reactor. The current activity for each specimen is defined as:

$$Activity_{C3}(t) = \frac{\dot{m}_{C3}}{m_{cat}} \left[\frac{kg}{gCat.hr} \right] \quad 5.5$$

$$Activity_{C2}(t) = \frac{\dot{m}_{C2}}{m_{cat}} \left[\frac{kg}{gCat.hr} \right] \quad 5.6$$

Here \dot{m}_{C3} is the mass flow rate of propylene, \dot{m}_{C2} is the mass flow rate of ethylene, and m_{cat} is the catalyst mass used for the polymerization experiment. Overall current reaction activity is thus defined as:

$$Activity(t) = Activity_{C3}(t) + Activity_{C2}(t) \left[\frac{kg}{gCat.hr} \right] \quad 5.7$$

A typical activity profile for a multi-stage impact-copolymerization experiment is depicted in figure 48. In the first hour, homo-polymerization of propylene takes place. The activity profile is obtained by calorimetric measurement outlined in chapter 4. Homo-polymerization is followed by a transition period, wherein the reaction conditions (pressure, gas composition), and reactor control mode is switched to the conditions desired for the gas phase. Once the system reaches steady-state conditions, the activity profile of the copolymerization can be extracted from the mass flow of species into the reactor and equation 5.7 (second half of figure 48).

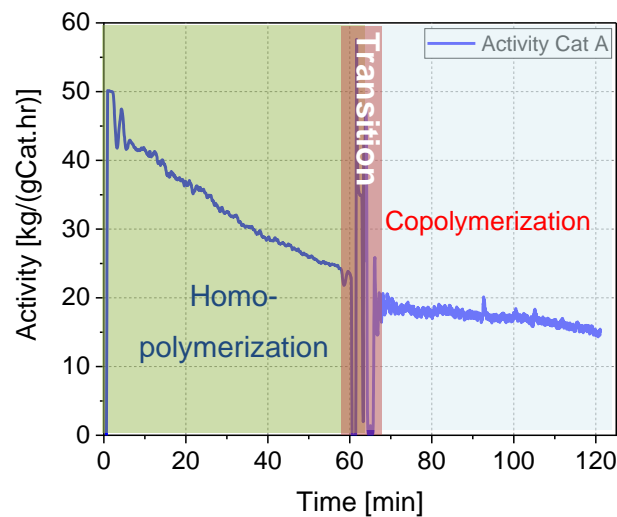


Figure 48. A typical activity profile of a multi-stage impact-copolymerization; Cat A; T=75 [°C], H₂=2.0 [mol%] in gas-phase, 10 [min] pre-polymerization, pre-contact=10 [s]

The overall copolymer production in the gas phase copolymerization stage can be calculated by integrating the mass flow rates of monomer and comonomer over copolymerization reaction time:

$$m_{cp} = \int_0^{t(copo)} (\dot{m}_{C3} + \dot{m}_{C2}) [kg] \quad 5.8$$

The multi-stage impact copolymerization process results in two separate polymer phases of homo-polymer matrix produced in the first stage, and the rubber phase copolymer which is

produced during the subsequent gas-phase stage. The rubber content of the product is a quantity for describing the amount of copolymer rubber relative to the entire product, and is calculated by dividing the copolymer mass by the mass of the entire product:

$$RC = \frac{m_{cp}}{m_{hp} + m_{cp}} * 100 [Mass\%] \quad 5.9$$

It must be noted that, the above-mentioned formula does not consider the polymer produced in the transition period, and therefore this can be a source of error for the kinetic measurement method. In section 5.1 it was demonstrated that the amount of homo-polymer matrix produced (m_{hp}) can be estimated online via calorimetric measurements and equation 5.2. The amount of copolymer rubber produced (m_{cp}) can be calculated online via equation 5.8, therefore the combined kinetic measurement method enables to produce impact copolymers with defined target rubber contents.

The copolymer composition, i.e. ethylene mole fraction in the rubber phase copolymer is calculated by the following equation:

$$xC_2 = \frac{\frac{\dot{m}_{C2}}{M_{wC2}}}{\frac{\dot{m}_{C2}}{M_{wC2}} + \frac{\dot{m}_{C3}}{M_{wC3}}} * 100 [mol\%] \quad 5.10$$

Herein \dot{m}_{C2} , and \dot{m}_{C3} [g/hr] are the average ethylene and propylene mass flow rates into the reactor during the gas-phase copolymerization. The quantity (xC_2) indicates the mole fraction of ethylene in the rubber phase copolymer and is an indication of how ethylene-rich the rubber phase is.

5.5.2 Establishment of reproducibility

For all multi-stage copolymerization experiments the initial homo-polymerization recipe and conditions have been kept fixed at standard homo-polymerization conditions of each catalyst tabulated in table 7 and 8. Therefore, all copolymerization experiments were carried out with 1 [mol%] hydrogen during the homo-polymerization stage. In results presented further in this chapter the hydrogen fraction in reaction recipe refers to the hydrogen mole fraction during the gas-phase copolymerization stage. Copolymerization kinetics of catalysts A and C are compared, and reproducibility has been established in standard copolymerization conditions. In standard copolymerization experiments an hour-long homo-polymerization stage is followed by an hour of gas-phase copolymerization in the conditions presented in table 14.

| Reaction conditions | Range |
|-----------------------------------------|---------------|
| Copolymerization pressure | 14 [bar] |
| Ethylene mole fraction in the gas phase | 17 [mol%] |
| Hydrogen mole fraction in the gas phase | 2 [mol%] |
| Ethylene composition in rubber | ~40 [mol%] |
| Homo-polymerization time | 60 [min] |
| Copolymerization time | 60 [min] |
| Resulting rubber content | 20-30 [mass%] |

Table 14. Standard gas-phase copolymerization conditions used for establishing reproducibility

Reaction pressure in the gas phase has been fixed at 14 [bar] for all experiments, activity profiles of catalyst A and catalyst C in these conditions are displayed in figure 49, As can be seen, outlined procedures is reproducible. As was observed in the kinetic study of homo-polymerizations, catalyst C displays higher activity. This is the case for the gas-phase copolymerization stage as well, where in similar conditions catalyst C displays 60% higher activity compared to catalyst A. Both catalysts show lower copolymerization activity at these conditions compared to homo-polymerization rates. A milder and fairly similar deactivation slope in gas-phase stage compared to bulk phase homo-polymerization stage is observed for catalyst A as well as catalyst C. The different deactivation behavior in the gas-phase reaction, i.e. the milder decline of activity and slight activation by start of the copolymerization might be caused by the increase in the amorphous fraction of the polymer, since the rubber phase copolymer is primarily amorphous.

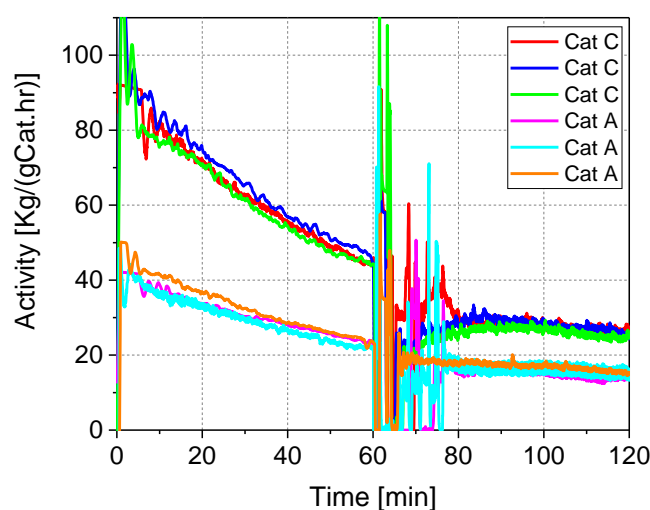


Figure 49. Reproducibility of the multi-stage impact copolymerization activity profiles; Cat A vs Cat C; T=75 [°C], H₂=2 [mol%], P=14 [bar]

The following table includes the statistics regarding the reproducibility of the standard copolymerization experiments:

| Catalyst | Mean gas-phase productivity [KgPP/(gCat)] | Number of runs | Standard deviation [KgPP/(gCat)] | Coefficient of variation |
|----------|-------------------------------------------|----------------|----------------------------------|--------------------------|
| Cat A | 15.12 | 5 | 2.45 | 16.18 |
| Cat C | 24.35 | 5 | 1.41 | 5.77 |

Table 15. Statistics; reproducibility of gas-phase polymerizations

5.5.3 Influence of comonomer composition

Copolymerizations with a range in gas-phase composition in the reactor have been carried out, which naturally result in different ethylene fractions in the resulting rubber phase. Copolymerization conditions to study the influence of monomer/comonomer ratio on copolymerization kinetics are listed in table 16:

| Reaction conditions | Range |
|-------------------------------------|---------------|
| Copolymerization pressure | 14 [bar] |
| Ethylene mole fraction in gas phase | 10-27 [mol%] |
| Hydrogen mole fraction in gas phase | 2 [mol%] |
| Ethylene composition in rubber | 27-59 [mol%] |
| Homo-polymerization time | 60 [min] |
| Copolymerization time | 60 [min] |
| Resulting rubber content | 20-40 [mass%] |

Table 16. Gas-phase copolymerization conditions used for studying the influence of ethylene composition

In order to avoid drifts in gas-phase composition over time, the following control-strategy was followed: The gas-phase composition at the beginning of the copolymerization was adjusted in a way, that consumption by reaction equals the monomers feed flow. This means that the monomer feed ratio between ethylene and propylene was set equal to the desired comonomer incorporation, the feed rates were controlled by the pressure control loop. The gas-phase composition at the beginning of the copolymerization was adjusted that way, that the μ -GC measurements do not show any drift in gas-phase composition throughout the copolymerization experiment.

The ethylene fraction needed in the gas-phase (measured by μ -GC) to achieve a certain ethylene incorporation in the copolymer is plotted in the following figure 50. A similar linear correlation can be established for both catalysts. This linear correlation helps to adjust the gas-

phase composition according to the desired ethylene incorporation in the copolymer. It is observed in figure 50 that ethylene fractions in the gas mixture in the reactor from 10 to 27 [mol%] result in ethylene fractions in the resulting rubber between 27-57 [mol%].

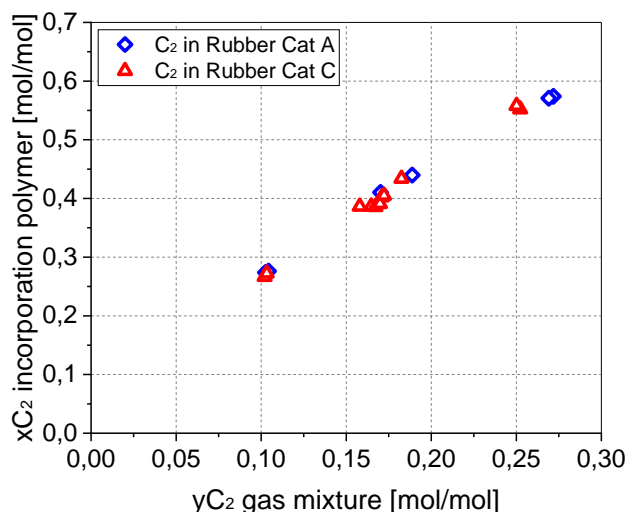


Figure 50. Gas-phase composition vs incorporation in polymer; Cat A vs Cat C; T=75 [°C], H₂=2 [mol%], P=14 [bar], x_{C₂}=27-57 [mol%], y_{C₂}=10-27 [mol%]

The influence of ethylene composition in rubber on the copolymerization activity profiles of catalyst A is depicted in figure 51 (this graph includes only the copolymerization activity profile). By an increase in ethylene composition in rubber, (x_{C₂} from 27 to 59 [mol%]) a boost in the copolymerization activity is observed. This is due to the higher reactivity of ethylene compared to propylene.

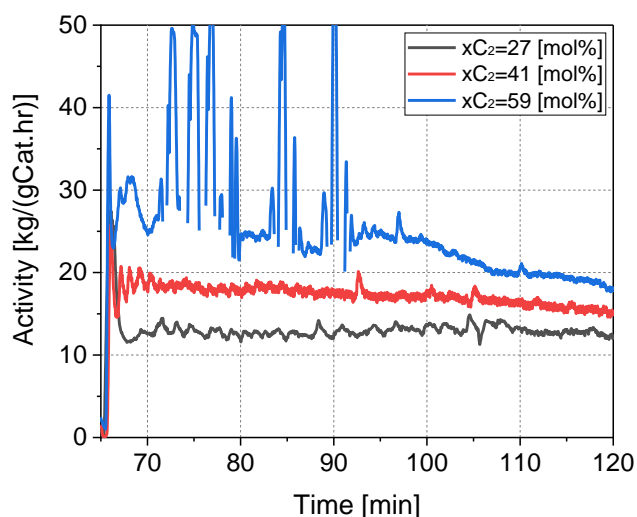


Figure 51. Influence of ethylene composition on copolymerization kinetics; Cat A; T=75 [°C], H₂=2 [mol%], P=14 [bar], x_{C₂}=27-59 [mol%], y_{C₂}=10-27 [mol%]

It has been reported that propylene/ethylene copolymerization rate reaches a peak activity, followed by deactivation [66]. In the experiment with lowest ethylene fraction ($x_{C_2}=27$ [mol%]) the peak activity occurs in a later stage of copolymerization, whereas for higher ethylene compositions peak activity occurs at the beginning of the copolymerization and is followed by deactivation.

Copolymerization activity profiles of catalyst C can be seen in figure 52. By an increase in ethylene composition from 27 to 41 [mol%] activity is increased, however for the highest ethylene composition tested, a sharper deactivation is observed.

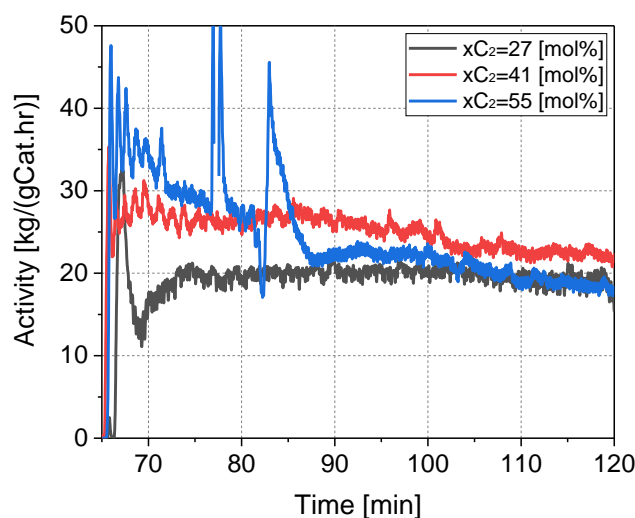


Figure 52. Influence of ethylene composition on copolymerization kinetics; Cat C; $T=75$ [°C], $H_2=2$ [mol%], $P=14$ [bar], $x_{C_2}=27-55$ [mol%], $y_{C_2}=10-27$ [mol%]

5.5.4 Product molecular weight

It was demonstrated in chapter 4.6, that for estimation of the weight average molecular weight of the homo-polymer samples in this study the melt flow rate method has been used. The following relationship between the weight average molecular weight of homo-polypropylene matrix and the resulting MFR is proposed by Bremner [138]:

$$M_{w, hp} = 538.445 [MFR_{hp}]^{-0,249} \quad 5.11$$

Since the hetero-phasic polypropylene impact copolymers, consist of the homo-polymer matrix and the immiscible rubber phase copolymer, final product MFR measured for the impact copolymer samples indicate the melt flow rate of the mixture of the homo-polymer matrix and the rubbery phase.

The final MFR of the impact copolymer sample can be formulated using a logarithmic mixing rule, e.g. using the following equation proposed by Wang and Doshev [141]:

$$\text{Log}(MFR_{Total}) = (1 - RC)\text{Log}(MFR_{hp}) + (RC)\text{Log}(MFR_{EPR}) \quad 5.12$$

In this mixing rule MFR_{Total} indicates the melt flow rate value of the final product including the homo-polymer matrix and the copolymer rubber phase. This value is available by direct measurement of the product MFR. RC [Mass%] is the rubber content and indicates the mass fraction of the rubber phase relative to the entire product (rubber mass plus matrix mass). Rubber content is known by the combined mass balance and calorimetry method of reaction kinetic measurement (equation 5.9).

In copolymerization experiments the homo-polymerization stage has always been carried out with a fixed hydrogen concentration of 1 [mol%] in the feed, therefore the matrix MFR had been fixed at around 57 [g/10min] on average. During the gas-phase copolymerization stage, the hydrogen fraction has been kept fixed for all experiments at 2 [mol%]. In addition to hydrogen concentration, the composition of the copolymer can influence the molecular weight of the rubber as well. Higher ethylene fractions in gas-phase and consequently in the polymer lead to higher molecular weight of the product [142].

Total MFR values of several samples with a fixed amount of hydrogen and ethylene composition in rubber (~40 [mol%]) and rubber contents ranging between 0 to 32 [mass%] are compared figure 53. Homo-polymer products with 0 [Mass%] rubber content have an average MFR value of about 57 [g/10min], this value is the result of the standard homo-polymerization conditions. With higher rubber contents, the MFR levels decline.

Both catalysts display similar behavior in this regard and have comparable MFR results. By fitting the total MFR values of samples with different rubber content using equation 5.12 (green dash line in figure 53) the MFR of the rubber phase can be roughly estimated with extrapolating equation 5.12 to 100 [Mass%] rubber content. It is observed that for this specific ethylene composition in rubber (40 [mol%]) and hydrogen concentration (2 [mol%]), the rubber phase must have an MFR of about 2.2 [g/10min]. This is a rough estimate since the samples might have slightly different ethylene composition or different matrix MFR's.

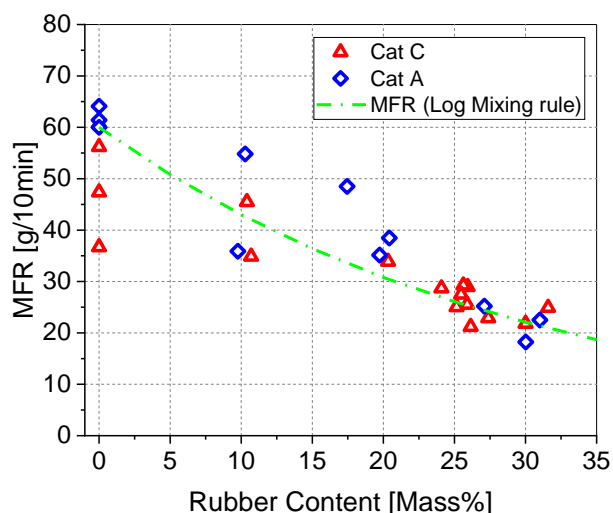


Figure 53. Final MFR; Cat A vs Cat C; rubber content= 0-32 [Mass%], T=75 [°C], H₂=2 [mol%], P=14 [bar], x_{C2}=40 [mol%],

Since the molecular weight of the rubber component cannot be measured directly, the copolymer samples are fractionated using boiling xylene (described in chapter 4.6.7). After fractionation of the copolymer samples, the extracted rubber phase is subjected to the intrinsic viscosity (IV) measurements. Figure 54 displays the IV results with regard to the composition of the rubber phase for samples with rubber content fixed at 20 [Mass%] and ethylene in rubber composition ranging between 30 to 55 [mol%]:

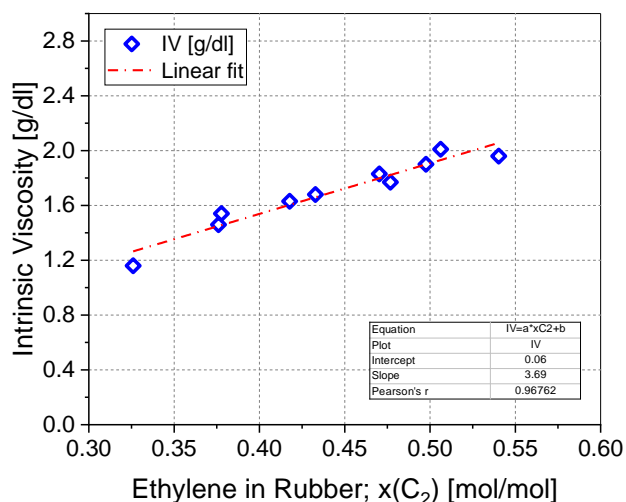


Figure 54. Intrinsic viscosity vs ethylene fraction in rubber; Cat A vs Cat C rubber content= 20 [Mass%], T=75 [°C], H₂=2 [mol%], P=14 [bar], x_{C2}=32-55 [mol%]

With larger fraction of ethylene in rubber, Intrinsic viscosity increases. However, the range of the samples produced in this work is not overly broad and intrinsic viscosity values lie between

1.2 to 2 [g/dl]. A linear fit, results in the following correlation between the intrinsic viscosity and ethylene fraction in rubber:

$$IV_{EPR} \left[\frac{g}{dl} \right] = 3.69 x C_2 + 0.06 \quad 5.13$$

Intrinsic viscosity measurements are an established method for indirect estimation of the molecular weight. The viscosity-average molecular weight M_v and IV are related by the Mark–Houwink equation [143]:

$$IV = K [M_v]^a \quad 5.14$$

The value of viscosity-average molecular weight M_v , lies between number and weight molecular weight averages (M_n, M_w). Constants (K, a) are measured by calibration with homogeneous fractions of the polymer with known molecular weight for specific solvent/temperature conditions, however for polypropylene produced with Ziegler-Natta catalysts, homogeneous fractions are not available and values for (K, a) are empirically determined to correlate with M_n or M_w , such correlations for homo-polypropylene have been proposed by Parrini and by Pasquon [144,145]. In case of propylene/ethylene impact copolymers, in work of Grein [146], after fractionation of copolymer samples, Intrinsic viscosity of the rubber phase has been analyzed and the results coupled with separate GPC measurements of M_n and M_w [kg/mol] of the copolymer phase were used to propose a correlation between molecular weight and intrinsic viscosity of the rubber phase:

$$IV_{EPR} = 0.0192 [M_{w,EPR}]^{0.8175} \quad 5.15$$

Therefore, the relationship between $M_{w,EPR}$ [kg/mol] and MFR_{EPR} is defined as:

$$MFR_{EPR} = 2 * 10^7 [M_{w,EPR}]^{-2.797} \quad 5.16$$

And respectively the relationship between intrinsic viscosity and MFR of the copolymer rubber is derived as:

$$MFR_{EPR} = 22.762 [IV_{EPR}]^{-3.331} \quad 5.17$$

By equation 5.15, and experimentally obtained values of intrinsic viscosity, weight average molecular weight of the rubber phase of copolymer samples produced in this work are calculated as:

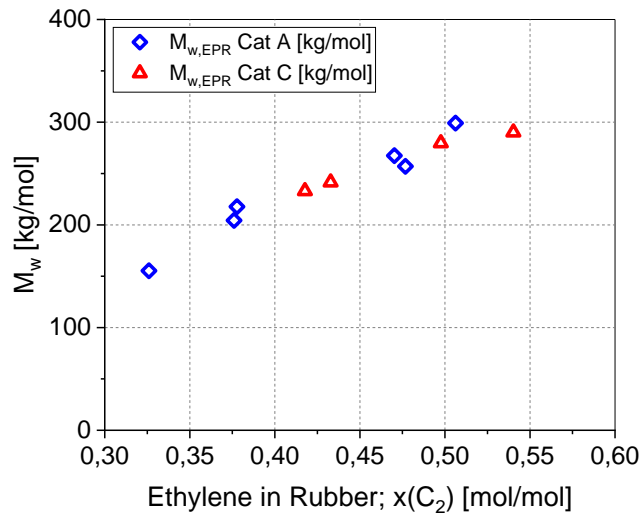


Figure 55. Weight average molecular weight of EPR vs ethylene fraction in rubber; Cat A vs Cat C rubber content= 20 [Mass%], $T=75$ [°C], $H_2=2$ [mol%], $P=14$ [bar], $x_{C_2}=32-55$ [mol%]

The weight average molecular weight of the homo-polymer matrix is about 200 [kg/mol] and as depicted in figure 55 the ethylene/propylene copolymer rubber phase has a molecular weight of between; 200 to 300 [kg/mol], depending on the ethylene composition. The Melt flow rate of the rubber phase with regard to the ethylene fraction in rubber can be calculated by equation 5.16 and the experimentally obtained IV values displayed in figure 56:

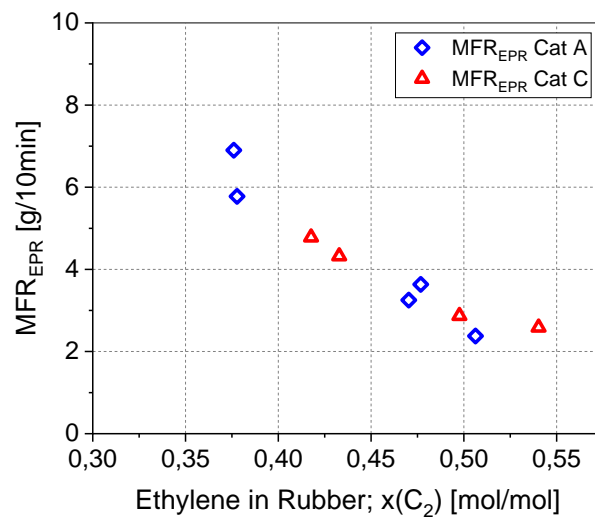


Figure 56. Rubber phase MFR vs ethylene fraction in rubber; Cat A vs Cat C; Rubber content= 20 [Mass%], $T=75$ [°C], $H_2=2$ [mol%], $P=14$ [bar], $x_{C_2}=32-55$ [mol%]

To evaluate the accuracy of the estimations of matrix and rubber phase MFR's and the mixing rule used, the final product MFR of samples with a range of ethylene in rubber (32~55 [mol%]) and a fixed rubber content of 20 [Mass%] are compared with the calculated MFR in the following graph:

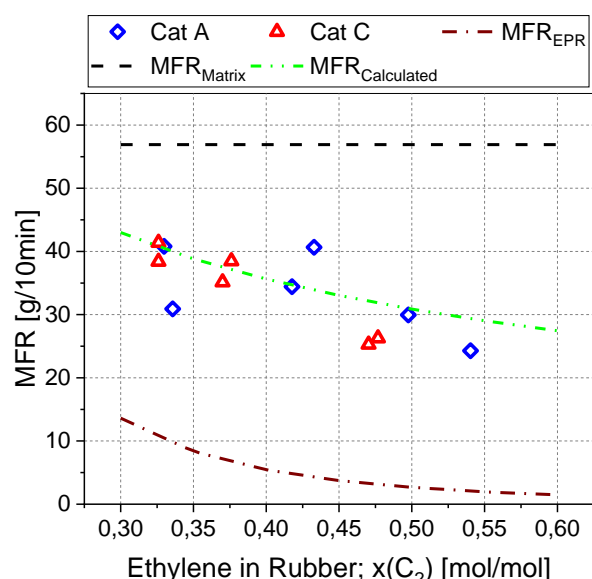


Figure 57. Final product MFR vs ethylene in rubber; Comparison between experiment and calculated values; Cat A vs Cat C rubber content= 20 [Mass%], $T=75$ [°C], $H_2=2$ [mol%], $P=14$ [bar], $x_{C_2}=32-55$ [mol%]

In figure 57, the data points indicate the total MFR measured for products of catalyst A and C. Both catalysts result in relatively similar overall product melt flow rate under similar conditions (hydrogen concentration, ethylene composition, rubber content). The black dashed line indicates the homo-polymer matrix MFR, which is fixed for all samples at about 57 [g/10min]. The brown dash-dot line indicates the calculated MFR of the rubber phase and is calculated by equations 5.13, 5.15 and 5.16. The green dash-dot-dot line indicates the total MFR calculated by the MFR value of matrix and rubber and the logarithmic mixing rule displayed in equation 5.12. It is observed that with an increase in ethylene composition in copolymer, the rubber phase MFR, and thus the total product MFR decreases. By IV measurements and estimation of the rubber MFR, the total product MFR can be estimated with logarithmic mixing rule with an acceptable accuracy.

5.6 Characterization results

In this section, the results of polymer characterization performed on homo-polymer and impact copolymer samples, produced in this study are presented. The characterization methods include, porosimetry measurements, bulk density determination, particle size distribution and electron microscopy measurements, which are carried out to investigate the particle morphology of the selected samples. Furthermore, DSC measurements are performed for determination of sample crystallinity, and FTIR measurements for determination of comonomer content and validation of the kinetic measurement principle.

5.6.1 Determination of ethylene content with FTIR method

It was demonstrated in section 5.5, that by means of mass balance, and the information provided by the kinetic measurement method, the amount of homo-polymer matrix, copolymer rubber, and the composition of the copolymer can be controlled. To validate the accuracy of the experimental method, FTIR measurements were carried out to experimentally measure the mass fraction of ethylene in the final impact-copolymer samples. The following parity diagram compares the ethylene mass fraction in the entire product measured by FTIR with the values calculated via mass balance:

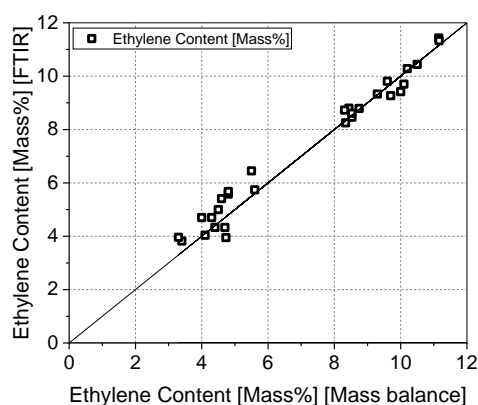


Figure 58. Ethylene mass fraction in entire product; Mass balance kinetics measurement method comparison with FTIR measurements

The parity diagram indicates an overall acceptable agreement between the calculated and measured values. Sources of error in calculated values can be:

1. Errors in calorimetry measurement and estimation of the amount of homo-polymer matrix since the calorimetry method cannot estimate the homo-polymer production in pre-polymerization and heat-up stages.
2. Polymer produced during the transition period from bulk phase homo-polymerization to gas phase copolymerization.

At lower ethylene contents the mass balance calculation displays higher error, since for these samples, the gas phase copolymerization reaction time is shorter and thus the error generated in the transition period is more amplified. For samples with higher ethylene content the combined calorimetry and mass balance calculations, display minor error.

5.6.2 Porosimetry measurements

Porosity of a number of samples were measured by the described method in section 4.6.2. The effect of pre-contacting on porosity has been studied. As was observed in chapter 5.4, pre-contacting had a considerable influence on polymerization reaction kinetics of catalyst A, whereas that was not the case for catalyst C. Influence of pre-contact time on the porosity of the homo-polymer particles produced by both catalysts is depicted in the following figure 59:

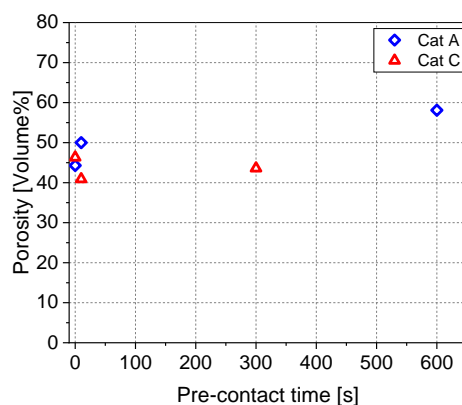


Figure 59. Influence of pre-contacting on homo-polymer particle porosity; Cat A vs Cat C; $T=75$ [°C], $H_2=1.8$ [mol%] for Cat A, $H_2=1.0$ [mol%] for Cat C, 10 [min] pre-polymerization, pre-contact=0-600 [s]

A trend in porosity is observed for catalyst A, in which with longer pre-contact time, the particles are more porous. It should be noted that the polymerization with no pre-contacting has the least activity, and the product has the least porosity. Overall, samples produced using catalyst C, are less porous compared to products of catalyst A and, with different pre-contact times do not display a meaningful trend in porosity.

In addition, porosity was measured for copolymer samples produced using both catalysts with rubber mass content ranging from 10 to 30 [Mass%]. While products of catalyst C generally have lower porosity, a similar trend was observed for both catalysts: porosity decreases with an increase in the rubber content. McKenna proposed a model for the morphological evolution of PP particles throughout the impact copolymerization stage and indicated that the rubber phase primarily fills the pores of homo-polymer matrix [147]. It was reported that a significant trend in bulk density of the powder up to a certain rubber content is not observed, and combined fractionation and microscopy results confirmed the proposed model. In this work porosity measurement results are in line with this hypothesis. The decline in porosity of polymer particles with the increase in rubber content, is an indication that the rubber material produced in the gas-phase copolymerization stage is primarily filling in the pores of the homo-polymer matrix.

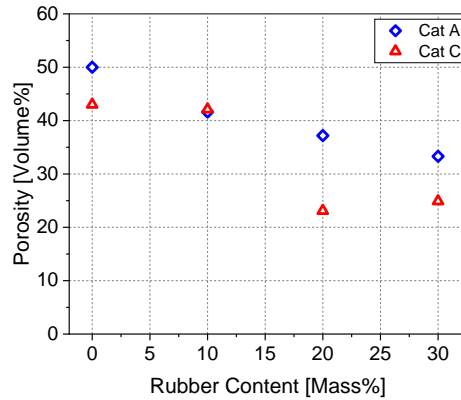


Figure 60. influence of rubber content on copolymer product's porosity; Cat A vs Cat C; rubber content=0-30 [Mass%], T=75 [°C], H₂=2 [mol%], P=14 [bar], x_{C2}=40 [mol%]

5.6.3 Particle size distribution

Particle size distribution of homo-polymer samples produced by catalyst A and C were measured by sieve grading (demonstrated in chapter 4.6.3) and the results are compared:

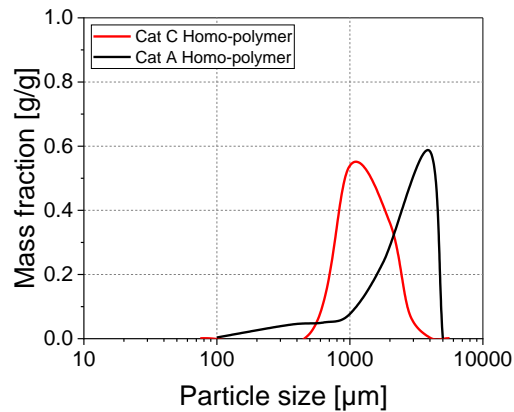


Figure 61. Homo-polymer particle size distribution; Cat A vs Cat C; T=75 [°C], H₂=1.0 [mol%] 10 [min] pre-polymerization, 10 [s] pre-contact

It is observed that samples produced by catalyst A in similar standard conditions have significantly larger particles compared to products of catalyst C. Largest mass fraction of homo-polymers produced by catalyst A are 4000 [µm] in size, whereas catalyst C results in particles mostly around 1000 to 2000 [µm] in diameter. It is worth mentioning that despite having smaller particles, catalyst C sample has a smaller fraction of fine powder (<75 [µm]).

The influence of pre-contacting on the particle size distribution of the resulting powder can be seen in the following figure 62:

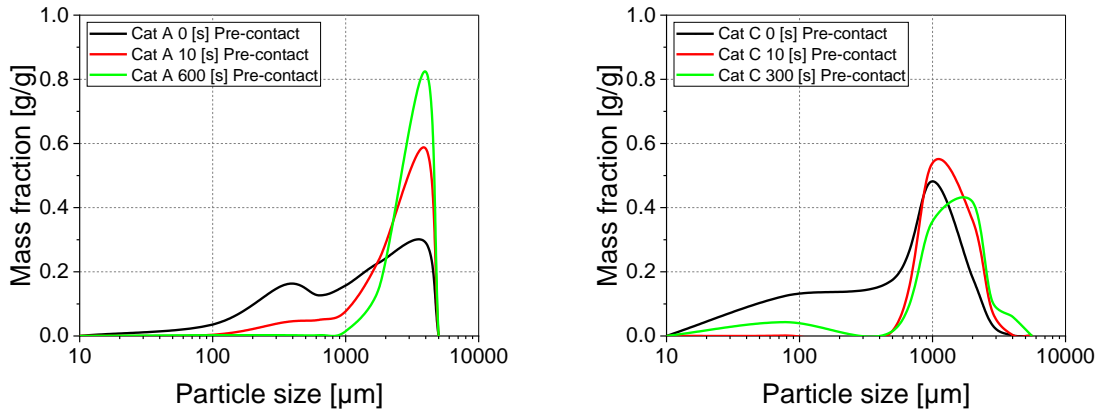


Figure 62. Influence of pre-contacting on homo-polymer particle size distribution; Cat A vs Cat C; $T=75$ [°C], $H_2=1.8$ [mol%] for Cat A, $H_2=1.0$ [mol%] for Cat C, 10 [min] pre-polymerization, pre-contact=0-600 [s]

Pre-contacting has a considerable influence on particle size of samples produced by catalyst A, where the sample produced without pre-contacting has a larger fraction of fines and a smaller fraction of particles grow to full size. By increasing the pre-contacting duration, the fraction of fines diminishes, and particles grow larger. The sample with 600 seconds of pre-contacting has negligible fraction of fines. In case of samples produced by catalyst C, in absence of pre-contacting a noticeable fraction of fines is apparent, and by pre-contacting particles grow in size and the fine powder fraction decreases, however overall, the effect is not as significant as that of catalyst A.

Influence of hydrogen on particle size distribution of the powder products (produced by catalyst A) is depicted in the following graph:

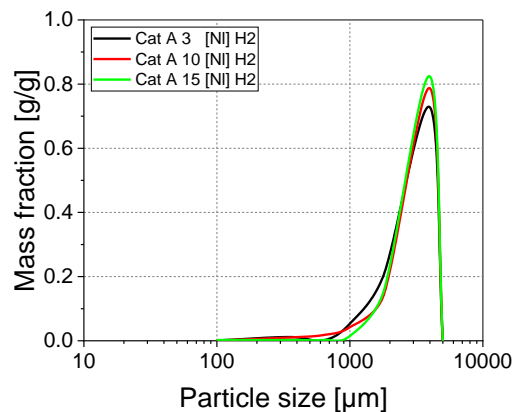


Figure 63. Influence of hydrogen on homo-polymer particle size distribution; Cat A; $T=75$ [°C], $H_2=0-1.8$ [mol%], 10 [min] pre-polymerization, 10 [s] pre-contact

It is observed that by incorporation of more hydrogen in the polymerization process the large particles fraction slightly increases. It must be noted that the experiment with more hydrogen has a higher activity and therefore particles grow slightly larger.

To study the evolution of particles size during the gas-phase copolymerization stage, three samples with 0 (homo-polymer) 20 and 40 [mass%] rubber were chosen for comparison (all produced using catalyst C):

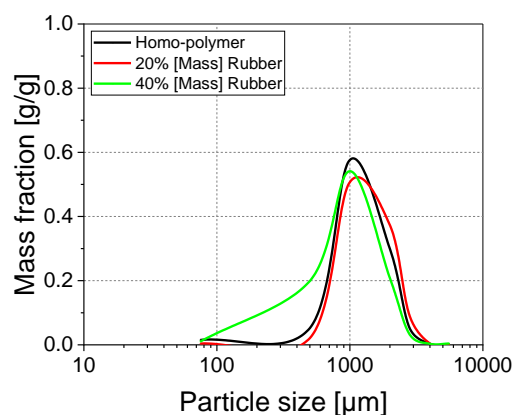


Figure 64. Influence of rubber content on copolymer particle size distribution; Cat C; Rubber content=0-40 [Mass%] T=75 [°C], H₂=2 [mol%], P=14 [bar], x_{C2}=40 [mol%]

It is observed that the sample containing 20 [mass%] rubber displays very similar particle size distribution compared to the homo-polymer sample, and the sample with 40 [mass%] rubber has slightly larger fraction of fines. Overall, it can be stated that copolymerization does not have a dramatic effect on particle size distribution. This is in-line with the hypothesis that the hetero-phasic copolymer rubber is primarily formed in the pores of the homo-polymer matrix particles.

5.6.4 Bulk density

Tapped bulk density of the samples produced, using catalysts A and C was measured, and influence of hydrogen, pre-contacting, and formation of rubber copolymer phase on the final product bulk density has been studied. Figure 65 demonstrates the influence of hydrogen presence on the final product bulk density. Samples produced without any hydrogen have higher bulk density compared to samples produced with standard hydrogen concentration (1 [mol%]). This is the case for both catalyst A and catalyst C. Overall, samples produced by catalyst C show slightly higher bulk density compared to products of catalyst A. This can be understood by taking a look back at the particle size distribution of the samples in figure 61, wherein it was demonstrated that catalyst C results in noticeably smaller particles.

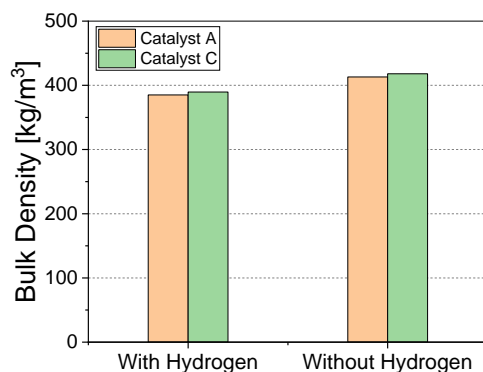


Figure 65. Influence of hydrogen on homo-polymer bulk density; Cat A vs Cat C; T=75 [°C], H₂=0-1.0 [mol%], 10 [min] pre-polymerization, 10 [s] pre-contact

The influence of pre-contacting on product bulk density was studied for samples produced without pre-contacting (0 [s]) and longer pre-contacting time (300 [s] for catalyst A and C). Pre-contacting reduces bulk density of products of both catalysts, wherein samples without pre-contacting result in bulk density of above 450 [kg/m³] and samples with pre-contacting have bulk density of about 400 [kg/m³]. This can be explained by reduction of fines as was observed in particle size distribution measurements, wherein the samples with pre-contacting displayed to have significantly smaller fraction of fine powder.

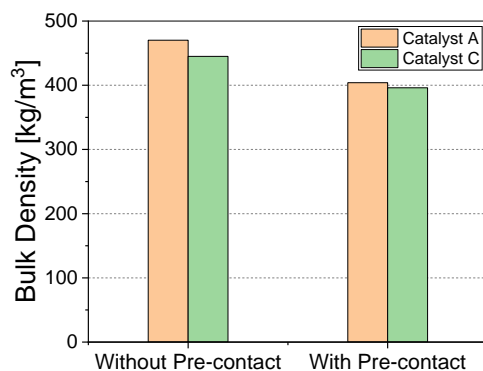


Figure 66. Influence of pre-contacting on homo-polymer bulk density; Cat A vs Cat C; T=75 [°C], H₂=1.0 [mol%], 10 [min] pre-polymerization, pre-contact=0-300 [s]

Samples with a range of rubber content (0~43 [Mass%]) were tested to study the influence of formation of the copolymer rubber phase on the product bulk density, displayed in figure 67. By formation of copolymer rubber phase up to 30 [Mass %], a meaningful trend in the bulk density is not observed, however the samples with about 40 [Mass %] rubber display a noticeable drop in bulk density.

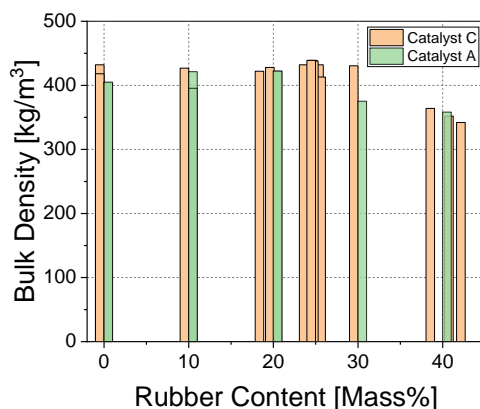


Figure 67. Influence of rubber content on copolymer bulk density; Cat A vs Cat C; T=75 [°C], H₂=2.0 [mol%], 10 [min] pre-polymerization, pre-contact=10 [s].

5.6.5 Microscopy

Particle morphology was studied using electron microscopy method as well. In the following figure 68, the morphology of a typical homo-polymer particle produced in standard homo-polymerization conditions (conditions in table 9 and 10) by catalysts A and C are compared. The two homo-polymer samples used for microscopy measurements have both been produced in similar standard homo-polymerization conditions (1.0 [mol%] H₂, T=75 [°C], 10 [s] of catalyst pre-contacting, and 10 [min] of pre-polymerization). For each sample, a picture of a typical particle with a magnification of 20 is depicted. Furthermore, a particle from each sample has been cut in half in order to obtain a picture with magnification of 150 from the inner side of the particle. As was observed in particle size distribution measurements, catalyst A results in larger particles (more than 2 [μm] in diameter on average) compared to catalyst C (about 1 [μm] in diameter on average). Homo-polymer products of both catalysts produced in standard conditions result in a spherical morphology with smooth surfaces (figure 68-a and c). The porosity of the homo-polymer particles is apparent in the pictures obtained from the particles that are cut in half (Figure 68-b and d).

The SEM pictures in figure 69 do show impact copolymer samples made by catalysts A and C, respectively. Both samples have been produced in similar conditions (2 [mol%] H₂ gas phase, 40 [mol%] ethylene in rubber, T=75 [°C]) with slightly different rubber contents; Figure 69-a (40 [Mass%] rubber content, catalyst A) and 69-c (30 [Mass%] rubber content, catalyst C). The impact-copolymer particles produced by either catalyst maintain a spherical morphology throughout copolymerization stage as well. Figures 69-b and 69-d display the inner side of the copolymer particles produced by catalysts A and C. Compared to homo-polymers

(figure 68-b and d) it can be observed that the formation of rubber phase copolymer has visibly reduced the porosity of the particle and the pores are filled.

In figures 70-a and b homo-polymer particles of catalyst A produced without pre-contacting of the catalyst and cocatalyst are displayed. Comparing with particle morphology displayed in figure 68-a and b (homo-polymer samples of catalyst A produced with 10 [s] of pre-contacting in otherwise similar conditions) a significant influence of pre-contacting on particle morphology can be observed. The sample produced without pre-contacting has significantly smaller particles (as was observed in particle size distribution measurements), the spherical shape is completely lost, and a sizable portion of the product is in fine powder form. In case of catalyst C, the homo-polymer sample produced without pre-contacting (figure 70-c and d) displays the spherical particle shape, however the particle has a number of visible cracks and the smooth surface resulting from 10 seconds of pre-contacting (figure 68-c) is lost.

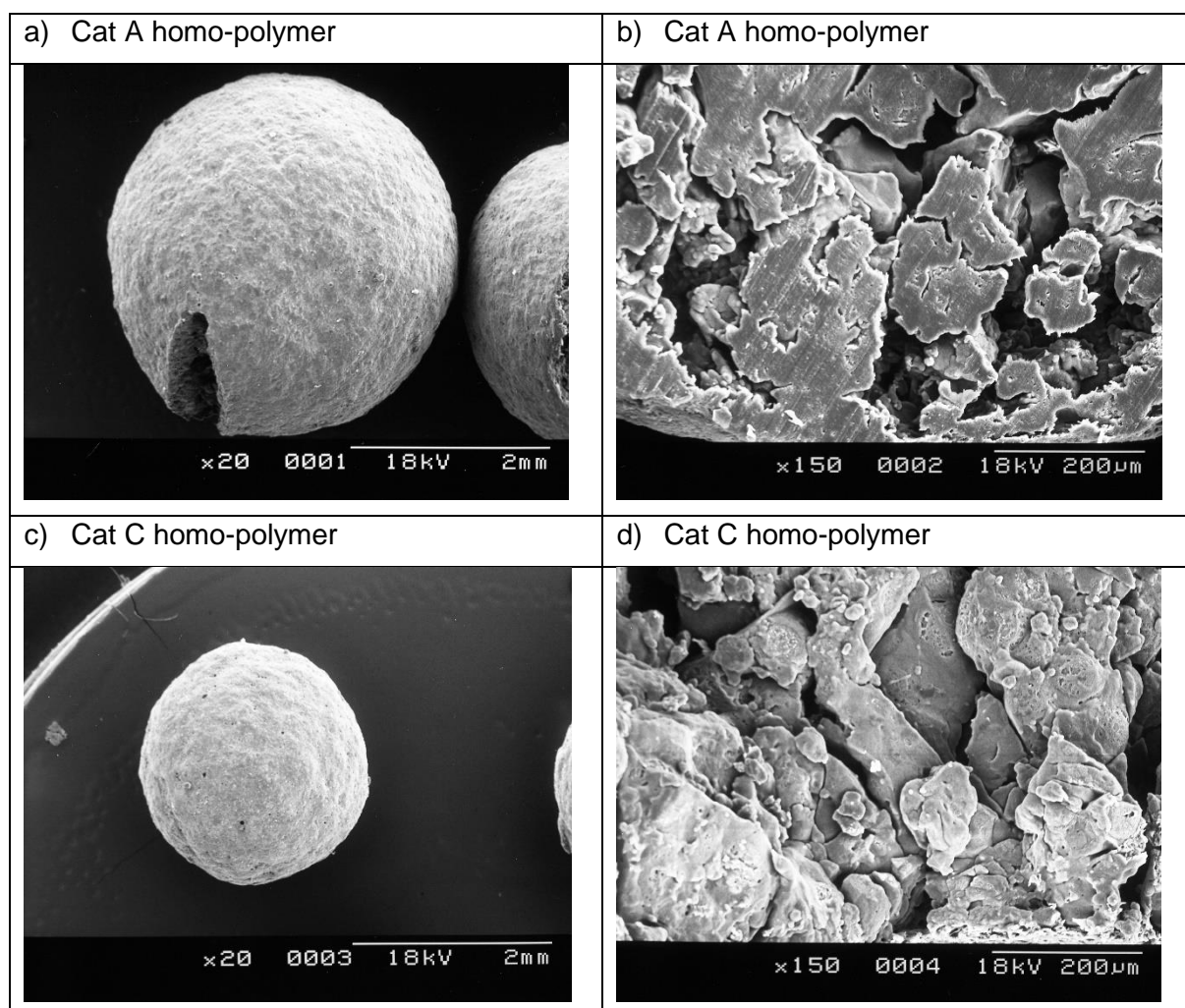


Figure 68.a) Homo-polymer produced by catalyst A b) Homo-polymer produced by catalyst A c) Homo-polymer produced by catalyst C d) Homo-polymer produced by catalyst C

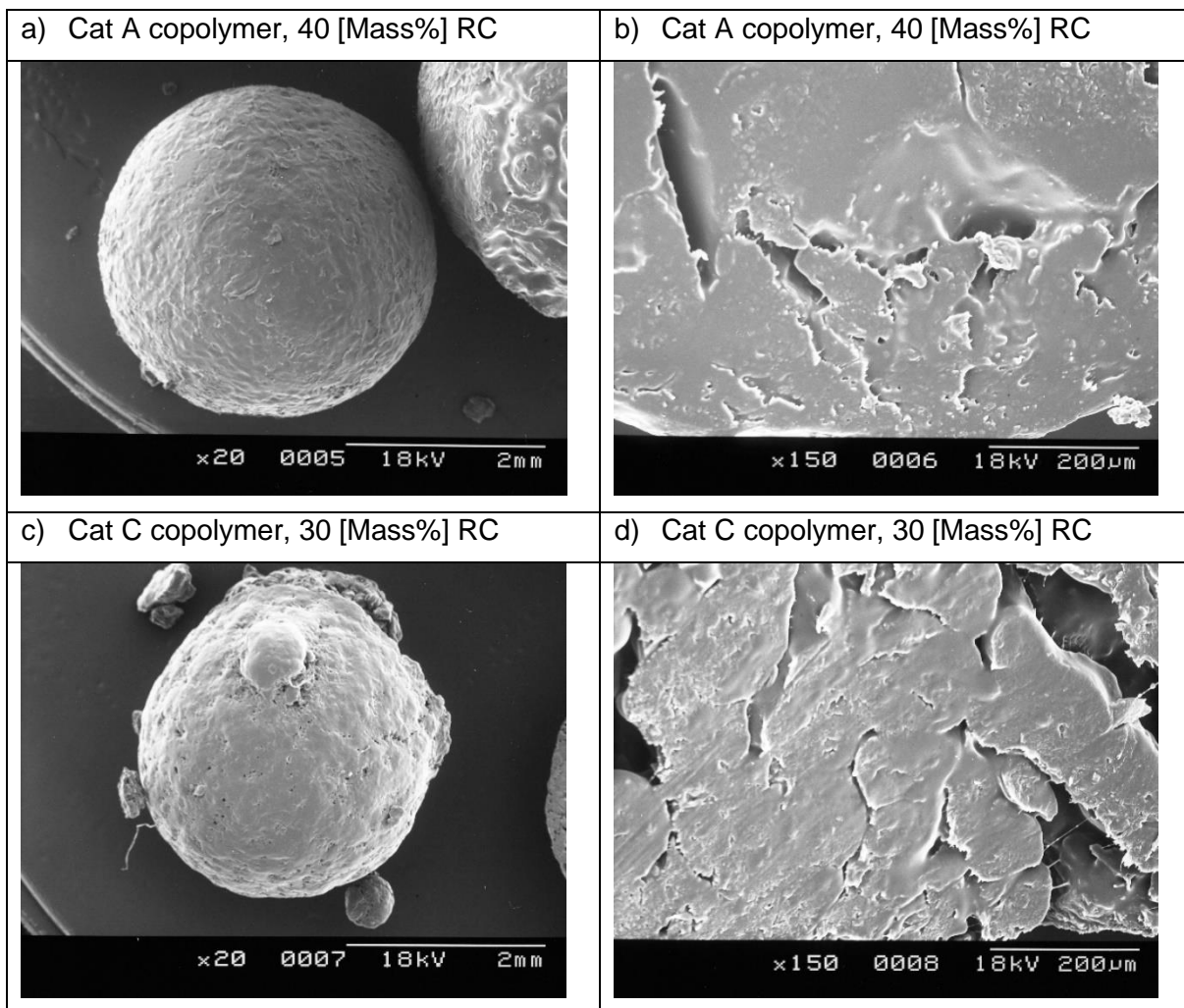
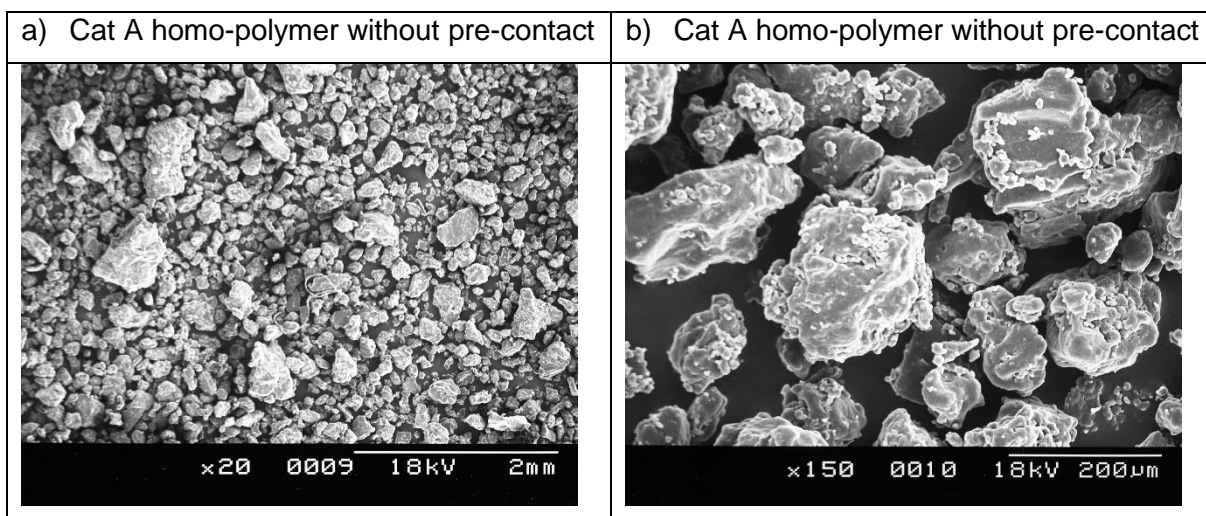


Figure 69.a) Copolymer produced by catalyst A b) Copolymer produced by catalyst A c) Copolymer produced by catalyst C d) Copolymer produced by catalyst C



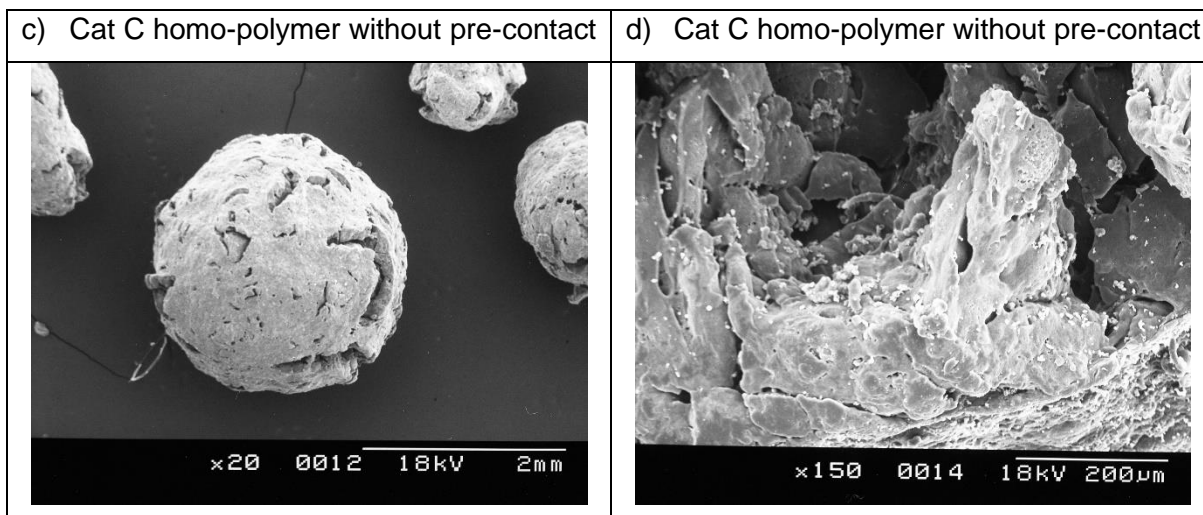


Figure 70. a) Homo-polymer produced by catalyst A without pre-contact b) Homo-polymer produced by catalyst A without pre-contact c) Homo-polymer produced by catalyst C without pre-contact d) Homo-polymer particle produced by catalyst C without pre-contact

5.6.6 Determination of crystallinity

Crystallinity of several homo-polymer samples has been tested using DSC technic. A typical DSC curve obtained for a homo-polymer sample is displayed below:

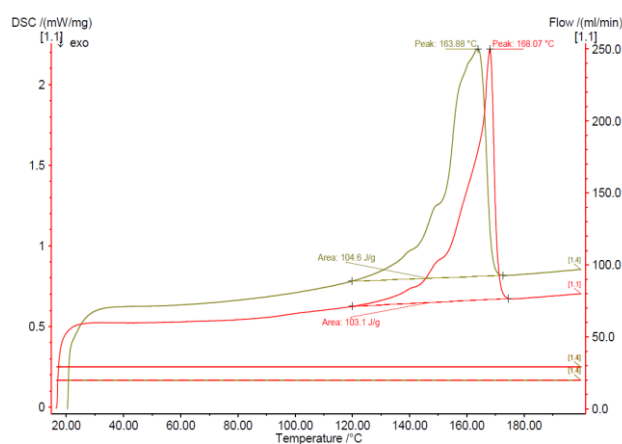


Figure 71. A typical DSC curve obtained for a homo-polymer sample

To calculate the crystallinity from the DSC curves the area under the curve, regarding the first heating ramp is considered, and the peak area is divided by the melting Enthalpy of 100% crystalline PP ($\Delta H^0=207$ j/g) [139]. The first heating ramp is chosen since the powder is in its closest state to polymer particles in the reactor during the polymerization. The degree of crystallinity has been calculated for several homo-polymer samples and is listed in the following table:

| Catalyst | Sample Type | Crystallinity [Mass %] |
|----------------|--------------|------------------------|
| C | Homo-polymer | 52,6 |
| C | Homo-polymer | 43,6 |
| C | Homo-polymer | 42,5 |
| C | Homo-polymer | 44,6 |
| C | Homo-polymer | 58,8 |
| C | Homo-polymer | 52,6 |
| C | Homo-polymer | 45,8 |
| C | Homo-polymer | 52,3 |
| Average | | 49,1 |

Table 17. Crystallinity of homo-polymer samples; Cat C; T=75 [°C], H₂=1.0 [mol%], 10 [min] pre-polymerization, pre-contact=10 [s]

The homo-polymer samples have an average crystallinity of 49 [weight %]. The crystallinity of the copolymer samples is estimated using the following correlation:

$$X_{cr}^{icp} = (1 - RC)X_{cr}^{hp} \quad 5.18$$

Where X_{cr}^{icp} [Mass%] is the crystallinity degree of the copolymer sample, RC [Mass%] is the rubber content, and X_{cr}^{hp} [Mass%] is the crystallinity degree of the homo-polymer. Zacur investigated the crystalline structure of ICP samples by temperature rising elution fractionation and DSC technic [148], and reported that the crystalline fraction in ICP samples is attributed to homo-polymer, and the copolymer rubber fraction is reported to be in amorphous phase. However, formation of PP or PE homo-polymer sequences during the copolymerization production stage is a possibility. As was reported by Goede [149] small traces of polyethylene crystals were detected in a fractionation study as well as homo-polymer polypropylene crystals in the EPR fractions. In this study, it is assumed that the rubber, produced in the gas-phase copolymerization stage is entirely amorphous.

6 Phase equilibria and mass transfer

In the first section of this chapter the phase equilibria between vapor and liquid phases in the bulk polymerization reactor is investigated, and by performing flash calculation, material balance of each phase, as well as composition of components (propylene and hydrogen) in liquid and vapor phases are estimated.

In the second section, the equilibrium solubility of penetrant gases (propylene and ethylene) in semi-crystalline polypropylene samples, is investigated by means of sorption measurements.

6.1 Vapor-liquid phase equilibria in bulk-phase propylene polymerization

To describe the phase equilibria between the liquid and vapor phases in the partially filled polymerization reactor the phi-phi approach is applied (equation 2.18). In order to derive fugacity terms of components in the reactor, the Peng-Robinson equation of state is used. The general expression of the Peng-Robinson equation of state is presented as the following [150]:

$$P = \frac{RT}{v-b} - \frac{a(T)}{v(v+b) + b(v-b)} \quad 6.1$$

According to [149] the compressibility factor Z for a pure component can be calculated by solving the following equation 6.3:

$$Z = \frac{Pv}{RT} \quad 6.2$$

$$Z^3 - (1-B)Z^2 - (A-3B^2-2B)Z - (AB-B^2-B^3) = 0 \quad 6.3$$

$$A = \frac{aP}{R^2T^2} \quad 6.4$$

$$B = \frac{bP}{RT} \quad 6.5$$

Where parameters; a and b for a substance at critical temperature (T_c) are defined as:

$$a(T_c) = 0.45724 \frac{R^2T_c^2}{P_c} \quad 6.6$$

$$b(T_c) = b(T_r) = 0.07780 \frac{RT_c}{P_c} \quad 6.7$$

$$Z_c = 0.307 \quad 6.8$$

At temperatures other than critical temperature

$$a(T_r) = a(T_c) [(1 + (0.37464 + 1.54226\omega - 0.26992\omega^2)(1 - \tilde{T}_r^{1/2}))^2] \quad 6.9$$

Where \tilde{T}_r is the reduced temperature and is defined as:

$$\tilde{T}_r = \frac{T}{T_c} \quad 6.10$$

ω is the acentric factor and has a specific experimentally determined value for each substance. In the following table values of the constant parameters of the Peng-Robinson equation of state for substances used in this work are listed [151]:

| Substance | T_c [K] | P_c [bar] | ω |
|-----------|-----------|-------------|----------|
| Propylene | 365.57 | 46.646 | 0.1408 |
| Ethylene | 282.35 | 50.418 | 0.0866 |
| Hydrogen | 33.145 | 12.964 | -0.219 |

Table 18. Critical pressure and temperature, and acentric factor of propylene, hydrogen, and ethylene

The following graph shows the accuracy of the Peng-Robinson equation of state, predicting the molar volume of pure propylene vapor at saturation (experimental data from national institute of standards and technology [152]):

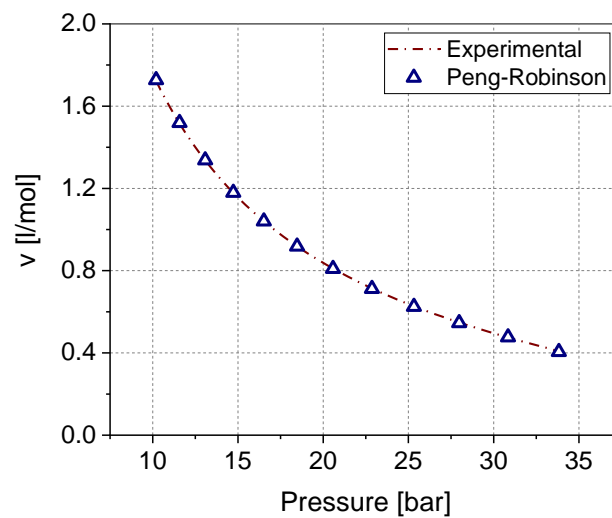


Figure 72. Propylene vapor molar volume at saturation; Comparison between experimental values and PR-Eos
 The compressibility factor of propylene can be calculated by equation 6.3. This equation has three roots, wherein the smallest root is attributed to the liquid phase compressibility factor, the largest root is the compressibility of the vapor, and the middle root has no physical meaning. The compressibility factor for pure propylene vapor, and liquid at saturation pressures and different temperatures are calculated by equation 6.3 and plotted in figure 73:

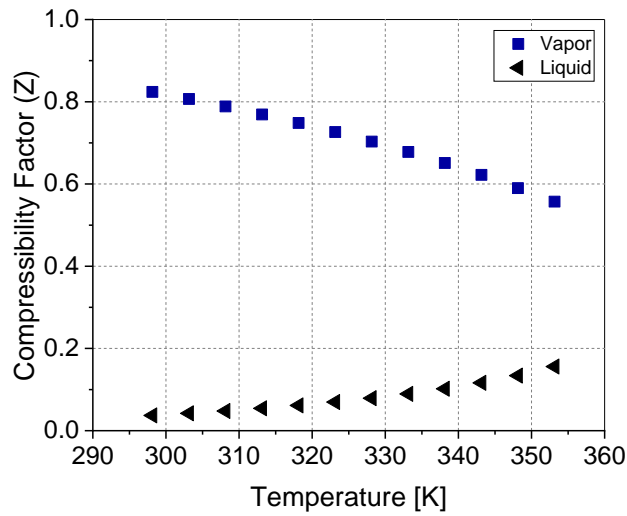


Figure 73. Propylene compressibility factor at saturation calculated by PR-Eos

By integrating equation 2.12 using the Peng-Robinson equation of state as presented in equation 6.1 to formulate the substance volume, the fugacity of a pure substance is derived:

$$\ln\left(\frac{f}{P}\right) = \ln(\varphi) = Z - 1 - \ln(Z - B) - \frac{A}{2\sqrt{2}B} \ln\left(\frac{Z + 2.414B}{Z - 0.414B}\right) \quad 6.11$$

For illustration, the liquid and vapor fugacity of pure propylene at 75 [°C] is calculated by equation 6.11 (compressibility factor (Z) needs to be inserted in the formula accordingly). It is observed that propylene fugacity starts to deviate from ideal behavior from about 5 [bar] pressure range. Propylene saturation pressure at this temperature is around 33.9 [bar], where in the figure 74 it is observed that above this pressure the liquid propylene fugacity is not a strong function of pressure.

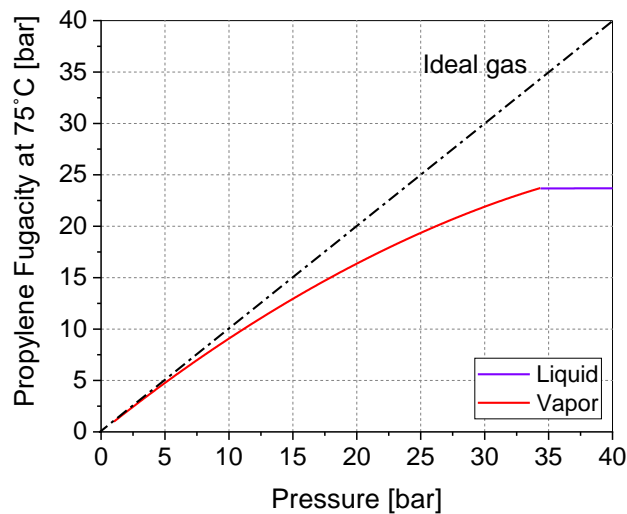


Figure 74. Propylene fugacity; T=75 [°C] P=0-40 [bar]

During the bulk polymerization of propylene, two components of hydrogen and propylene coexist in vapor liquid equilibrium. Based on the phi-phi formulation, the condition for equilibrium of a component in a mixture between two phases is:

$$x_i \hat{\phi}_i^l = y_i \hat{\phi}_i^v \quad 6.12$$

Herein $\hat{\phi}_i^l$, and $\hat{\phi}_i^v$ indicate the fugacity coefficient of component i in the liquid and vapor mixtures. Equilibrium constant of component i is hence defined as:

$$K_i = \frac{y_i}{x_i} = \frac{\hat{\phi}_i^l}{\hat{\phi}_i^v} \quad 6.13$$

Fugacity coefficient of component i in a mixture is derived by Peng-Robinson equation of state as:

$$\ln(\hat{\phi}_i) = \frac{b_i}{b} (Z - 1) - \ln(Z - B) - \frac{A}{2\sqrt{2}B} \left(\frac{2\sum_i X_i a_{ij}}{a} - \frac{b_i}{b} \right) \ln \left(\frac{Z + 2.414B}{Z - 0.414B} \right) \quad 6.14$$

$$a = \sum_i \sum_j y_i y_j a_{ij}; \quad b = \sum_i y_i b_i; \quad a_{ij} = (1 - \delta_{ij}) a_i^{0.5} a_j^{0.5} \quad 6.15$$

This equation can be used to calculate the fugacity of propylene and hydrogen in both liquid and vapor phase (compressibility factor and constant parameters must be adjusted accordingly). y_i is the mole fraction of component i , and δ_{ij} is the temperature dependent binary interaction parameter between the two components and must be determined empirically. The following equation is proposed by Pater to estimate a temperature dependent interaction parameter for a binary mixture of propylene and hydrogen [49]:

$$\delta_{ij} = 7,524 * 10^{-4} T^2 - 0,4829T + 77,0879 \quad 6.16$$

6.1.1 Flash calculation procedure

For determination of the heat transfer to the jacket (see chapter 4.4.3) the filling level in the reactor must be known. For determination of the filling level, flash calculations must be performed in order to determine the partitioning of propylene between vapor and liquid phase.

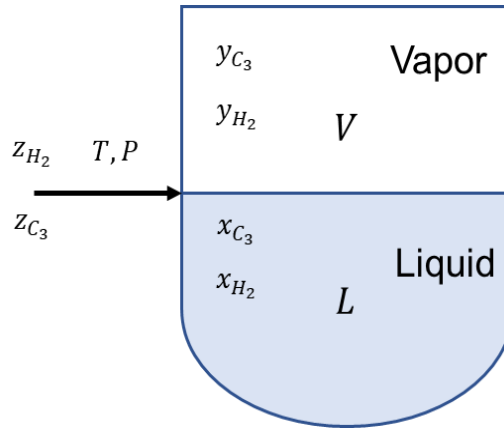


Figure 75. Schematic depiction of material partitioning in the partially filled reactor

According to Rachford-Rice [153] calculations the material balances in a two-phased system can be written as:

$$L + V = 1 \quad 6.17$$

Where L is the fraction of material in liquid, and V is the fraction of material in the vapor phase. For component i the mass balance in the reactor is therefore written as:

$$Lx_i + Vy_i = z_i \quad 6.18$$

Where z_i is the mole fraction of component i in the reactor (all phases) this equation can be rewritten as:

$$z_i = x_i(1 - V) + Vy_i \quad 6.19$$

And the mole fraction of component i in liquid and vapor phase from equation 6.19 are thus derived as:

$$x_i = \frac{z_i}{1 + V(K_i - 1)} \quad 6.20$$

And,

$$y_i = \frac{z_i K_i}{1 + V(K_i - 1)} \quad 6.21$$

Since the summation of fractions of all components in each phase is naturally equal to one, the following equations can be derived:

$$\sum_i x_i = \sum_i \frac{z_i}{1 + V(K_i - 1)} = 1 \quad 6.22$$

$$\sum_i y_i = \sum_i \frac{z_i K_i}{1 + V(K_i - 1)} = 1 \quad 6.23$$

$$F_y = \sum_i \frac{z_i K_i}{1 + V(K_i - 1)} - 1 = 0 \quad 6.24$$

$$F_x = \sum_i \frac{z_i}{1 + V(K_i - 1)} - 1 = 0 \quad 6.25$$

$$F = F_y - F_x = \sum_i \frac{z_i(K_i - 1)}{1 + V(K_i - 1)} = 0 \quad 6.26$$

Equation 6.26 needs to be solved in an iterative approach to calculate V (the fraction of materials existing in vapor phase). The algorithm displayed in figure 76 is used to perform the iterative flash calculations according to [116]:

1. Input: pressure, temperature, and the composition of materials in the reactor (z_i). Pressure and temperature values in the reactor are readily available by the setup. The overall composition of hydrogen in the reactor (z_{H_2}) is thus calculated as:

$$z_{H_2} = \frac{n_{H_2}}{n_{H_2} + n_{C_3}} \quad 6.27$$

n_{H_2} , and n_{C_3} are the total moles of hydrogen and propylene fed to the reactor and are measured by mass flow meters in the setup.

2. Mole fraction of components in each phase are guessed (x_i, y_i)
3. Equation 6.14 is used to calculate fugacity coefficients of components in vapor and liquid mixtures ($\hat{\phi}_i^v, \hat{\phi}_i^l$).
4. Equilibrium constant of each component is calculated by equation 6.13.
5. Equation 6.26 is solved to calculate V (mole fraction of material in vapor phase)
6. Using equation 6.20, and 6.21 new values for (x_i, y_i) are calculated.
7. By comparing the new values of (x_i, y_i) with values from the previous step, it is determined if the iterative solution has converged to an accurate enough result.

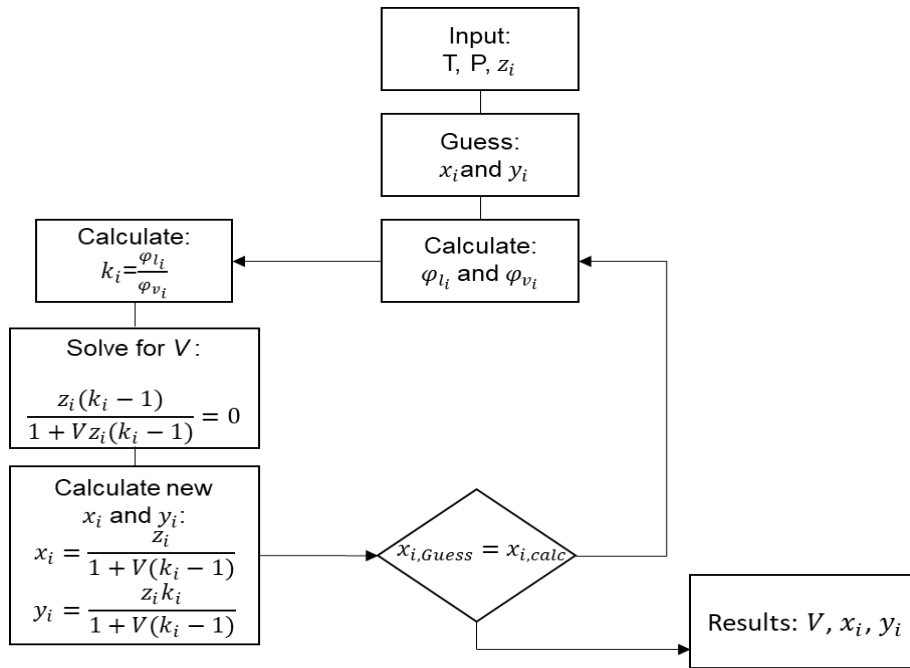


Figure 76. Flash calculation algorithm

Providing reasonable initial guesses is a crucial factor in convergence of the iterative flash calculation procedure. A semi-empirical approach for guessing the initial values of hydrogen and propylene has been used in this work. As was outlined in section 4.1.4, the reactor setup is equipped with a μ -GC setup, that is capable of measuring the composition of materials in the gas phase. A series of calibration measurements were performed, in which the reactor was filled with a known amount of propylene and hydrogen and the composition of the gas phase above the liquid in the reactor was measured by μ -GC (depiction of phases and corresponding parameters in figure 75). The following plot displays the measured gas composition of hydrogen (y_{H_2}) with regard to composition of hydrogen in the feed (z_{H_2}):

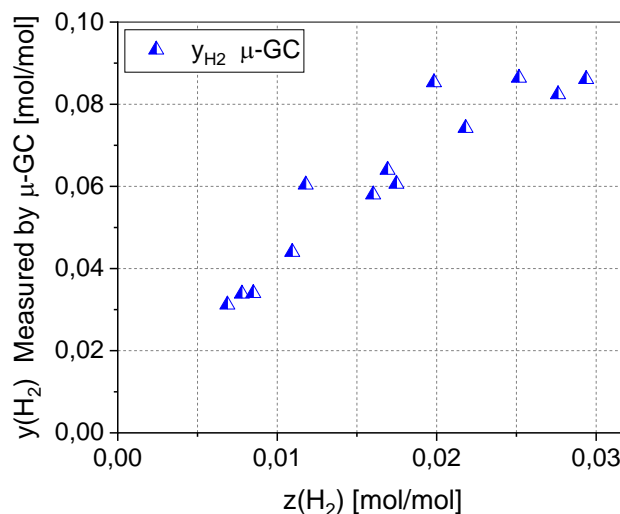


Figure 77. Hydrogen mole fraction in the gas phase measured by μ -GC; T=75 [°C] P=35-41 [bar]

According to the mole fraction of hydrogen in the feed (z_{H_2}), the experimental gas composition measured by μ -GC setup can provide a reasonable initial guess for y_{H_2} .

The parity diagram in figure 78 compares the experimental results of gas chromatography setup with the calculated values using the outlined flash calculation procedure for mole fraction of hydrogen in the gas phase (y_{H_2}). The flash calculation procedure results are in acceptable agreement with the experimental values measured by μ -GC. Pressure drop and composition drift during calibration measurements by μ -GC can be sources of disparity between calculations and measurements.

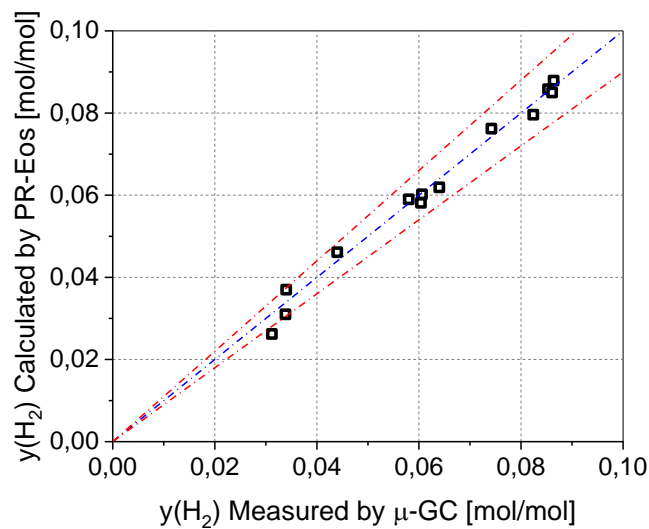


Figure 78. Parity diagram: Flash calculation vs measurements by μ -GC

The following graph displays the mole fraction of hydrogen in the liquid phase regarding the reactor pressure, calculated through the flash calculation procedure in figure 76:

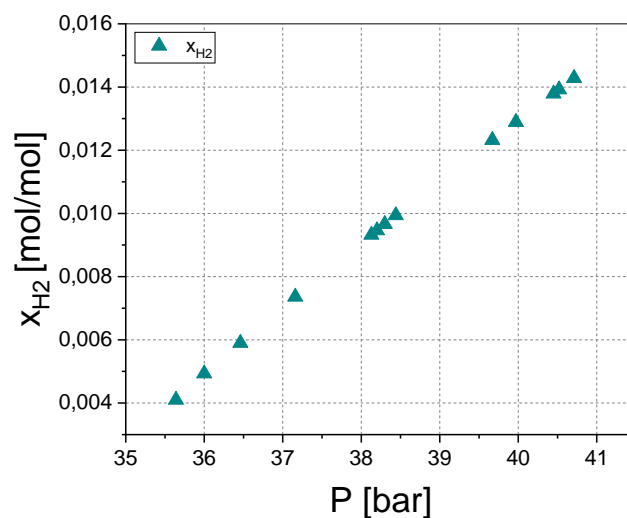


Figure 79. Hydrogen mole fraction in liquid propylene determined by flash calculation; T=75 [°C] P=35-41 [bar]

As expected, the hydrogen mole fraction in liquid propylene is significantly smaller than the fraction in vapor phase and is typically below 1 [mol%] in the operational range of this work.

6.1.2 Determination of liquid level in the reactor

By determining the material balance of the liquid and vapor phases through the flash calculation procedure in figure 76, the number of moles in each phase can be calculated via:

$$n_{H_2} + n_{C_3} = n_T \quad 6.28$$

$$n_{liquid} = n_T L \quad 6.29$$

$$n_{vapor} = n_T V \quad 6.30$$

And thus, the volume occupied by the liquid and vapor phase can be calculated as:

$$V_{liquid} = n_{liquid} / \rho_{liquid,(P,T)} \quad 6.31$$

$$V_{vapor} = n_{vapor} ZRT / P \quad 6.32$$

Where $\rho_{liquid} [\frac{mol}{l}]$ is the molar density of pure liquid propylene at the operating conditions of the reactor (changes in liquid propylene density due to dissolution of small amounts of hydrogen is neglected). In equation 6.32 the compressibility factor regarding the vapor mixture of propylene and hydrogen (Z) is calculated via PR-Eos (equation 6.3). In figure 80 the liquid propylene volume regarding the mass of entire propylene feed to the reactor is plotted (data in appendix III).

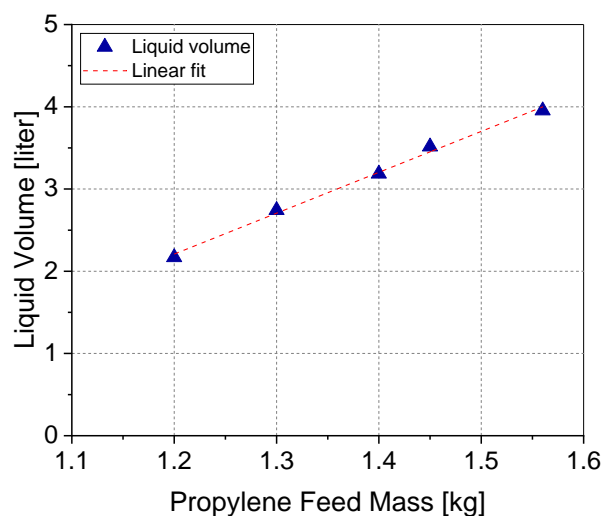


Figure 80. Liquid propylene volume vs propylene feed; T=75 [°C], P=38-40 [bar]

In a batch bulk polymerization process, as the polymer is forming in the liquid pool of monomer, due to the much higher density of polypropylene compared to liquid propylene [136,152], the liquid volume level in the reactor is decreasing. The volume occupied by the liquid and the suspended polymer particles in the reactor at a given moment during polymerization is:

$$V_{occupied}(t) = V_{liquid}(t) + V_p(t) = \frac{m_{liquid}(t)}{\rho_{liquid}} + \frac{m_p(t)}{\rho_p} \quad 6.33$$

Where $m_p(t)$ is the polymer mass produced up to the given point of the reaction and is obtained by the polymerization rate and the mass-balance based algorithm demonstrated in figure 23, and equation 5.2. $m_{liquid}(t)$ is the mass of the liquid propylene in the reactor at the given moment and is estimated by the results of flash calculation (displayed in figure 80), based on the amount of entire remaining propylene in the reactor.

Once the volume occupied by liquid and polymer is determined, the effective heat transfer area (wetted surface) can be calculated. Determination of the heat transfer area is necessary for determining the heat transfer coefficient of the reactor and to calibrate the calorimetric measurements. The change in the filling liquid volume during a typical homo-polymerization reaction is illustrated in the following figure 81:

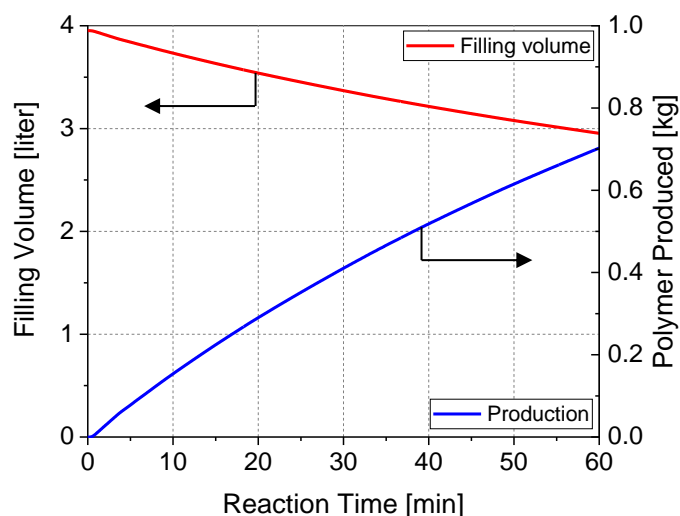


Figure 81. Change in volume occupied by liquid during a standard homo-polymerization; Cat A; T=75 [°C], H₂=1 [mol%], 10 [min] pre-polymerization, 10 [s] pre-contact

6.2 Sorption equilibrium

For kinetic modelling, the concentration of the reaction partners must be known.

In this work, a high-pressure magnetic sorption balance has been used to experimentally determine the equilibrium solubility of gaseous propylene and ethylene in homo-polymer and copolymer products, in conditions (pressure, temperature) close to that of polymerization reactions conducted.

6.2.1 Sorption balance setup

The sorption balance setup consists of a stainless-steel chamber with maximum pressure of 25 [bar]. The chamber is connected to a magnetic coupling (Rubotherm, Bochum), which transfers the load of the sample and the sample holder in the closed chamber to a high precision laboratory balance (Mettler Toledo AT261, accuracy of 0.01 [mg]) placed in ambient conditions outside the pressure chamber. Sorption of gases into the polymer can be measured by the balance with an accuracy of 0.01 [mg].

The chamber is submerged in a thermostated (Lauda E300) water bath. The magnet coupling is thermostated by a jacket using a separate water thermostat (Lauda E300) as well. The measurement temperature is controlled in isoperibolic mode, where the water bath temperature is set constant at 2-3 [°C] above the measurement temperature and the jacket thermostat is set at the desired measurement temperature. Chamber pressure is monitored using a Wakai pressure sensor. The measurement chamber is connected to a gas mixing cylinder by a needle valve, through which the gas samples can be dosed with desired pressure. There are vacuum and nitrogen connections to the mixing tank and the measurement chamber for removing remaining gases or air after sample placement and for blank measurements using nitrogen gas. The gas mixing cylinder is heated up using an electrical heating band and a Horst HLE 10 power regulator to the desired measurement temperature before dosing gases to the chamber.

The data generated by the setup, including chamber and bath temperature, chamber pressure and the mass measured by the balance are collected by a DasyLab data acquisition software, where it can be viewed online during the measurement. The magnetic sorption balance setup is sketched in figure 82.

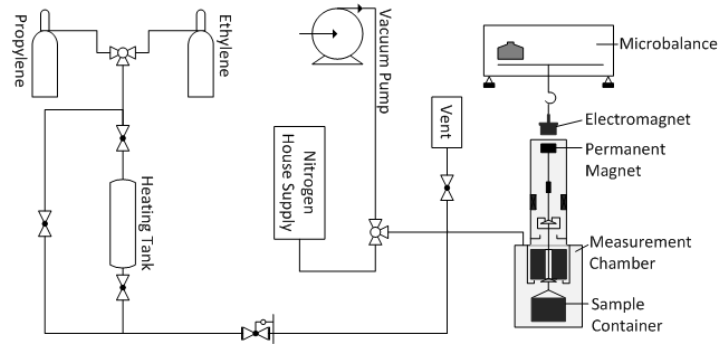


Figure 82. Sorption balance setup outline

6.2.2 Sorption measurement procedure

For sorption experiments around 1 gram of polymer powder is placed in a basket and is hooked on the magnetic coupling in the measurement chamber. The pressure chamber is closed and to remove the air in the chamber as well as remaining monomer gas in the polymer powder, the chamber is placed under vacuum for two hours with a rotary-vane pump. The chamber temperature is adjusted to the measurement temperature as well as the gas reservoir cylinder temperature. The desired measurement pressure is set at the pressure regulator and the gas is dosed to the measurement chamber. The gas filling causes a spike of around 2 [°C] in the chamber temperature for about 2 minutes. The mass uptake of the polymer sample is monitored online and depending on the sample and the type of penetrant, the measurement for each pressure step lasts between 30 minutes to one hour to reach equilibrium.

6.2.3 Data interpretation

During the sorption measurements, the magnetic balance measures the weight of sample holder basket and the sample, however the buoyance force of the gas in the chamber needs to be considered in order to calculate the corrected mass uptake of the sample. The buoyance force generated by the sample and the basket in a fluid is given as:

$$Buoyance = \rho_{gas}(V_P + V_{basket}) \quad 6.34$$

The corrected mass measurement, and thus the mass uptake can be calculated by the following equation:

$$m_{corr} = m_{balance} + \rho_{gas}(V_P + V_{basket}) \quad 6.35$$

m_{corr} is the corrected weight, $m_{balance}$ is the value measured by the magnetic balance. ρ_{gas} indicates the density of the gas in the chamber and is estimated by the Peng-Robinson

equation of state (see chapter 6.1). The term $(V_p + V_{basket})$ is the combined volume of the polymer sample and the basket. The basket volume is determined by blank measurements, in which the container is subjected to nitrogen gas at different pressures. The sample volume (V_p) includes both, the initial polymer volume (before sorption measurement), and the increase in polymer volume during sorption measurement due to the swelling effect.

To estimate the initial polymer sample volume the weighted sample mass is divided by polypropylene density.

$$V_p^0 = \frac{m_p}{\rho_p} \quad 6.36$$

ρ_p is the density of the semi-crystalline polypropylene and is directly influenced by the degree of crystallinity of the sample, formulated as:

$$\rho_p(T) = v_{cr}\rho_{cr}(T) + (1 - v_{cr})\rho_{am}(T) \quad 6.37$$

v_{cr} is the volume fraction of crystalline polymer and is assumed to be constant throughout the sorption measurements. ρ_{cr} and ρ_{am} are the temperature dependent crystalline and amorphous polypropylene density, and are estimated by Tait equation at the measurement temperature [154,155]:

$$\rho_{am/cr}(T) = \frac{1}{v_0 e^{\alpha_0 T}} \quad 6.38$$

With:

| | Amorphous | Crystalline |
|----------------------------|-----------------------|-----------------------|
| v_0 [cm ³ /g] | 1.1606 | 0.9430 |
| α_0 [1/°C] | 6.70*10 ⁻⁴ | 3.77*10 ⁻⁴ |

Table 19. Constant parameters of Tait equation for amorphous and crystalline polypropylene

Crystalline volume fraction is dependent on the degree of crystallinity of the polymer, which for homo-polypropylene is formulated as:

$$v_{cr} = \frac{V_{cr}}{V_p} = \frac{V_{cr}}{V_{cr} + V_{am}} = \frac{\frac{X_{cr}^{hp}}{\rho_{cr}}}{\frac{X_{cr}^{hp}}{\rho_{cr}} + \frac{(1 - X_{cr}^{hp})}{\rho_{am}}} \quad 6.39$$

V_{cr} is the crystalline volume of the polymer, V_p is the volume of the entire polymer and X_{cr}^{hp} is the degree of crystallinity of the homo-polymer sample. It was demonstrated in chapter 5.6.6, that the homo-polymer samples tested in this study have an average degree of crystallinity of

49 [Mass%], therefore the crystalline volume fraction for homo-polymer samples is estimated to have the constant value of 44.8 [Vol%], however the copolymer samples have a varying degree of crystallinity based on the rubber content (equation 6.40), and hence the crystalline volume fraction of the copolymer samples is formulated as:

$$X_{cr}^{cp} = (1 - RC)X_{cr}^{hp} \quad 6.40$$

$$v_{cr} = \frac{\frac{(1 - RC)X_{cr}^{hp}}{\rho_{cr}}}{\frac{(1 - RC)X_{cr}^{hp}}{\rho_{cr}} + \frac{(1 - (1 - RC)X_{cr}^{hp})}{\rho_{am}}} \quad 6.41$$

By inserting the crystalline volume fraction in equation 6.37 the polymer sample density is estimated.

6.2.3.1 Effect of swelling

The polymer volume can increase due to swelling of gases in the polymer:

$$V_p = V_p^0 + \Delta V_{swelling} \quad 6.42$$

$\Delta V_{swelling}$ indicates the increase in volume of amorphous fraction of the polymer sample. Swelling of polypropylene and polyethylene due to sorption of gases has been studied by researchers. As an example, Bobak used video microscopy [156] [157], and proposed the following experimental correlation to estimate the change in volume based on the mass of sorbed material in amorphous polymer:

$$\Delta V_{swelling} = 1.7844 \frac{m_{sorbed}}{m_p} V_p^0 \quad 6.43$$

m_{sorbed} is the absorbed mass into the polymer (subtracting the mass of the sample basket (m_{basket}) and the sample mass (m_p) from the corrected mass (m_{corr})). By considering the swelling influence and combining equations 6.43 and 6.35, the sorbed mass is given as:

$$m_{sorbed} = \frac{m_{corr} - m_{basket} - m_p}{1 - 1.7844 \frac{\rho_{gas}}{\rho_{pp}}} \quad 6.44$$

The solubility of the penetrant gas in polymer is thus defined as absorbed mass per mass of polymer:

$$S_{gas} = \frac{m_{sorbed}}{m_p} \quad 6.45$$

6.2.4 Experimental plan

The experimental sorption study is conducted aimed at two objectives:

1. Estimation of liquid propylene concentration in polymer, in conditions close to that of homo-polymerization reaction (propylene saturation pressure; $P=33.9$ [bar], $T=75$ [°C]), by fitting and extrapolating the experimentally obtained solubility data of propylene gas to saturation conditions.
2. Determination of equilibrium solubility of propylene and ethylene gases, and thus concentration of species in homo-polymer and copolymer samples in conditions close to that of copolymerization reaction ($P=14$ [bar], $T=75$ [°C]).

Equilibrium solubilities of ethylene and propylene gases in homo-polymer and copolymer samples have been measured at 75 [°C] and pressures ranging between 5 to 25 [bar]. Four different homo-polymer samples produced with two different catalysts in similar conditions were chosen to check the reproducibility of the measurements and to determine whether samples produced with different catalysts display different equilibrium gas solubility. Copolymer samples used for sorption measurements have a rubber content of ranging between 10 to 30 [Mass%], and a fixed ethylene in rubber fraction of 40 [mol%], to study the influence of rubber content on penetrant concentration in amorphous phase.

| Sample number | Catalyst | Sample type | Average crystallinity [Mass%] | Rubber content [Mass%] | C ₂ in Rubber [mol%] |
|---------------|----------|--------------|-------------------------------|------------------------|---------------------------------|
| Hp53 | Cat A | Homo-polymer | 49 | 0 | 0 |
| Hp267 | Cat A | Homo-polymer | 49 | 0 | 0 |
| Hp190 | Cat C | Homo-polymer | 49 | 0 | 0 |
| Hp192 | Cat C | Homo-polymer | 49 | 0 | 0 |
| lcp248 | Cat C | Copolymer | 44.1 | 10 | 40 |
| lcp258 | Cat C | Copolymer | 39.2 | 20 | 40 |
| lcp244 | Cat C | Copolymer | 34.3 | 30 | 40 |

Table 20. Sorption experiments experimental plan

6.2.5 Solubility of gases in homo-polymer samples

The following plot depicts a typical sorption experiment, wherein sorption of propylene gas in a homo-polypropylene sample at 75 [°C] and 10 [bar] pressure is displayed. As penetrating gas propylene is dosed into the measurement chamber, an initial instability in reading of the magnetic balance is observed due to the injection effect, however shortly after the signal

stabilizes and the mass uptake can be observed. Mass uptake starts with a sharper initial slope and after typically 15 to 20 minutes (for samples studied in this work) levels off at the equilibrium solubility level.

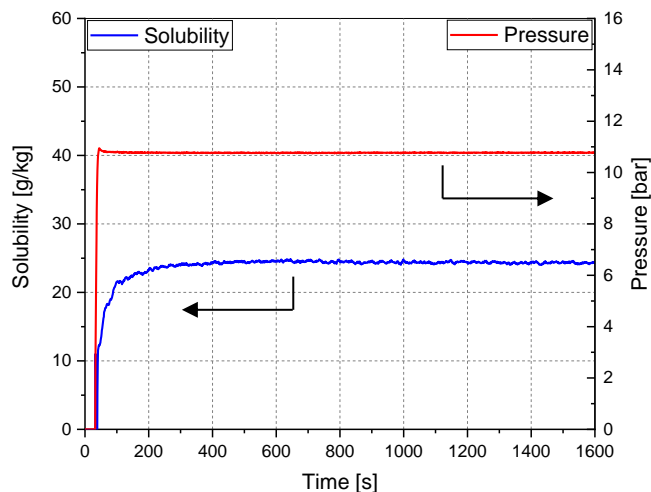


Figure 83. Typical propylene sorption measurement mass uptake curve; $T=75$ [°C] $P=6$ [bar]

The equilibrium value in the graph above indicates the equilibrium solubility at the measurement pressure and temperature.

Equilibrium solubility of propylene gas in four different homo-polymer samples produced with two different catalysts in similar conditions has been measured. It is observed that products of catalysts A and C follow a very similar regime, and the slight possible differences in crystallinity of the samples do not cause a dramatic disparity in resulting equilibrium solubility of propylene.

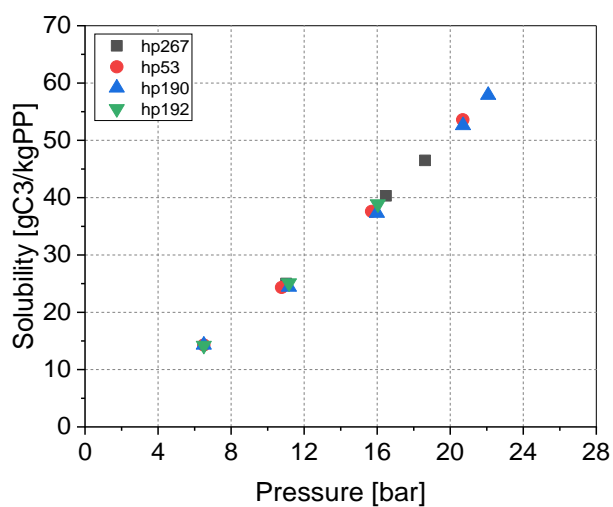


Figure 84. Propylene solubility in different homo-polymer samples; test of reproducibility; $T=75$ [°C] $P=5-23$ [bar]

The equilibrium solubility of ethylene and propylene in a homo-polypropylene sample at 75 [°C] and pressures up to 24 [bar] are presented in the following figure 85:

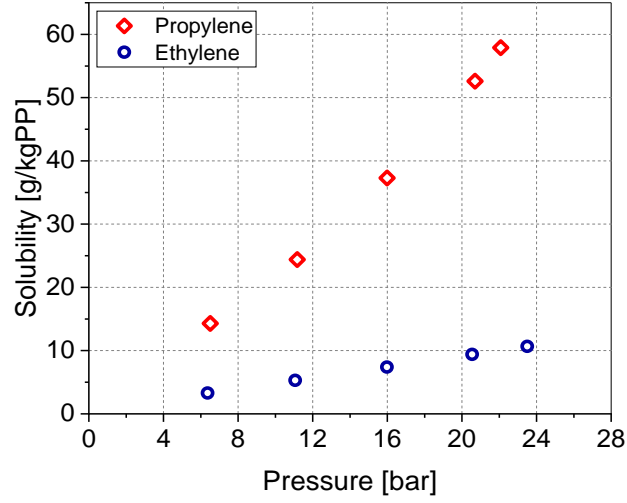


Figure 85. Propylene and ethylene equilibrium solubility in a homo-polymer sample; T=75 [°C] P=5-24 [bar]

The equilibrium solubility results can be used to calculate the concentration of a penetrant in amorphous phase of polymer given as:

$$C_{am} = \frac{n_{sorbed}}{V_{am}} \quad 6.46$$

Where n_{sorbed} is moles of penetrant gas absorbed in polymer, and V_{am} is the volume of the amorphous fraction of the polymer. Swelling of the amorphous polymer phase should be considered, therefore the amorphous phase volume is formulated as:

$$V_{am} = V_{am}^0 + \Delta V_{swelling} = \frac{m_P(1 - X_{cr}^{hp})}{\rho_{am}} + \Delta V_{swelling} \quad 6.47$$

V_{am}^0 is the initial volume of the amorphous phase and $\Delta V_{swelling}$ is the increased volume due to swelling caused by sorption of the penetrant. Equation 6.43 can be used to calculate $\Delta V_{swelling}$.

Therefore, equation 6.46 is reformulated as:

$$C_{am} = \frac{S_{gas}}{M_W(1 - v_{cr} + 1.7844S_{gas})} \quad 6.48$$

Where S_{gas} [gC₃/kgPP] is the solubility measured by the balance, v_{cr} is the volume fraction of crystalline polymer, and M_W is the molecular weight of the penetrant gas. The equilibrium concentrations of ethylene and propylene in amorphous fraction of the homo-polymer samples at 75 [°C] are therefore calculated by equation 6.48 from the solubility data and depicted in figure 86:

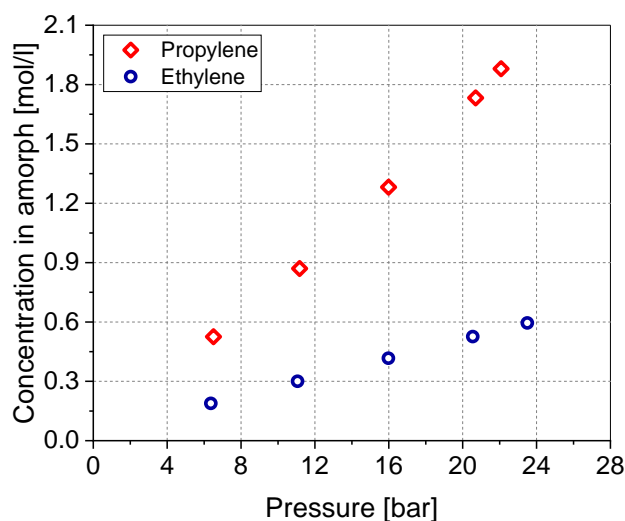


Figure 86. Propylene and ethylene concentration in amorphous fraction of homo-polymer; T=75 [°C] P=5-24 [bar] Propylene has significantly higher concentration in amorphous polymer in similar conditions compared to ethylene. As depicted in figure 86, ethylene concentration appears to be following a linear relation with pressure and can be described by Henry's law in the pressure range of up to 25 [bar] displayed in figure 87. The concentration of ethylene in the amorphous fraction of homo-polypropylene in the pressure range measured in this work can be estimated by the following Henry constant:

$$C_{C2} = H_{C2}P = 0.0238 \text{ [mol/l/bar]} * P \quad 6.49$$

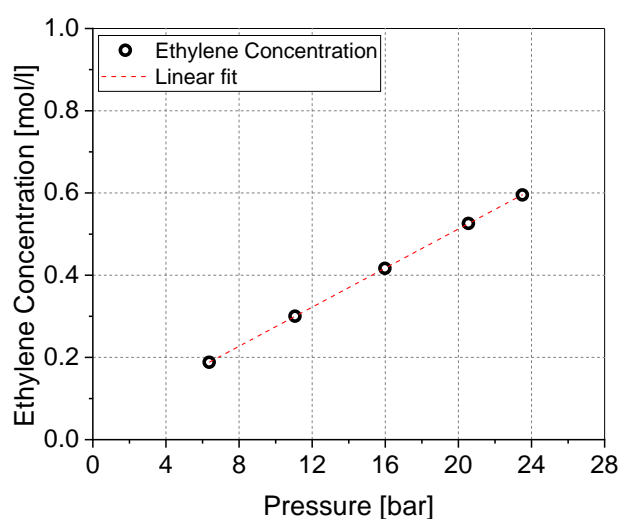


Figure 87. Ethylene concentration in amorphous fraction of homo-polymer; T=75 [°C] P=5-24 [bar]

Propylene concentration deviates from a linear behavior, especially at higher pressures and cannot be described by Henry's law at these higher pressures. Therefore, to fit the experimental solubility data an alternative method needs to be applied. Different approaches have been proposed in literature, e.g. calculation of propylene's gas solubility based on the Flory-Huggins Theory [121] and a semiempirical approach proposed by Hutchinson [125].

A further method is adopting an equation of state for describing the phase equilibria between polymer and penetrant. Sanchez-Lacombe equation of state (SL-Eos) [158] is often used in literature to describe the phase behavior of α -olefins/polyolefins systems [123,124,159–161]. SL-Eos is relatively simple and adopts three molecular parameters to describe a fluid. The theory is based on a lattice–fluid model, aiming to describe, mainly polymer–solvent phase behavior. The general expression of SL-Eos is given as [162]:

$$\bar{\rho}^2 + \bar{P} + \bar{T} \left[\ln(1 - \bar{\rho}) + \left(1 - \frac{1}{r}\right) \bar{\rho} \right] = 0 \quad 6.50$$

Where r is the number of lattice sites occupied by one molecule, \bar{P} , \bar{T} , $\bar{\rho}$ are reduced pressure, temperature, and density are defined as:

$$\bar{\rho} = \frac{1}{\bar{v}} = \frac{rv^*}{v}, v^* = \frac{1}{\rho^*} \quad 6.51$$

$$\bar{T} = \frac{RT}{\varepsilon^*}, T^* = \frac{\varepsilon^*}{R} \quad 6.52$$

$$\bar{P} = \frac{Pv^*}{\varepsilon^*}, P^* = \frac{\varepsilon^*}{v^*} \quad 6.53$$

Where ρ^* , T^* , and P^* are the characteristic values of each substance and are determined experimentally for each substance. In this work, the following characteristic values for propylene and polypropylene are used [163]:

| Substance | T^* [K] | P^* [bar] | ρ^* [kg/m ³] |
|-----------|-----------|-------------|-------------------------------|
| Propylene | 360.4 | 3100 | 670.8 |
| PP | 724.3 | 2800 | 938.9 |

Table 21. Characteristic parameters of SL-Eos

In general, there are three solutions to equation 6.50. The higher density solution corresponds to a liquid while the lower density corresponds to a gas (amorphous polymer phase is considered to behave as a liquid).

In a binary system such as the mixture of propylene gas and the amorphous polypropylene, the characteristic parameters are defined as:

$$v_{ij}^* = \frac{(v_i^* + v_j^*)}{2}, \quad \varepsilon_{ij}^* = \sqrt{\varepsilon_i^* \varepsilon_j^*} (1 - k) \quad 6.54$$

k is the binary interaction parameter and is unique for each binary system. In this study the binary interaction parameter is adjusted to match the experimental data obtained by sorption measurements to describe the Homo-polymer/propylene binary system.

As was illustrated by equation 2.18 The equilibrium between two phases can be established when the condition of equality of the chemical potential of the phases is met. This can be extended to the equilibrium between polymer and penetrant as well. The equilibrium between the penetrant and amorphous polymer phase can be described in terms of fugacity, this condition can be reformulated for the equilibrium between polymer and penetrant as:

$$\hat{\phi}_i^v = x_i \hat{\phi}_i^l \quad 6.55$$

In this formulation the amorphous polymer is assumed to be in liquid phase, and the presence of polymer in gas phase is assumed to be negligible. Fugacity coefficient formulated by SL-Eos is calculated for propylene gas and amorphous polypropylene polymer in order to estimate the mole fraction of propylene in polymer at equilibrium (x_i), and respectively propylene concentration. Fugacity coefficient of a species in mixture by SL-Eos is formulated as:

$$\ln(\hat{\phi}_i) = -\ln(Z) + r_i \left[-2 \frac{\bar{\rho}}{\bar{T}} - \ln(1 - \bar{\rho}) \right] + \left(\frac{Z - 1}{r} \right) \left[\frac{nr}{v^*} \left(\frac{\partial v^*}{\partial n_i} \right) \right] - \frac{\bar{\rho}}{\bar{T}} \left[\frac{nr}{\varepsilon^*} \left(\frac{\partial v^*}{\partial n_i} \right) \right] \quad 6.56$$

To fit the experimentally obtained solubility data of propylene gas in the amorphous fraction of homo-polypropylene, the binary interaction parameter (k) between the propylene gas and the amorphous polymer is adjusted to match the present data set in the measurement range. During the bulk homo-polymerizations, polymer particles are submerged in liquid propylene (at pressures greater than saturation pressure 33.9 [bar]), whereas the sorption measurements can only be performed for gases with pressure up to 25 [bar] (due to limitations of the experimental setup). To estimate the concentration of liquid propylene in amorphous polymer, the values of monomer concentration calculated by SL-Eos, are extrapolated to the saturation pressure of propylene at 75 [°C] ($P_{\text{sat}}=33.9$ [bar]).

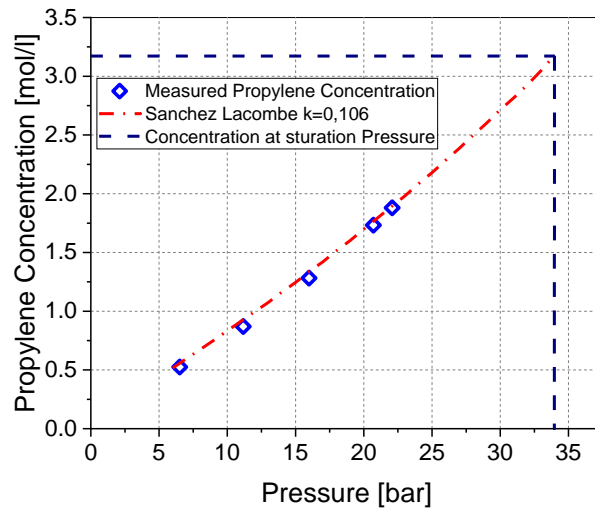


Figure 88. Propylene concentration in amorphous fraction of homo-polymer; T=75 [°C] P=0-33.9 [bar]

By extrapolating the values calculated by SL-Eos to the saturation pressure of propylene, the liquid propylene concentration at 75 [°C] is calculated to be 3.17 [mol/l]. This concentration is assumed to stay constant during the bulk homo-polymerization experiments and is used in the kinetic model in this work. To calculate the concentration of liquid propylene in amorphous polypropylene in existing literature a common method is to use Flory-Huggins theory. This method has been used by Kettner, Samson, and Patzlaff [74] [164]. These results and the values calculated by SL-Eos based on experimental measurements in this work are presented and compared in the following graph:

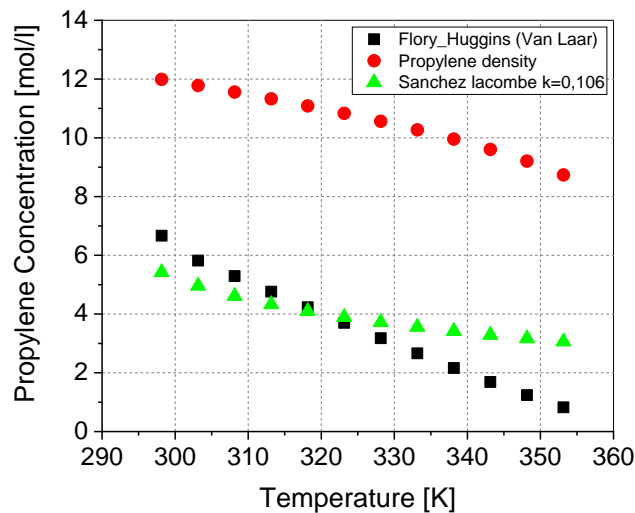


Figure 89. Liquid propylene concentration in amorphous polypropylene at saturation pressure; T=25-80 [°C]; Comparison between Flory, SL Eos, and propylene density

6.2.6 Solubility of gases in copolymer samples

In this section, the experiments conducted were aimed at studying the influence of rubber content of the hetero-phasic copolymers, on the equilibrium solubility of gases and thus concentration in amorphous polymer. Gross equilibrium solubility of propylene and ethylene gases in samples with a range of rubber content have been measured (0~30 [Mass%]) and depicted in figures 90, and 91. These samples all had a similar fraction of ethylene in rubber (~40 [mol%]).

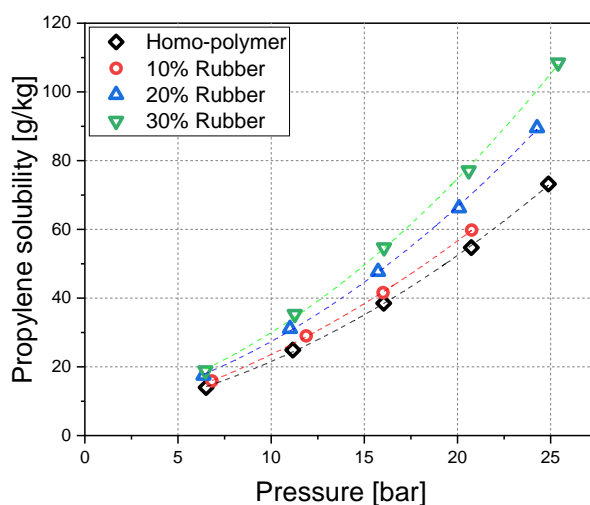


Figure 90. Propylene solubility in copolymer samples; T=75 [°C] P=0-25 [bar] RC=0-30 [Mass%]

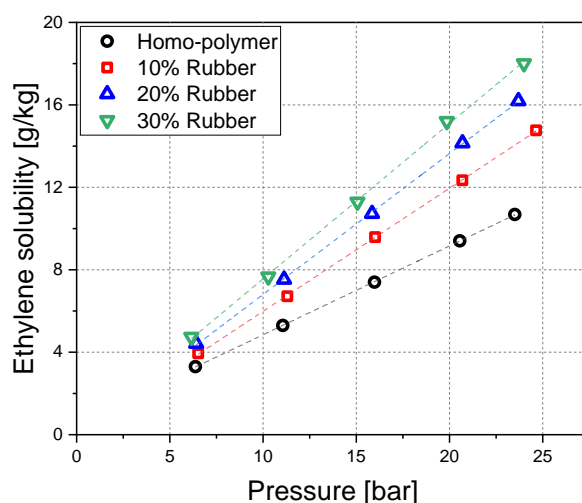


Figure 91. Ethylene solubility in copolymer samples; T=75 [°C] P=0-25 [bar] RC=0-30 [Mass%]

It is observed that by an increase in rubber content, gross gas solubility per mass of the sample increases. This is expected, since the rubber phase is amorphous and causes the overall

crystallinity of the sample to decrease. Gas solubility in hetero-phasic copolymer samples is formulated as:

$$S_{Total} = S_{hp} + S_{cp} = \frac{m_{sorbed,cp} + m_{sorbed,hp}}{m_{sample}} \quad 6.57$$

S_{Total} is the gas solubility in the copolymer sample, S_{hp} is gas solubility in amorphous fraction of the semi-crystalline homo-polymer, and S_{cp} is gas solubility in the amorphous rubber phase. The concentration of each species is calculated via the following equation:

$$C_{am} = \frac{S_{Total}}{M_W(1 - v_{cr} + 1.7844S_{Total})} \quad 6.58$$

Where S_{Total} [g/kg] is the solubility of the species measured by the balance, M_W is the molecular weight of the penetrant, and v_{cr} is the volume fraction of crystalline polymer, and for a copolymer sample is calculated by equation 6.41. The concentration of gases in amorphous polymer (including both, the amorphous fraction of homo-polymer and the copolymer rubber) is depicted in the following graph:

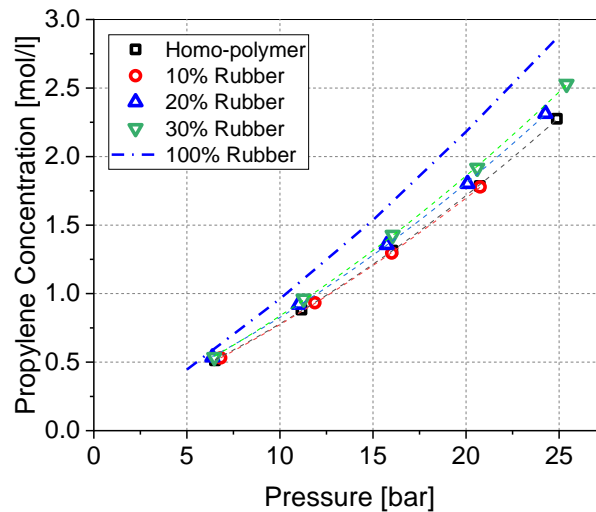


Figure 92. Propylene concentration in amorphous polymer; T=75 [°C] P=0-25 [bar] RC=0-30 [Mass%]

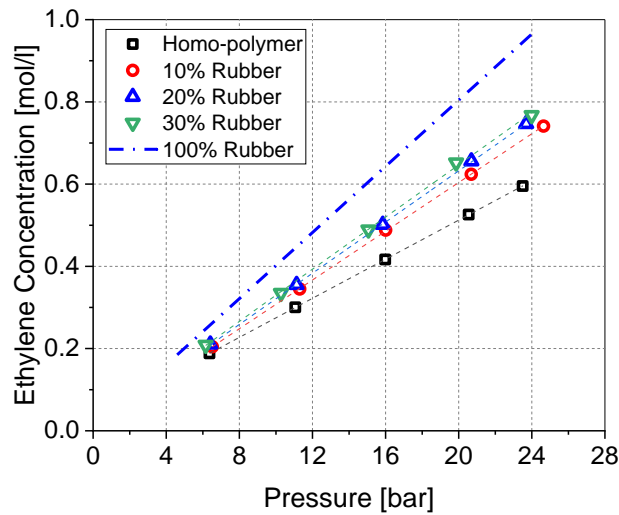


Figure 93. Ethylene concentration in amorphous polymer; T=75 [°C] P=0-25 [bar] RC=0-30 [Mass%]

By extrapolating experimentally measured gas concentration to 100% rubber content, monomer concentration in the (amorphous) rubber phase, can be compared with the concentration in the amorphous fraction of the homo-polymer (equal to 0% rubber content). Both ethylene, and propylene concentrations in the rubber phase copolymer are significantly higher compared to the concentration in the amorphous fraction of homo-polymer.

6.2.7 Concentration of reaction partners during polymerization

In section 6.2.5 the concentration of propylene in the amorphous homo-polymer during bulk-phase homo-polymerization was estimated using Sanchez-Lacombe equation of state for extrapolation the experimentally obtained sorption data to saturation conditions relevant for bulk-phase polymerization in liquid propylene. For the gas-phase copolymerization, this approach however is not needed, since all copolymerization experiments in this study have been carried out at 14 [bar] and lie within possible measurement range of the magnetic sorption balance.

During the gas-phase copolymerization, a mixture of propylene and ethylene gases exist in the reactor. Considering the partial pressure of each species, experimentally measured data for propylene and ethylene concentration are used to determine the concentration of reaction partners. Partial pressures of different species are calculated according to:

$$P_i = y_i P_{copo} \quad 6.59$$

y_i is the mole fraction of each gas in the reactor during copolymerization and is directly measured by the μ -GC setup, and P_{copo} is the copolymerization pressure. The mixing effect on gas solubility of the samples is neglected.

Propylene concentration is formulated in the reaction kinetic model (chapter 7) following the partial pressure of propylene, and the semi-empirical approach introduced by Hutchinson [125] to fit and interpolate between the experimentally obtained data points (displayed in figure 92):

$$C_{C3} = P_{C3} A_H e^{B_H C_{C3}} \quad 6.60$$

In case of ethylene, the concentration in copolymer samples still follows a linear correlation in regard to pressure (figure 91) and can be described by Henry's law.

To estimate the hydrogen concentration during polymerization reactions the following equation is used

$$C_{H2} = x_{H2} C_{C3} \quad 6.61$$

Due to the lack of solubility data for hydrogen in polymer phase, the hydrogen mole fraction in reaction medium (in liquid propylene during homo-polymerization and the subsequent gas mixture in copolymerization stage) is used to estimate the hydrogen concentration in polymer phase.

7 Kinetic modeling

A simplified phenomenological kinetic model has been developed to describe the polymerization kinetics of the two catalysts used in this study. The objective of the model is to describe the experimentally obtained polymerization yields, catalyst activity profiles during the homo-polymerization and copolymerization experiments, as well as product molecular weight (obtained by MFR, and intrinsic viscosity measurements). The model is focused on simulating the conducted experiments in this study, and to estimate the specific kinetic parameters of each catalyst used.

The hydrogen response in homo-polymerization kinetics have been modeled for both catalysts, therein the influence of hydrogen concentration on catalyst activity and homo-polymer product molecular weight has been modeled. Since pre-contacting has no notable influence on homo-polymerization kinetics of catalyst C, Influence of pre-contacting on polymerization activity has only been modeled for catalyst A. Copolymerization kinetics have been modeled for both catalysts, therein the influence of comonomer composition on catalyst activity and the resulting copolymer composition, as well as product molecular weight is simulated. The model has been developed in the commercial software package gPROMS Model Builder 5.1 (Process Systems Enterprise).

7.1 Model assumptions

Ziegler-Natta catalysts have multiple active sites [8] which result in broad molecular weight distributions. By considering multiple types of active centers, kinetic modeling can become relatively complex, therefore the homo-polymerization kinetics in this work have been modeled by incorporating only one type of active center. However, this approach appeared not feasible in case of copolymerization experiments, and thus to describe the copolymerization kinetics more accurately, a second type of active sites was considered to be activated by introduction of comonomer to the system. The kinetic scheme is similar amongst both active center types, however after parameter estimation some rate constants at different sites have to be assigned different values to better match the experimental results.

In the kinetic model it is assumed that mass and heat transfer at the particle scale do not affect the polymerization rate, and no transport limitations are present. Monomer and comonomer concentrations are assumed to be equal to equilibrium concentration and no concentration and temperature gradients in particle are considered:

$$\frac{\partial C_i}{\partial r_p} = 0 \text{ at } (r, t) \quad 7.1$$

$$C_i = C_{eq} \text{ at } (r, t) \quad 7.2$$

$$\frac{\partial T_p}{\partial r_p} = 0 \text{ at } (r, t) \quad 7.3$$

The lab-scale reactor used in this work is considered to be an ideal batch reactor, in terms of mixing and heat removal. During the bulk phase homo-polymerizations the reactor is considered to be in isothermal conditions, and the minor deviations due to process control issues are neglected. During the gas phase semi-batch operation of the reactor in copolymerization stage, iso-baric and isothermal conditions are assumed. The reaction rate parameters are assumed to be constant throughout the polymerization experiments.

The pre-polymerization and heat-up stages are neglected and polymerizations in model simulations are considered to begin at the main reaction temperature and the corresponding pre-polymerization degree.

7.2 Kinetic scheme

The kinetic scheme used in the model is based on the following experimental findings:

Homo-polymerization:

- Hydrogen enhances the homo-polymerization activity for both catalysts in similar fashion.
- By an increase in hydrogen concentration, the products molecular weight decreases.
- An optimum duration of pre-contacting enhances the homo-polymerization activity of catalyst A, whereas longer pre-contacting leads to lower polymerization rate.

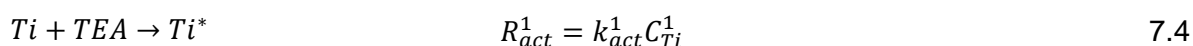
Copolymerization:

- Higher ethylene fraction in gas mixture, enhances the overall activity.
- Higher ethylene fraction in copolymer leads to higher copolymer molecular weight.

Here the kinetic scheme for one type of active centers, including the elementary reaction steps are presented. In each step, the elementary reaction wherein a polymer chain of specific length part takes is outlined, however the reaction rates and mass balances are formulated for chains of all lengths.

Active site formation:

Catalyst titanium components are activated by reacting with the cocatalyst.



k_{act}^1 is the activation rate constant, and C_{Ti}^1 is the concentration of the titanium species in the polymer phase. To simplify, the concentration of the cocatalyst at the active site is not included in this rate equation, and activation is assumed to occur spontaneously. Heterogeneous Ziegler-Natta catalysts mainly consist of $MgCl_2$ support and a fraction of titanium chloride. Catalysts used in this work each have a unique amount titanium (Cat A: 0.026 [g_{Ti}/g_{Cat}], Cat C: 0.037 [g_{Ti}/g_{Cat}]). Only a fraction of titanium species are active in polymerization reactions. This can be due to incomplete activation step by cocatalyst, poisoning, reacting with functional groups of the support material or steric hinderance by the support surface [14].

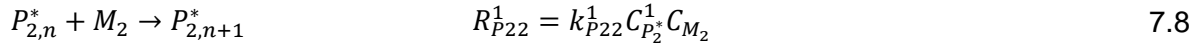
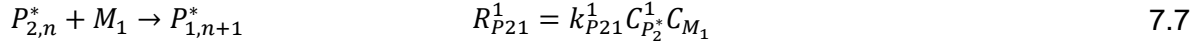
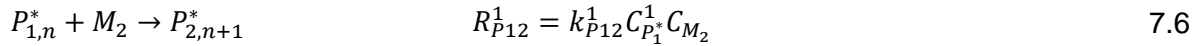
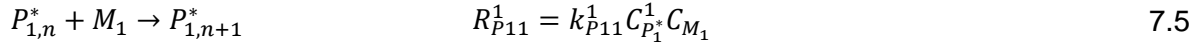
Chain initiation:

The activated catalyst titanium sites instantaneously react with either monomer or comonomer, initiating a polymer chain. Naturally during the homo-polymerization only propylene ended polymer chains are formed.



Chain propagation:

By coordination of monomer to the catalyst active sites, chain propagation occurs.



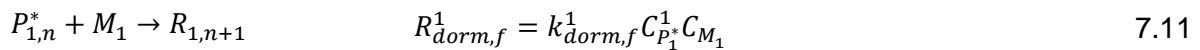
In homo-polymerization, chain propagation only occurs by addition of a propylene molecule to an active chain (equation 7.5). whereas during copolymerization stage propagation can either occur by reaction between a propylene molecule and an active chain ending with propylene or ethylene (equations 7.5 or 7.7), or addition of an ethylene molecule to an active chain ending with propylene or ethylene (equations 7.6 or 7.8). reactivity ratios (r_1 and r_2) for a propylene/ethylene system are defined as:

$$r_1 = \frac{k_{p11}}{k_{p12}} \quad 7.9$$

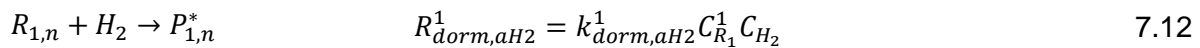
$$r_2 = \frac{k_{p22}}{k_{p21}} \quad 7.10$$

Influence of hydrogen on catalyst activity is explained by the dormant site theory. This theory indicates that dormant polymer chains are formed by 2,1-misinsertion of propylene to the active center, which leads to sterical hinderance, and thus making the active site less reactive. The dormant sites can be reactivated either spontaneously or by reacting with a small molecule such as hydrogen. In this model dormant site formation and reactivation by hydrogen is assumed to happen only to chains ending with propylene.

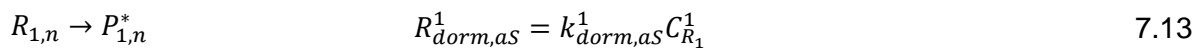
Dormant site formation:



Dormant site reactivation by hydrogen:

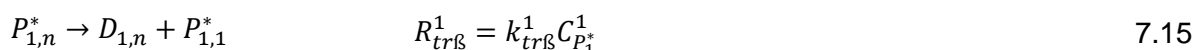
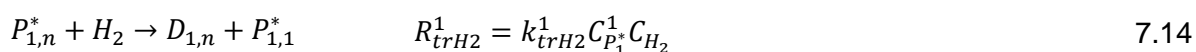


Spontaneous dormant site reactivation:



The influence of hydrogen concentration on product molecular weight, wherein higher hydrogen concentration leads to lower product molecular weight, can be explained with presence of chain transfer reactions. Chain transfer to hydrogen occurs when an active polymer chain reacts with a hydrogen molecule and forms a dead polymer chain and a vacant active site. In order to model the MFR measured for homo-polymer samples produced without any hydrogen (MFR≈0.3 [g/10min]), it was assessed that further transfer reactions must be present. Therefore, in addition to chain transfer to hydrogen, spontaneous chain transfer (by β-hydride elimination) is considered to be present in the polymerization as well. By β-hydride elimination an active chain spontaneously forms a dead chain and a vacant active site.

Chain transfer:



In order to model the molecular weight of copolymer products, initially, chain transfer from chains ending with ethylene was considered, however model calculations revealed that the prominent influence on product molecular weight is posed by chain transfer from active chains ending with propylene, and thus chain transfer from ethylene ended active chains was neglected in the applied kinetic scheme.

Deactivation



The decline over time in activity profiles is explained by deactivation of active sites, therein either an active chain turns into a dead chain, or a vacant site turns into a dead catalyst site. It was reported by Kettner [63] that the deactivation rate is independent of monomer concentration, and as was observed in normalized activity profiles (section 5.6) the deactivation rate is independent of hydrogen concentration. Therefore, it is assumed that deactivation takes place spontaneously. For modeling the copolymerization kinetics different deactivation rate constants for chains ending with ethylene and propylene are incorporated.

To describe the kinetics of the copolymerization reactions a second type of active site is assumed to be activated by introduction of ethylene to the system. The kinetic scheme for the second type of active sites is otherwise identical to the first type. The final kinetic scheme for both type of sites is listed in the following table:

| Kinetic Scheme | Site 1 | Site 2 |
|-----------------------------------|---------------------------------------------------|---------------------------------------------------|
| Activation | $R_{act}^1 = k_{act}^1 C_{Ti}^1$ | $R_{act}^2 = k_{act}^2 C_{Ti}^2$ |
| Propagation | $R_{P11}^1 = k_{P11}^1 C_{P1^*}^1 C_{M1}$ | $R_{P11}^2 = k_{P11}^2 C_{P1^*}^2 C_{M1}$ |
| | $R_{P12}^1 = k_{P12}^1 C_{P1^*}^1 C_{M2}$ | $R_{P12}^2 = k_{P12}^2 C_{P1^*}^2 C_{M2}$ |
| | $R_{P21}^1 = k_{P21}^1 C_{P2^*}^1 C_{M1}$ | $R_{P21}^2 = k_{P21}^2 C_{P2^*}^2 C_{M1}$ |
| | $R_{P22}^1 = k_{P22}^1 C_{P2^*}^1 C_{M2}$ | $R_{P22}^2 = k_{P22}^2 C_{P2^*}^2 C_{M2}$ |
| Chain Transfer | $R_{trH2}^1 = k_{trH2}^1 C_{P1^*}^1 C_{H2}$ | $R_{trH2}^2 = k_{trH2}^2 C_{P1^*}^2 C_{H2}$ |
| | $R_{trR}^1 = k_{trR}^1 C_{P1^*}^1$ | $R_{trR}^2 = k_{trR}^2 C_{P1^*}^2$ |
| Dormant chain formation | $R_{dorm,f}^1 = k_{dorm,f}^1 C_{P1^*}^1 C_{M1}$ | $R_{dorm,f}^2 = k_{dorm,f}^2 C_{P1^*}^2 C_{M1}$ |
| Dormant chain reactivation | $R_{dorm,aH2}^1 = k_{dorm,aH2}^1 C_{R1}^1 C_{H2}$ | $R_{dorm,aH2}^2 = k_{dorm,aH2}^2 C_{R1}^2 C_{H2}$ |
| | $R_{dorm,aS}^1 = k_{dorm,aS}^1 C_{R1}^1$ | $R_{dorm,aS}^2 = k_{dorm,aS}^2 C_{R1}^2$ |
| Deactivation | $R_{d1}^1 = k_{d1}^1 C_{P1^*}^1$ | $R_{d1}^2 = k_{d1}^2 C_{P1^*}^2$ |
| | $R_{d2}^1 = k_{d2}^1 C_{P2^*}^1$ | $R_{d2}^2 = k_{d2}^2 C_{P2^*}^2$ |

Table 22. Final kinetic scheme applied in kinetic model

7.3 Derivation of mass balances

The general mass balance for a reaction partner 'i' is given by:

$$\frac{dn_i}{dt} = V_R \sum_j R_{i,j} \quad 7.18$$

$R_{i,j}$ are the rate expressions of the elementary reactions (j), in which component 'i' takes part according to the reaction scheme outlined in the previous section and table 22.

V_R is the reaction volume, which corresponds to the amorphous part of the semi-crystalline polymer since monomer is only soluble in the amorphous fraction of the polymer. Therefore, equation 7.18 can be rearranged as:

$$\frac{dn_i}{dt} = V_P (1 - v_{cr}) \sum_j R_{i,j} \quad 7.19$$

v_{cr} is the volume fraction of crystalline polymer and is directly proportional to the degree of crystallinity of the polymer (equations 6.39 And 6.41), and V_P is the volume of the entire

polymer. The degree of crystallinity is constant throughout homo-polymerization, whereas during copolymerization, crystallinity decreases with rubber formation since the rubber phase is entirely amorphous.

During the polymerization, the reaction volume is increasing due to formation of the polymer phase. This increase in reaction volume on the other hand causes a decrease in the concentration of the active species (dilution effect). One simple way to treat the dilution effect, is to balance the active components not in concentrations, but in moles (the product of volume and concentration), since these only change due to chemical reaction. As an example, the propagation rate expression can be formulated as:

$$V_R R_{P11}^1 = V_R k_{P11}^1 C_{P1}^1 C_{M1} = V_P (1 - v_{cr}) k_{P11}^1 C_{P1}^1 C_{M1} \quad 7.20$$

With

$$n_{P1}^1 = V_P C_{P1}^1 \quad 7.21$$

Since it is assumed, that the catalyst active sites and their subsequent transformations (active, dead, or dormant polymer chains) are uniformly distributed in the polymer phase, this can be rearranged to:

$$V_R R_{P11}^1 = (1 - v_{cr}) k_{P11}^1 n_{P1}^1 C_{M1} \quad 7.22$$

In the same manner, the following material balances of the species have been obtained, starting from the reaction scheme outlined in table 22.

For site type 1, active chains of all lengths ended by propylene, the following balance is obtained:

$$\begin{aligned} \frac{dn_{P1}^1}{dt} = R_{P1}^1 V_R = V_P (1 - v_{cr}) (R_{act}^1 + R_{dorm,as}^1 + R_{dorm,aH2}^1 + R_{P21}^1 - R_{P12}^1 - R_{dorm,f}^1 - \\ R_{d1}^1) = (1 - v_{cr}) (k_{act}^1 n_{Ti}^1 + k_{dorm,aH2}^1 n_{R1}^1 C_{H2} + k_{dorm,as}^1 n_{R1}^1 + k_{P21}^1 n_{P2}^1 C_{M1} - \\ k_{P12}^1 n_{P1}^1 C_{M2} - k_{dorm,f}^1 n_{P1}^1 C_{M1} - k_{d1}^1 n_{P1}^1) \end{aligned} \quad 7.23$$

$$n_{P1}^1(t = 0) = 0$$

The initial number of active titanium species that in turn can potentially initiate a propylene ended active chain at site type one, is formulated as:

$$n_{Ti}^1(t = 0) = \frac{x_{active} \cdot m_{cat} \cdot x_{Ti}}{M_{wTi}} \quad 7.24$$

Where, x_{Ti} is the mass fraction of titanium in catalyst, x_{active} is the fraction of active titanium centers, m_{cat} is the catalyst mass used in the polymerization experiment, and M_{wTi} is the molar mass of titanium. Some experimental techniques for determination of the fraction of active species in polymerizations of Ziegler-Natta catalysts have been developed such as active site tagging with alcohols or carbon monoxide and the stopped flow technique. In general terms it is believed that between 1-10% off the titanium atoms are activated during polymerization [165–167].

The fraction of active titanium species of both catalysts in this model is considered to be fixed at 2% in all process simulations, with the exception of experiments with different duration of pre-contacting, therein the fraction of titanium active species is adjusted to describe the catalyst activity accordingly.

Balancing leads for site type 2, active chains of all lengths ended by propylene, to the following mass-balance:

$$\begin{aligned} \frac{dn_{P_1^*}^2}{dt} = R_{P_1^*}^2 V_R = V_P (1 - v_{cr}) (R_{dorm,as}^2 + R_{dorm,aH_2}^2 + R_{P_{21}}^2 - R_{P_{12}}^2 - R_{dorm,f}^2 - R_{d_1}^2) = \\ (1 - v_{cr}) (k_{dorm,aH_2}^2 n_{R_1}^2 C_{H_2} + k_{dorm,as}^2 n_{R_1}^2 + k_{P_{21}}^1 n_{P_2^*}^2 C_{M_1} - k_{P_{12}}^2 n_{P_1^*}^2 C_{M_2} - \\ k_{dorm,f}^2 n_{P_1^*}^2 C_{M_1} - k_{d_1}^2 n_{P_1^*}^2) \end{aligned} \quad 7.25$$

$$n_{P_1^*}^2(t = 0) = 0$$

Propylene ended active chains of site type 2 are formed respectively via, dormant site reactivation (with hydrogen or spontaneous), and propagation reaction between active chains ending with ethylene and a propylene molecule. Propylene active species are consumed via deactivation, dormant site formation, and cross propagation with an ethylene molecule. Naturally, during homo-polymerization stage the terms in the balance that include concentration of ethylene and ethylene ended chains are equal to zero and disappear. It must be noted that, as displayed in the kinetic scheme the transfer reactions do not influence the total number of active chains, since by consuming an active chain of a certain length an un-initiated active site is recreated and in our assumed kinetic scheme, chain initiation is instantaneous.

The mass balance for the active chains ending with ethylene is derived as:

Site type 1:

$$\frac{dn_{P_2^*}^1}{dt} = V_P(1 - v_{cr})(R_{P_{12}}^1 - R_{P_{21}}^1 - R_{d2}^1) = (1 - v_{cr})(k_{P_{12}}^1 n_{P_1^*}^1 C_{M_2} - k_{P_{21}}^1 n_{P_2^*}^1 C_{M_1} - k_{d2}^1 n_{P_2^*}^1) \quad 7.26$$

$$n_{P_2^*}^1(t = 1 \text{ hr}) = 0$$

Site type 2:

$$\frac{dn_{P_2^*}^2}{dt} = V_P(1 - v_{cr})(R_{act}^2 + R_{P_{12}}^2 - R_{P_{21}}^2 - R_{d2}^2) = (1 - v_{cr})(k_{act}^2 n_{Ti}^2 + k_{P_{12}}^2 n_{P_1^*}^2 C_{M_2} - k_{P_{21}}^2 n_{P_2^*}^2 C_{M_1} - k_{d2}^2 n_{P_2^*}^2) \quad 7.27$$

$$(t = 1 \text{ hr}) = 0$$

Ethylene ended active chains are produced by reaction between propylene ended active chains and ethylene molecules, and by formation of active chains at the second site through activation reaction. Ethylene ended active chains are consumed by reacting with propylene molecules and through deactivation reaction. In mass balance of active chains ending with ethylene, the terms for dormant site formation and reactivation are absent.

The activation and initiation reactions at the second site type are considered to only result in ethylene initiated active chains, hence the activation term was absent from the balance for the propylene ended active chains of site type 2. By activation of site type 2 a number of new titanium centers are introduced to the polymerization environment. The mole number of re-introduced potential titanium centers is assumed to be proportional to the ethylene mole fraction in the system, hence with a higher ethylene concentration in reaction, a larger number of active centers are created, which in turn instantaneously initiate an active chain by reacting with an ethylene molecule. This approach was applied to describe the activation effect of ethylene on the copolymerization reaction.

$$n_{Ti}^2 \text{ at } (t = 1 \text{ hr}) = y_{C_2} \frac{x_{active}^2 m_{cat} x_{Ti}}{M_{wTi}} \quad 7.28$$

The mass balance for dormant chains of all lengths of both site types are derived as (dormant chains are only propylene ended):

$$\begin{aligned} \frac{dn_R}{dt} = V_P(1 - v_{cr})(R_{dorm,f}^1 + R_{dorm,f}^2 - R_{dorm,aH_2}^1 - R_{dorm,aS}^1 - R_{dorm,aH_2}^2 - \\ R_{dorm,aS}^2) = (1 - v_{cr})(k_{dorm,f}^1 n_{P_1^*}^1 C_{M_1} + k_{dorm,f}^2 n_{P_1^*}^2 C_{M_1} - k_{dorm,aH_2}^1 n_{R_1}^1 C_{H_2} - \\ k_{dorm,aS}^1 n_{R_1}^1 - k_{dorm,aH_2}^2 n_{R_1}^2 C_{H_2} - k_{dorm,aS}^2 n_{R_1}^2) \end{aligned} \quad 7.29$$

$$n_{R_1}(t = 0) = 0$$

Dormant chains are formed through the dormant chain formation reaction (1-2 miss insertion) and consumed (reactivated) via reacting with hydrogen molecules and spontaneous reactivation reaction.

Mass balance of entire dead chains of all lengths and all end species of both site types:

$$\begin{aligned} \frac{dn_D}{dt} = & V_P(1 - v_{cr})(R_{d1}^1 + R_{d1}^2 + R_{d2}^1 + R_{d2}^2 + R_{trH_2}^1 + R_{trH_2}^2 + R_{trB}^1 + R_{trB}^2) = (1 - \\ & v_{cr})(k_{d1}^1 n_{P_1}^1 + k_{d1}^2 n_{P_1}^2 + k_{d2}^1 n_{P_2}^1 + k_{d2}^2 n_{P_2}^2 + k_{trH_2}^1 n_{P_1}^1 C_{H_2} + k_{trH_2}^2 n_{P_1}^2 C_{H_2} + k_{trB}^1 n_{P_1}^1 + \\ & k_{trB}^2 n_{P_1}^2) \end{aligned} \quad 7.30$$

$$n_D(t = 0) = 0$$

Dead chains are formed through transfer and deactivation reactions. The initial values for the number of dead, dormant and active chains are set at zero in the model. The amount of polymer produced over reaction time is equal to the total consumed monomer and comonomer. The overall rate of propylene consumption is formulated as:

$$R_{C_3} = (R_{P_{11}}^1 + R_{P_{21}}^1 + R_{P_{11}}^2 + R_{P_{21}}^2)V_P(1 - v_{cr}) \quad 7.31$$

propylene consumption by the formation of dormant chains is neglected, since the overall number of dormant chains is negligible.

Overall rate of ethylene consumption is formulated as:

$$R_{C_2} = (R_{P_{22}}^1 + R_{P_{12}}^1 + R_{P_{22}}^2 + R_{P_{12}}^2)V_P(1 - v_{cr}) \quad 7.32$$

Overall polymer production rate is therefore derived as:

$$\frac{dm_p}{dt} = -(R_{C_2}M_{W_{C_2}} + R_{C_3}M_{W_{C_3}}) \quad 7.33$$

Consumption rate is expanded as:

$$\begin{aligned} \frac{dm_p}{dt} = & -[(k_{P_{11}}^1 n_{P_1}^1 C_{M_1} + k_{P_{21}}^1 n_{P_2}^1 C_{M_1} + k_{P_{11}}^2 n_{P_1}^2 C_{M_1} + k_{P_{21}}^2 n_{P_2}^2 C_{M_1})M_{W_{C_3}} + \\ & (k_{P_{22}}^1 n_{P_2}^1 C_{M_2} + k_{P_{12}}^1 n_{P_1}^1 C_{M_2} + k_{P_{22}}^2 n_{P_2}^2 C_{M_2} + k_{P_{12}}^2 n_{P_1}^2 C_{M_2})M_{W_{C_2}}](1 - v_{cr}) \end{aligned} \quad 7.34$$

And thus, activity is derived as:

$$Activity \left[\frac{kg}{gCat.hr} \right] = \frac{dm_p}{dt} \frac{1}{m_{cat}} \frac{3600 \left[\frac{s}{hr} \right]}{1000 \left[\frac{g}{kg} \right]} \quad 7.35$$

7.4 Method of moments

Species population balances for all species of different chain lengths in the polymerization, result in a set of ordinary differential equations. These ODE equations can be numerically solved to achieve the complete molecular weight distribution. This approach, however, requires significant computational effort. In many publications regarding mathematical modeling of olefin polymerization kinetics, for simplifying the computations the method of moments is adopted. The method of moments permits one to statistically calculate the number and weight averages of polymer chains as well as polydispersity index. Method of moments cannot predict the full molecular weight distribution rather; it predicts the molecular weight averages. Method of moments has been applied in studies to describe the molecular weight averages resulting from catalytic polymerization and copolymerization of olefins [102,168,169]. The i^{th} moment of a species in polymerization is defined as:

$$m^i = \sum_{n=1}^{\infty} n^i \cdot c_{mn} = \sum_{n=1}^{\infty} n^i \cdot n_{mn} \quad 7.36$$

The exponent i corresponds to the moment order. c_{mn}, n_{mn} correspond to concentration and respectively mole number of species m , and the subscript n indicates the chain length. By using the mass balances for different species, the following equation for 0th, 1st and 2nd moments corresponding to species present in the homo-polymerization are derived.

| Order | Species | Equation |
|-------------------------------------|----------------|----------------------------------------------------------------------------------------------------------------------------------------------------------------------------------------------------------|
| 0th order moments | Active chains | $dQ_1^0/dt = k_{act}^1 n_{Ti}^1 + (k_{dorm,aH2}^1 C_{H2} + k_{dorm,aS}^1) R^0 - (k_{dorm,f}^1 C_{M1} + k_{d1}^1) Q_1^0$ |
| | Dormant chains | $dR^0/dt = k_{dorm,f}^1 C_{M1} Q_1^0 - (k_{dorm,aH2}^1 C_{H2} + k_{dorm,aS}^1) R^0$ |
| | Dead chains | $dD^0/dt = (k_{trH2}^1 C_{H2}^{0.5} + k_{trB}^1 + k_{d1}^1) Q_1^0$ |
| 1st order moments | Active chains | $dQ_1^1/dt = k_{act}^1 n_{Ti}^1 + k_{p11}^1 C_{M1} Q_1^0 + (k_{dorm,aH2}^1 C_{H2} + k_{dorm,aS}^1) R^1 - (k_{dorm,f}^1 C_{M1} + k_{d1}^1) Q_1^1 + (k_{trH2}^1 C_{H2}^{0.5} + k_{trB}^1) (Q_1^0 - Q_1^1)$ |
| | Dormant chains | $dR^1/dt = k_{dorm,f}^1 C_{M1} Q_1^1 - (k_{dorm,aH2}^1 C_{H2} + k_{dorm,aS}^1) R^1$ |
| | Dead chains | $dD^1/dt = (k_{trH2}^1 C_{H2}^{0.5} + k_{trB}^1 + k_{d1}^1) Q_1^1$ |

| Order | Species | Equation |
|-------------------------------|----------------|---------------------------------------------------------------------------------------------------------------------------------------------------------------------------------------------------------------------|
| 2 nd order moments | Active chains | $dQ_1^2/dt = k_{act}^1 n_{Ti}^1 + k_{p11}^1 C_{M1} (2Q_1^1 + Q_1^0) + (k_{dorm,aH2}^1 C_{H2} + k_{dorm,aS}^1) R^2 - (k_{dorm,f}^1 C_{M1} + k_{d1}^1) Q_1^2 + (k_{trH2}^1 C_{H2}^{0.5} + k_{trB}^1) (Q_1^0 - Q_1^2)$ |
| | Dormant chains | $dR^2/dt = k_{dorm,f}^1 C_{M1} Q_1^2 - (k_{dorm,aH2}^1 C_{H2} + k_{dorm,aS}^1) R^2$ |
| | Dead chains | $dD^2/dt = (k_{trH2}^1 C_{H2}^{0.5} + k_{trB}^1 + k_{d1}^1) Q_1^2$ |

Table 23. Species moments during homo-polymerization

It must be noted that during copolymerization stage, a second separate phase of polymer is produced, and therefore a separate set of equations for moments corresponding to species during copolymerization are derived and incorporated in the kinetic model. The balancing for derivation of the moments during copolymerization is performed separately for each active site type:

| Order | Species | Equation |
|-------------------------------|---------------------------------------------|----------------------------------------------------------------------------------------------------------------------------------------------------------------------------------------------------------------------------------------------------------------------------------------------------------------------------------|
| 0 th order moments | Active chains (propylene Ended) Site type 1 | $dQ_{1,cp1}^0/dt = k_{act}^1 n_{Ti}^1 + (k_{p21}^1 C_{M1}) Q_{2,cp1}^0 - (k_{p12}^1 C_{M2}) Q_{1,cp1}^0 + (k_{dorm,aH2}^1 C_{H2} + k_{dorm,aS}^1) R_{cp1}^0 - (k_{dorm,f}^1 C_{M1} + k_{d1}^1) Q_{1,cp1}^0$ |
| | Active chains (propylene Ended) Site type 2 | $dQ_{1,cp2}^0/dt = (k_{p21}^2 C_{M1}) Q_{2,cp2}^0 - (k_{p12}^2 C_{M2}) Q_{1,cp2}^0 + (k_{dorm,aH2}^2 C_{H2} + k_{dorm,aS}^2) R_{cp2}^0 - (k_{dorm,f}^2 C_{M1} + k_{d1}^2) Q_{1,cp2}^0$ |
| | Active chains (ethylene Ended) Site type 1 | $dQ_{2,cp1}^0/dt = (k_{p12}^1 C_{M2}) Q_{1,cp1}^0 - (k_{p21}^1 C_{M1}) Q_{2,cp1}^0 - (k_{d2}^1) Q_{2,cp1}^0$ |
| | Active chains (ethylene Ended) Site type 2 | $dQ_{2,cp2}^0/dt = k_{act}^2 n_{Ti}^2 + (k_{p12}^2 C_{M2}) Q_{1,cp2}^0 - (k_{p21}^2 C_{M1}) Q_{2,cp2}^0 - (k_{d2}^2) Q_{2,cp2}^0$ |
| | Dormant chains Site type 1 | $dR_{cp1}^0/dt = (k_{dorm,f}^1 C_{M1}) Q_{1,cp1}^0 - (k_{dorm,aH2}^1 C_{H2} + k_{dorm,aS}^1) R_{cp1}^0$ |
| | Dormant chains Site type 2 | $dR_{cp2}^0/dt = (k_{dorm,f}^2 C_{M1}) Q_{1,cp2}^0 - (k_{dorm,aH2}^2 C_{H2} + k_{dorm,aS}^2) R_{cp2}^0$ |
| | Dead chains Site type 1 | $dD_{cp1}^0/dt = (k_{d2}^1) Q_{2,cp1}^0 + (k_{d1}^1 + k_{trH2}^1 C_{H2}^{0.5} + k_{trB}^1) Q_{1,cp1}^0$ |
| | Dead chains Site type 2 | $dD_{cp2}^0/dt = (k_{d2}^2) Q_{2,cp2}^0 + (k_{d1}^2 + k_{trH2}^2 C_{H2}^{0.5} + k_{trB}^2) Q_{1,cp2}^0$ |
| 1 st order moments | Active chains (propylene Ended) Site type 1 | $dQ_{1,cp1}^1/dt = k_{act}^1 n_{Ti}^1 + (k_{p11}^1 C_{M1}) Q_{1,cp1}^0 + (k_{p21}^1 C_{M1}) (Q_{2,cp1}^0 + Q_{2,cp1}^1) - (k_{p12}^1 C_{M2}) Q_{1,cp1}^1 + (k_{dorm,aH2}^1 C_{H2} + k_{dorm,aS}^1) R_{cp1}^1 - (k_{dorm,f}^1 C_{M1} + k_{d1}^1) Q_{1,cp1}^1 + (k_{trH2}^1 C_{H2}^{0.5} + k_{trB}^1) (Q_{1,cp1}^0 - Q_{1,cp1}^1)$ |
| | Active chains (propylene Ended) Site type 2 | $dQ_{1,cp2}^1/dt = (k_{p11}^2 C_{M1}) Q_{1,cp2}^0 + (k_{p21}^2 C_{M1}) (Q_{2,cp2}^0 + Q_{2,cp2}^1) - (k_{p12}^2 C_{M2}) Q_{1,cp2}^1 + (k_{dorm,aH2}^2 C_{H2} + k_{dorm,aS}^2) R_{cp2}^1 - (k_{dorm,f}^2 C_{M1} + k_{d1}^2) Q_{1,cp2}^1 + (k_{trH2}^2 C_{H2}^{0.5} + k_{trB}^2) (Q_{1,cp2}^0 - Q_{1,cp2}^1)$ |
| | Active chains (ethylene Ended) Site type 1 | $dQ_{2,cp1}^1/dt = (k_{p22}^1 C_{M2}) Q_{2,cp1}^0 - (k_{p21}^1 C_{M1}) Q_{2,cp1}^1 + (k_{p12}^1 C_{M2}) (Q_{1,cp1}^0 + Q_{1,cp1}^1) - (k_{d2}^1) Q_{2,cp1}^1$ |

| Order | Species | Equation |
|-------------------------------------|---------------------------------------------|---------------------------------------------------------------------------------------------------------------------------------------------------------------------------------------------------------------------------------------------------------------------------------------------------------------------------------------------------------------|
| 1st order moments | Active chains (ethylene Ended) Site type 2 | $dQ_{2,cp2}^1/dt = k_{act}^2 n_{Ti}^2 + (k_{p22}^2 C_{M2}) Q_{2,cp2}^0 - (k_{p21}^2 C_{M1}) Q_{2,cp2}^1 + (k_{p12}^2 C_{M2})(Q_{1,cp2}^0 + Q_{1,cp2}^1) - (k_{d2}^2) Q_{2,cp2}^1$ |
| | Dormant chains Site type 1 | $dR_{cp1}^1/dt = (k_{dorm,f}^1 C_{M1}) Q_{1,cp1}^1 - (k_{dorm,aH2}^1 C_{H2} + k_{dorm,as}^1) R_{cp1}^1$ |
| | Dormant chains Site type 2 | $dR_{cp2}^1/dt = (k_{dorm,f}^2 C_{M1}) Q_{1,cp2}^1 - (k_{dorm,aH2}^2 C_{H2} + k_{dorm,as}^2) R_{cp2}^1$ |
| | Dead chains Site type 1 | $dD_{cp1}^1/dt = (k_{d2}^1) Q_{2,cp1}^1 + (k_{d1}^1 + k_{trH2}^1 C_{H2}^{0.5} + k_{trB}^1) Q_{1,cp1}^1$ |
| | Dead chains Site type 2 | $dD_{cp2}^1/dt = (k_{d2}^2) Q_{2,cp2}^1 + (k_{d1}^2 + k_{trH2}^2 C_{H2}^{0.5} + k_{trB}^2) Q_{1,cp2}^1$ |
| 2nd order moments | Active chains (propylene Ended) Site type 1 | $dQ_{1,cp1}^2/dt = k_{act}^1 n_{Ti}^1 + (k_{p11}^1 C_{M1})(2Q_{1,cp1}^1 + Q_{1,cp1}^0) + (k_{p21}^1 C_{M1})(Q_{2,cp1}^1 + 2Q_{2,cp1}^0 + Q_{2,cp1}^1) - (k_{p12}^1 C_{M2}) Q_{1,cp1}^2 + (k_{dorm,aH2}^1 C_{H2} + k_{dorm,as}^1) R_{cp1}^2 - (k_{dorm,f}^1 C_{M1} + k_{d1}^1) Q_{1,cp1}^2 + (k_{trH2}^1 C_{H2}^{0.5} + k_{trB}^1)(Q_{1,cp1}^0 - Q_{1,cp1}^1)$ |
| | Active chains (propylene Ended) Site type 2 | $dQ_{1,cp2}^2/dt = (k_{p11}^2 C_{M1})(2Q_{1,cp2}^1 + Q_{1,cp2}^0) + (k_{p21}^2 C_{M1})(Q_{2,cp2}^1 + 2Q_{2,cp2}^0 + Q_{2,cp2}^1) - (k_{p12}^2 C_{M2}) Q_{1,cp2}^2 + (k_{dorm,aH2}^2 C_{H2} + k_{dorm,as}^2) R_{cp2}^2 - (k_{dorm,f}^2 C_{M1} + k_{d1}^2) Q_{1,cp2}^2 + (k_{trH2}^2 C_{H2}^{0.5} + k_{trB}^2)(Q_{1,cp2}^0 - Q_{1,cp2}^1)$ |
| | Active chains (ethylene Ended) Site type 1 | $dQ_{2,cp1}^2/dt = (k_{p22}^1 C_{M2})(Q_{2,cp1}^0 + 2Q_{2,cp1}^1) + (k_{p12}^1 C_{M2})(Q_{1,cp1}^0 + 2Q_{1,cp1}^1 + Q_{1,cp1}^1) - (k_{p21}^1 C_{M1}) Q_{2,cp1}^2 - (k_{d2}^1) Q_{2,cp1}^2$ |
| | Active chains (ethylene Ended) Site type 2 | $dQ_{2,cp2}^2/dt = k_{act}^2 n_{Ti}^2 + (k_{p22}^2 C_{M2})(Q_{2,cp2}^0 + 2Q_{2,cp2}^1) + (k_{p12}^2 C_{M2})(Q_{1,cp2}^0 + 2Q_{1,cp2}^1 + Q_{1,cp2}^1) - (k_{p21}^2 C_{M1}) Q_{2,cp2}^2 - (k_{d2}^2) Q_{2,cp2}^2$ |
| | Dormant chains Site type 1 | $dR_{cp1}^2/dt = (k_{dorm,f}^1 C_{M1}) Q_{1,cp1}^2 - (k_{dorm,aH2}^1 C_{H2} + k_{dorm,as}^1) R_{cp1}^2$ |
| | Dormant chains Site type 2 | $dR_{cp2}^2/dt = (k_{dorm,f}^2 C_{M1}) Q_{1,cp2}^2 - (k_{dorm,aH2}^2 C_{H2} + k_{dorm,as}^2) R_{cp2}^2$ |
| | Dead chains Site type 1 | $dD_{cp1}^2/dt = (k_{d2}^1) Q_{2,cp1}^2 + (k_{d1}^1 + k_{trH2}^1 C_{H2}^{0.5} + k_{trB}^1) Q_{1,cp1}^2$ |
| | Dead chains Site type 2 | $dD_{cp2}^2/dt = (k_{d2}^2) Q_{2,cp2}^2 + (k_{d1}^2 + k_{trH2}^2 C_{H2}^{0.5} + k_{trB}^2) Q_{1,cp2}^2$ |

Table 24. Species moments during copolymerization

Weight average molecular weight and number average molecular weight by method of moments for homo-polymer are derived as:

$$M_{n,hp} = \frac{Q^1 + R^1 + D^1}{Q^0 + R^0 + D^0} Mw_{C3} \quad 7.37$$

$$M_{w,hp} = \frac{Q^2 + R^2 + D^2}{Q^1 + R^1 + D^1} Mw_{C3} \quad 7.38$$

Weight average molecular weight and number average molecular weight by method of moments for rubber phase copolymer are derived as:

$$M_{n,EPR} = \frac{Q_{2,cp1}^1 + Q_{1,cp1}^1 + Q_{2,cp2}^1 + Q_{1,cp2}^1 + R_{cp1}^1 + R_{cp2}^1 + D_{cp1}^1 + D_{cp2}^1}{Q_{2,cp1}^0 + Q_{1,cp1}^0 + Q_{2,cp2}^0 + Q_{1,cp2}^0 + R_{cp1}^0 + R_{cp2}^0 + D_{cp1}^0 + D_{cp2}^0} \bar{M} \quad 7.39$$

$$M_{w,EPR} = \frac{Q_{2,cp1}^2 + Q_{1,cp1}^2 + Q_{2,cp2}^2 + Q_{1,cp2}^2 + R_{cp1}^2 + R_{cp2}^2 + D_{cp1}^2 + D_{cp2}^2}{Q_{2,cp1}^1 + Q_{1,cp1}^1 + Q_{2,cp2}^1 + Q_{1,cp2}^1 + R_{cp1}^1 + R_{cp2}^1 + D_{cp1}^1 + D_{cp2}^1} \bar{M} \quad 7.40$$

\bar{M} is the average mass of repeating unit in the polymer chain and is defined as the following, with x_{C_2} as the mole fraction of ethylene in copolymer:

$$\bar{M} = x_{C_2} M_{wC_2} + (1 - x_{C_2}) M_{wC_3} \quad 7.41$$

Polydispersity is calculated as:

$$PDI = \frac{M_w}{M_n} \quad 7.42$$

The model calculates the molecular weight of homo-polymer matrix and rubber phase copolymer separately, in order to match the experimentally obtained values of weight average molecular weight, and thus melt flow rate of each polymer phase.

The aim of the model is to describe the influence of hydrogen concentration in homo-polymerization on homo-polymer matrix molecular weight, and the effect of ethylene composition of copolymer on rubber phase molecular weight. The following experimental correlations between weight average molecular weight of each polymer phase and the corresponding melt flow rate have been incorporated in the model (see chapter 5.5.4):

Homo-polymer Matrix:

$$MFR_{hp} = 9.3 * 10^{10} [M_{w,hp}]^{-4.016} \quad 7.43$$

Rubber phase copolymer:

$$MFR_{EPR} = 2 * 10^7 [M_{w,EPR}]^{-2.797} \quad 7.44$$

And the total MFR of the final product (including both homo-polymer and rubber), is calculated in the model by the following mixing rule:

$$\text{Log}(MFR_{Total}) = (1 - RC)\text{Log}(MFR_{hp}) + (RC)\text{Log}(MFR_{EPR}) \quad 7.45$$

7.5 Model implementation and parameter estimation

The model has been implemented in the commercial software package gPROMS Model Builder 5.1 (Process Systems Enterprise). The rate equations presented in the kinetic scheme, the differential equation of species balances, and polymer chain moments are given under "Model" section in gPROMS. By assigning values for rate constants, reaction conditions, and catalyst specific parameters, a process can be defined, therein gPROMS enables to simulate the polymerization reaction. The following information about experiments are defined for each process in gPROMS: the experiment duration, the initial conditions, and values of time invariant quantities.

Under "performed experiment" section, the experimentally obtained data is given to the software. Measurements of key quantities (corresponding to model variables) are taken throughout the duration of an experiment. Each measurement consists of three pieces of information:

The value of the measured quantity, the time at which the measurement was taken, and the uncertainty to which the measurement is known, which is expressed as the statistical standard deviation of the measurement, and in this case corresponds to the standard deviation associated with the experimental polymerization procedure.

In this model the activity profiles, and the corresponding melt flow rate of the product and ethylene composition in resulting polymer are given to the software. For reducing the computation load for each performed experiment only up to 24 data points at selected times from the experimentally obtained activity profiles are chosen. A constant variance model with variation of 3.5% is defined for the experimental data points based on information presented in table 9.

By parameter estimation process the kinetic constant parameters are fitted by gPROMS to match the measured experimental data. The process of fitting these parameters to laboratory or plant data is called "parameter estimation" in the software and is based on the maximum likelihood formulation, which includes simultaneous estimation of parameters. When solving a maximum likelihood parameter estimation problem, gPROMS attempts to determine values for the uncertain parameters that maximize the probability that the mathematical model will predict the measurement values obtained from the experiments.

Since a high number of parameters must be estimated, the following stepwise procedure was used separately for each catalyst:

Initially, a standard homo-polymerization experiment was considered (with 1 [mol%] hydrogen): While keeping the active titanium fraction fixed at 2%, the propagation rate constant of propylene (k_{p11}^1) was adjusted to match experimental yield. At this step, rest of the rate constants regarding dormant site formation and reactivation ($k_{dorm,f}$, $k_{dorm,aH}$, $k_{dorm,aS}$), deactivation (k_{d1}^1), and transfer rate parameters (k_{trH2}^1 , k_{trB}^1) were set at values from models presented by Kettner and Zacca for propylene polymerization kinetics as starting points [63,91].

Next, the homo-polymerization experiment without hydrogen was considered. Since there is no hydrogen present in the reactor, no dormant site reactivation by hydrogen takes place. Experimental yield of the experiment without hydrogen was matched by adjusting the spontaneous dormant site reactivation rate constant ($k_{dorm,aS}$), while keeping other rate constants fixed.

Subsequently, experimental data from homo-polymerizations with various hydrogen concentrations (0~2 [mol%]) were inserted in the software and the parameter estimation procedure by gPROMS was performed, therein the active fraction of titanium centers was kept fixed at 2% and chain propagation rate constant as well as spontaneous dormant site reactivation rate constant were set fixed at the values obtained in previous steps. The rest of parameters ($k_{dorm,f}$, $k_{dorm,aH}$, k_d^1) were adjusted simultaneously by gPROMS to find a suitable fit for the range of the experiments. Since the second site only activates during the copolymerization stage, these rate constants correspond only to the first type of active site.

In order to model the influence of hydrogen concentration on homo-polymer products molecular weight, first the homo-polymerization experiment without hydrogen was considered and the experimental MFR value of the product was matched by adjusting the spontaneous (β -hydride) chain transfer parameter. For experiments with hydrogen, the chain transfer to hydrogen rate parameter was adjusted to describe the influence of hydrogen on the product MFR. These parameters all correspond to the first type of active sites.

Once the homo-polymerization kinetics and respectively the hydrogen response was adequately represented, and the kinetic parameters of the first site during homo-polymerization were determined, the copolymerization experiments were considered. In this step the goal was to model the influence of gas-phase composition on the rubber phase copolymer composition, copolymerization kinetics, rubber phase molecular weight and the resulting product's total MFR.

Initially, the copolymer composition was modeled, herein the reactivity ratios of monomer and comonomer were adjusted (at two different type of active sites) in order to match the

experimentally obtained polymer composition vs gas phase monomer/comonomer composition (displayed in figure 50). As initial guesses, the values of propagation and reactivity ratios proposed by Kröner [65] were implemented in the model calculations. Once the reactivity ratios were estimated, the parameter estimation step for copolymerization experiments was carried out.

Experimentally obtained copolymerization activity profiles corresponding to various mole fractions of ethylene in the feed were used for parameter estimation. In parameter estimation step the kinetic parameters of site one corresponding to homo-polymerization kinetics and reactivity ratios of both sites were kept fixed at the values determined in previous steps. Propagation rate constants of ethylene at both sites as well as and deactivation parameters of the second site were determined simultaneously by parameter estimation function to find the most suitable fit.

To model the molecular weight of the copolymer, the chain transfer to hydrogen at the second site was adjusted to match the experimentally obtained data regarding the weight average molecular weight of the rubber phase, while the chain transfer to hydrogen rate parameter at site 1, and the spontaneous transfer rate parameter from propylene ended chains at both sites were at the values determined for homo-polymerizations experiments.

The model implementation and parameter estimation results of catalysts A and C are listed in the following table

| Parameter | Catalyst A Site type 1 | Catalyst A Site type 2 | Catalyst C Site type 1 | Catalyst C Site type 2 | Unit |
|------------------|----------------------------------|----------------------------------|----------------------------------|----------------------------------|-------------|
| k_{act} | $5.00 \cdot 10^{-2}$ | $5.00 \cdot 10^{-2}$ | $5.00 \cdot 10^{-2}$ | $5.00 \cdot 10^{-2}$ | 1/s |
| k_{p11} | $3.05 \cdot 10^4$ | $1.21 \cdot 10^5$ | $3.93 \cdot 10^4$ | $4.58 \cdot 10^4$ | l/(mol.s) |
| k_{p22} | $3.01 \cdot 10^6$ | $1.93 \cdot 10^6$ | $2.68 \cdot 10^6$ | $3.68 \cdot 10^5$ | l/(mol.s) |
| r_1 | 0.25 | 0.09 | 0.25 | 0.09 | - |
| r_2 | 27.86 | 7.00 | 27.86 | 7.00 | - |
| k_{d1} | $3.7 \cdot 10^{-4}$ | $1.5 \cdot 10^{-4}$ | $3.45 \cdot 10^{-4}$ | $4.53 \cdot 10^{-5}$ | 1/s |
| k_{d2} | $8.9 \cdot 10^{-4}$ | $3.5 \cdot 10^{-4}$ | $4.59 \cdot 10^{-5}$ | $6.25 \cdot 10^{-5}$ | 1/s |
| k_{trH2} | 143 | 643 | 212 | 90 | l/(mol.s) |
| $k_{tr\beta}$ | 11.40 | 11.40 | 17.50 | 17.50 | 1/s |
| $k_{dorm,f}$ | $9.6 \cdot 10^{-2}$ | $9.6 \cdot 10^{-2}$ | $9.6 \cdot 10^{-2}$ | $9.6 \cdot 10^{-2}$ | l/(mol.s) |

| Parameter | Catalyst A Site type 1 | Catalyst A Site type 2 | Catalyst C Site type 1 | Catalyst C Site type 2 | Unit |
|-----------------|---------------------------|---------------------------|---------------------------|---------------------------|-----------|
| $k_{dorm,aH}$ | $1.8 \cdot 10^{+1}$ | $1.8 \cdot 10^{+1}$ | $1.8 \cdot 10^{+1}$ | $1.8 \cdot 10^{+1}$ | l/(mol.s) |
| $k_{dorm,aS}$ | $1.8 \cdot 10^{-2}$ | $1.8 \cdot 10^{-2}$ | $1.0 \cdot 10^{-2}$ | $1.0 \cdot 10^{-2}$ | l/(mol.s) |
| $x_{Active} \%$ | 2.00 | 2.00 | 2.00 | 2.00 | Mass% |

Table 25. Parameter estimation results

Activation rate constants are set to a large enough value to describe how fast does the polymerization reach the maximum initial activity. Similar values for both catalysts at both types of active sites have been determined.

A larger chain propagation rate constant with propylene at site 1 was estimated for catalyst C compared to catalyst A. This agrees with the experimental results of homo-polymerizations, wherein catalyst C displays higher activity.

As expected, chain propagation with ethylene is assigned a higher rate constant for both catalysts and has been estimated by parameter estimation option in gPROMS to fit the experimental activity profiles of copolymerization experiments.

For both catalysts, the experimental results regarding the copolymer composition vs monomer composition in the gas phase could be described with similar values of the reactivity ratios.

Deactivation rate constant regarding chains ending with propylene were estimated to be relatively similar at site 1 for both catalysts, as was depicted in normalized homo-polymerization activity profiles. Despite having different activity levels, both catalysts display similar deactivation behavior. The deactivation rate constants of propylene ended chains at the second type of active sites as well as deactivation parameter regarding chains ending with ethylene at sites 1 and 2 have been assigned smaller values for catalyst C compared to catalyst A, to fit the activity profiles of copolymerization experiments.

Similar results regarding dormant site formation and reactivation with hydrogen have been estimated for both catalysts, with an exception of spontaneous dormant site reactivation, herein catalyst A displays a higher rate of spontaneous dormant site reactivation compared to catalyst C, these values are determined by fitting the experiments performed without hydrogen. The dormant site formation and reactivation parameters at the second type of active sites have been assigned similar values as for site type 1.

Despite having similar MFR results with regard to hydrogen concentration, catalyst C displays a higher chain transfer to hydrogen and spontaneous chain transfer rate constants compared to catalyst A at site type one. This can be explained by higher chain propagation rate of catalyst

C, therein chains grow faster compared to polymerizations with catalyst A, and thus to result in similar final weight average molecular weight, chain transfer rate parameter needs to be assigned a larger value. These parameters are estimated to describe the influence of hydrogen concentration on homo-polymer product's molecular weight and respectively MFR results.

Chain transfer to hydrogen rate constant at the second type of active sites for catalyst A has been assigned a larger value compared to that of catalyst C to match the experimentally obtained values for molecular weight of the rubber phase copolymer.

7.6 Model simulation results; hydrogen response

In this section the experimental results including homo-polymerization yield, product MFR and individual activity profiles are compared with the model simulations. In the following figure experimental polymerization yield and model simulated yields with regard to hydrogen mole fraction in the feed are compared for both catalysts:

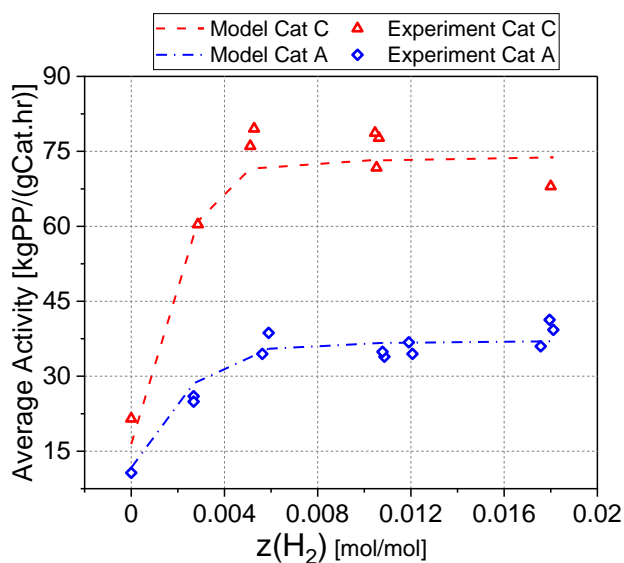
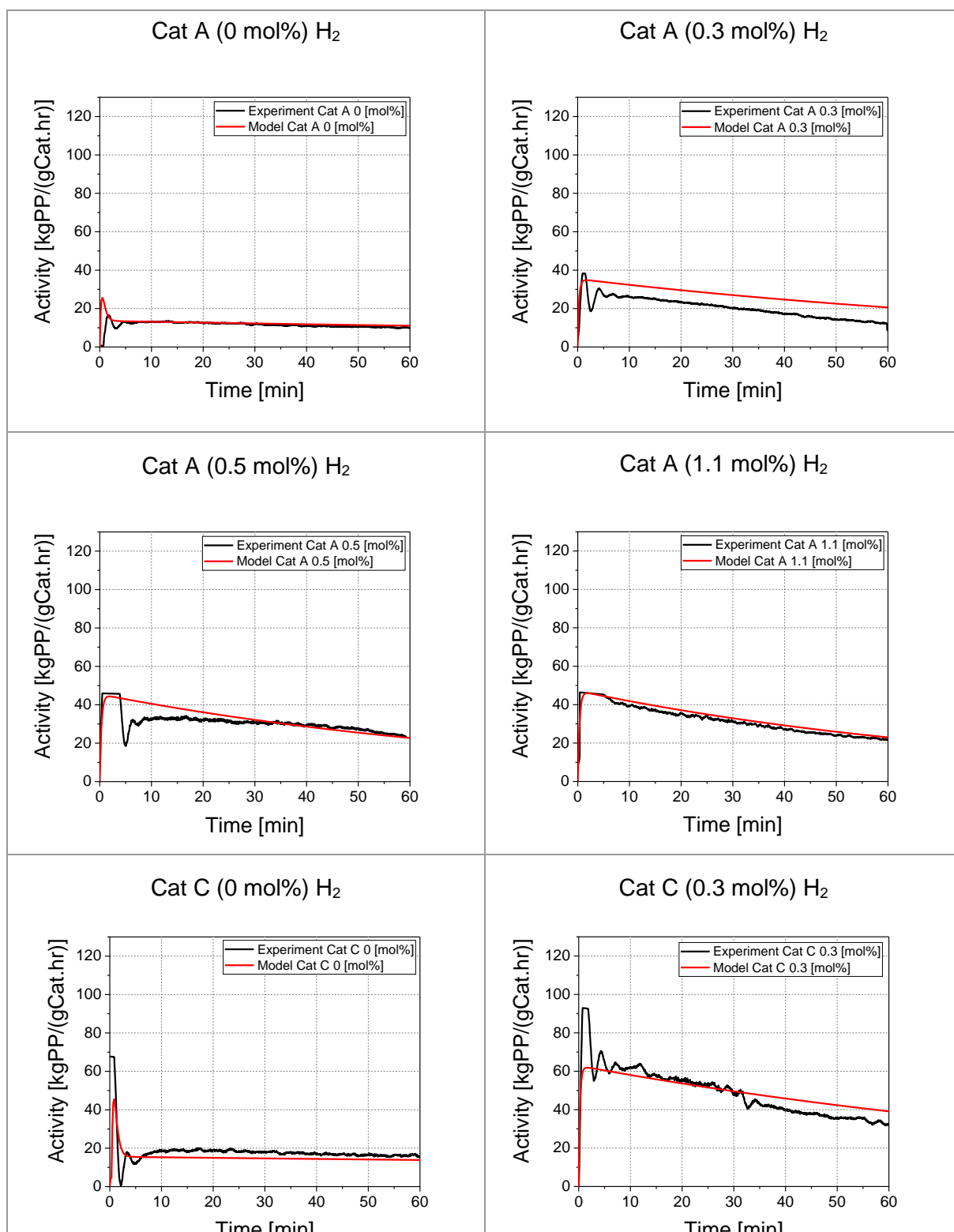


Figure 94. Hydrogen response Cat A vs Cat C; Comparison with model; T=75 [°C], H₂=0-1.8 [mol%]

Model simulations are capable of capturing the hydrogen response of both catalysts with acceptable accuracy. The hydrogen response includes the rise in activity by introduction of up to 0.5 [mol%] hydrogen in the feed, where the activity increases and reaches a plateau there after. This is due to adaptation of the dormant site theory in the kinetic scheme of the model. The experiments without presence of hydrogen show the least activity and include the highest number of dormant species calculated by the kinetic model, however during experiments with about 1.0 [mol%] hydrogen in the feed, up to 93% of the dormant chains are reactivated either spontaneously or by reacting with hydrogen. Activity profiles of homo-polymerization

experiments using catalyst A and C with various hydrogen mole fractions in the feed (0~1.0 mol%) are displayed and compared with model simulations in the following graphs:



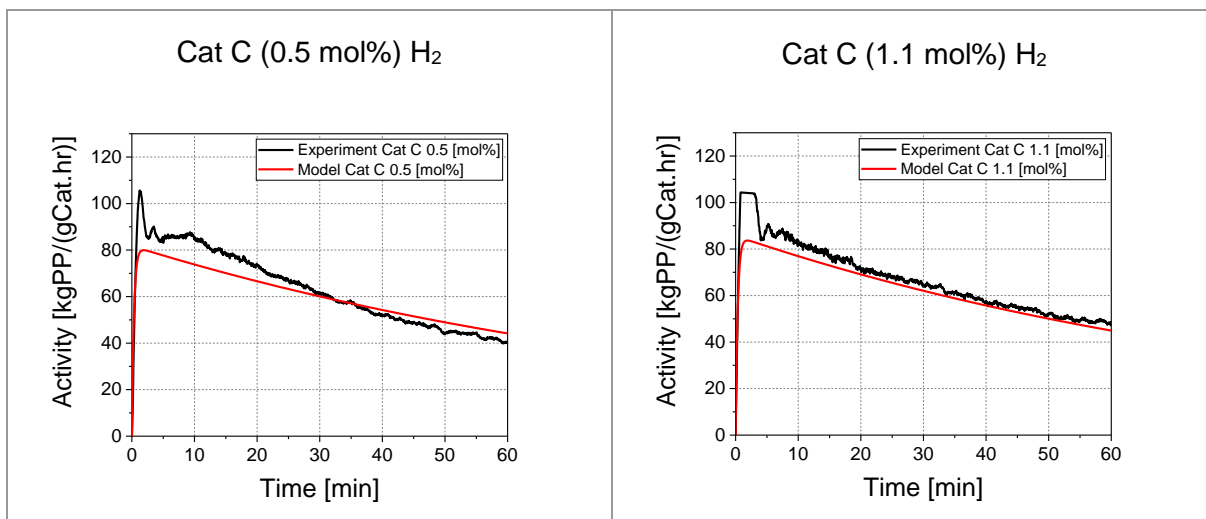


Figure 95. Hydrogen response activity profiles; Cat A vs Cat C; Comparison with model; T=75 [°C], H₂=0-1.1 [mol%]

The weight average molecular weight of the homo-polymer matrix is calculated by the method of moments and set of equations displayed in table 23. The model estimates the homo-polymer MFR from the weight average molecular weight ($M_{w, hp}$), by the experimental correlation displayed in equation 7.43. Influence of hydrogen on homo-polymer products' molecular weight and thus MFR is depicted with regard to mole fraction of hydrogen in liquid propylene, in the following diagram and compared with model simulations:

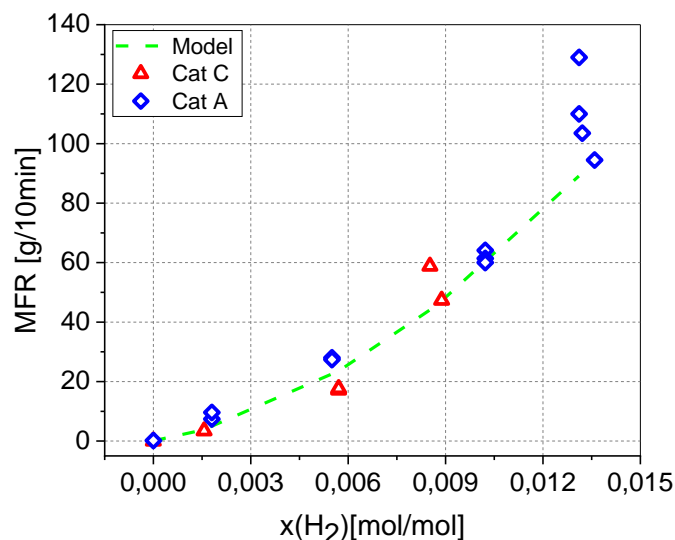


Figure 96. Influence of hydrogen on Homo-polymer product's MFR; Cat A vs Cat C; Comparison with model; T=75 [°C], H₂=0-1.8 [mol%]

7.7 Model simulation results; pre-contact influence

In this section, the influence of pre-contacting on homo-polymerization kinetics of catalyst A is modeled by adjusting the maximum number of active titanium sites that can potentially be

activated during the polymerization. For modeling the hydrogen response, where all experiments were carried out with the optimum pre-contacting time of 10 seconds, the fraction of potentially active titanium centers was kept fixed at 2%. In this step the estimated parameters for modeling the hydrogen response (chain propagation, deactivation, dormant site formation and reactivation) are kept fixed, and x_{active} is adjusted to match the effect of pre-contacting on the homo-polymerization kinetics of catalyst A. Since pre-contacting does not display a notable influence on polymerization kinetics of catalyst C, this approach for catalyst C is not necessary. It was observed that pre-contacting does not influence product molecular weight with a meaningful trend, hence the chain transfer rate constants were kept at the values, obtained by modeling hydrogen response experiments. Results of parameter estimation to model the influence of pre-contacting on catalyst activity are listed in the following table:

| Pre-contact time [s] | x_{Active} [Mass%] Cat A (Site type 1) |
|----------------------|---------------------------------------------|
| 0 | 0.80 |
| 10 | 2.00 |
| 60 | 1.95 |
| 300 | 1.50 |

Table 26. Fraction of active titanium species adjusted to describe pre-contacting influence on homo-polymerization kinetics of catalyst A

It must be noted all other kinetic parameters are similar to those displayed in table 25 except for fraction of potentially active titanium centers, that are adjusted to match the influence of pre-contacting on catalyst activity. The model simulations well describe the influence of pre-contacting on the polymerization yield and the average activity as depicted in the following:

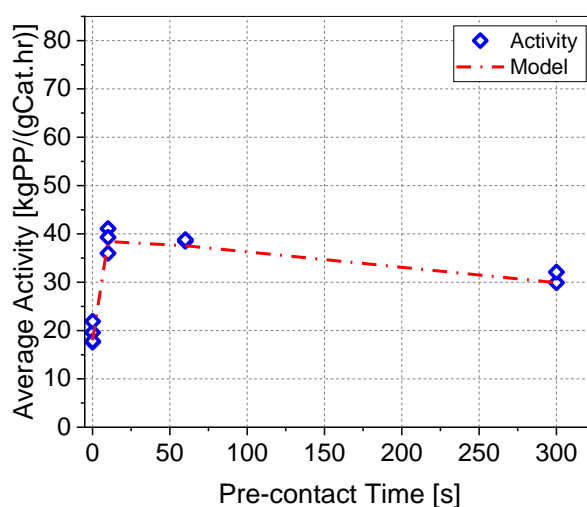


Figure 97. Average activity catalyst A; pre-contacting influence; Comparison with model; T=75 [°C], H₂=1.8 [mol%], pre-contact=0-300 [s]

Activity profiles of catalyst A with different pre-contacting times are presented and compared with the model simulations in the following figures:

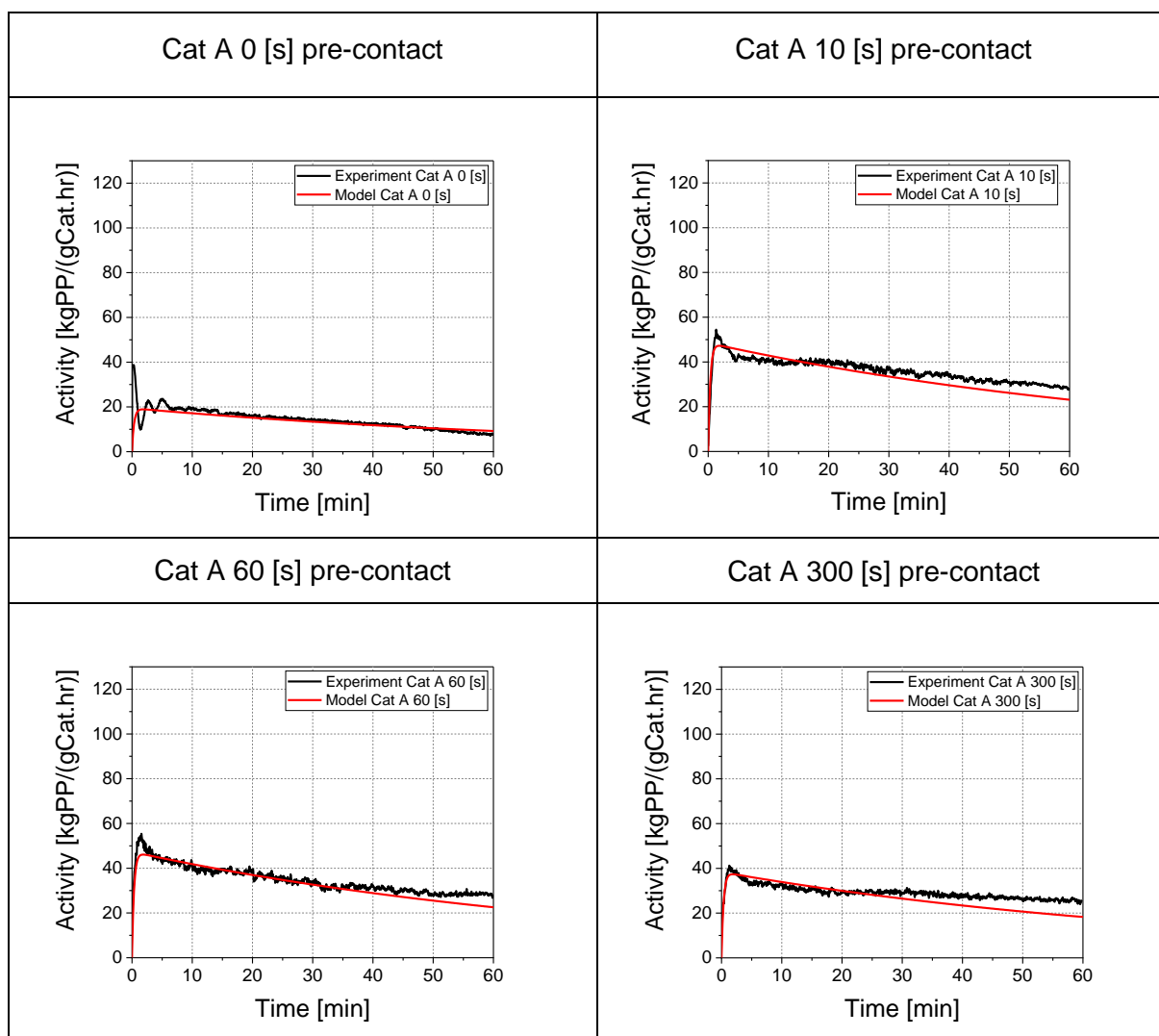


Figure 98. Activity profiles of catalyst A; pre-contact influence, Comparison with model; $T=75$ [°C], $H_2=1.8$ [mol%], pre-contact=0-300 [s]

7.8 Model simulation results; copolymerization kinetics

In this section model simulation results of copolymerization experiments are presented. The simulations include describing the copolymer composition, copolymerization activity profiles, and copolymer molecular weight, as well as overall product melt flow rate. Results of model simulations with regard to ethylene fraction in the gas phase and ethylene incorporation in the resulting copolymer is depicted in the following graph:

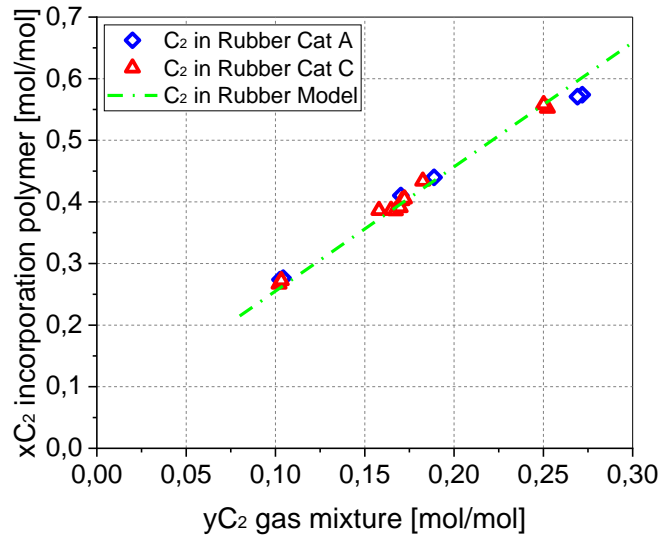


Figure 99. Gas composition vs ethylene in rubber; Comparison with model; Cat A vs Cat C; $T=75$ [°C], $H_2=2$ [mol%], $P=14$ [bar], $x_{C_2}=27-57$ [mol%], $y_{C_2}=10-27$ [mol%]

By adjusting the reactivity ratios, the model simulations are capable of describing the copolymer composition with acceptable accuracy. Both catalysts display similar behavior and are modeled with similar reactivity ratios (displayed in table 25). Results of model simulation for a typical copolymerization experiment of catalyst A and catalyst C is displayed in the following graph (ethylene in gas phase $y_{C_2}=17$ [mol%], ethylene in rubber $x_{C_2}=40$ [mol%]).

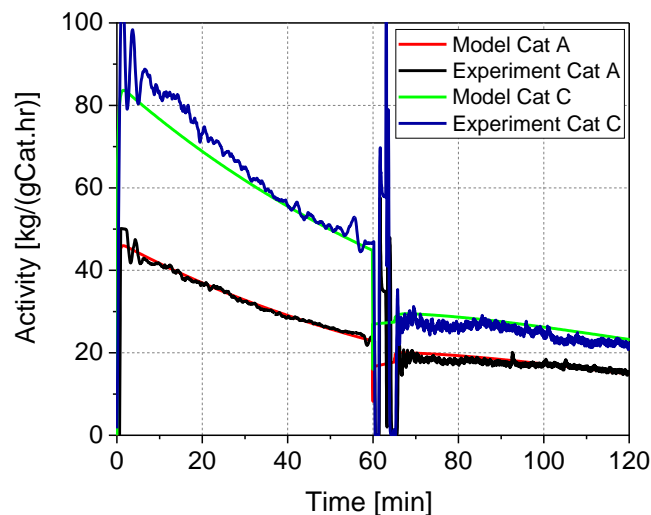


Figure 100. Copolymerization activity profile, Comparison with model; Cat A vs Cat C; $T=75$ [°C], $H_2=2$ [mol%], $P=14$ [bar], $x_{C_2}=40$ [mol%], $y_{C_2}=17$ [mol%]

The model predicts the homo-polymerization activity profile followed by the copolymerization stage. The following graph displays the individual activity profiles of ethylene, propylene, and the overall activity in the copolymerization stage of the standard experiment of catalyst A in figure 101.

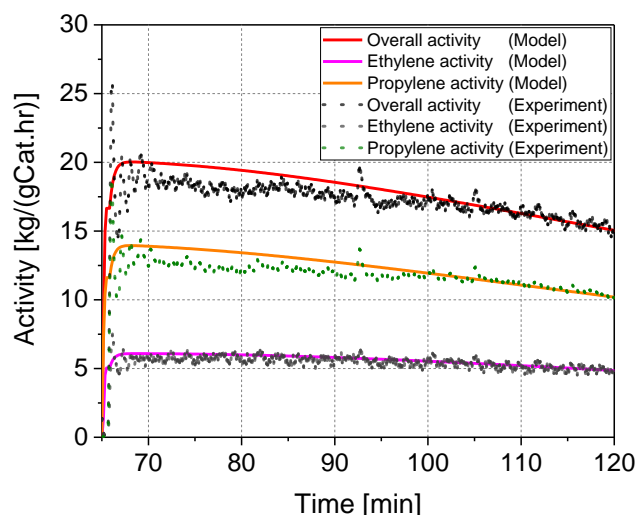


Figure 101. Activity profile, Comparison with model; Cat A; $T=75$ [°C], $H_2=2$ [mol%], $P=14$ [bar], $x_{C_2}=40$ [mol%], $y_{C_2}=17$ [mol%]

The model provides an acceptable match with experimental overall activity profile, as well as individual ethylene and propylene activity profiles. The influence of ethylene fraction in copolymer, on activity is correctly represented. The following graphs depict the effect of ethylene mole fraction in copolymer on overall activity profiles of catalyst A and catalyst C in heco stage, and a comparison with the experimentally obtained activity profiles, the ethylene fraction in rubber for these experiments ranges between (27 to 59 [mol%]):

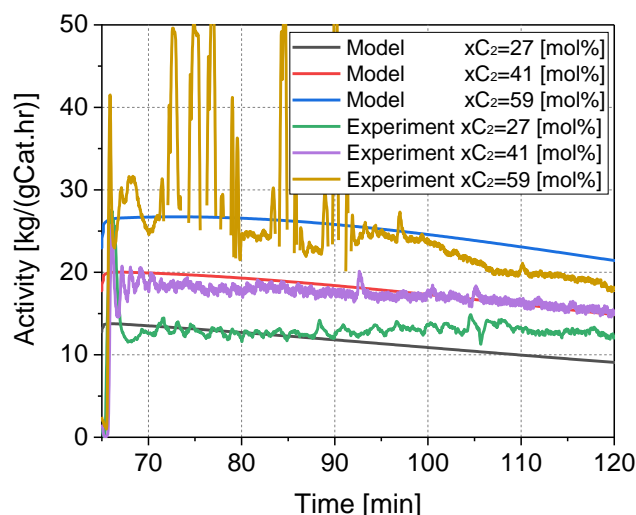


Figure 102. Influence of ethylene mole fraction in rubber on overall activity of gas phase copolymerization stage; Comparison with model; Cat A; $T=75$ [°C], $H_2=2$ [mol%], $P=14$ [bar], $x_{C_2}=27-59$ [mol%], $y_{C_2}=10-27$ [mol%]

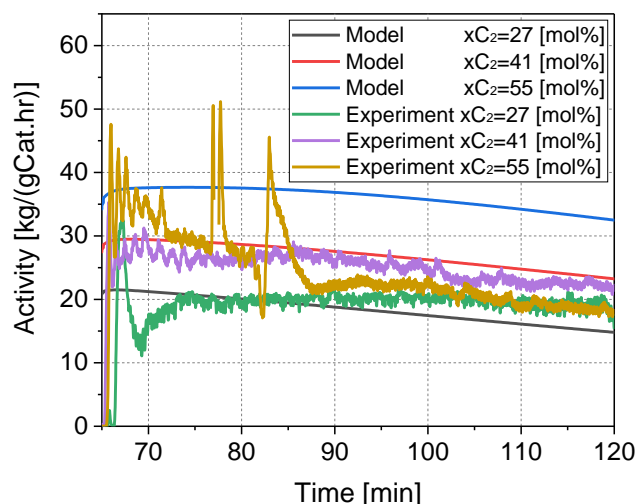


Figure 103. Influence of ethylene mole fraction in rubber on overall activity of gas phase copolymerization stage; Comparison with model; Cat C; T=75 [°C], H₂=2 [mol%], P=14 [bar], x_{C2}=27-55 [mol%], y_{C2}=10-27 [mol%]

With an increase in fraction of ethylene in copolymer (x_{C_2}) from 27 to 59 [mol%] initial catalyst activity nearly doubles. This experimental observation is captured in the model by introducing a second type of active sites that activate with ethylene and thus with higher concentration of ethylene the number of active sites during copolymerization increases. Furthermore, as an example for catalyst A, ethylene ($k_{p22}=3.01 \cdot 10^{+6}$) is more reactive compared to propene ($k_{p11}=3.05 \cdot 10^{+4}$) as indicated by the results of the parameter estimation. Therefore, an increase in ethylene fraction leads in higher overall activity. In case of catalyst C, at higher ethylene fractions, a sharp deactivation in activity is recorded. This deactivation might be attributed to possible formation of semi-crystalline polyethylene during copolymerization. In all previous simulations it is assumed that the rubber phase is entirely amorphous. To demonstrate how formation of a semi-crystalline polymer in copolymerization stage might affect the resulting overall polymerization rate, in the following figure 104 two hypothetical simulations are presented, wherein copolymerizations resulting in semi-crystalline or fully amorphous rubber phase are compared. It is clearly demonstrated in the simulations that by formation of fully amorphous copolymer rubber, an activation effect in the copolymerization stage is captured by the model, this is well in-line with the experimental findings. The model is able to capture this effect due to how the balancing of species were performed in equation 7.19, which allowed to include the fraction of crystalline polymer in the mass balance differential equations. From these simulations and the experimental findings one can conclude that in addition to kinetical and thermodynamical effects, the forming polymer micro-structure can have a significant influence on overall catalyst activity.

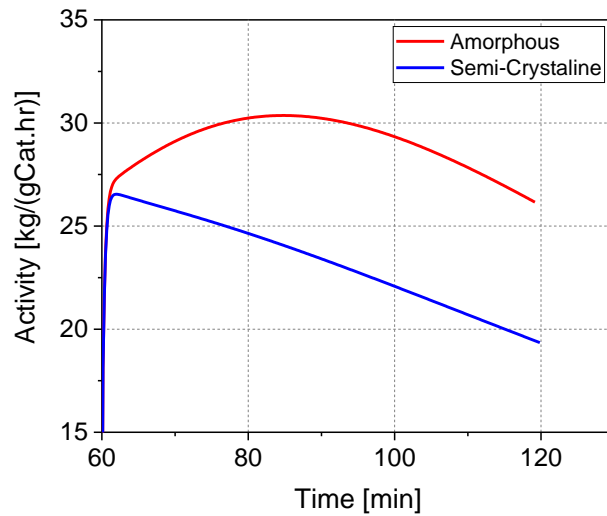


Figure 104. Simulated case, influence of forming polymer crystallinity on overall copolymerization activity profile. The weight average molecular weight of the rubber phase copolymer is calculated by the model using the method of moments and equations displayed in table 24. The model calculations describe the influence of ethylene composition in copolymer on the molecular weight of the copolymer phase.

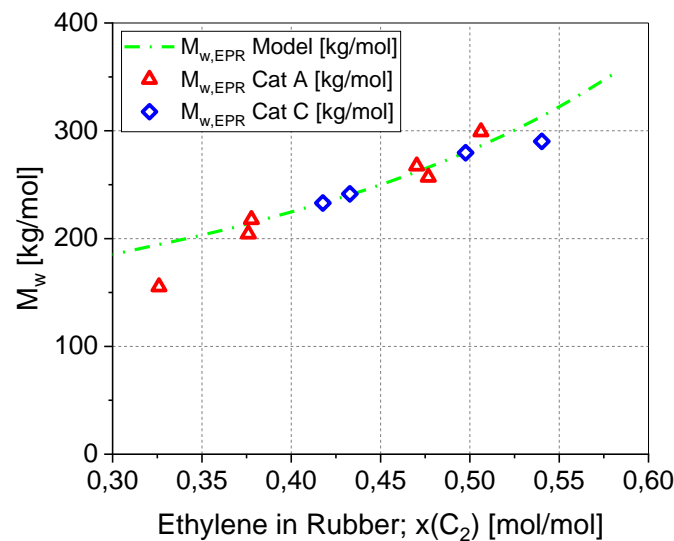


Figure 105. Weight average molecular weight of EPR vs ethylene fraction in rubber; Cat A vs Cat C; Comparison with model; rubber content= 20 [Mass%], $T=75$ [°C], $H_2=2$ [mol%], $P=14$ [bar], $x_{C_2}=32-55$ [mol%]

In figure above, the data points indicate the weight average molecular weight of the copolymer samples of both catalysts measured by fractionation followed by intrinsic viscosity measurements. The line in the graph indicates the model calculations and is obtained by simulating the copolymerization experiments of catalyst A. Both catalysts despite having different chain transfer parameters, result in products with similar molecular weights in similar conditions (2 [mol%] hydrogen in copolymerization stage for all experiments).

By the correlation displayed in equation 7.44 the MFR values of the rubber phase is calculated from weight average molecular weight and displayed in the following graph:

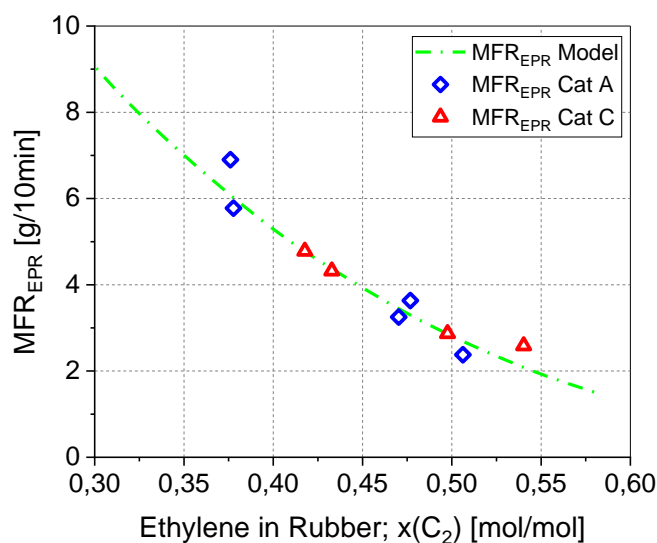


Figure 106. Rubber phase MFR vs ethylene fraction in rubber; Cat A vs Cat C; Comparison with model; rubber content= 20 [Mass%], T=75 [°C], H₂=2 [mol%], P=14 [bar], x_{C2}=32-55 [mol%]

The resulting influence of ethylene in rubber on the final product MFR (including matrix and the rubber phase) is depicted in figure 107 for catalyst A. in which the rubber content was fixed at 20 [Mass%] and ethylene fraction in rubber was varied between 30 to 55 [mol%]:

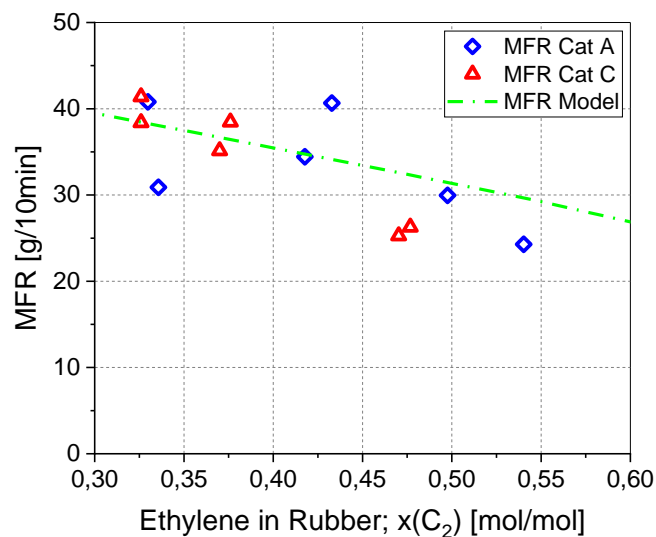


Figure 107. Final product MFR vs ethylene in rubber; Comparison with model; Cat A vs Cat C rubber content= 20 [Mass%], T=75 [°C], H₂=2 [mol%], P=14 [bar], x_{C2}=32-55 [mol%]

The model captures the decline in total MFR with regard to ethylene composition in rubber, by accounting for the matrix MFR and the rubber phase MFR separately (equations 7.43 and 7.44) and calculating the total MFR by the mixing rule displayed in equation 7.45.

8 Summary

The aim of this work was to study and compare polymerization kinetics of two different Ziegler-Natta catalysts in a multi-step copolymerization consisting of a bulk-phase propylene homo-polymerization step in which the polypropylene homopolymer matrix is generated, and a subsequent gas-phase polymerization, in which an elastomeric propylene/ethylene copolymer acting as impact modifier, is synthesized.

For studying kinetics in the first polymerization step, bulk-phase homo-polymerization of propylene, a calorimetric measurement approach was established. An existing 5-liter reactor setup was equipped with a power compensation heater (purchased from PRT GmbH, Ahaus DE). The resulting calorimeter setup was calibrated, and the required operational procedures were developed. For correct interpretation of the measured data, changes in the heat flow to the jacket due to changes in the filling level of the reactor had to be considered. For this purpose, a software-sensor for online evaluation of the calorimetric measurements was developed. The software sensor combines a material-balance and flash-calculations for propylene with calibration measurements and allows to estimate the (changing) heat flow to the jacket and thus the chemical heat flow of the reaction, online at any time during the reaction. The power compensation method offers excellent temperature control throughout the reaction. The accuracy of the calorimetric measurements were validated by comparing the weighted polymerization yield with the values determined by the reaction calorimetry method and the setup offered an error range of well below 10%.

For the experiments with subsequent gas-phase copolymerization step, the reaction kinetics in gas-phase conditions were studied by semi-batch operation of the reactor in a pressure control loop. For controlling and monitoring the gas phase composition in the reactor, a μ -GC was added to the reactor setup. The combined calorimetric and gas-phase kinetic measurement principle enabled production of hetero-phasic copolymer samples with defined rubber content and controlled rubber composition. The accuracy of the combined kinetic measurement method was validated by comparing expected and measured ethylene content in the final samples (determined by FTIR measurements).

In case of bulk propylene homo-polymerization experiments, after establishing reproducibility of the polymerization procedure, the hydrogen responses of the used catalysts were studied.

It was observed that catalyst C displayed with an average activity in bulk conditions of up to $78 \text{ kg}_{\text{PP}}/(\text{g}_{\text{cat}} \cdot \text{hr})$ nearly double the activity of catalyst A. However, both catalysts displayed similar type of hydrogen response, wherein by an increase in hydrogen concentration from 0 to 0.5 [mol%], the average catalyst activity increased and reached a plateau thereafter. The influence of hydrogen on homo-polymer product molecular weight was investigated by means of melt flow rate measurements. It was observed that homo-polymer products of both catalysts produced in this work have a weight average molecular weight of in between 200 to 800 [kg/mol], depending on the hydrogen concentration in the polymerization process ($\text{H}_2=0-1.8$ [mol%]).

Influence of pre-contacting on the homo-polymerization kinetics was studied as well. It was observed that 10 seconds of pre-contacting resulted in a maximum activity for catalyst A. In experiments without pre-contacting, catalyst A displayed 50% lower activity. Longer pre-contacting durations led to a decline in activity of catalyst A. In case of catalyst C, it was observed that pre-contacting had no influence on homo-polymerization kinetics. Furthermore, electron microscopy measurements revealed that pre-contacting significantly enhances powder morphology of products of both catalysts.

In the multi-stage propylene/ethylene impact-copolymerization experiments, a standard bulk-phase propylene homo-polymerization ($T=75$ [°C], $\text{H}_2=1$ [mol%]) was followed by the gas-phase copolymerization step. Reaction pressure in gas-phase was fixed at 14 [bar] for all experiments. After establishing reproducibility of copolymerization procedure, the influence of monomer/comonomer ratio on copolymerization kinetics was studied. Both catalysts showed a similar comonomer incorporation behavior. For an ethylene content of about 18 [mol%] in gas-phase, a comonomer incorporation of about 40 [mol%] ethylene in the copolymer was observed, for both catalyst A and C. For both catalysts, increasing ethylene fraction in copolymer enhances copolymerization activity. Catalyst C displayed 60% higher activity in gas-phase copolymerization experiments, compared to catalyst A in similar conditions.

While the weight average molecular weight of the homo-polymer matrix was determined by melt flow rate method to be about 200 [kg/mol] in standard conditions ($T=75$ [°C], $\text{H}_2=1$ [mol%]), the molecular weight of the extracted copolymer rubber was determined by intrinsic viscosity measurements. The molecular weight of the rubber was in between 200 to 300 [kg/mol], depending on the ethylene fraction in copolymer ($T=75$ [°C], gas phase composition: $x_{\text{H}_2}=2$ [mol%] and $x_{\text{C}_2}=30-55$ [mol%]).

Moreover, the particle morphology of the impact copolymer samples was characterized by means of electron microscopy, particle size distribution, porosimetry and bulk density

measurements. It was illustrated that the rubber phase copolymer is primarily forming within the pores of the homo-polymer matrix particles.

To describe the vapor-liquid phase equilibria in bulk-phase polymerization of propylene, Peng-Robinson equation of state was used. A MATLAB program was developed to calculate fugacity coefficients of the components present in the reactor and to perform flash calculations. As a result, the liquid filling volume in the reactor throughout polymerization as well as mole fraction of hydrogen and propylene in each phase can be calculated. The accuracy of the flash calculations was validated by comparing the calculation results with experimental mole fractions in the reactor measured with the μ -GC setup. Phase equilibria between the semi-crystalline polypropylene and the penetrant gases were studied in a high-pressure sorption balance. Propylene and ethylene equilibrium gas solubilities were experimentally measured in pressures up to 25 [bar] at $T=75$ [$^{\circ}\text{C}$], polymer swelling was considered. In order to estimate the liquid propylene concentration in polymer during the bulk-phase homo-polymerization, the experimentally obtained data points were extrapolated to propylene saturation pressure ($p=33.9$ [bar], $T=75$ [$^{\circ}\text{C}$]) by using the Sanchez-Lacombe equation of state. This approach led to an estimated equilibrium concentration of propylene in polypropylene in bulk-homopolymerization conditions of about 3.17 [mol/l].

Finally, the experimental results obtained were compiled in a simplified phenomenological kinetic model, with data sets for both catalysts. Purpose of the model is to describe both homo-polymerization and copolymerization kinetics and the resulting polymers with respect to the corresponding reaction conditions. The model was implemented in gPROMS 5.1 model-builder software platform. While for description of homo-polymerization just one type of active sites is considered, for copolymerization a second type of active sites, which is activated by ethylene, was incorporated. The effect of hydrogen on polymerization activity is described via the dormant site theory. For description of product molecular weights, the method of moments was implemented in the model and transfer reactions (both spontaneous and to hydrogen) are considered. The model is based on equilibrium concentrations, mass-transfer has been neglected. A stepwise procedure was used to determine the catalyst-specific reaction rate parameters. Polymerization yield and activity profiles simulated by model calculations delivered reasonable agreement with the experimentally obtained data, over the whole measurement range studied. The model provides an adequate description of the experimentally observed comonomer incorporation in the copolymerization stage. Molecular weights predicted by the model were compared to experimental data in terms of melt-flow rate and exhibit a reasonable agreement to experimental data.

The developed model and the kinetic data determined can be applied for e.g. model-based product development, scale-up considerations, and process optimization.

9 List of symbols

| Abbreviations | Description |
|----------------|------------------------------------------|
| C ₂ | Ethylene |
| C ₃ | Propylene |
| DEAC | Diethyl aluminum chloride |
| DSC | Differential scanning calorimetry |
| EPDM | Ethylene propylene diene elastomer |
| EPR | Ethylene propylene rubber |
| FTIR | Fourier transform infrared spectroscopy |
| GC | Gas chromatography |
| GPC | Gel permeation chromatography |
| ICP | High-impact ethylene propylene copolymer |
| IV | Intrinsic viscosity |
| MAO | Methylaluminoxane |
| MFR | Melt flow rate |
| MGM | Multi-grain model |
| PFM | Polymeric flow model |
| PP | Polypropylene |
| PR-Eos | Peng-Robinson equation of state |
| SEM | Scanning electron microscopy |
| SL-Eos | Sanchez-Lacombe equation of state |
| RC | Rubber content |
| TEA | Triethylaluminium |
| Ti | Titanium |
| ZN | Ziegler-Natta catalyst |
| XRD | X-ray diffraction |

| Capital letters | Description | Unit |
|-----------------------|-------------------------------------|----------------------------------------|
| <i>A</i> | PR-Eos constant parameter | [bar/J ² mol ²] |
| <i>A</i> | Heat transfer area | [m ²] |
| <i>A_H</i> | Hutchinson semi empirical parameter | [mol/l/bar] |
| <i>B</i> | PR-Eos constant parameter | [bar/K] |
| <i>B_H</i> | Hutchinson semi empirical parameter | [l/mol] |
| <i>C_{am}</i> | Concentration in amorphous | [mol/l] |
| <i>C_i</i> | Concentration of species "i" | [mol/l] |

| | | |
|--------------------|-------------------------------------------------|------------|
| H_i | Henry's constant of component "i" | [bar] |
| K_i | Equilibrium constant of component "i" | - |
| L | Fraction of material in liquid phase | [mol/mol] |
| M_n | Number average molecular weight | [kg/mol] |
| M_w | Weight average molecular weight | [kg/mol] |
| $M_{w,hp}$ | Weight average molecular weight of homo-polymer | [kg/mol] |
| $M_{w,cp}$ | Weight average molecular weight of copolymer | [kg/mol] |
| N | Stirring speed | [rpm] |
| P | Compensation heater power | [W] |
| P | Pressure | [bar] |
| P_c | Critical pressure | [bar] |
| \dot{Q}_{chem} | Chemical heat flow | [W] |
| \dot{Q}_{disp} | Heat loss at ambient temperature | [W] |
| \dot{Q}_{jacket} | Heat flow to the reactor jacket | [W] |
| \dot{Q}_{loss} | Heat loss | [W] |
| R | Gas constant | [J/mol. K] |
| $R_{i,j}$ | Gross rate of reactions including component i | [mol/s] |
| R_{C2} | Gross consumption rate of ethylene | [mol/s] |
| R_{C3} | Gross consumption rate of propylene | [mol/s] |
| R_p | Polymerization rate | [mol/s] |
| S_{eq} | Equilibrium solubility | [g/kg] |
| T | Temperature | [K] |
| T_{amb} | Ambient temperature | [K] |
| T_c | Critical temperature | [K] |
| T_r | Reactor temperature | [K] |
| T_j | Jacket temperature | [K] |
| V | Volume | [l] |
| V | Fraction of material in vapor phase | [mol/mol] |
| V_{am} | Amorphous polymer volume | [l] |
| V_{cr} | Crystalline polymer volume | [l] |
| V_{liquid} | Liquid propylene volume in the reactor | [l] |
| V_p | Polymer volume | [l] |
| X_{cr} | Degree of crystallinity | [Mass%] |

| Small letters | Description | Unit |
|----------------------|----------------------------------------------|--------------------------|
| a | PR-Eos constant parameter | - |
| a_i | Activity of a substance | - |
| b | PR-Eos constant parameter | [J/mol. K] |
| d | Reactor wall thickness | [m] |
| f | fugacity | [bar] |
| \hat{f}_i^v | Fugacity of component i in vapor mixture | [bar] |
| \hat{f}_i^l | Fugacity of component i in liquid mixture | [bar] |
| h_c | Heat transfer coefficient of coolant | [W/ (m ² .K)] |
| h_r | Convective heat transfer coefficient | [W/ (m ² .K)] |
| k_{loss} | Heat loss coefficient | [W/K] |
| k_l | Effective heat transfer coefficient | [W/m ² K] |
| m_p | Polymer mass | [kg] |
| m_{hp} | Homo-polymer mass | [kg] |
| m_{cp} | Copolymer mass | [kg] |
| \dot{m}_{C3} | Propylene mass flow | [kg/hr] |
| \dot{m}_{C2} | Ethylene mass flow | [kg/hr] |
| $\bar{\dot{m}}_{C2}$ | Average ethylene mass flow | [kg/hr] |
| $\bar{\dot{m}}_{C3}$ | Average propylene mass flow | [kg/hr] |
| \dot{m}_{C3} | Propylene mass flow | [kg/hr] |
| \dot{m}_{C2} | Ethylene mass flow | [kg/hr] |
| n_i | Mole number of a component | [mol] |
| r_p | Particle radius | [m] |
| r_1 | Reactivity ratio | - |
| r_2 | Reactivity ratio | - |
| v_{cr} | Crystalline volume fraction | - |
| v | Molar volume | [l/mol] |
| x_{C2} | Ethylene fraction in copolymer rubber phase | [mol/mol] |
| x_i | Mole fraction of a component in liquid | [mol/mol] |
| y_i | Mole fraction of a component in vapor | [mol/mol] |
| z_i | Mole fraction of a component in reactor feed | [mol/mol] |

| Greek letters | Description | Unit |
|---------------|-----------------------------|----------------------|
| ρ_p | Polymer density | [kg/m ³] |
| ρ_{cr} | Crystalline polymer density | [kg/m ³] |

| | | |
|-----------------------|-------------------------------------------------------|----------------------|
| ρ_{am} | Amorphous polymer density | [kg/m ³] |
| δ_{ij} | Binary interaction parameter of PR-Eos | - |
| ΔH_f | Formation enthalpy | [kJ/mol] |
| φ | Fugacity coefficient | - |
| $\hat{\varphi}_i^v$ | Fugacity coefficient of component i in vapor mixture | - |
| $\hat{\varphi}_i^l$ | Fugacity coefficient of component i in liquid mixture | - |
| ϕ | Thermal resistance | [W/mK] |
| χ | Flory-Huggins theory interaction parameter | - |
| μ | Chemical potential | [J/mol] |
| γ | Liquid activity | - |
| ΔT | Temperature difference | [K] |
| ω | Acentric factor | - |
| $\Delta V_{swelling}$ | Volume change by swelling | [m ³] |
| λ | Thermal conductivity | [W/m/K] |

10 Appendix

Appendix I

Polymerization experiments results are listed in this appendix.

1 Polymerization results for establishing reproducibility of polymerization process:

The following experiments were all performed at 75 [°C] using Catalyst A and catalyst C with 10 [NI] of hydrogen:

| Run number | Catalyst type | Catalyst amount [mg] | Hydrogen amount [NI] | Activity [kgPP/gCat.hr] | MFR [g/10min] |
|------------|---------------|----------------------|----------------------|-------------------------|---------------|
| Re80 | A | 16.0 | 10 | 36.8 | 60 |
| Re81 | A | 19.4 | 10 | 34.5 | 61 |
| Hp222 | A | 17.7 | 10 | 33.9 | 55.3 |
| Hp272 | A | 18.2 | 10 | 35.3 | 58.5 |
| Hp278 | A | 17.4 | 10 | 34.9 | 64.1 |
| Hp173 | C | 10.5 | 10 | 72.6 | 63.7 |
| Hp176 | C | 10.5 | 10 | 75.0 | 54.3 |
| Hp184 | C | 10.6 | 10 | 71.7 | 47.4 |
| Hp188 | C | 9.1 | 10 | 74.6 | 64.4 |
| Hp190 | C | 10.2 | 10 | 69.0 | 53.2 |

Table 27. Polymerization results for establishing reproducibility of polymerization process; Cat A vs Cat C; T= 75 [°C]

2 Polymerization results for studying hydrogen response

The following experiments were all performed at 75 [°C] using catalyst A:

| Run Code | Catalyst type | Catalyst amount [mg] | zH ₂ [mol/mol] | Activity [kg/(gCat.hr)] | MFR [g/10min] | Mw [kg/mol] |
|----------|---------------|----------------------|---------------------------|-------------------------|---------------|-------------|
| Hp288 | A | 18.0 | 0 | 10.7 | 0.3 | 726 |
| Hp302 | A | 17.2 | 0 | 10.5 | 0.2 | 803 |
| Hp280 | A | 17.7 | 0.00268 | 26.0 | 7.4 | 327 |
| Hp279 | A | 18.0 | 0.00267 | 24.9 | 9.63 | 306 |
| Re92 | A | 18.4 | 0.0059 | 38.7 | 28 | 23 |
| Re91 | A | 17.1 | 0.00563 | 34.5 | 27.4 | 236 |
| Hp222 | A | 17.7 | 0.01086 | 33.9 | 55.3 | 198 |
| Hp278 | A | 17.4 | 0.01078 | 34.9 | 64.1 | 191 |
| Re81 | A | 19.1 | 0.01206 | 34.5 | 61.4 | 193 |
| Re79 | A | 15.9 | 0.01191 | 36.8 | 60 | 194 |
| Re57 | A | 17.6 | 0.01757 | 36.0 | 110 | 167 |
| Re55 | A | 17.7 | 0.01811 | 39.3 | 94.7 | 173 |
| Hp284 | A | 15.7 | 0.01795 | 41.3 | 129 | 160 |
| Re73 | A | 19.2 | 0.01769 | 42.5 | 109 | 167 |

Table 28. Polymerization results for studying hydrogen response; Cat A vs Cat C; T= 75 [°C]

The following experiments were all performed at 75 [°C] using Catalyst C:

| Run Code | Catalyst type | Catalyst amount [mg] | zH ₂ [mol/mol] | Activity [kg/(gCat.hr)] | MFR [g/10min] | Mw [kg/mol] |
|----------|---------------|----------------------|---------------------------|-------------------------|---------------|-------------|
| Hp289 | C | 9.8 | 0 | 21.5 | 0.1 | 955 |
| Hp301 | C | 9.2 | 0 | 21.2 | 0.13 | 894 |
| Hp182 | C | 10.6 | 0.01062 | 77.7 | 58.8 | 195 |
| Hp184 | C | 10.6 | 0.01053 | 71.7 | 47.3 | 206 |
| Hp195 | C | 9.3 | 0.00527 | 79.5 | 17.2 | 265 |
| Hp196 | C | 9.7 | 0.00511 | 76.0 | 17.6 | 263 |
| Hp276 | C | 10.2 | 0.00286 | 60.4 | 3.5 | 394 |
| Hp277 | C | 13.9 | 0.0029 | 59.7 | 2.2 | 442 |
| Hp194 | C | 12.5 | 0.01046 | 78.7 | 36.7 | 219 |

Table 29. Polymerization results for studying hydrogen response; Cat A vs Cat C; T= 75 [°C]

3 The polymerization experiments carried out for studying the influence of pre-contact:

The following experiments were all performed at 75 [°C] using Catalyst C:

| Run Code | Catalyst type | Catalyst amount [mg] | Activity [kg/(gCat.hr)] | MFR [g/10min] | Pre-contact time [s] |
|----------|---------------|----------------------|-------------------------|---------------|----------------------|
| Hp173 | C | 10.5 | 72.4 | 63.7 | 0 |
| Hp176 | C | 10.5 | 75.0 | 54.3 | 0 |
| Hp182 | C | 10.6 | 77.7 | 58.8 | 10 |
| Hp184 | C | 10.6 | 71.7 | 47.4 | 10 |
| Hp188 | C | 9.1 | 74.6 | 64.4 | 10 |
| Hp192 | C | 9.0 | 78.2 | 86.0 | 10 |
| Hp190 | C | 10.2 | 69.0 | 53.2 | 60 |
| Hp191 | C | 10.2 | 75.5 | 59.1 | 60 |
| Hp198 | C | 10.5 | 76.0 | 60.7 | 300 |
| Hp199 | C | 9.6 | 76.5 | 56.2 | 300 |

Table 30. Polymerization results for studying the influence of pre-contacting; Cat A vs Cat C; T= 75 [°C]

The following experiments were all performed at 75 [°C] using Catalyst A:

| Run Code | Catalyst type | Catalyst amount [mg] | Activity [kg/(gCat.hr)] | MFR [g/10min] | Pre-contact time [s] |
|----------|---------------|----------------------|-------------------------|---------------|----------------------|
| Re24 | A | 12.6 | 19.6 | - | 0 |
| Re118 | A | 18.7 | 19.6 | - | 0 |
| Hp267 | A | 17.0 | 17.6 | 142 | 0 |
| Hp270 | A | 17.8 | 17.8 | 148 | 0 |
| Hp271 | A | 18.7 | 21.9 | - | 0 |
| Re57 | A | 16.3 | 39.3 | 111 | 10 |
| Re55 | A | 17.7 | 36.0 | 94.5 | 10 |
| Hp284 | A | 15.7 | 41.1 | - | 10 |
| Re54 | A | 17.1 | 38.5 | 84 | 60 |
| Re53 | A | 18.1 | 38.8 | 86 | 60 |
| Re58 | A | 16.3 | 29.9 | 117 | 300 |
| Re61 | A | 19.5 | 32.1 | 112 | 300 |

Table 31. Polymerization results for studying the influence of pre-contacting; Cat A vs Cat C; T= 75 [°C]

Appendix II

In this appendix the results of intrinsic viscosity and MFR measurements regarding a number of impact copolymer samples are listed. These samples are produced with both catalysts A

and C. In the following table the calculated MFR values of either polymer phase is compared with experimentally obtained results:

| Sample Nr | Catalyst | Rubber Content [Mass%] | Ethylene in rubber (FTIR) [mol/mol] | MFR Total (Measured) [g/10min] | MFR Matrix (Estimated) [g/10min] | IV EPR (measured) [g/dl] | MFR EPR (Calculated) [g/10min] | Mw EPR (Calculated) [kg/mol] |
|-----------|----------|------------------------|-------------------------------------|--------------------------------|----------------------------------|--------------------------|--------------------------------|------------------------------|
| ICP257 | C | 20 | 0.42 | 34.5 | ~57 | 1.63 | 4.5 | 233 |
| ICP258 | C | 20 | 0.43 | 40.7 | ~57 | 1.68 | 4.0 | 242 |
| ICP260 | C | 20 | 0.49 | 30.0 | ~57 | 1.90 | 2.7 | 280 |
| ICP261 | C | 20 | 0.54 | 24.3 | ~57 | 1.96 | 2.4 | 290 |
| ICP250 | A | 10 | 0.38 | 35.9 | ~57 | 1.54 | 5.4 | 218 |
| ICP239 | A | 20 | 0.32 | 38.5 | ~57 | 1.16 | 13.8 | 155 |
| ICP255 | A | 20 | 0.38 | 38.5 | ~57 | 1.46 | 6.4 | 204 |
| ICP264 | A | 20 | 0.47 | 25.3 | ~57 | 1.83 | 3.0 | 267 |
| ICP265 | A | 20 | 0.48 | 26.3 | ~57 | 1.77 | 3.4 | 257 |
| ICP232 | A | 30 | 0.51 | 22.5 | ~57 | 2.01 | 2.2 | 299 |

Table 32. Impact copolymer samples molecular weight analysis

Appendix III

In this section the results of experiments for investigating the phase equilibria between liquid and vapor in the polymerization reactor are presented. The following experiments were performed to investigate the partitioning of hydrogen in two phases. The values calculated by the flash calculation procedure are compared with the experimentally measured data points obtained by μ -GC setup:

| z_{H_2} [mol/mol] | y_{H_2} (Measured by μ -GC) [mol/mol] | y_{H_2} (Flash calculation) [mol/mol] | x_{H_2} (Flash calculation) [mol/mol] | Pressure [bar] | k_{H_2} |
|---------------------|---------------------------------------------|-----------------------------------------|-----------------------------------------|----------------|-----------|
| 0.00687 | 0.0312 | 0.02620 | 0.00410 | 35.64 | 6.390 |
| 0.00778 | 0.0339 | 0.03100 | 0.00493 | 36.00 | 6.285 |
| 0.00850 | 0.0340 | 0.03700 | 0.00590 | 36.46 | 6.271 |
| 0.01094 | 0.0440 | 0.04611 | 0.00736 | 37.16 | 6.267 |
| 0.01179 | 0.0604 | 0.05814 | 0.00932 | 38.13 | 6.240 |
| 0.01748 | 0.0606 | 0.06020 | 0.00966 | 38.30 | 6.234 |
| 0.01692 | 0.0640 | 0.06190 | 0.00994 | 38.44 | 6.225 |
| 0.01983 | 0.0853 | 0.08580 | 0.01392 | 40.52 | 6.164 |
| 0.02182 | 0.0742 | 0.07620 | 0.01232 | 39.67 | 6.185 |

| | | | | | |
|---------|--------|---------|---------|-------|-------|
| 0.02516 | 0.0864 | 0.08789 | 0.01428 | 40.71 | 6.155 |
| 0.02761 | 0.0824 | 0.07960 | 0.01289 | 39.97 | 6.175 |
| 0.02938 | 0.0861 | 0.08500 | 0.01379 | 40.45 | 6.164 |
| 0.01602 | 0.0580 | 0.05899 | 0.00946 | 38.20 | 6.238 |

Table 33. Mole fraction of hydrogen in gas phase measured by μ -GC vs calculated values by flash calculation procedure; T= 75 [°C], P=35-41 [bar]

The equilibrium constant for each measurement in table 31 is a result of the convergence of the iterative flash calculation procedure and varies slightly for different data points. In the following plot the calculated equilibrium constants are plotted against the experiment pressure. It is observed that the equilibrium constant of hydrogen in a binary mixture with propylene decreases at higher pressures, which can be an indication of higher solubility of hydrogen in liquid propylene at higher pressures:

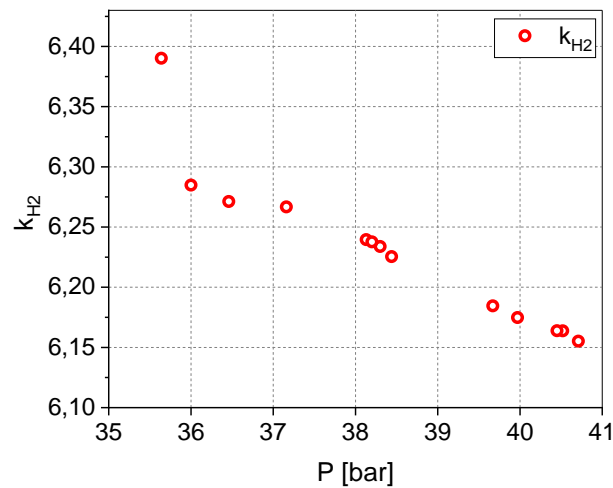


Figure 108. Hydrogen equilibrium constant in a binary mixture with propylene; T=75 [°C], P=35-41 [bar]

The amount of material in the liquid phase for different amounts of propylene in the feed is estimated, following the flash calculation procedure, and presented in the following table:

| n_{H_2} [mol] | m_{C_3} [kg] | n_{C_3} [mol] | n_T [mol] | z_{H_2} [mol/mol] | Pressure [bar] | V_{liquid} [liter] |
|--------------------|-------------------|--------------------|----------------|------------------------|-------------------|-------------------------|
| 0.675 | 1.200 | 28.57 | 29.25 | 0.0231 | 38.78 | 2.17 |
| 0.675 | 1.300 | 30.95 | 31.63 | 0.0213 | 39.23 | 2.74 |
| 0.675 | 1.400 | 33.33 | 34.01 | 0.0198 | 39.59 | 3.19 |
| 0.675 | 1.450 | 34.52 | 35.20 | 0.0192 | 39.97 | 3.52 |
| 0.675 | 1.560 | 37.14 | 37.82 | 0.0178 | 40.42 | 3.95 |

Table 34. Amount of material in the liquid phase for different amounts of propylene in the feed; T= 75 [°C]- P=35-41 [bar]

References

- [1] Plastics Europe Facts 2019 FINAL_web_version_Plastics available at: https://www.plasticseurope.org/application/files/9715/7129/9584/FINAL_web_version_Plastics_the_facts2019_14102019.pdf.
- [2] Kutsch, O. 2021 *Polypropylene Market Report: Global Industry Analysis*. <https://www.ceresana.com/en/market-studies/plastics/polypropylene/polypropylene-market-share-capacity-demand-supply-forecast-innovation-application-growth-production-size-industry.html>. Accessed 11 March 2021.
- [3] Karian, H. G. 2003 *Handbook of polypropylene and polypropylene composites*. Plastics engineering, vol 51. New York: Marcel Dekker.
- [4] Malpass, D. B. & Band, E. 2012 *Introduction to Industrial Polypropylene. Properties, Catalysts Processes*. EBL-Schweitzer, 1., Auflage. New York, NY: John Wiley & Sons.
- [5] Moore, E. P. 1996 Polypropylene handbook. Polymerization, characterization, properties, processing, applications.
- [6] Derosa, C. & Auriemma, F. 2006 Structure and physical properties of syndiotactic polypropylene: A highly crystalline thermoplastic elastomer. *Progress in Polymer Science* **31**, 145–237.
- [7] Paukkeri, R. & Lehtinen, A. 1993 Thermal behaviour of polypropylene fractions: 1. Influence of tacticity and molecular weight on crystallization and melting behaviour. *Polymer* **34**, 4075–4082.
- [8] Alburnia, A., Prades, F. & Jeremic, D. 2019 *Multimodal Polymers with Supported Catalysts. Design and Production*. Cham: Springer International Publishing.
- [9] Kaminsky, W. & Laban, A. 2001 Metallocene catalysis. *Applied Catalysis A: General* **222**, 47–61.
- [10] van der Ven, S. 2014 *Polypropylene and other Polyolefins. Polymerization and Characterization*. Studies in Polymer Science, v. 7. Amsterdam: Elsevier Science.
- [11] Gahleitner, M., Tranninger, C. & Doshev, P. 2013 Heterophasic copolymers of polypropylene: Development, design principles, and future challenges. *J. Appl. Polym. Sci.* **130**, 3028–3037.
- [12] Karger-Kocsis, J. 1995 *Polypropylene Structure, blends and composites. Volume 2 Copolymers and Blends*. Dordrecht: Springer Science.
- [13] Sato, H. & Ogawa, H. 2009 *Review on Development of Polypropylene Manufacturing Process*.
- [14] Soares, J. B. P. 2013 *Polyolefin Reaction Engineering*. Weinheim: Wiley.
- [15] LyondellBasell. 2020 *Licensed Polyolefin Technologies and Services. Spheripol*. <https://www.lyondellbasell.com/en/products-technology/technology/polypropylene-technologies/>. Accessed 30 November 2020.
- [16] Mitsui Chemicals Inc. *Hypol-II for Licensed PP Technology*. <https://jp.mitsuichemicals.com/en/techno/license>. Accessed 12 January 2020.
- [17] McKenna, T. 2019 Condensed Mode Cooling of Ethylene Polymerization in Fluidized Bed Reactors. *Macromolecular Reaction Engineering* **13**.
- [18] Lummus Technology. 2020 *Novolen® Gas-Phase Process | Lummus Technology*. <https://www.lummustechnology.com/Process-Technologies/Petrochemicals/Polypropylene-Production/Novolen-Gas-Phase-Process>. Accessed 2 December 2020.

- [19] Grace Materials Technologies. 2021 *UNIPOL Polypropylene Process Licensing*. <https://grace.com/en-us/capabilities/process-licensing>. Accessed 12 March 2021.
- [20] LyondellBasell *Licensed Polyolefin Technologies and Services. Spherizone*. <https://www.lyondellbasell.com/globalassets/products-technology/technology/spherizone-brochure.pdf>. Accessed 30 November 2020.
- [21] Ziegler, K., Breil, H., Holzkamp, E. & Martin, H. 1960 Verfahren zur Herstellung von hochmolekularen Polyäthylenen. Patent Nr. DE973626 C.
- [22] Corradini, P., Busico, V., Cavallo, L., Guerra, G., Vacatello, M. & Venditto, V. 1992 Structural analogies between homogeneous and heterogeneous catalysts for the stereospecific polymerization of 1-alkenes. *Journal of Molecular Catalysis* **74**, 433–442.
- [23] Keii, T. 1986 *Catalytic polymerization of olefins. Proceedings*. Studies in surface science and catalysis, vol 25. Amsterdam, Tokyo: Kodansha.
- [24] Kissin, Y. V. 2008 *Alkene polymerization reactions with transition metal catalysts*. Studies in surface and catalysis, vol 173. Amsterdam, London: Elsevier.
- [25] Kissin, Y. V., Chadwick, J. C., Mingozzi, I. & Morini, G. 2006 Isoselectivity Distribution of Isospecific Centers in Supported Titanium-Based Ziegler-Natta Catalysts. *Macromol. Chem. Phys.* **207**, 1344–1350.
- [26] Natta, G., Pino, P., Mazzanti, G. & Giannini, U. 1957 A CRYSTALLIZABLE ORGANOMETALLIC COMPLEX CONTAINING TITANIUM AND ALUMINUM. *J. Am. Chem. Soc.* **79**, 2975–2976.
- [27] Hermans, J. P. & Henriouille, P. 1975 Process for the preparation of a ziegler-natta type catalyst. <https://patents.google.com/patent/ca962654a/en-20us4325121.pdf>.
- [28] Correa, A., Piemontesi, F., Morini, G. & Cavallo, L. 2007 Key Elements in the Structure and Function Relationship of the MgCl₂/TiCl₄/Lewis Base Ziegler–Natta Catalytic System. *Macromolecules* **40**, 9181–9189.
- [29] Parodi, S., Nocci, R., Giannini, U., Barbè, P. C. & Scata, U. 1982 Components and catalysts for the polymerization of olefins. Patent Nr. US4399054A.
- [30] Cecchin, G., Morini, G. & Pelliconi, A. 2001 Polypropene product innovation by reactor granule technology. *Macromolecular Symposia* **173**, 195–210.
- [31] Morini, G., Albizzati, E., Balbontin, G., Mingozzi, I., Sacchi, M. C., Forlini, F. & Tritto, I. 1996 Microstructure Distribution of Polypropylenes Obtained in the Presence of Traditional Phthalate/Silane and Novel Diether Donors: A Tool for Understanding the Role of Electron Donors in MgCl₂-Supported Ziegler–Natta Catalysts. *Macromolecules* **29**, 5770–5776.
- [32] Kaminsky, W. 2004 The discovery of metallocene catalysts and their present state of the art. *Journal of Polymer Science Part A: Polymer Chemistry* **42**, 3911–3921.
- [33] Kaminsky, W. 1996 New polymers by metallocene catalysis. *Macromolecular Chemistry and Physics* **197**, 3907–3945.
- [34] Jian Yang & Lubin Lou. 2018 Supported metallocene catalyst systems for polymerization. Patent Nr. US 10723821 B2.
- [35] Alshaiban, A. & Soares, J. B. P. 2013 Effect of Hydrogen and External Donor on the Microstructure of Polypropylene Made with a 4th Generation Ziegler-Natta Catalyst. *Macromolecular Reaction Engineering* **7**, 135–145.
- [36] Busico, V., Cipullo, R. & Corradini, P. 1992 Hydrooligomerization of propene: a “fingerprint” of a Ziegler-Natta catalyst, 1. Preliminary results for MgCl₂-supported systems. *Die Makromolekulare Chemie, Rapid Communications* **13**, 15–20.

- [37] Corradini, P., Busico, V. & Cipullo, R. 1992 Hydroooligomerization of propene: a “fingerprint” of a Ziegler-Natta catalyst, 2. A reinterpretation of results for isospecific homogeneous systems. *Die Makromolekulare Chemie, Rapid Communications* **13**, 21–24.
- [38] Guastalla, G. & Giannini, U. 1983 The influence of hydrogen on the polymerization of propylene and ethylene with an MgCl₂ supported catalyst. *Makromol. Chem., Rapid Commun.* **4**, 519–527.
- [39] Ali, M. A., Betlem, B., Roffel, B. & Weickert, G. 2006 Hydrogen response in liquid propylene polymerization: Towards a generalized model. *AIChE J.* **52**, 1866–1876.
- [40] Soares, J. & Hamielec, A. E. 1996 Kinetics of propylene polymerization with a non-supported heterogeneous Ziegler-Natta catalyst—effect of hydrogen on rate of polymerization, stereoregularity, and molecular weight distribution. *Polymer* **37**, 4607–4614.
- [41] Kissin, Y. V., Rishina, L. A. & Vizen, E. I. 2002 Hydrogen effects in propylene polymerization reactions with titanium-based Ziegler-Natta catalysts. II. Mechanism of the chain-transfer reaction. *Journal of Polymer Science Part A: Polymer Chemistry* **40**, 1899–1911.
- [42] Varshouee, G. H., Heydarinasab, A., Shaheen, U., Aborehab, M. A. S., Vaziri, A., Ouadi, Y. E., Roozbahani, B., Bouyanzer, A., Hammouti, B. & Ben Hadda, T. 2018 Hydrogen effect modeling on Ziegler-Natta catalyst and final product properties in propylene polymerization. *AJOL* **32**, 371–386.
- [43] Chadwick, J., Miedema, A. & Sudmeijer, O. 1994 Hydrogen activation in propene polymerization with MgCl₂-supported Ziegler-Natta catalysts: the effect of the external donor. *Macromolecular Chemistry and Physics* **195**, 167–172.
- [44] Choi, K. & Ray, W. H. 1985 The dynamic behaviour of fluidized bed reactors for solid catalysed gas phase olefin polymerization. *Chemical Engineering Science* **40**, 2261–2279.
- [45] Mikhail A. Matsko, Gennadii D. Bukatov, Tatiana B. Mikenas & Vladimir A. Zakharov. 2001 Ethylene Polymerization with Supported Vanadium-Magnesium Catalyst: Number of Active Centers and Propagation Rate Constant. *Macromolecular Chemistry and Physics* **202**, 1435–1439.
- [46] Pater, J. T. M., Weickert, G., Loos, J., van S. & Wim P. M. 2001 High precision prepolymerization of propylene at extremely low reaction rates—kinetics and morphology. *Chemical Engineering Science* **56**, 4107–4120.
- [47] Pater, J. T. M., Weickert, G. & van, S., Wim P. M. 2003 Polymerization of liquid propylene with a fourth-generation Ziegler-Natta catalyst: Influence of temperature, hydrogen, monomer concentration, and prepolymerization method on powder morphology. *Journal of Applied Polymer Science* **87**, 1421–1435.
- [48] Weickert, G., Meier, G. B., Pater, J. & Westerterp, K. R. 1999 The particle as microreactor: catalytic propylene polymerizations with supported metallocenes and Ziegler–Natta catalysts. *Chemical Engineering Science* **54**, 3291–3296.
- [49] Pater, J. T. M., Weickert, G. & van S., W. P. M. 2003 Propene bulk polymerization kinetics: Role of prepolymerization and hydrogen. *AIChE J.* **49**, 180–193.
- [50] Samson, J. J. C., van Middelkoop, B., Weickert, G. & Westerterp, K. R. 1999 Gas-phase polymerization of propylene with a highly active ziegler-natta catalyst. *AIChE J.* **45**, 1548–1558.
- [51] Kettner, J., Valaei, S. & Bartke, M. 2020 Reaction Calorimetry for Studying Kinetics in Bulk Phase Polymerization of Propene. *Macromol. React. Eng.*, 2000031.

- [52] Busico, V., Corradini, P., Ferraro, A. & Proto, A. 1986 Polymerization of propene in the presence of MgCl₂-supported Ziegler-Natta catalysts, 3. Catalyst deactivation. *Makromol. Chem.* **187**, 1125–1130.
- [53] Chien, J. C. W., Wu, J.-C. & Kuo, C.-I. 1982 Magnesium chloride supported high-mileage catalysts for olefin polymerization. I. Chemical composition and oxidation states of titanium. *J. Polym. Sci. Polym. Chem. Ed.* **20**, 2019–2032.
- [54] Shimizu, F., Pater, J. T. M., van Swaaij, W. P. M. & Weickert, G. 2002 Kinetic study of a highly active MgCl₂-supported Ziegler-Natta catalyst in liquid pool propylene polymerization. II. The influence of alkyl aluminum and alkoxy silane on catalyst activation and deactivation. *Journal of Applied Polymer Science* **83**, 2669–2679.
- [55] Kissin, Y. V. 2012 Active centers in Ziegler–Natta catalysts: Formation kinetics and structure. *Journal of Catalysis* **292**, 188–200.
- [56] José Cancelas Sanz, A. 2017 *High impact polypropylene : structure evolution and impact on reaction*.
- [57] Bahareh Raisi. 2010 Effects of Catalyst Pre-contact Procedure on Kinetics, Properties and Morphology of Propylene Polymerization.
- [58] Aigner, P., Paulik, C., Krallis, A. & Kanellopoulos, V. 2016 Optimal Catalyst and Cocatalyst Precontacting in Industrial Ethylene Copolymerization Processes. *Journal of Polymers* **2016**, 1–10.
- [59] Tan, N., Yu, L., Tan, Z. & Mao, B. 2015 Kinetics of the propylene polymerization with prepolymerization at high temperature using Ziegler-Natta catalyst. *J. Appl. Polym. Sci.* **132**, n/a-n/a.
- [60] Choi, K. & Ray, W. H. 1985 Recent Developments in Transition Metal Catalyzed Olefin Polymerization—A Survey. II. Propylene Polymerization. *Journal of Macromolecular Science, Part C* **25**, 57–97.
- [61] Meier, G. B., Weickert, G. & van Swaaij, W. P. M. 2001 Comparison of gas- and liquid-phase polymerization of propylene with heterogeneous metallocene catalyst. *Journal of Applied Polymer Science* **81**, 1193–1206.
- [62] Meier, G. B., Weickert, G. & van Swaaij, W. P. M. 2001 Gas-phase polymerization of propylene: Reaction kinetics and molecular weight distribution. *J. Polym. Sci. A Polym. Chem.* **39**, 500–513.
- [63] Kettner, J. 2019 *Kinetic investigation of different supported catalysts for the polymerization of propylene under industrially relevant conditions*. Göttingen: Cuvillier Verlag.
- [64] Piduhn, M. 1999 *Metallocen-katalysierte Polymerisation von Propen und Ethen aus der Gasphase*.
- [65] Kröner, T. 2014 *Mass Transport and Kinetics in the Heterophasic Copolymerization of Propylene*. Berlin: Mensch & Buch.
- [66] Debling, J. A. & Ray, W. H. 2001 Morphological development of impact polypropylene produced in gas phase with a TiCl₄/MgCl₂ catalyst. *Journal of Applied Polymer Science* **81**, 3085–3106.
- [67] Keii, T., Suzuki, E., Tamura, M., Murata, M. & Doi, Y. 1982 Propene polymerization with a magnesium chloride-supported ziegler catalyst, 1. Principal kinetics. *Makromol. Chem.* **183**, 2285–2304.
- [68] Andersen, H. M. 1966 Isothermal kinetic calorimeter applied to emulsion polymerization. *Journal of Polymer Science Part A-1: Polymer Chemistry* **4**, 783–791.

- [69] Kröner, S., Eloranta, K., Bergstra, M. F. & Bartke, M. 2007 Kinetic Study of the Copolymerisation of Ethylene with a Single Site Catalyst in Propane Slurry Polymerisation. *Macromol. Symp.* **259**, 284–294.
- [70] Zhang, B., Qian, Q., Yang, P., Jiang, B., Fu, Z. & Fan, Z. 2021 Responses of a Supported Ziegler–Natta Catalyst to Comonomer Feed Ratios in Ethylene–Propylene Copolymerization: Differentiation of Active Centers with Different Catalytic Features. *Ind. Eng. Chem. Res.* **60**, 4575–4588.
- [71] Nedorezova, P. M., Tsvetkova, V. I., Aladyshev, A. M., Savinov, D. V., Dubnikova, I. L., Optov, V. A., Lemenovskii, D. A. 2000 Stereospecific bulk polymerization of propylene. *Polymer* **45**, 333–338.
- [72] Matos, V., Mattos Neto, A. G., Nele, M. & Pinto, J. C. 2002 Method for quantitative evaluation of kinetic constants in olefin polymerizations. II. Kinetic study of a high-activity Ziegler-Natta catalyst used for bulk propylene polymerizations. *J. Appl. Polym. Sci.* **86**, 3226–3245.
- [73] Batyrshin, A. Z., Bukatov, G. D., Salakhov, I. I., Sergeev, S. A., Mats'ko, M. A., Barabanov, A. A. & Sakhabutdinov, A. G. 2019 Effect of Polymerization Conditions on Polypropylene Synthesis in Liquid Monomer. *Pet. Chem.* **59**, 167–173.
- [74] Patzlaff, M. 2006 *Kinetische Untersuchung der Polymerisation von Propylen mit neuartigen Ziegler-Natta Katalysatoren in Gas- und Flüssigphase*: Technische Universität Berlin.
- [75] Landau, R. N. 1996 Expanding the role of reaction calorimetry. *Thermochimica Acta* **289**, 101–126.
- [76] Tisse, V. F., Sheibat-Othman, N. & McKenna, T. F. L. 2010 A lab-scale reaction calorimeter for olefin polymerization. *Can. J. Chem. Eng.* **88**, n/a-n/a.
- [77] Lahti, M., Avela, A. & Seppälä, J. 1995 Polymerization calorimeter. Part 1. Modelling and characterization. *Thermochimica Acta* **262**, 13–31.
- [78] Karcz, J. & Cudak, M. 2002 Efficiency of the heat transfer process in a jacketed agitated vessel equipped with an eccentrically located impeller. *Chemical Papers- Slovak Academy of Sciences* **56**.
- [79] Stoessel, F. 1997 Applications of reaction calorimetry in chemical engineering. *Journal of Thermal Analysis and Calorimetry* **49**, 1677–1688.
- [80] Schlegel, M. & Löwe, A. 1998 A reaction calorimeter with compensation heater and differential cooling. *Chemical Engineering and Processing: Process Intensification* **37**, 61–67.
- [81] Samson, J. J. C., Weickert, G., Heerze, A. E. & Westerterp, K. R. 1998 Liquid-phase polymerization of propylene with a highly active catalyst. *AIChE J.* **44**, 1424–1437.
- [82] Korber, F., Hauschild, K. & Fink, G. 2001 Reaction Calorimetric Approach to the Kinetic Investigation of the Propylene Bulk Phase Polymerization. *Macromol. Chem. Phys.* **202**, 3329–3333.
- [83] Stoessel, F. 2020 *Thermal Safety of Chemical Processes. Risk Assessment and Process Design*, 2nd edition edition. Weinheim: Wiley-VCH.
- [84] Moritz U. H. 1989 *Polymerization calorimetry. A powerful tool for reactor control, Proceedings of the Third Berlin International Workshop on Polymer Reaction Engineering*.
- [85] Ali, M. A., Betlem, B., Roffel, B. & Weickert, G. 2007 Estimation of the Polymerization Rate of Liquid Propylene Using Adiabatic Reaction Calorimetry and Reaction Dilatometry. *Macromol. React. Eng.* **1**, 353–363.

- [86] Carloff, R., Proß, A. & Reichert, K.-H. 1994 Temperature oscillation calorimetry in stirred tank reactors with variable heat transfer. *Chem. Eng. Technol.* **17**, 406–413.
- [87] Andersen, H. M. 1969 Polymerization rates by calorimetry. II. *Journal of Polymer Science Part A-1: Polymer Chemistry* **7**, 2889–2896.
- [88] Dobre, A. C., Yaacoub, E.-J. & Schumpe, A. 2003 Kinetic and Thermodynamic Studies of Emulsion Polymerization of a Sugar Monomer by Calorimetry with Compensation Heating and Differential Cooling. *Macromol. Mater. Eng.* **288**, 516–524.
- [89] Zogg, A., Stoessel, F., Fischer, U. & Hungerbühler, K. 2004 Isothermal reaction calorimetry as a tool for kinetic analysis. *Thermochimica Acta* **419**, 1–17.
- [90] Debling, J. A., Han, G. C., Kuijpers, F., Verburg, J., Zacca, J. & Ray, W. H. 1994 Dynamic modeling of product grade transitions for olefin polymerization processes. *AIChE J.* **40**, 506–520.
- [91] Zacca, J. J. & Ray, W. H. 1993 Modelling of the liquid phase polymerization of olefins in loop reactors. *Chemical Engineering Science* **48**, 3743–3765.
- [92] Yiannoulakis, H., Yiagopoulos, A., Pladis, P. & Kiparissides, C. 2000 Comprehensive Dynamic Model for the Calculation of the Molecular Weight and Long Chain Branching Distributions in Metallocene-Catalyzed Ethylene Polymerization Reactors. *Macromolecules* **33**, 2757–2766.
- [93] Válter Matos, Antônio G. Mattos Neto & José Carlos Pinto. 2001 Method for quantitative evaluation of kinetic constants in olefin polymerizations. I. Kinetic study of a conventional Ziegler–Natta catalyst used for propylene polymerizations. *Journal of Applied Polymer Science* **79**, 2076–2108.
- [94] Luo, Z.-H., Su, P.-L., Shi, D.-P. & Zheng, Z.-W. 2009 Steady-state and dynamic modeling of commercial bulk polypropylene process of Hypol technology. *Chemical Engineering Journal* **149**, 370–382.
- [95] Khare, N. P., Lucas, B., Seavey, K. C., Liu, Y. A., Sirohi, A., Ramanathan, S., Lingard, S., Song, Y. & Chen, C.-C. 2004 Steady-State and Dynamic Modeling of Gas-Phase Polypropylene Processes Using Stirred-Bed Reactors. *Ind. Eng. Chem. Res.* **43**, 884–900.
- [96] McKenna, T. F. & Soares, J. B. 2001 Single particle modelling for olefin polymerization on supported catalysts: A review and proposals for future developments. *Chemical Engineering Science* **56**, 3931–3949.
- [97] McKenna, T. & Mattioli, V. 2001 Progress in describing particle growth for polyolefins: a look at particle morphology. *Macromolecular Symposia* **173**, 149–162.
- [98] Arlman, E. 1964 Ziegler-Natta catalysis II. Surface structure of layer-lattice transition metal chlorides. *Journal of Catalysis* **3**, 89–98.
- [99] Arlman, E. 1964 Ziegler-Natta catalysis III. Stereospecific polymerization of propene with the catalyst system. *Journal of Catalysis* **3**, 99–104.
- [100] Cossee, P. 1964 Ziegler-Natta catalysis I. Mechanism of polymerization of alpha;-olefins with Ziegler-Natta catalysts. *Journal of Catalysis* **3**, 80–88.
- [101] Shaffer, W. K. A. & Ray, W. H. 1997 Polymerization of olefins through heterogeneous catalysis. XVIII. A kinetic explanation for unusual effects. *Journal of Applied Polymer Science* **65**, 1053–1080.
- [102] Soares, J. B. P. 2001 Mathematical modelling of the microstructure of polyolefins made by coordination polymerization: a review. *Chemical Engineering Science* **56**, 4131–4153.

- [103] Huang, K. & Xie, R. 2014 Modeling of molecular weight distribution of propylene slurry phase polymerization on supported metallocene catalysts. *Journal of Industrial and Engineering Chemistry* **20**, 338–344.
- [104] Xie, T., McAuley, K. B., Hsu, J. C. C. & Bacon, D. W. 1994 Gas Phase Ethylene Polymerization: Production Processes, Polymer Properties, and Reactor Modeling. *Ind. Eng. Chem. Res.* **33**, 449–479.
- [105] Cheng, X., Feng, L., Gu, X., Chen, X., Zhen-Guo & McAuley, K. B. 2020 Modeling of sequence length distribution for olefin copolymerization with vanadium-based catalyst. *AIChE Journal* **66**, e16784.
- [106] Tian, Z., Xue-Ping, G., Feng, L.-F. & Guo-Hua, H. 2013 A model for the structures of impact polypropylene copolymers produced by an atmosphere-switching polymerization process. *Chemical Engineering Science* **101**, 686–698.
- [107] Soares, J. B. P. & Hamielec, A. E. 1996 Copolymerization of Olefins in a Series of Continuous Stirred-Tank Slurry-Reactors Using Heterogeneous Ziegler-Natta and Metallocene Catalysts. I. General Dynamic Mathematical Model. *Polymer Reaction Engineering* **4**, 153–191.
- [108] Ghafelebashi Zaranda, S. M. & Safinejad, A. 2020 Determination of kinetic parameters for ethylene polymerization (with and without hydrogen) by Ziegler-Natta catalyst. *Polyolefins Journal* **7**, 121–130.
- [109] Schmeal, W. R. & Street, J. R. 1971 Polymerization in expanding catalyst particles. *AIChE J.* **17**, 1188–1197.
- [110] Bartke, M. & Reichert, K.-H. 2000 Calculation of Molecular Weight Distributions of Polymerization Reactions Using Standard Simulation Software. *Chem. Eng. Technol.* **23**, 1062–1065.
- [111] Yermakov, I. Mikhaichenko, V. Besco, Y.P Grabovski. 1970 The role of transfer processes in gaseous phase polymerization of ethylene.
- [112] Nagel, E. J., Kirillov, V. A. & Ray, W. H. 1980 Prediction of Molecular Weight Distributions for High-Density Polyolefins. *Ind. Eng. Chem. Prod. Res. Dev.* **19**, 372–379.
- [113] Floyd, S., Choi, K. Y., Taylor, T. W. & Ray, W. H. 1986 Polymerization of olefines through heterogeneous catalysis IV. Modeling of heat and mass transfer resistance in the polymer particle boundary layer. *Journal of Applied Polymer Science* **31**, 2231–2265.
- [114] Hutchinson, R. A., Chen, C. M. & Ray, W. H. 1992 Polymerization of olefins through heterogeneous catalysis X: Modeling of particle growth and morphology. *Journal of Applied Polymer Science* **44**, 1389–1414.
- [115] Angus, S., Armstrong, B. & Reuck, K. M. de. 1980 *International Thermodynamic Tables of the Fluid State-7 Propylene*, International Union of Pure and Applied Chemistry: Elsevier Ltd.
- [116] Smith, J. M. & van Ness, H. C. 1975 *Introduction to chemical engineering thermodynamics*. McGraw-Hill chemical engineering series, 3. ed. Tokyo: McGraw-Hill.
- [117] Huron, M.-J. & Vidal, J. 1979 New mixing rules in simple equations of state for representing vapour-liquid equilibria of strongly non-ideal mixtures. *Fluid Phase Equilibria* **3**, 255–271.
- [118] Rogers, C. E., Stannett, V. & Szwarc, M. 1960 The sorption, diffusion, and permeation of organic vapors in polyethylene. *Journal of Polymer Science* **45**, 61–82.
- [119] Michaels, A. S. & Bixler, H. J. 1961 Flow of gases through polyethylene. *Journal of Polymer Science* **50**, 413–439.

- [120] Li, N. N. & Long, R. B. 1969 Permeation through plastic films. *AIChE Journal* **15**, 73–80.
- [121] Flory, P. J. 1942 Thermodynamics of High Polymer Solutions. *The Journal of Chemical Physics* **10**, 51–61.
- [122] Bashir, M., Kanellopoulos, V., Al-haj Ali, M. & McKenna, T. 2020 Applied Thermodynamics for Process Modeling in Catalytic Gas Phase Olefin Polymerization Reactors. *Macromolecular Reaction Engineering* **14**, 1900029.
- [123] Cancelas, A. J., Plata, M. A., Bashir, M., Bartke, M., Monteil, V. & McKenna, T. F. L. 2018 Solubility and Diffusivity of Propylene, Ethylene, and Propylene-Ethylene Mixtures in Polypropylene. *Macromol. Chem. Phys.* **219**, 1700565.
- [124] Bashir, M., Al-haj Ali, M., Kanellopoulos, V., Seppälä, J., Kokko, E. & Vijay, S. 2013 The Effect of Pure Component Characteristic Parameters on Sanchez-Lacombe Equation-of-State Predictive Capabilities. *Macromol. React. Eng.* **7**, 193–204.
- [125] Hutchinson, R. A. & Ray, W. H. 1990 Polymerization of olefins through heterogeneous catalysis. VIII. Monomer sorption effects. *Journal of Applied Polymer Science* **41**, 51–81.
- [126] Patzlaff, M., Wittebrock, A. & Reichert, K.-H. 2006 Sorption studies of propylene in polypropylene. Diffusivity in polymer particles formed by different polymerization processes. *Journal of Applied Polymer Science* **100**, 2642–2648.
- [127] Sato, Y., Tsuboi, A., Sorakubo, A., Takishima, S., Masuoka, H. & Ishikawa, T. 2000 Vapor–liquid equilibrium ratios for hexane at infinite dilution in ethylene+impact polypropylene copolymer and propylene+impact polypropylene copolymer. *Fluid Phase Equilibria* **170**, 49–67.
- [128] Bartke, M., Kröner, S., Wittebrock, A., Reichert, K., Iliopoulos, I. & Dittrich, C. 2007 Sorption and Diffusion of Propylene and Ethylene in Heterophasic Polypropylene Copolymers. *Macromolecular Symposia* **259**, 327–336.
- [129] Kröner, T. & Bartke, M. 2013 Sorption of Olefins in High Impact Polypropylene - Experimental Determination and Mass Transport Modeling. *Macromol. React. Eng.* **7**, 453–462.
- [130] Ben Mrad, A., Sheibat-Othman, N., Valaei, S., Bartke, M. & McKenna, T. F. L. 2022 Diffusivity of Multicomponent Gas Mixtures in Polyethylene. *Macromolecular Chemistry and Physics* **223**, 2100406.
- [131] Ben Mrad, A., Sheibat-Othman, N., Hill, J., Bartke, M. & McKenna, T. F. 2021 A novel approach for the estimation of the Sanchez-Lacombe interaction parameters for the solubility of ternary polyolefins systems. *Chemical Engineering Journal* **421**, 127778.
- [132] Novak, A., Bobak, M., Kosek, J., Banaszak, B. J., Lo, D., Widya, T., Harmon Ray, W. & Pablo, J. J. de. 2006 Ethylene and 1-hexene sorption in LLDPE under typical gas-phase reactor conditions: Experiments. *Journal of Applied Polymer Science* **100**, 1124–1136.
- [133] Slipecevic, A., Storti, G. & Morbidelli, M. 2000 Measurement of diffusivity and solubility of olefins in polypropylene by gas chromatography. *Journal of Applied Polymer Science* **78**, 464–473.
- [134] Polymer reactor technology GmbH, Ahaus Germany. 2016 *Power Compensation calorimeter manual*.
- [135] 2019 *Glove Box for the Research and Laboratory - GP(Campus)*. <https://www.jacomex.com/glove-box/gpcampus/>. Accessed 6 June 2020.
- [136] Karian, H. G. 2003 *Handbook of Polypropylene and Polypropylene Composites*. Plastics engineering, 2nd ed. Hoboken: Marcel Dekker Inc.

- [137] Ogawa, T. & Inaba, T. 1977 Gel permeation chromatography of ethylene–propylene copolymerization products. *Journal of Applied Polymer Science* **21**, 2979–2990.
- [138] Bremner, T., Rudin, A. & Cook, D. G. 1990 Melt flow index values and molecular weight distributions of commercial thermoplastics. *Journal of Applied Polymer Science* **41**, 1617–1627.
- [139] Raka, L. & Bogoeva-Gaceva, G. 2017 Crystallization of polypropylene: application of differential scanning calorimetry part ii. crystal forms and nucleation. *Contributions* **29**.
- [140] Brandrup, J. 1999 *Polymer handbook*, 4. ed. Hoboken, N. J.: Wiley.
- [141] Wang, J. & Doshev, P. 2015 Heterophasic Polypropylene Polymer. Patent Nr. EP 2891667 B1.
- [142] Grein, C., Gahleitner, M., Knogler, B. & Nestelberger, S. 2007 Melt viscosity effects in ethylene–propylene copolymers. *Rheol Acta* **46**, 1083–1089.
- [143] Flory, P. J. ca. 2006 *Principles of polymer chemistry*, 19. print. Ithaca, NY: Cornell Univ. Press.
- [144] Parrini, P., Sebastiano, F. & Messina, G. 1960 Intrinsic viscosity and molecular weight of isotactic polypropylene. *Makromol. Chem.* **38**, 27–38.
- [145] Pasquon, I. 1967 Some aspects of the mechanism of the stereospecific polymerization of α -olefins. *Pure and Applied Chemistry* **15**, 465–480.
- [146] Grein, C., Bernreitner, K., Hauer, A., Gahleitner, M. & Neißl, W. 2003 Impact modified isotactic polypropylene with controlled rubber intrinsic viscosities: Some new aspects about morphology and fracture. *Journal of Applied Polymer Science* **87**, 1702–1712.
- [147] McKenna, T. F., Bouzid, D., Matsunami, S. & Sugano, T. 2003 Evolution of Particle Morphology During Polymerisation of High Impact Polypropylene. *Polymer Reaction Engineering* **11**, 177–197.
- [148] Zacur, R., Goizueta, G. & Capiati, N. 2000 Dispersed phase morphology of impact PP copolymers. Effects of blend composition as determined by TREF. *Polym. Eng. Sci.* **40**, 1921–1930.
- [149] Goede, E. de, Mallon, P. & Pasch, H. 2010 Fractionation and Analysis of an Impact Poly(propylene) Copolymer by TREF and SEC-FTIR. *Macromol. Mater. Eng.* **295**, 366–373.
- [150] Peng, D.-Y. & Robinson, D. B. 1976 A New Two-Constant Equation of State. *Ind. Eng. Chem. Fund.* **15**, 59–64.
- [151] Missen, R. W. 1989 “Chemical and Engineering Thermodynamics” by Stanley I. Sandler, 2nd ed., 1989, xxiii+622 pp., Wiley, New York. Price U.S. \$58.95. *The Canadian Journal of Chemical Engineering* **67**, 879–880.
- [152] 2020 *National Institute of Standards and Technology | NIST*. <https://www.nist.gov/>. Accessed 12 April 2020.
- [153] Rachford, H. H. & Rice, J. D. 1952 Procedure for Use of Electronic Digital Computers in Calculating Flash Vaporization Hydrocarbon Equilibrium. *Journal of Petroleum Technology* **4**, 19-3.
- [154] Sato, Y., Yurugi, M., Yamabiki, T., Takishima, S. & Masuoka, H. 2001 Solubility of propylene in semicrystalline polypropylene. *Journal of Applied Polymer Science* **79**, 1134–1143.
- [155] Zoller, P. 1979 Pressure–volume–temperature relationships of solid and molten polypropylene and poly(butene-1). *Journal of Applied Polymer Science* **23**, 1057–1061.

- [156] Bobak, M., Gregor, T., Bachman, B. & Kosek, J. 2008 Estimation of Morphology Characteristics of Porous Poly(propylene) Particles from Degassing Measurements. *Macromolecular Reaction Engineering* **2**, 176–189.
- [157] Podivinská, M., Jindrová, K., Chmelař, J. & Kosek, J. 2017 Swelling of polyethylene particles and its relation to sorption equilibria under gas-phase polymerization conditions. *J. Appl. Polym. Sci.* **134**, 45035.
- [158] Sanchez, I. C. & Lacombe, R. H. 1976 An elementary molecular theory of classical fluids. Pure fluids. *J. Phys. Chem.* **80**, 2352–2362.
- [159] Kanellopoulos, V., Mouratides, D., Pladis, P. & Kiparissides, C. 2006 Prediction of Solubility of α -Olefins in Polyolefins Using a Combined Equation of State Molecular Dynamics Approach. *Ind. Eng. Chem. Res.* **45**, 5870–5878.
- [160] Kiparissides, C., Dimos, V., Boultouka, T., Anastasiadis, A. & Chasiotis, A. 2003 Experimental and theoretical investigation of solubility and diffusion of ethylene in semicrystalline PE at elevated pressures and temperatures. *Journal of Applied Polymer Science* **87**, 953–966.
- [161] Hill, J. 2021 *Kinetics and Catalyst Overheating in the Gas Phase Polymerization of Propylene*. Martin-Luther Universität Halle-Wittenberg. Halle (Saale).
- [162] Neau, E. 2002 A consistent method for phase equilibrium calculation using the Sanchez–Lacombe lattice–fluid equation-of-state. *Fluid Phase Equilibria* **203**, 133–140.
- [163] Khare, N. P. 2003 *Predictive Modeling of Metal-Catalyzed Polyolefin Processes*: Virginia Tech.
- [164] Samson, J. J. C., Bosman, P. J., Weickert, G. & Westerterp, K. R. 1999 Liquid-phase polymerization of propylene with a highly active Ziegler-Natta catalyst. Influence of hydrogen, cocatalyst, and electron donor on the reaction kinetics. *J. Polym. Sci. A Polym. Chem.* **37**, 219–232.
- [165] Yaluma, A. K., Tait, P. & Chadwick, J. 2006 Active center determinations on MgCl₂-supported fourth- and fifth-generation Ziegler-Natta catalysts for propylene polymerization. *J. Polym. Sci. A Polym. Chem.* **44**, 1635–1647.
- [166] Thakur, A., Wada, T., Chammingkwan, P., Terano, M. & Taniike, T. 2019 Development of Large-Scale Stopped-Flow Technique and its Application in Elucidation of Initial Ziegler-Natta Olefin Polymerization Kinetics. *Polymers* **11**, 1012.
- [167] McKenna, T., Tioni, E., Ranieri, M., Alizadeh, A., Boisson, C. & Monteil, V. 2013 Catalytic olefin polymerisation at short times: Studies using specially adapted reactors. *Can. J. Chem. Eng.* **91**, 669–686.
- [168] Tian, Z., Xue-Ping, G., Feng, L.-F. & Guo-Hua, H. 2013 A model for the structures of impact polypropylene copolymers produced by an atmosphere-switching polymerization process. *Chemical Engineering Science* **101**, 686–698.
- [169] Soares, J. B. P. & Hamielec, A. E. 1996 Bivariate chain length and long chain branching distribution for copolymerization of olefins and polyolefin chains containing terminal double-bonds. *Macromol. Theory Simul.* **5**, 547–572.

Curriculum vitae

Personal information

Name Valaei, Sina
Birth 01.09.1990 Hamedan, Iran
Nationality Iranain/German
Address Klaavuntie 4, 00910 Helsinki, Finland
Telephone +358503794217
E-mail sina.valaei@outlook.com

Work experience

09/2021 - **Senior Scientist I**
Borealis Polymers Oy,
Polymerization and catalysts competence center
Porvoo, Finland

04/2021 – 08/2021 **Project manager**
Polymer reactor technology GmbH,
Ahaus, Germany

01/2018 – 03/2021 **Research scientist**
Martin-Luther-University Halle-Wittenberg,
Halle, Germany

Academic education

01/2018 – 03/2021 **PhD Student**
Martin-Luther-University Halle-Wittenberg, Germany
“Kinetic study of bulk propylene homo-polymerization, and gas phase impact copolymerization”

10/2013 – 10/2016 **Master of Polymer Materials Science**
Martin-Luther-University Halle-Wittenberg, Germany
Master thesis: “Kinetic study of bi-modal propylene polymerization”

09/2008 – 06/2013 **Bachelor of Chemical Engineering**
University of Tehran, Iran
Thesis: “Modeling heat transfer in polystyrene foam”

09/2004 – 06/2008 **High school**
NODET, Hamedan, Iran

List of publications

Valaei, S., Bartke, M., "Multistep Bulk-/Gas-Phase Polymerization of Propene in a Reaction Calorimeter", *Macromol. React. Eng.*, 2022

Kettner, J., Valaei, S., Bartke, M., "Reaction Calorimetry for Studying Kinetics in Bulk Phase Polymerization of Propene", *Macromol. React. Eng.*, 2020

Ben Mrad, A., Sheibat-Othman, N., Valaei, S., Bartke, M. & McKenna, T. F. L., "Diffusivity of Multicomponent Gas Mixtures in Polyethylene", *Macromolecular Chemistry and Physics.*, 2022

Conference contributions:

Valaei, S., Bartke, M., "Kinetics and Modeling of multi-step propylene/ethylene Impact Copolymerization", CHISA Conference, Virtually, 15.-18. March 2021

Valaei, S., Bartke, M., "Power compensation calorimetry, a tool for studying the kinetics of bulk Propylene polymerization", 13th International Workshop on Polymer Reaction Engineering, Hamburg, 11.-14. June 2019

Valaei, S., Bartke, M., "Kinetic Study of bimodal propylene polymerization", Polymer Reaction Engineering X Conference, Punta Cana (Dominican Republic), 20.-25. May 2018

Eidesstattliche Erklärung

Ich erkläre an Eidesstatt, dass ich meine Dissertation selbstständig und ohne fremde Hilfe verfasst, keine anderen als die von mir angegebenen Quellen und Hilfsmittel benutzt und die den benutzten Werken wörtlich oder inhaltlich entnommenen Stellen als solche kenntlich gemacht habe. Desweiteren erkläre ich, dass ich erstmals eine Dissertation einreiche und diese noch bei keiner anderen wissenschaftlichen Institution eingereicht habe. Ich bin nicht vorbestraft und es gibt keine laufenden Ermittlungsverfahren gegen meine Person.
